



**CANADIAN MINING INDUSTRY RESEARCH
ORGANIZATION (CAMIRO) EXPLORATION DIVISION**

**CAMIRO PROJECT 10E01
Phase I**

**Quality Control Assessment of Portable XRF Analysers:
Development of Standard Operating Procedures,
Performance on Variable Media and Recommended Uses**

**Gwendy Hall
Angelina Buchar
Graeme Bonham-Carter**

**June 9, 2011
Minor revisions October 10, 2012
Minor revisions October 16, 2013**

Table of Contents

Executive summary and recommendations to users	4
1. Introduction	12
2. Background	14
2.1 Basic principles and operation of portable ED-XRF.....	14
2.1.1 Principles.....	14
2.1.2 Instrumentation.....	18
2.1.3 Interferences in ED-XRF.....	21
2.1.4 Calibration strategies.....	23
2.1.5 Optimization.....	24
2.1.6 Daily operating procedure.....	25
2.2 Literature review.....	27
3. Methods	35
3.1 Instruments used in this study.....	35
3.2 Suite of samples under study.....	39
3.3 Optimization of beam time.....	42
3.4 Evaluation of accuracy.....	42
3.5 Evaluation of precision and detection limits.....	42
3.6 Data analysis.....	42
3.7 Thin-film study.....	45
4. Results	48
4.1 Silica blanks.....	48
4.2 Optimization of beam time.....	50
4.3 Accuracy and precision.....	53
4.3.1 Introduction.....	53
4.3.2 Discussion of results by element.....	58
4.3.2.1 Major and minor elements.....	61
4.3.2.2 Anions, P, S, Cl.....	66
4.3.2.3 Trace elements.....	67
4.3.3 Summary and discussion of accuracy and precision graphs.....	80
4.4 Precision and detection limits.....	89
4.5 Thin-film study.....	94
4.6 Drift.....	101
5. Recommendations for manufacturers of pXRF analysers	104
6. References	109

List of Appendices

- 1 NRCan certification booklet (appendix_1.pdf)
- 2a University of California X-ray data booklet (appendix_2a.pdf)
- 2b Table 1-3 from U.C. X-ray data booklet (appendix_2b.pdf)
- 3 CRM data. Recommended and selected values (appendix_3.xls)
- 4a X-Y graphs. Soil mode. (appendix_4a.pdf)
- 4b X-Y graphs. Mining mode. (appendix_4b)
- 5 Beam time study. (compressed file: appendix_5.zip)
- 6 CRM/XRF data. Soil mode. (appendix_6.xls)
- 7a CRM/XRF data. Mining mode. Elements Ag-Ni (appendix_7a.xls)
- 7b CRM/XRF data. Soil mode. Elements P-Zr (appendix_7b.xls)
- 8a Precision data. Soil mode. All elements. (appendix_8a.xls)
- 8b Precision data. Mining mode. Elements Ag-Mn. (appendix_8b.xls)
- 8c Precision data. Mining mode. Elements Mo-Zr. (appendix_8c.xls)

Note: *The appendices are either pdfs or tabbed Excel files or a compressed zip file (appendix 5). These named files are independently saved to make them easier to use, but are an integral part of the report.*

EXECUTIVE SUMMARY

The CAMIRO study by G. Hall *et al.* was funded by 31 companies and in collaboration with the Natural Resources Canada, three manufacturers of portable XRF instruments (Bruker Elemental, Olympus InnovX and Thermo Fisher Scientific Niton) and analytical support of two commercial laboratories (ALS Global and SGS). The study was proposed to provide independent guidelines and protocols for practical and safe use of instruments in the field and collection and interpretation of data. Within a month of start-up we quickly realized that analysis using 5 to 6 instruments is a monumental task. As well, we realized that the challenge of measuring and interpreting data required, first, a fundamental review of frequently measured elements in common rock and mineralized samples of certified reference powders. The results and guidelines reported here constitute a singular report that all sponsors can use to guide their field and interpretative uses. However, there is a need for further work on the challenges of working with *real* field materials (rock, core, soils, wet sediments). We are proposing a follow-up study, Phase 2, to start in late 2011.

A suite of 41 control reference materials (CRMs), which had been augmented by several samples from sponsors, was used to evaluate the performance of portable energy-dispersive X-ray fluorescence (pXRF) instruments in the analysis of geological materials. This suite encompasses both a wide range of geological matrices in soils, rocks and ores and a wide range in concentration of elements. The fine powdered CRMs were used to establish the figures of merit – accuracy, precision and detection limits – obtained in the operation of three handheld and two benchtop pXRF instruments from InnovX (Olympus), Niton (Thermo Fisher Scientific) and Bruker Elemental. The accepted concentrations of elements in the CRMs, against which the pXRF data were compared, were derived from recommended (certified) values and, where these were missing, from total element analyses carried out by ALS Laboratories of Vancouver and by SGS Laboratories of Toronto.

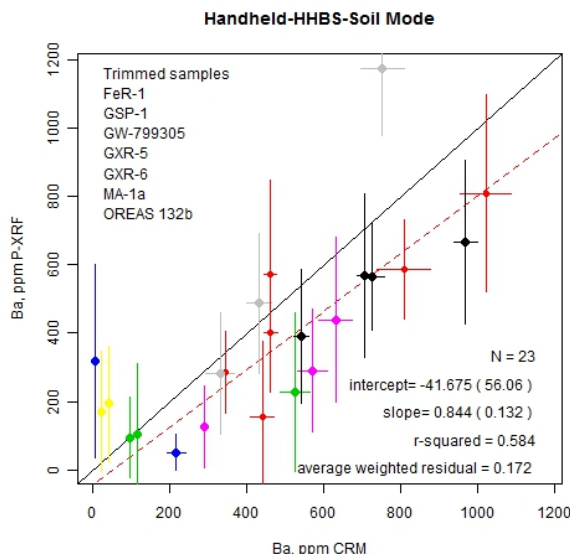
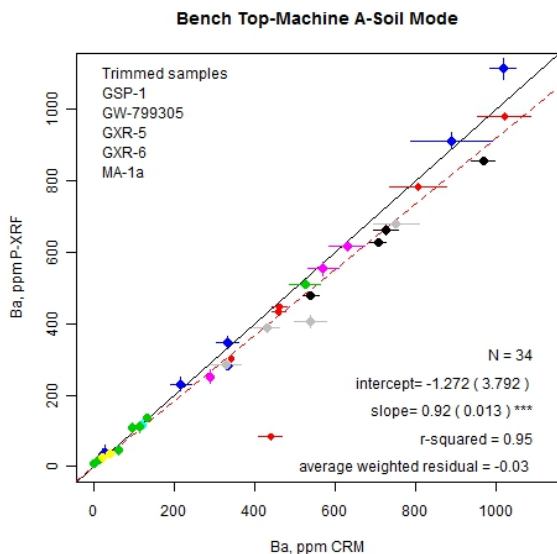
The only parameter optimized in the analysis is beam time and this was thoroughly evaluated with three CRMs, from 10 s to 120 s with 10 readings for each sample at each value of ‘t’. Accuracy was determined from 10 replicate analyses of each of the 41 samples in both the mining (‘Fundamental Parameter’ type of calibration) and the soil (with Compton normalization) mode. Precision, in the sense of measurement repeatability, was determined using a subset of 10 CRMs, and analysing them 10 times each in a random order (i.e. the sample was moved off the viewing area each time). Detection limits, based on the definition of three times the standard deviation of a sample at low concentration (within 10 times of the expected detection limit), were derived using this subset of 10 CRMs (excluding ores and rare-earth element enriched samples). Different makes and thicknesses of thin-film, used to cover the sample when encapsulated for analysis, were studied to determine the effect on the transmittance of fluorescence photons for the light elements (e.g. Mg, Al, Si) in particular. Drift of instruments over the course of a day was also investigated.

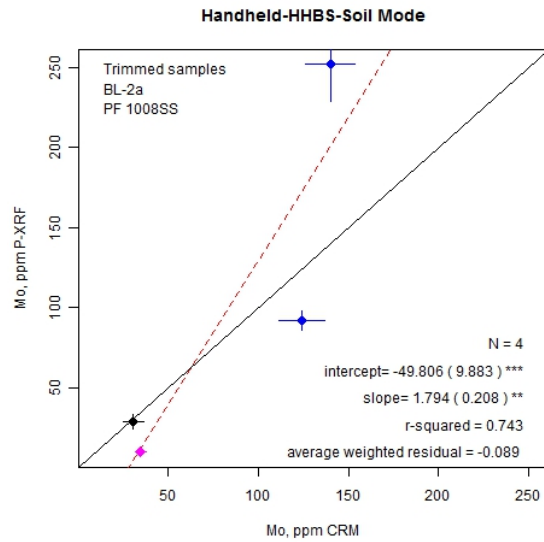
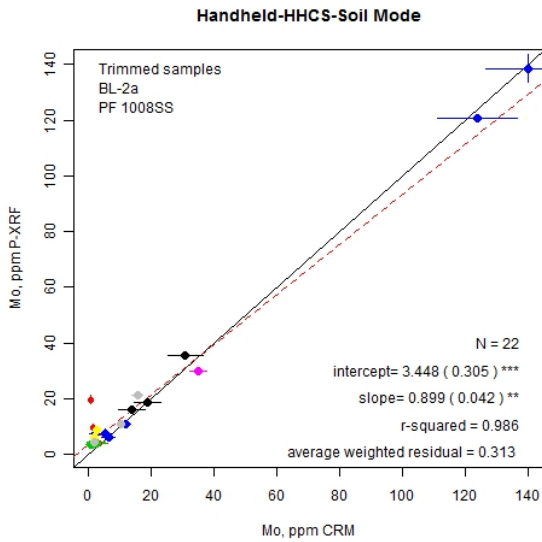
The accuracy data are reported in Excel spreadsheets and are plotted (pXRF vs accepted value) as x-y graphs using the Ripley-Thompson functional linear relationship method. Samples were colour-coded according to their matrix (e.g. mafic/ultramafic group) in order to identify any trends in the data. The values of the slope and r^2 (used as a measure of goodness of fit) from these graphs were

then used to summarize the performance of the instruments for each element by each mode, in addition to a discussion of each element in detail.

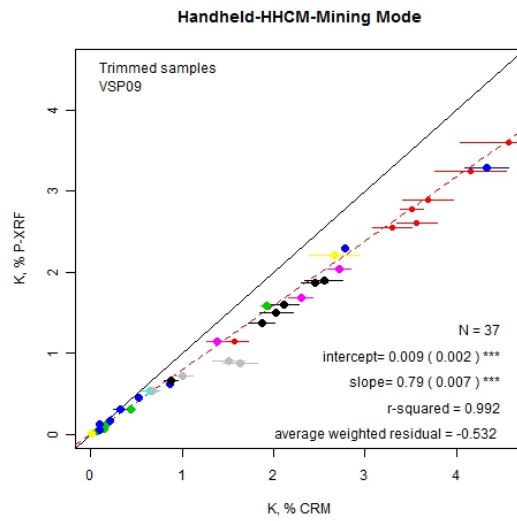
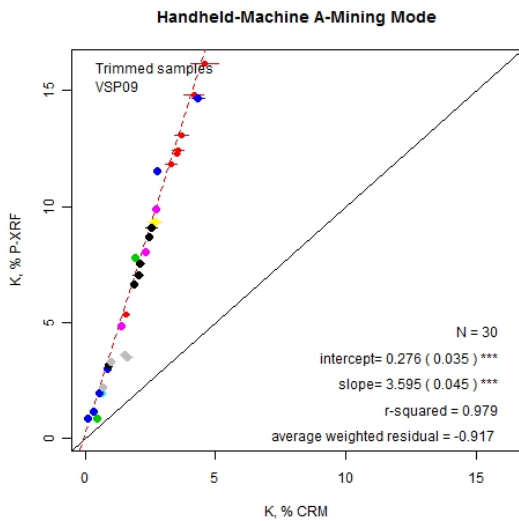
A *beam (count) time* of 60 s was chosen as a compromise between good precision of measurement and productivity. Precision, and hence detection limit, should improve with time and in most instances this is the case. However, one handheld model shows no improvement in noise with time for many trace elements in the soil mode. A large increase in absolute concentration, accompanied by a decrease in precision, after 40-60 s is evident for Al, Mg, Si and S by another instrument in the mining mode. A shift of ~18 to ~22 % in a Si value dependent on beam time is hard to understand. Furthermore, worse precision at the longest beam times (100, 120 s) is seen for Ti, V, Cr and Ca for this instrument. The manufacturers are investigating the causes of these unexpected trends with increasing beam time. Users should establish the optimum beam time appropriate for their objectives; less than 50 s is not advised.

Perhaps the most surprising discovery is the *inconsistency in performance* from one instrument to another, and not necessarily from one manufacturer to another, although that was mostly the case. Large differences in accuracy are evident for many elements, mostly the traces. An example of extremes in performance is shown below for Ba at levels below 1000 ppm (i.e. trimmed data-set): note the excellent goodness of fit (r^2 of 0.95) and very small pXRF error bars using Benchtop A contrasted with the unacceptably poor precision shown by Handheld B. Another example is afforded by Mo at levels below 150 ppm (shown below), where Handheld C performs well, with an r^2 of 0.99 and a slope of 0.90 but Handheld B has such poor sensitivity that it can only report on the four highest samples. No one instrument does well across the elements; the order of best to worst performance depends on the element and the matrix. This makes conclusions challenging but also implies that a company should not mix instruments within a survey, or if they do, then to cross-calibrate them (not always legitimate if interferences are handled differently by the proprietary software). Although evaluation of pXRF across five instruments was very time-consuming, conclusions based only on one instrument would have been extremely misleading given the stark contrast in performance for many elements.





With the exception of Mg, the major elements are generally well to adequately determined in the *mining mode*. We did not carry out calibrations specific to the matrices being analysed as there were too many to do within the time-frame but the colour-coding allowed any linear trends to be observed. Only several such trends were noted that pertained to the behaviour of a particular group. While results are usually accurate to within $\pm 20\%$ for Fe, Ca and Si, they certainly are not for Al (e.g. $\pm 40\%$ at levels $>0.4\%$ Al) and Mg. In the mining mode, slopes are often significantly different from 1.0 (e.g. 0.7 to 1.3) but linearity is commonly good (with the exception of difficult matrices such as the ores and the REE-enriched samples). This suggests that accuracy could be improved immensely by recalibration. An example of differences in slope but excellent r^2 values is given below: K by Handheld A would report very high indeed (slope of 3.6!) without recalibration whereas Handheld C would report low by $\sim 20\%$ (slope of 0.79).



Many users are unaware that they should calibrate with their own standards of similar matrix to the samples being analysed. This is hardly surprising as more than one manufacturer has advertised, quote, “*Fundamental Parameters is the preferred analysis tool for mining....applications. Using this powerful in-factory calibrated instrument, an analyzer can then measure the full range of element concentrations in a wide variety of samples for years without any additional calibrations or user input of any kind.*” This is not true! If accuracy is desired in the mining mode (i.e. for major elements), then the user MUST carry out a calibration of their own, thereby altering the factory settings for the intercept and slope.

Using the summary of r^2 and slope across the instruments, the overall sequence of elements in the mining mode from ‘good’ to ‘bad’ in this mode is Fe, Ca, Zn, Pb, Cu, Si, K, Al, S, Cr, As, Ni, Mn, Ti, Sr, Rb, P, Mg. In considering only precision (r^2), this sequence changes slightly to Ca, Zn, K, Rb, Sr, Fe, Mn, Cu, S, Ni, Pb, P, Ti, Cr, Al, Si, Mg. If several instruments perform badly and others well for an element, its position in this sequence is compromised when in fact the capability of pXRF to measure that element could indeed be good. These differences in performance amongst the instruments make such classification of elements only rough guides.

In the *soil mode*, the sequence from best to worst element is Sr, Rb, Cu, Ca, K, Zn, Fe, Ti, Zr, As, Mn, Th, Pb, Nb, Ba, Cd, Cr, U and Sb. For these elements, a minimum of one ‘good’ rating for accuracy (slope of 0.96-1.04) or goodness of fit ($r^2 > 0.9$) was assigned to at least one instrument. However, elements where all ratings are ‘fair’ (slope of 0.9-0.95 or 1.05-1.1; r^2 of 0.8-0.9) ‘poor’ or ‘bad’ (slope of < 0.8 or > 1.2 ; $r^2 < 0.5$) include Mo, V, Ni, Co, S and Sn. Given the diversity of sample types in the suite under study, these criteria used to assess performance are probably rather stringent. Elements determined by only one or two instruments include La, Y, Ce, Ag, Au, Sm, Se, W, P, Hg, Nd and Ta. Of these, La and Y show good precision and accuracy by one instrument, Ag shows good precision by one instrument, but the rest are overwhelmingly rated as ‘bad’.

Elements where highly erroneous results were obtained include Au, Bi, Cs, Hf, Hg, Sc, Pd, Pt, Se, Ta, Te and W. While many values are below detection limits set by the factory, others are reported in some samples at ~10 to 1000 times higher levels than the accepted concentrations. Clearly these elements suffer from acute interferences, made far more prominent by the element’s normal abundance in the ppb rather than ppm concentration range. In these cases where interferences play such a critical role, the practice of some manufacturers to simply report values as being below the element’s detection limit (‘<DL’ or ‘<LOD’) should be adopted universally.

Repeatability of measurement by pXRF is usually excellent, often better than $\pm 10\%$, depending on concentration and region of the spectrum being measured. From this work using 10 CRMs (excluding ores and REE-enriched samples), typical RSDs for the CRMs fall into the following groups: $< 2.5\%$ for Fe, Ca, K, Si; 2.5-4.9% for Mn, Rb, Sr, Ti, Y, Zn, Zr; 5-10% for Ag, Cr, Cu, Pb, V, Al, S; 11-20% for As, Ba, Cd, Co, Ni, S, Th, U, Mg; and $> 20\%$ for Sb, Se, Sn and P.

The *detection limits* (3σ) measured in this project, using samples containing elements at ‘background’ concentrations, are similar to those provided by most manufacturers, in the 5-50 ppm range for many trace elements. However, these detection limits are *ideal* and are degraded

dramatically by the presence of interfering elements, a situation that can be expected to arise in many geological applications. The most problematic samples in terms of accuracy are the two REE-enriched samples supplied by Great Western Minerals and several other CRMs containing high levels of REEs (SY-3 and a stream sediment). The various ores also created numerous ‘fliers’ in the elemental data-sets.

Sometimes a *problem with accuracy* will be indicated by a high standard deviation (counting statistics) reported by the instrument and/or by imprecise results for replicate analyses. However, there were many instances in this project where this was not the case, as, for example, in the well-known spectral interferences of U on Mo, Pb on As and Zn on Au. The syenite, SY-3, contains 650 ppm U but only 1.0 ppm Mo; however, Mo is reported in SY-3 at 15 ± 3.2 ppm up to 34.4 ± 1.6 ppm, all 10 replicate analyses being reported by each instrument. These standard deviations are certainly acceptable and the instrumental standard deviation for each measurement is low, in the order of $\sim \pm 10\%$. Similarly, Mo is reported, with good precision, in the range 74–272 ppm across four instruments in the U ore BL-2a (4260 ppm U) but its certified concentration is only 15 ppm Mo. How is the user to know that these reported values are not Mo but are actually caused by the presence of U? Similarly, three instruments do not report As in the Zn-Pb ore OREAS 132b (3.88% Pb), presumably programmed to recognize this magnitude of interference, but two instruments do report As as 923 ± 73 ppm and 1064 ± 95 ppm ($n=10$, with reasonable individual SDs) when in fact OREAS 132b contains only 155 ppm As. If one company can guard against such huge errors and get their software right, why cannot others?

For some instruments, very random concentrations were reported at levels that were clearly below the detection capability for that particular matrix. For example, one instrument reported 0 ppm Co in MRG-1 and 300 ppm the next reading (the randomness indicating an interference problem), and yet in another less problematic matrix Co might be determined with good precision at concentrations lower than 300 ppm. The geochemist is not in the habit of taking multiple readings so he/she would either follow up on a false anomaly or miss one by not realizing that the region of the *real* detection limit has changed. It would be safer for the user if the software was designed to work with variable detection limits and eliminate reporting concentrations below these limits according to the degree of interference encountered, as indeed some manufacturers do.

Drift over the course of a day is unacceptable for some groups of elements (specific to a beam) determined by several instruments. In at least one case the drift is related to change in the live-time and this needs to be addressed by the manufacturer.

The *thin-film study* demonstrates the significant differences in transmittance of the fluorescence signal that the thickness of the film can make. Mylar, for example, at $2.5 \mu\text{m}$ transmits $\sim 79\%$ of the Si signal (five samples tested on two instruments), but only $\sim 57\%$ when its thickness increases to $6.0 \mu\text{m}$. The elements most affected are the light elements: from Mg (worst), through Al, Si, P, S, K to Ca. At the same thickness, Prolene (polypropylene) transmits to a higher degree than Mylar (e.g. $\sim 90\%$ at $3 \mu\text{m}$ for Si), probably because it is less dense than Mylar and the transmittance is less affected by thickness. These materials contain elements such as S, P and Ca as contaminants that the user should be aware of, particularly if they are analysing samples containing low levels of these analytes.

Although the benchtop instruments are operated at higher power than the handhelds, and therefore should be superior for elements whose lines are of higher energy, there was no perceptible difference in overall performance.

For *rare-earth elements* (REE), instruments equipped with radioactive sources such as ^{55}Fe , ^{57}Co , ^{109}Cd and ^{241}Am are to be preferred to those operated with X-ray tubes, regardless of the disadvantage of licensing and shipping requirements and decay of the sources. The added power is needed to excite the K lines of the REEs. Only one instrument reported Ce, La, Nd, and Sm: the results are highly erroneous for Nd and while detection at the tens of ppm level was very challenging for Ce, La, and Sm, some of the results for La are accurate, though very imprecise (25-100 % RSDs). Cerium, La, Nd and Sm could be measured with adequate precision in the REE-enriched samples but with variable accuracy. Yttrium, used as a surrogate for REEs, was determined with excellent accuracy and precision by the two instruments reporting this element.

The suite of CRMs used in this study is certainly varied in sample type and element concentration so perhaps it is not surprising that so many spectral interferences or incorrect results were encountered. Much is being asked of the algorithms to correct for interferences over wide ranges of element concentration. It must be borne in mind that this is a *direct* analysis, without a fusion, digestion or dilution step which serves to suppress problems from different matrices in other analytical techniques such as ICP-MS. It is the geologist or geochemist who operates the pXRF instrument, without the benefit of a geoanalyst who is well aware of the strengths and weaknesses of the technique. An analyst in an established laboratory, for example, would be fully cognizant of the pitfalls, would be able to recognize the interferences and would set detection limits at realistic levels dependent on the sample type. Each mining company is strongly encouraged to designate someone with technical acumen within their group to be their pXRF specialist, to take the training (e.g. offered by University of Western Ontario, a week's course), to be responsible for the maintenance and calibrations of their pXRF instruments, and to train others in the company in the operation before they go to the field.

Portable XRF is capable of producing extremely valuable data in the field (e.g. to guide a survey) or at the mine-site (e.g. sorting core). If calibrated properly, it can certainly provide data that are fit for these purposes. However, it should not be used as a replacement for acquiring data from an accredited laboratory using established analytical techniques that produce high quality data.

Two instrument breakdowns, demanding return to the factory, and significant communication with technical staff suggest that pXRF is not yet in a robust state. At the end of this report is a section on recommendations to manufacturers and below are recommendations to users.

There is a lot of information in this report. To obtain details on specific elements of interest, the reader is directed to the individual pertinent areas and to the appendices containing all the data and graphs.

Recommendations to users

- Be prepared to carry out a calibration to suit your sample type/matrix, certainly for elements to be determined using the mining mode (i.e. at higher than trace levels). Establish a suite of at least five CRMs, over the expected concentration range, by preparing them to be as homogeneous as possible and having them analysed by several accredited laboratories for total concentrations of the elements of interest. If accuracy is of paramount importance, this may be necessary in the soil mode also but test the factory soil calibration first.
- Become very familiar with the performance of your instrument before taking it to the field. Ascertain the optimum beam time in each mode appropriate for your analytical goals and use both the CRMs supplied with the instrument (usually one or more of the NIST soils used in this project) and your own CRMs to establish figures of merit (i.e. *realistic* detection levels, accuracy, precision). Your CRMs may well exhibit data of lesser quality than the NIST standards but that is to be expected. Ensure that the thin-film being used is the same as that employed by the factory in their calibration. If not, then a correction factor needs to be established for the light elements (Mg, Si, Al).
- Learn to anticipate serious spectral interferences by using the Periodic Table Guide of element lines provided by the manufacturers and in this report (the more detailed guide to lines is provided in Appendices 2a, b). In most cases, the spectral interferences are not complex. Poor counting statistics precision can alert the user to a likely interference on that element but this is certainly not always the case. Check the spectrum for that element. If the result reported is unexpected (usually high), then analyse again and later check it by a different analytical technique.
- If a *spatial trend* in a survey is being sought and accuracy is not of concern, then prior calibration is not mandatory. However, ensure that a false trend in the data is not generated by any obvious interferences incurred. This could happen when the matrix being analysed changes significantly (e.g. from dry to wet conditions in a soil survey; changing horizons in a soil survey; moving down-core), leading to physical effects, absorption/enhancement effects or direct spectral overlap from hitherto trace-level elements. Data can often be corrected ‘after-the-fact’ by establishing a calibration to suit the changes in matrix later in the lab/office.
- If a sample is being analysed through a bag of some sort, then that bag’s level of contamination must be established and its absorption characteristics for the light elements (Mg, Al, Si) known. Use pure SiO₂ and a low-level CRM as samples to ascertain these figures and correct for them.
- Ensure the depth of sample being analysed is adequate, especially if its density is low. Remember critical penetration depth for light elements such as Si is in the μm range compared to heavy elements in the mm range.
- Follow the manufacturer’s instructions (hopefully the manuals are improving!), e.g. run the supplied coupon/disc as an energy check daily. Run the SiO₂ blank at least daily or whenever it is suspected that the window has become dirty (the blank concentration levels should be familiar). The rate at which one or more CRMs is analysed is up to the user/organization but a rate of 1 in 20 to 1 in 40 is recommended. This will facilitate drift correction later if necessary or alert the user to another problem. Running a sample of similar matrix to those under study at a similar rate is also useful.
- Download data from the analyser at least daily and check for any ‘oddities’ such as change in element order or column shifts. Check the livetime readings: if they are highly variable or decreasing, this may be indicative of a problem with the tube, detector or multichannel analyser.

- Be consistent!
- Don't combine data from different instruments unless they have been thoroughly cross-calibrated.
- At the present state of the technology, avoid using data for the elements Au, Bi, Cs, Hf, Hg, Sc, Pd, Pt, Se, Ta, Te and W. If one or more of these elements is important, then construct a calibration with CRMs of similar matrix at the appropriate concentration range and carefully check spectra of the survey samples.
- pXRF is a very useful tool for guiding surveys and sorting samples and drill-core. It is by no means a replacement for the high quality data generated by an accredited geochemistry laboratory.

1. INTRODUCTION

Portable energy-dispersive (ED) XRF has improved dramatically in recent years, thanks to the semi-conductor industry, miniaturization of components such as the X-ray tube and the development of sensitive detectors such as the silicon drift detector (SDD). The literature is replete with applications of this technique in the analysis of cultural artifacts, artwork and archaeology: the non-destructive nature of the technique combined with its ability to analyse small areas and detection limits in the ppm range have made it particularly alluring to these fields of study. Another successful application is in the analysis of alloys; this is apparent when one reads the manuals of pXRF instrumentation which contain specific methods for this medium. In the last few years the appeal of rapid on-site analysis in the field or at the mine using a compact instrument delivering ppm-to-percent level measurement has encouraged many in the exploration and mining industry to purchase these tools. However, the results have not always measured up to the claims of the advertising literature proffered by the vendors, not only in terms of detection capability but most importantly in terms of accuracy. Claims that may be true in the application of pXRF to alloy analysis can fail drastically when the medium under study is a complex geological matrix such as a soil, rock or ore. It is in this environment that the proposal to evaluate pXRF for specific application to the mining industry was formulated.

Organization for this project began in earnest in September 2010. Gwendy Hall, formerly a research scientist in geoanalysis at the Geological Survey of Canada (GSC) for 35 years, agreed to accept the leadership of the project. Discussions were held with the GSC management to carry out the laboratory work on-site at the 601 Booth St location of the GSC, and in so doing, the project would benefit from the existing knowledge and experience in the field of XRF of the scientific staff. The Letter of Agreement was signed in December when GSC became an in-kind sponsor of the project and a laboratory was identified for use. Meanwhile in October interviews were held at the University of Ottawa for the technical position of operating the instruments and carrying out the day-to-day analyses. Six (pending) M.Sc. and PhD graduates were interviewed and Angelina Buchar, with an M.Sc. from the University of Ottawa (subject of research is in trace chemicals in the Arctic environment), won the competition. The necessary one-day of training was arranged and given to Angelina Buchar and others at the GSC on November 8th. In record time, on November 10th, Angelina passed the mandatory exam (Level 1) to operate a portable XRF analyser in Canada. The very useful ‘Certification Information and Examination Preparation Booklet’, produced by Natural Resources Canada, is attached as it not only contains information on the principles and operation of an XRF but it describes best practices in terms of *safety of use* (Appendix 1: NRCan Certification).

The portable XRF (pXRF) instrument manufacturers - InnovX (Olympus), Niton (Thermo Scientific) and Bruker (Elemental) – agreed to lend their instruments to the project without charge and to train A. Buchar and G. Hall in their operation at the GSC. Work in the laboratory began in January, when Angelina was completely free and after receiving the first instruments in mid-December. Delivery of the analysers was staggered

through the project so that the period in which they were in CAMIRO's custody was not over-extended. The last delivery was made in April.

The objectives of the project included:

1. Optimization of operating parameters and calibration methodology (e.g. Compton normalization with Fundamental Parameters) for both exploration and mining applications. Clarification of the use of 'modes' of operation.
2. Determination of the method detection limit for each target element.
3. Evaluation of accuracy and precision for a wide variety of control reference materials (CRM) (i.e. different matrices).
4. Measurement of the effects of spectral and chemical interferences likely to be present in geochemical samples.
5. Comparison of the performance of the handheld vs bench-top instruments.
6. Documentation of the skills and training required to operate both types of instruments.
7. A literature review of pXRF.

Sponsors initially wanted to see these objectives expanded to include the development of protocols for the analysis of rocks, cores, soils etc. However, given the very wide range in target elements and matrices (from 'background' soils to drill cores) already tabled, it was agreed that this phase of the work would concentrate on deriving the figures of merit (accuracy, precision, detection limits) for powdered geological control reference materials (CRM) only. Sponsors were given the list of potential CRMs and asked to suggest or provide other samples if their interests were not covered. The fact that this work was to be conducted across 5-6 instruments put a large constraint on the scope of the project because of time. In fact, initially there were 7 instruments but one broke down and, while some work was done on the Bruker benchtop, the S2 Ranger, it is not included here as it is not really a portable model as are the others (rather it is a sophisticated, lab-style benchtop with an automated multi-sampler).

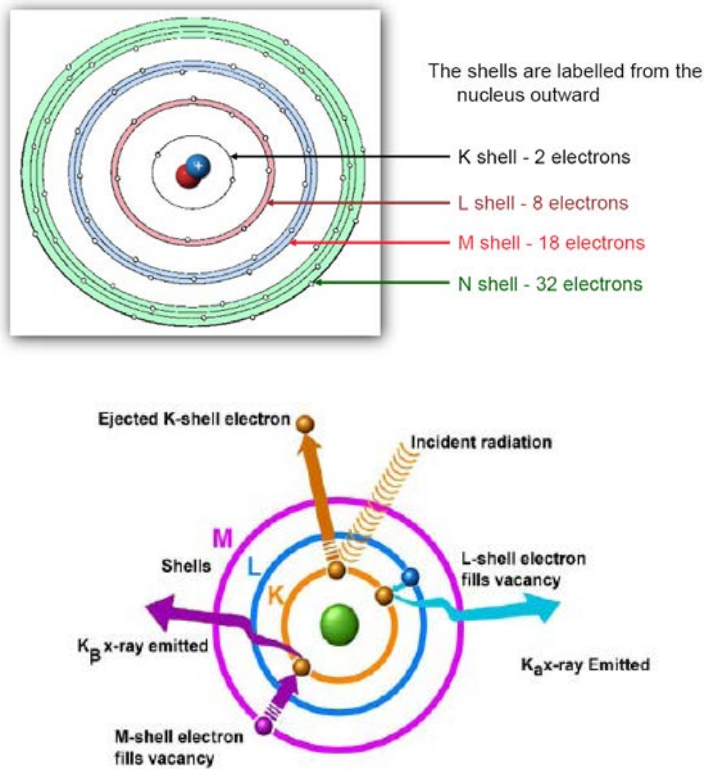
2. BACKGROUND

2.1 Basic Principles and Operation of Portable ED-XRF

2.1.1 Principles

X-ray fluorescence, using either wavelength- or energy-dispersive spectrometry, is a well established multi-element, non-destructive, analytical technique with a wide dynamic range (from ppm to %) (Potts, 1987). Portable XRF (pXRF), based on energy-dispersive spectrometry, has developed rapidly in recent years owing to advances in semi-conductor technology and miniaturization.

Atoms fluoresce at specific energies when excited by X-rays and detection of specific fluorescent photons enables the quantitative measurement of the elements in a sample. Below is a simplified diagram of the electron shell configuration of an atom, after Niels Bohr, accompanied by a schematic showing the impact of an X-ray beam on an atom and the typical reactions this causes.



When a sample is irradiated with X-rays, an electron from an inner shell of the atom with an appropriate absorption energy may be ejected, as shown here where an electron has been ejected from the K-shell. An outer shell electron then falls in to fill this inner shell vacancy as the atom regains its ground state. This process, known as *the photo-electric effect*, produces photons with energy equivalent to the difference in energy between the two shells. For example, here if an electron from the L-shell fills the vacancy in the K-shell, a K_α X-ray is emitted whereas if the electron originated in the M-shell, a K_β X-ray

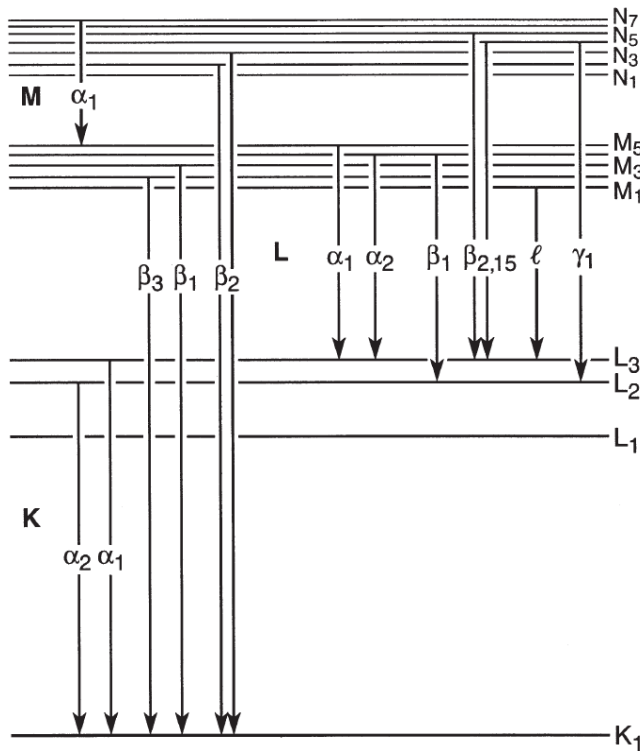
would be produced. Typically it is the K and L electrons which are affected in XRF analysis. The K-shell electrons have the highest binding energy and hence they require a higher energy X-ray to remove them than would L-shell electrons. Each atom has an X-ray line spectrum that consists of a series of discrete energies with intensities related to the probability that a particular transition will occur. The X-rays emitted are characteristic of the atom and provide qualitative identification of the element while their intensities provide quantitative analysis.

Moseley's Law (1913) describes the relationship between the wavelength of an X-ray emission (λ) and the atomic number of an element Z :

$$1/\lambda = k(Z-\alpha)^2$$

where k is a constant for a particular series of lines (K, L etc) and α is a shielding constant (the effective nuclear charge available to an outer orbital electron is *shielded* by intervening electrons). Thus energy is proportional to Z^2 .

X-ray spectra are more complicated than suggested by the Bohr atom. In reality, orbital electrons interact with one another to split the energy levels of each shell into subshells. The K-shell is always mono-energetic but the L-shell can split into three subshells (L_I , L_{II} and L_{III}) and the M-shell into five. Transitions from each subshell to a vacant orbital are governed by selection rules that are defined by quantum theory; some transitions are allowed and others forbidden. The magnitude of the split increases as the number of electrons in the atom increases and therefore low atomic number elements will have relatively simple spectra whereas those of heavier elements will be more complex. Transitions from one shell to another that give rise to various X-ray emission lines are illustrated below.



PERIODIC TABLE OF XRF FLUORESCENCE DATA

Including K and L line energies & detection limits

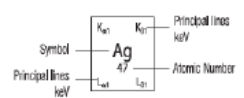


H 1	IIA																He 2																																																	
0.06 Li 3	0.11 Be 4																	0.18 B 5	0.28 C 6	0.39 N 7	0.62 O 8	0.68 F 9	0.85 Ne 10																																											
1.04 Na 11	1.25 Mg 12																	1.49 Al 13	1.74 Si 14	2.01 P 15	2.14 S 16	2.31 Cl 17	2.48 Ar 18	2.90 Kr 36	3.19 Xe 54																																									
IIIB		IVB		VB		VIB		VIIB		Group VII		IB		IIB		IIIA		IVA		VA		VIA		VIIA																																										
3.01 K 19	3.69 Ca 20	3.69 Sc 21	4.01 Ti 22	4.46 V 23	4.09 Cr 24	4.46 Mn 25	4.83 Fe 26	5.43 Co 27	5.41 Ni 28	5.96 Cu 29	5.9 Zn 30	6.40 Ga 31	6.4 Ge 32	7.06 As 33	7.06 Se 34	7.85 Br 35	8.02 Kr 36	7.85 Rb 37	7.95 Sr 38	7.48 Y 39	8.29 Zr 40	8.05 Nb 41	8.91 Mo 42	8.94 Tc 43	9.57 Ru 44	9.57 Rh 45	9.57 Pd 46	9.57 Ag 47	9.57 Cd 48	10.26 In 49	10.26 Sn 50	10.26 Sb 51	10.26 Te 52	10.26 I 53	10.26 Xe 54	10.26 Ba 56	10.26 La 57	10.26 Ce 58	10.26 Pr 59	10.26 Nd 60	10.26 Pm 61	10.26 Sm 62	10.26 Eu 63	10.26 Gd 64	10.26 Tb 65	10.26 Dy 66	10.26 Ho 67	10.26 Er 68	10.26 Tm 69	10.26 Yb 70	10.26 Lu 71	10.26 Ac 89	10.26 Th 90	10.26 Pa 91	10.26 U 92	10.26 Np 93	10.26 Pu 94	10.26 Am 95	10.26 Cm 96	10.26 Bk 97	10.26 Cf 98	10.26 Es 99	10.26 Fm 100	10.26 Md 101	10.26 No 102	10.26 Lr 103
13.4 Rb 37	14.96 Sr 38	14.17 Y 39	15.84 Zr 40	14.96 Nb 41	10.74 Mo 42	14.96 Tc 43	15.84 Ru 44	17.07 Rh 45	16.02 Pd 46	18.02 Ag 47	17.48 Cd 48	18.01 In 49	18.37 Sn 50	20.02 Sb 51	19.28 Te 52	21.06 I 53	20.22 Xe 54	22.72 Ba 56	21.18 La 57	23.62 Ce 58	21.18 Pr 59	23.62 Nd 60	21.18 Pm 61	23.62 Sm 62	21.18 Eu 63	23.62 Gd 64	21.18 Tb 65	23.62 Dy 66	21.18 Ho 67	23.62 Er 68	21.18 Tm 69	23.62 Yb 70	21.18 Lu 71	23.62 Ac 89	21.18 Th 90	23.62 Pa 91	21.18 U 92	23.62 Np 93	21.18 Pu 94	23.62 Am 95	21.18 Cm 96	23.62 Bk 97	21.18 Cf 98	23.62 Es 99	21.18 Fm 100	23.62 Md 101	21.18 No 102	23.62 Lr 103																		
1.69 Cs 55	1.75 Ba 56	1.81 La 57	1.87 Ce 58	1.92 Pr 59	1.92 Nd 60	1.92 Pm 61	1.92 Sm 62	1.92 Eu 63	1.92 Gd 64	1.92 Tb 65	1.92 Dy 66	1.92 Ho 67	1.92 Er 68	1.92 Tm 69	1.92 Yb 70	1.92 Lu 71	1.92 Ac 89	1.92 Th 90	1.92 Pa 91	1.92 U 92	1.92 Np 93	1.92 Pu 94	1.92 Am 95	1.92 Cm 96	1.92 Bk 97	1.92 Cf 98	1.92 Es 99	1.92 Fm 100	1.92 Md 101	1.92 No 102	1.92 Lr 103	1.92 Ac 89	1.92 Th 90	1.92 Pa 91	1.92 U 92	1.92 Np 93	1.92 Pu 94	1.92 Am 95	1.92 Cm 96	1.92 Bk 97	1.92 Cf 98	1.92 Es 99	1.92 Fm 100	1.92 Md 101	1.92 No 102	1.92 Lr 103																				
86.1 Fr 87	97.47 Ra 88	97.47 Ac 89	100.13 Th 90	100.13 Pa 91	100.13 U 92	100.13 Np 93	100.13 Pu 94	100.13 Am 95	100.13 Cm 96	100.13 Bk 97	100.13 Cf 98	100.13 Es 99	100.13 Fm 100	100.13 Md 101	100.13 No 102	100.13 Lr 103	100.13 Ac 89	100.13 Th 90	100.13 Pa 91	100.13 U 92	100.13 Np 93	100.13 Pu 94	100.13 Am 95	100.13 Cm 96	100.13 Bk 97	100.13 Cf 98	100.13 Es 99	100.13 Fm 100	100.13 Md 101	100.13 No 102	100.13 Lr 103	100.13 Ac 89	100.13 Th 90	100.13 Pa 91	100.13 U 92	100.13 Np 93	100.13 Pu 94	100.13 Am 95	100.13 Cm 96	100.13 Bk 97	100.13 Cf 98	100.13 Es 99	100.13 Fm 100	100.13 Md 101	100.13 No 102	100.13 Lr 103																				

Lanthanides 57-71	33.44 La 57	37.3 Ce 58	34.72 Pr 59	39.26 Nd 60	36.03 Pm 61	40.75 Sm 62	37.28 Eu 63	42.27 Gd 64	38.72 Tb 65	43.83 Dy 66	40.12 Ho 67	45.41 Er 68	41.54 Tm 69	47.04 Yb 70	43 Lu 71	44.48 Ac 89	50.28 Th 90	46 Pa 91	52.12 U 92	47.55 Np 93	53.88 Pu 94	49.13 Am 95	56.68 Cm 96	50.74 Bk 97	57.62 Cf 98	52.93 Es 99	60.37 Fm 100	54.07 Md 101	61.28 No 102	54.07 Lr 103	
	4.95 Cs 55	5.04 Ba 56	4.84 La 57	5.26 Ce 58	5.03 Pr 59	5.49 Nd 60	5.22 Pm 61	5.72 Sm 62	5.43 Eu 63	5.96 Gd 64	5.64 Tb 65	6.21 Dy 66	5.85 Ho 67	6.45 Er 68	6.05 Tm 69	6.71 Yb 70	6.27 Lu 71	6.98 Ac 89	6.5 Th 90	7.25 Pa 91	6.72 U 92	7.53 Np 93	6.95 Pu 94	7.81 Am 95	7.18 Cm 96	8.1 Bk 97	7.42 Cf 98	8.4 Es 99	7.86 Fm 100	8.71 Md 101	
Actinides 89-103	90.86 Ac 89	102.85 Th 90	93.35 Pa 91	105.61 U 92	96.87 Np 93	108.43 Pu 94	98.44 Am 95	111.3 Cm 96	101.09 Bk 97	114.18 Cf 98	103.66 Es 99	117.16 Fm 100	106.26 Md 101	120.19 No 102	109.10 Lr 103	122.24 Ac 89	111.99 Th 90	126.36 Pa 91	114.76 U 92	126.64 Np 93	117.66 Pu 94	132.78 Am 95	120.89 Cm 96	138.08 Bk 97	117.66 Cf 98	132.78 Es 99	120.89 Fm 100	138.08 Md 101	117.66 No 102	138.08 Lr 103	
	12.65 Cs 55	15.71 Ba 56	12.97 La 57	16.2 Ce 58	13.29 Pr 59	16.7 Nd 60	13.51 Pm 61	17.22 Sm 62	13.95 Eu 63	17.74 Gd 64	14.28 Tb 65	18.28 Dy 66	14.62 Ho 67	18.83 Er 68	14.96 Tm 69	19.39 Yb 70	15.21 Lu 71	19.97 Ac 89	15.63 Th 90	20.56 Pa 91	19.02 U 92	21.17 Np 93	16.38 Pu 94	21.73 Am 95	19.02 Cm 96	21.17 Bk 97	16.38 Cf 98	21.73 Es 99	16.38 Fm 100	21.73 Md 101	16.38 No 102

Alloy Elements and Detection Limit Guidelines:
 Elements Detected: Magnesium (Mg, Z=12) through Silicon (Si, Z=14) and Titanium (Ti, Z=22) through Platinum (Pt, Z=78) typically 0.1% - some elements as low as 0.01%

Low-Density Sample Types (Soils, powders, liquids)



- Requires vacuum, LOD 0.2 – 3%
- LOD 1% - 5%
- 250 - 2,500 ppm
- 10 - 100 ppm
- 50 - 150 ppm
- Not Measured

Adapted from Innov-X handout for handheld XRF analyzers
 Note similar reference tables available from other XRF vendors

Detection limits are a function of testing time, sample matrix and presence of interfering elements.
 Detection limits are estimates based on 1-2 minutes test times and detection confidence of 3σ(99.7% confidence).
 Interference-free detection limits are intended as guidelines; please contact Innov-X Systems to discuss your specific application.

On the previous page is a useful table, provided by most pXRF instrument manufacturers, which shows the energies of the K and L lines for each element of the Periodic Table. The $K\alpha$ and $K\beta$ lines are used for elements with low to medium Z values as they require X-rays of reasonably low energy. However, the energies required to eject an electron from the K-shell of heavier elements, from say Ba onwards, are so high that the L-lines are preferentially used for analysis. The L-lines of low Z elements are so low in energy that photons of this energy range would not be transmitted in air (i.e. absorbed) and indeed the K-lines of elements Mg to Ca require a path containing a vacuum or inert gas for optimal determination. $K\alpha$ and $K\beta$ lines are quite close together, \sim several keV apart, and typically have an intensity ratio of \sim 5:1; $L\alpha$ and $L\beta$ lines are more comparable in their intensities.

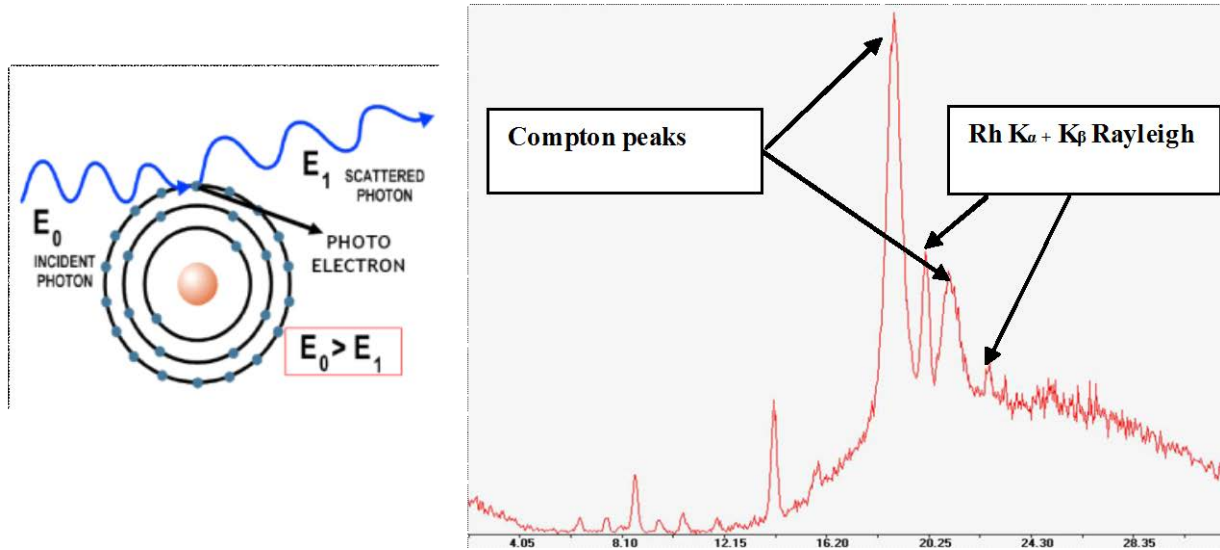
The energy of the *absorption edge* corresponds to the energy required to ionize a particular electron (from a K-shell, or an L-shell etc) from the atom and thus the most effective X-ray photons for exciting a sample are those with energies just above the absorption edge. For example, an X-ray tube with a Cr anode that emits characteristic lines at 5.41 keV (Cr $K\alpha_{1,2}$) and 5.95 keV (Cr $K\beta$) effectively excites Ca (absorption edge of 4.04 keV) but Fe would not be excited at all, as its absorption edge of 7.11 keV is significantly higher. The degree of attenuation of an X-ray beam due to an individual element absorber (undergoing the photoelectric effect) is described by the *mass attenuation coefficient* of that element, i.e. the proportion of incident X-rays attenuated per unit area per unit mass of the element.

Besides the characteristic X-rays from the target anode, an X-ray tube produces a continuum spectrum, having energies ranging from close to 0 up to the operating potential of the tube and this is termed '*Bremsstrahlung*'. This radiation is created when primary electrons are decelerated by interaction with the outer electrons of atoms of the target material. The continuum effectively extends the useful range of excitation of an X-ray tube and is especially important in exciting the light elements.

Rayleigh scatter, or coherent (elastic) scatter, results from the interaction of X-rays with inner orbital electrons that are so strongly bound to the nucleus that excitation is impossible. This absorbed radiation is then re-irradiated from the atom at the same energy level but with a random angular correlation with respect to the incident photon. Elements of higher Z have a larger proportion of electrons tightly bound to the nucleus and are therefore more efficient in producing Rayleigh scattering than lighter elements and likewise low-energy tubes would create a higher degree of Rayleigh scatter than those at higher voltages. Rayleigh scatter peaks tend to be sharp in shape and are easy to recognize as they correspond to the X-ray tube's target element.

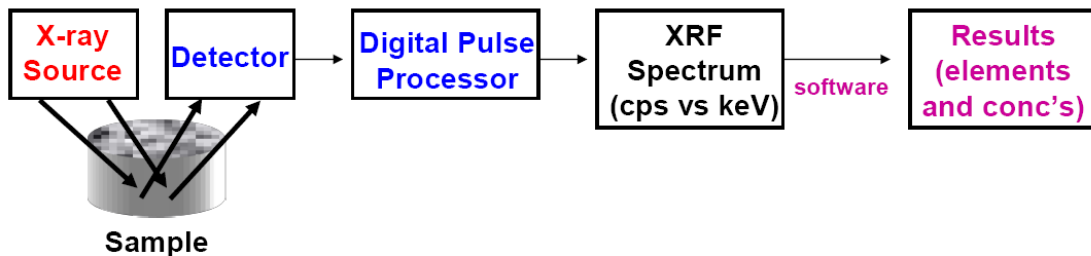
Compton scatter, or incoherent (inelastic) scatter, results from the interaction of X-ray photons with the more loosely bound outer shell electrons of an atom. While a proportion of the energy is used to ionize the electron, the rest is re-irradiated as a lower-energy photon. The intensity of the scatter photons varies as a function of the scatter angle and this fact is taken into account in the design of the spectrometer. The intensity of the Compton scatter spectrum is strongly related to the mean atomic number of the sample: the lower the mean Z , the higher the intensity of the Compton scatter (as the binding energy between outer electrons and the nucleus is lower due to the smaller positive charge on the nucleus). The Compton peak is typically broader than the Rayleigh peak and at lower energy. The process of generating the Compton scatter is illustrated

below. The spectrum of Intensity (counts per second) vs Energy (keV) for a sample irradiated with X-rays from a Rh anode shows the Rayleigh peaks coincident with the Rh $K\alpha$ (20.21 keV) and $K\beta$ (22.72 keV) lines and the corresponding Compton peaks for these Rh lines at somewhat lower energies. The phenomenon that the intensities of these peaks depend upon the mean Z (average composition) of the sample forms the basis of a matrix correction procedure.



2.1.2 Instrumentation

Portable XRF instrumentation consists of three main components: an X-ray source, a detector and a pulse processing electronics system.



The pXRF instruments today use, as sources, either an X-ray tube or radioisotopes. The former creates X-rays by the action of electrons, accelerated through a potential gradient under an electrostatic field, striking the anode (made of Rh, Ag, Ta, W or Cr, for example). Thus, characteristic X-rays of the target anode itself are produced as well as a continuum having energies up to the operating potential of the X-ray tube. The choice of anode is a consideration when determining the optimum instrumentation for a particular analytical application. For example, a Cr anode would effectively excite K-lines of Na to Ti in the Periodic Table, a Mo anode for Ca to As, and an Ag or Rh anode for Ca to Mo. To facilitate further optimization of

excitation conditions, some instruments allow the user to select the tube kV (typically up to ~50 kV) and μA (up to ~ 200 μA) and sometimes the primary beam filter, consisting of a thin metal foil placed between the tube and the sample, to modify the tube spectrum (i.e. attenuate certain unwanted lines coming from the tube). Clearly, the higher the energy of the X-rays produced by the tube the more efficient will be the excitation of the sample, particularly for the higher Z elements. Various filters can be employed to tailor the X-ray spectrum striking the sample in order to minimize or negate certain spectral interferences (characteristic and continuum) depending on the element determined and the matrix analysed.

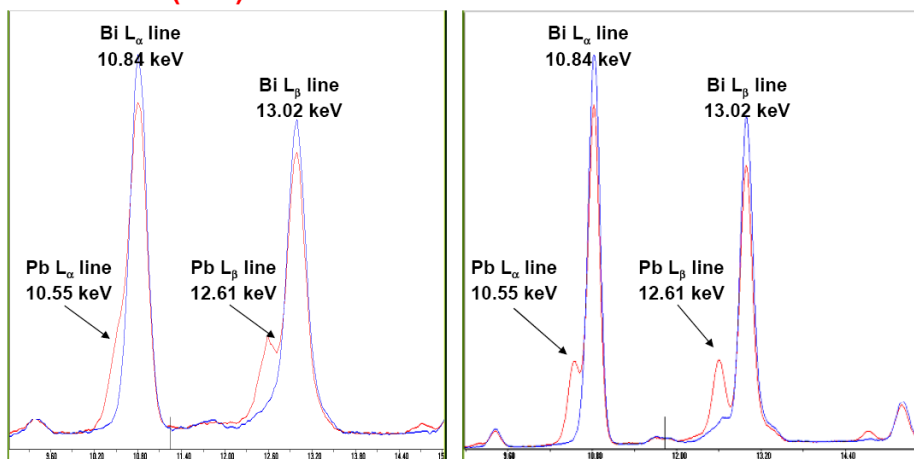
Most commonly used radioisotope sources include ^{55}Fe , ^{57}Co , ^{109}Cd and ^{241}Am . Each gives off radiation at specific energy levels and therefore efficiently excites elements within a specific atomic number range. Hence no single isotopic source is sufficient for exciting the entire range of elements of interest and instruments would be fitted with two or three sources (^{55}Fe , ^{109}Cd and ^{241}Am would provide a comprehensive range). The rare-earth elements (REE) require these more powerful sources (cf X-ray tube) to excite their high-energy K lines. The half-life, such as 270 days for ^{57}Co and 2.7 years for ^{55}Fe , is an important consideration: compensation has to be made for loss of intensity with time.

The development of the non-cryogenic semi-conductor detector has been critical in the advancement of pXRF. Examples of these devices include the Si(PIN) detector, the silicon drift detector (SDD), HgI_2 and cadmium-zinc-telluride (CZT). The SDD is particularly advantageous in allowing detection at much higher count rates while retaining performance with only Peltier cooling. The detector converts the energies of the X-ray photons into voltage pulses that can be counted to provide a measurement of the total X-ray flux. The pulse processing electronics integrate the electronic charge created in the detector crystal each time an X-ray is detected and then convert it into a signal that can contribute to the acquisition of the fluorescence spectrum in a multichannel analyser. The analyser is used to separate the spectrum of voltage pulses into narrow bands (*'regions of interest'*) for measurement of individual energies. Most instruments are supplied with matrix correction and appropriate quantification packages.

The *resolution* of the detector is a very important parameter. It is commonly defined as the full width half maximum (FWHM) at the Mn $K\alpha$ line (5.9 keV). The worse the resolution of a detector, the higher will be the contribution of the background intensity to the measurement of an emission line. This affects both the precision (peak-to-background ratio) and the detection limits. Secondly, poor resolution increases the degree of overlap between adjacent X-ray lines and hence decreases accuracy.

Older Si(PIN) detector

Newer SDD



Above are the spectra for two samples: one of Bi alone (blue line) and the other (red line) after Pb was added to the Bi sample. The L_{α} and L_{β} lines of Pb and Bi are not separated using the Si(PIN) detector which has a resolution of ~ 200 eV but resolution is much improved, and determination of Pb (with deconvolution) is possible, using the SDD with a resolution of ~ 150 eV.

The table below, taken from Potts (1987, p. 293), shows that the effect of detector resolution is much less marked for higher-energy photopeaks. The overlap of K K_{β} on Ca K_{α} changes from 33 to 39 to 44% as resolution degrades from 138 to 151 to 165 eV. The corresponding data for the overlap between higher energy Mo K_{α} – Zr K_{β} interference at ~ 17.5 keV are 23 to 25 to 27%, an overall increase of only 4% (cf 11%). Thus the effect of detector resolution is more critical at the lower energy region of the spectrum.

Analysed peak			Interfering peak	% Overlap				
		keV			keV	FWHM: 138 eV	FWHM: 151 eV	FWHM: 165 eV
Th	M_{α}	2.996	U	M_{β}	3.145	12	18	23
Ca	K_{α}	3.690	K	K_{β}	3.589	33	39	44
Fe	K_{α}	6.400	Mn	K_{β}	6.489	47	51	54
Mo	K_{α}	17.44	Zr	K_{β}	17.67	23	25	27

Besides resolution, the area of the detector plays a role in the quality of the pXRF analysis. The larger the area of the detector, the more efficiently it can gather and process counts.

For specific spatial analysis, the instrument's X-ray beam can be collimated to focus in on a particular area of the sample. Collimators range in size from <1 to 8 mm in diameter.

All instruments used in this project were equipped with X-ray tubes as sources and SDDs as detectors.

2.1.3 Interferences in ED-XRF

Spectral interferences

Appendix 2a is an extremely useful ‘X-ray booklet’ published by the University of California at Berkeley and put together by Thompson *et al.* (2009). Within this document are two comprehensive tables. The first (Table 1-2) provides the photon energies of principal K-, L- and M-shell emission lines for the elements (to Am, Z 95). The second (Table 1-3, attached separately for convenience as Appendix 2b, or alternatively go to http://xdb.lbl.gov/Section1/Table_1-3.pdf), a page of which is given below, details the photon energies and relative intensities of all these lines organized in order of ascending energy. This second table is extremely valuable in (a) identifying the principal lines of elements, (b) identifying spectral interferences from other elements and (c) judging whether the interferences would be significant. Users of pXRF are *strongly encouraged to refer to this table* when encountering unexpectedly high results for particular elements and when analysing a ‘new’ matrix that might pose spectral interferences on trace elements. Another useful tool is the interactive Periodic Table at <http://csrii.iit.edu/periodic-table.html>. In addition to the element lines there is such information as the X-ray cross-sections (for photo-electric, coherent and incoherent effects) at any energy one selects.

X-Ray Data Booklet Table 1-3. Photon energies and relative intensities of K-, L-, and M-shell lines shown in Fig. 1-1, arranged by increasing energy. An intensity of 100 is assigned to the strongest line in each shell for each element.

Energy (eV)	Element	Line	Relative intensity	Energy (eV)	Element	Line	Relative intensity	Energy (eV)	Element	Line	Relative intensity
54.3	3 Li	K $\alpha_{1,2}$	150	524.9	8 O	K $\alpha_{1,2}$	151	851.5	28 Ni	L $\alpha_{1,2}$	111
108.5	4 Be	K $\alpha_{1,2}$	150	556.3	25 Mn	L $\alpha_{1,2}$	15	868.8	28 Ni	L β_1	68
183.3	5 B	K $\alpha_{1,2}$	151	572.8	24 Cr	L $\alpha_{1,2}$	111	883	58 Ce	M α_1	100
277	6 C	K $\alpha_{1,2}$	147	582.8	24 Cr	L β_1	79	884	30 Zn	L $\alpha_{1,2}$	7
348.3	21 Sc	L $\alpha_{1,2}$	21	615.2	26 Fe	L $\alpha_{1,2}$	10	929.2	59 Pr	M α_1	100
392.4	7 N	K $\alpha_{1,2}$	150	637.4	25 Mn	L $\alpha_{1,2}$	111	929.7	29 Cu	L $\alpha_{1,2}$	111
395.3	22 Ti	L $\alpha_{1,2}$	46	648.8	25 Mn	L β_1	77	949.8	29 Cu	L β_1	65
395.4	21 Sc	L $\alpha_{1,2}$	111	676.8	9 F	K $\alpha_{1,2}$	148	957.2	31 Ga	L $\alpha_{1,2}$	7
399.6	21 Sc	L β_1	77	677.8	27 Co	L $\alpha_{1,2}$	10	978	60 Nd	M α_1	100
446.5	23 V	L $\alpha_{1,2}$	28	705.0	26 Fe	L $\alpha_{1,2}$	111	1,011.7	30 Zn	L $\alpha_{1,2}$	111
452.2	22 Ti	L $\alpha_{1,2}$	111	718.5	26 Fe	L β_1	66	1,034.7	30 Zn	L β_1	65
458.4	22 Ti	L β_1	79	742.7	28 Ni	L $\alpha_{1,2}$	9	1,036.2	32 Ge	L $\alpha_{1,2}$	6
500.3	24 Cr	L $\alpha_{1,2}$	17	776.2	27 Co	L $\alpha_{1,2}$	111	1,041.0	11 Na	K $\alpha_{1,2}$	150
511.3	23 V	L $\alpha_{1,2}$	111	791.4	27 Co	L β_1	76	1,081	62 Sm	M α_1	100
519.2	23 V	L β_1	80	811.1	29 Cu	L $\alpha_{1,2}$	8	1,097.9	31 Ga	L $\alpha_{1,2}$	111
				833	57 La	M α_1	100	1,120	33 As	L $\alpha_{1,2}$	6
				848.6	10 Ne	K $\alpha_{1,2}$	150	1,124.8	31 Ga	L β_1	66

The most common spectral overlap is that from a K β line of element Z-1 with the K α line of element Z (‘K α /K β interference’); of less concern are K/L, K/M and L/M overlaps. Element Z-1 would have to be present at high concentrations to interfere because the K α /K β intensity ratio for a given element is generally at least 5:1. For example, the Fe K α and K β lines are at 6.40 and 7.06 keV, respectively. If Co is being determined in the presence of high amounts of Fe there could well be severe overlap (false positive for Co) because the Co K α line has an energy of 6.92 keV, only 140 eV removed from the Fe K β line and the resolution of today’s detectors is usually higher than 140 eV (~ 150-175 eV). An example of a K/L interference is that of As K α /Pb L α (10.54 eV/10.55eV). The alternate lines – As K β (11.73 keV) and Pb L β (12.61 keV) – could be used but at the sacrifice of sensitivity as, for example the As K β line is ~ 7 times less sensitive.

On the other hand, a mathematical correction could be made for Pb at the As K α line but this would increase the detection limit for As and is really only feasible at ratios of Pb/As of 10:1 or less, often not adequate in geological applications.

The interaction of X-ray fluorescent photons with the detector can give rise to artifact peaks in an XRF spectrum, two of which are known as *sum or pile-up peaks* and *escape peaks*. A *sum peak* occurs when two photons arrive at the detector at exactly the same time (e.g. K α and K α , K α and K β , or K β and K β). For example, two Fe K α photons each of energy 6.40 keV would then appear in the spectrum at 12.80 keV. The greater the concentration of an element, the greater the presence of sum peaks so the strategy to minimize this interference would be to keep the count rate low. The greatest effect would clearly be that of a major element on a trace element. An *escape peak* is formed by a partial loss of energy of the arriving photon by interaction with the Si atom of the detector and the Si K α X-ray thus formed escapes from the detector without further interaction. An escape peak would then be visible in the X-ray spectrum of the sample at 1.74 keV (i.e. energy of the Si K α line) below the energy of the particular X-ray being measured. This phenomenon would lead to a low XRF result for the element being measured and may also create a spectral interference at that E-1.74 keV region. The magnitude of this escape peak varies as a function of incident photon energy and thus is more prevalent for elements of low Z. Escape peaks are much less intense than the characteristic peaks from which they are derived. As with sum peaks, using conditions that keep the count rate low minimizes this interference. These peaks can be automatically corrected (to a degree) by the manufacturer's computer algorithms.

Naturally the pXRF user also must be aware of elemental contaminants from materials containing the sample (i.e. the film covering the sample cup or the sample bag) and the unit's window.

Matrix (absorption/enhancement) interferences

All XRF measurements are subject to non-linear effects resulting from the attenuation, and also enhancement, of fluorescent X-ray intensities by interaction with the sample matrix. When a primary X-ray penetrates a sample, it suffers from progressive attenuation, to a degree governed by photon energy (the lower the energy, the more the attenuation) and sample matrix (the higher the mean Z, the greater the attenuation). Fluorescent X-rays generated within the sample also suffer attenuation before they can escape and reach the detector. Furthermore, enhancement effects can occur due to excitation by fluorescent X-rays from another element within the sample. For example, fluorescence from Fe (K α of 6.4 keV) within a sample may excite the fluorescence of Cr: the net result would be a low result for Fe (absorption) and a high result for Cr (enhancement). Many mathematical models have been developed to account for these absorption-enhancement effects (Potts and Webb, 1992). They fall into two categories, based either on the fundamental parameter approach or on empirically determined influence coefficients, or indeed on a combination of the two. Matrix corrections can also be made by estimating the mass attenuation coefficients using the Compton scatter intensity.

The sample's moisture content affects the accuracy of the analysis. As the moisture level increases, the sample dilution decreases the apparent concentration. This effect is most severe for analytes with low-energy X-ray lines (< 5 keV) and may be negligible for elements such as Pb with high Z. To a degree, dilution may be countered by reduced matrix absorption for the analyte

X-ray lines as H₂O replaces the higher Z (and hence more absorbing) components. Most reports state that a moisture content of $\leq 20\%$ is tolerable but samples wetter than that should be dried.

Sample morphology - particle size distribution, uniformity, heterogeneity and surface condition – of course affects the XRF results. If powdered samples are stored in cups, settling effects may have occurred. Finer particles tend to gather around the film if the cup is stored upside down: samples should be lightly shaken and the cups tapped prior to analysis.

Ambient temperatures changes can affect the gain of the amplifiers in the electronic processing system, thus producing drift. Instruments have an automatic gain control to correct for this.

It is important to appreciate the variable degree of attenuation suffered by fluorescent X-rays within the sample. The *critical penetration depth (CPD)* is the depth below the sample surface beyond which fluorescence X-rays are totally absorbed within the sample and hence are not seen by the detector. The magnitude of the critical penetration depth depends upon the mean mass attenuation coefficient of the sample and on the photon energy. Clearly the CPDs for heavy elements will be greater than those for light elements. For example, in the case of a silicate powder pellet of density 2.1 kg m^{-3} , the CPD of the Si K α line is only 0.013 mm whereas it is 1.4 mm for Nb and 10.6 mm for La (Potts, 1992). Thus, the XRF signals from elements of higher Z represent much greater volumes of the sample than do those of low-Z elements such as Si which may well not reflect the true composition if the sample is not homogeneous.

2.1.4 Calibration strategies

Most pXRF instruments today come with two factory-installed calibrations for geological applications: the *mining* mode, for use at higher elemental concentrations (i.e. for major elements, $> \sim 0.2\text{-}0.5\%$) based on ‘Fundamental Parameters’ (FP), and a *soil* mode (focusing on minor and trace elements) using Compton normalization.

The *FP* iterative approach uses X-ray theory to mathematically pre-determine inter-element matrix effects combined with pure element or known standard intensity responses to develop a quantitative algorithm for a certain sample type. It is based on mathematical equations that describe the physical properties of X-ray excitation and attenuation in terms of the appropriate fundamental parameters such as mass attenuation coefficients, fluorescent yields etc (Sherman 1955; Lachance and Traill 1966). Modern models combine the theoretical exactness of the FP technique with the practical flexibility of the Lachance-Traill influence coefficient approach (the influence or alpha coefficient quantifies the interaction of one element on another). Rousseau (1989) further developed this technique for geological samples, demonstrating that large numbers of standards were no longer required to set up a calibration as long as those that were used were known accurately and that matrix correction procedures were then not a major limitation to the accuracy of XRF results.

The FP approach is based on summing constituents to 100 % and thus, if the concentrations of some major elements (of low Z and hence a difficult analysis by pXRF) are not well known, the calibration will be inexact for numerous elements. Many users of the FP mode in pXRF are

unaware that they should modify the factory FP calibration using a few known standards of the same matrix as their samples. Some of the advertising literature is certainly responsible for this misconception, as is the common reference to the FP approach as a ‘standardless calibration’. This project demonstrates the quality of results obtained by not modifying the FP calibration and the improvement gained by adjusting the factors by the response of several matrix-matched standards.

The *Compton normalization* calibration for trace elements is a complementary method for correcting matrix interferences: it incorporates elements of both empirical and FP calibration. It is not based on a mathematical model of absorption/enhancement effects but rather on direct measurement of the intensity of the Compton scatter peak of the tube $K\alpha$ line. The intensity of the Compton peak is inversely proportional to the mean mass attenuation coefficient of the sample and thus matrix effects can be corrected by normalizing the intensity of the fluorescence line to that of the Compton scatter peak, both measurements being made on the sample being analysed. Manufacturers use a suite of well-characterized reference samples to establish this calibration. However, if the analyte line and the Compton peak are on different sides of a major element absorption edge, this procedure breaks down and the magnitude of the absorption edge must be taken into account. In geological applications, this procedure can be applied to elements that have fluorescent lines of energy greater than that of the Fe absorption edge (7.1 keV), Fe being the highest (Z) major element in most samples. If an ore is being analysed, where a ‘trace’ element is now the major constituent, this procedure can lead to errors. The K-lines of Rh, Ag and Mo anode X-ray tubes all efficiently excite trace element lines above the Fe adsorption edge and produce a convenient Compton peak. Compton normalization is similar to the use of internal standards in other analytical techniques.

The methods of empirical (with a suite of well characterized matrix-matched standards) and standard addition calibration are laboratory-based techniques that would not be used by most practitioners of pXRF in geochemistry.

2.1.5 Optimization

The tube voltage and current (i.e. power) are important parameters for generating X-ray fluorescence in different regions of the Periodic Table. These are usually established by the manufacturer and divided into ‘Beam 1’, ‘Beam 2’ etc but they can also be changed by the user. The lowest voltage (e.g. 10 kV) would be used for the light elements – the ‘majors’ in geoanalysis - which may be excited by the continuum or L lines of the Ag or Rh anode. The thickness of the beryllium window fitted to the tube is especially important for these elements (i.e. lower is preferable). Three beams could well be used for optimum efficiency of excitation, the uppermost being operated at up to 50 kV for elements of high Z.

Filters, made of metal foil ~10-150 μm thick, are selected depending upon the excitation source and the elements to be determined. The primary beam filter should: (a) transmit a large proportion of higher energy tube radiation (characteristic and continuum) that is capable of exciting the elements of interest; and (b) attenuate the lower energy tube continuum radiation that would otherwise be available for scatter of the sample and hence contribute to the background spectrum. There are ‘white’ filters and ‘absorption edge’ filters; discussion of their

roles can be found in Potts (1987) and references therein. The combination of tube potential and filter usage is designed by the manufacturer to preferentially excite the X-ray radiation of the particular elements in that grouping (or 'beam'): changing such combinations would require more knowledge and experience than would be expected of the geochemist operating a portable XRF instrument.

Beam or count time is one parameter that is selected by the pXRF user and clearly has an influence on precision and detection limits obtainable (signal/noise proportional to the square root of the measurement time). Expediency may limit the selection of beam time to a value in the range 30-90 s per beam, if the figures of merit are acceptable for the particular study or survey. This parameter has been thoroughly examined in this project.

Sample heterogeneity is a dominant factor in the accuracy and precision obtained in analysis by pXRF. If, rather than analysing the sample of soil or rock directly, it can be dried and sieved to pass 200-mesh, the results would obviously be more representative of the bulk material (if the goal is bulk and not spatial analysis). Loose sieved or powdered samples can be placed in cups and then tightly covered with thin (2-6 μm) plastic (Mylar, Prolene etc) film. The absorption properties of the film for low-Z elements should be measured and corrected for. Similarly if a sample bag is used in the field then its absorption and contaminant properties need to be measured. If the analysis is being carried out in a laboratory, a pressed pellet could be made. Typically, 5-15 g of powdered sample are mixed well with a suitable binder (e.g. a mixture of methyl cellulose and polyvinylpyrrolidone dissolved in a water/alcohol medium) or wax and pressed under pressure (e.g. 10-15 tons/in²) to form a disc of 30-50 mm diameter. If the binder is of significant quantity, its dilution effect must be taken into account.

2.1.6. Daily operating procedure

The manufacturers' manuals should be scrutinized to ensure day-to-day analytical procedures are consistent with any recommendations.

An energy calibration check is used to confirm that the instrument is operating within resolution and stability tolerances (i.e. no shifts in energy line positions, regions of interest, or shift in gain control due to temperature changes). This should be carried out each day with the manufacturer's check ('coupon'), often an alloy or pure metal, or if drift is suspected.

A blank, usually silica, a PTFE block or 'clean' sand supplied with the instrument, is run at the beginning and end of each day, or more often if a problem with contamination is suspected. This procedure essentially indicates if the window has become dirty. The blanks will obviously generate positive results if they have an inherent impurity but will also show lines originating from the X-ray tube and any components of the system that may fluoresce. Users should become familiar with the 'typical' spectrum of their blank sample.

A 'method' blank is different in that it should reflect any contamination introduced by whatever preparation has been carried out on the sample prior to analysis. In the case of this project, a method blank is unwarranted as the samples under study are already prepared.

The manufacturers usually supply a reference standard with an instrument, often one or more of the NIST standards, preferably an appropriate one such as the soil SRM 2709, 2710 or 2711. These should be run at least several times a day; US EPA 6200 (<http://www.epa.gov/osw/hazard/testmethods/sw846/pdfs/6200.pdf>) recommends every 20 samples but that is probably too frequent for many exploration/mining purposes. The tolerance limits EPA sets are $\pm 20\%$ of the certified value and, if the data do not fall within those limits, recalibration is necessary and the samples are to be rerun. Because of the nature of this particular investigation using only reference materials, insertion of a standard was unnecessary but it is highly recommended for users. Such a calibration check could also serve to monitor precision so it could be run ~ 5-10 times (RSDs should be $\leq 20\%$ for most elements).

Although not mentioned in manuals, a warm-up time at the start of the day is a good idea. EPA 6200 recommends 15-30 minutes.

2.2 Literature Review

The principles and practice of WD- and ED-XRF are well-known and are thoroughly discussed in Chapters 8 and 9 of Potts (1987) and the numerous references therein. Overviews with respect to pXRF in particular are provided by Kalnicky & Singhvi (2001), Wegrzynek *et al.* (2003) and Hou *et al.* (2004). Potts and West (2008) recently edited a multi-authored book, ``Portable X-Ray Fluorescence Spectrometry. Capabilities for In-situ Analysis``, wherein the reader is given an insight into the strengths and limitations of the technique together with demonstrations of its application into nine areas of scientific interest, geochemical prospecting being one.

A search, using the search engine SCOPUS, of > 7,200 journals (including Conference Proceedings) with the keywords ‘portable’ and ‘XRF’ in the title and/or abstract from 2000 to March 23rd 2011 resulted in only 207 papers. The overwhelming majority of these focused on the application of the technique to studying cultural artefacts, artwork, and archaeology, and, to a lesser extent, air filters, food and alloys. Only 23 of these papers were concerned with the use of pXRF in geochemistry, oriented to application in either environmental or mineral exploration, and some were in Chinese only. Internal government or industry publications are not covered within SCOPUS, though articles in trade journals often are. The publications relevant to exploration geochemistry are discussed here.

Phil Potts and his colleagues at the Open University in England are undoubtedly the most prolific leaders in contributing to our understanding of, and improving, the analysis of geological matrices by ED-XRF. Potts is well known in geanalysis for his tome ‘A Handbook of Silicate Rock Analysis’ (Potts 1987, 622 pp) and for his numerous papers on both WD-XRF and ED-XRF (see references in Potts, 1987 and Potts and Webb, 1992). Potts *et al.* in 1995 provided a preliminary assessment of pXRF in the analysis of silicate rocks. They employed a handheld Tracor Northern Spectrace TN 9000 instrument fitted with three radioactive isotope excitation sources - ^{55}Fe , ^{109}Cd and ^{241}Am - and a mercury(II) iodide X-ray detector of 260 eV resolution. The objective was to measure detection limits, precision and accuracy, under ideal lab conditions, for pressed pellets of 70 international CRMs, mostly of silicate composition. They employed the Tracor FP program using coefficients calculated off-line for a silicate rock matrix and a livetime of 200 s per source. They found detection limits (e.g. 6-14 ppm for Rb, Sr, Y, Zr, Nb), accuracy and precision (e.g. 0.5-2 % RSD for major elements) to be acceptable for K, Ca, Ti, Mn, Fe, Ba, Nb, Rb, Sr, Y and Zr in ‘normal’ silicate rocks but only higher or mineralized concentrations of Co, Cr, Cu, Ga, La, Nd, Ni, V and Zn could be determined adequately.

Later, using the same instrumentation, Potts *et al.* (1997a) devised a simple procedure to correct for surface irregularity effects in a rock sample. Firstly, they used 44 silicate reference materials of widely ranging composition to measure scatter peak – Compton and Rayleigh – intensities as a function of sample composition. Data for the Raleigh peak intensity derived from the scatter of the ^{55}Fe Mn K lines show the least dependence on matrix (compared to the scatter peaks from the ^{109}Cd Ag K α /K β lines and the ^{241}Am 59.9 keV γ line) and therefore its intensity was considered constant over this category or group of silicate rocks. Secondly, using a slab of dolerite and one of grey granite, the air gap between the analyser unit and the sample was progressively increased (using washers) from 0 to 12.6 mm. A plot of intensities of selected fluorescence (e.g. for Rb, Sr, Zr, Nb, Ba) and scatter peaks normalized to the values at 0 mm air gap shows an almost

exponential drop-off with distance. However, this change in intensity can be corrected for by normalizing to the intensity of the Fe K line. The decrease in intensity of the scatter peaks does not fall off as rapidly as the fluorescence lines for air gaps above ~ 3 mm and thus the procedure does not work under these conditions for larger air gaps or irregularities. For lower atomic weight elements such as K, Ca and Ti, the correction procedure is affected by air attenuation and hence breaks down. A further limitation is that as the distance between analyser and sample is increased, the source-sample-detector scatter angle increases, thus causing a relative increase in the total scatter intensity.

Using the same handheld Spectrace TN9000 instrument, Potts *et al.* (1997b) examined the limitations of pXRF caused by mineralogy in the direct analysis of *in-situ* silicate rocks ranging from a fine-grained dolerite, andesite and microgranite through a medium-grained granite (feldspar typically 3 mm; quartz and mafic minerals up to 3 mm) to a coarse-grained granite (feldspar and quartz typically 7 mm). The critical penetration depths of different X-ray K lines (from low to high energy: K, Ca, Ti, Fe, Rb, Zr, Ba, Ce) were calculated for samples of basaltic, andesitic and rhyolitic composition to estimate the different sample volumes from which the X-ray signals originate. For example, 50% of the signal in a basalt originates from a depth of 4.6 and 1164 mm for K and Ce (the extreme cases studied), respectively, and 99 % of that signal would represent a depth of 30.2 and 7730 mm, respectively. This clearly demonstrates the influence of the near-surface chemistry and mineralogy on the analytical result and the different sample volumes actually represented for different elements. Using a grid placed on the excitation window (25 mm diameter) with different placements of 'samples' of wires of Ti (for the ⁵⁵Fe beam), Mo (¹⁰⁹Cd) and Ag (²⁴¹Am), 3-D surface contour graphs of the variation in detected XRF intensity across the analyser window were produced. Fluorescence intensities were ~ 6-10 times higher near the centre of the window than at the periphery and therefore the results would be influenced by not only the size and distribution of minerals in the excited volume but also by the position in the window of the individual minerals. They then analysed slabs of the five silicates, focusing at random on 10 non-overlapping sites for each sample. From these data they calculated the number of analyses required for specific values of precision. For example, to achieve RSDs for Ba (230 ppm) in the dolerite of 2 % and 20 %, 20 and 1 analyses, respectively, are required. However, in the coarse-grained Shap granite, with a mean Ba concentration of 536.4 ± 499.2 ppm, the equivalent number of determinations would be 2166 and 22! In practical terms, for those elements where the concentration is 10 times greater than the average counting precision, this work showed that only one analysis would suffice for a precision of ~ 10 % for the four fine- to medium-grained granites but the Shap granite would require 5 analyses to obtain an average sampling precision of 20 %. Clearly these figures pertain to these samples in particular but they serve to guide work for other rock types.

Argyraki *et al.* (1997), also from the Open University, evaluated the application of pXRF to mapping contaminated land for Pb using the handheld Spectrace TN9000 instrument. They compared results obtained using pXRF *in-situ* after removing the top 30 mm of soil with those obtained later in the lab on a 0-150 mm core of soil, of 25-mm diameter, that had been dried, sieved to <2 mm and ground to <100 µm. The lab techniques were pXRF and ICP-AES following an HNO₃-HClO₄ digestion. Calibration for pXRF was reported to be by fundamental parameters established (by the manufacturer one assumes) with a 'typical' soil; in-house soils standards, some of similar matrix to the unknowns, were run to establish instrumental precision.

Duplicate measurements were taken at each sampling point at a distance of 2 mm from the initial sampling location, so that an estimate could be made of measurement precision (including sampling error). For all three sets of data, the combined sampling and analytical variance was less than 20% of the total variance (i.e. geochemical variance dominated). For both field and lab-based pXRF, a bias of -11% shown by the NIST SRM 2710 was thought to be due to the difference in composition of this reference material and that of a 'typical' soil used to determine the fundamental parameter coefficients required for the matrix correction procedure. Lead concentrations in the soils analysed were in the range ~0.1-2.3 %. A direct comparison of results for Pb by *in-situ* pXRF against those by ICP-AES showed a rotational 'bias' of $-57 \pm 6\%$ (1s) in the former method. This could have been due to the fact that *in-situ* pXRF analysed only essentially the top ~1.5 mm for Pb whereas the average composition of the 15-cm core was being measured by ICP-AES; however, individual analyses of 11 slices of 6-mm layers of the core showed little systematic spatial trend with depth and indeed no depletion of Pb at surface. When the bias for Pb between *in-situ* pXRF and laboratory-based pXRF was compared, a similar rotational 'bias' was apparent, i.e. $-52 \pm 7\%$ (1s). Two potential causes for the low bias of the *in-situ* pXRF results are the moisture content of the soil and the rough surface of the soil used for excitation. When a correction was made for moisture (9-19 % water content), an initial bias of -20 % against ICP-AES determinations for this particular experiment was reduced to -7 %. In order to compensate for the unevenness of the soil surface, a Rayleigh scatter correction was made. After this correction, the bias was effectively eliminated. Thus, correction for moisture content and matrix by Raleigh normalization greatly improved the accuracy of *in-situ* pXRF. The technique was deemed 'fit for purpose', with the suggestion that the use of appropriate reference materials, though hard to find to simulate the unknown soils in their natural state, could be useful for the elimination of bias of the *in-situ* measurements.

In an excellent paper by Jones *et al.* (2005), the same instrument as used by Argyraki *et al.* (1997) was employed to measure geochemical variations within and between dolerite outcrops in south Wales. With calibration modified by using a range of reference materials, and rock surface relief compensated for using a correction based on the intensity of back-scatter peaks from the ^{55}Fe spectrum (Potts *et al.*, 1997a), the fundamental parameter mode was employed to determine five major and minor elements (K, Ca, Ti, Mn and Fe) and seven trace elements (Ba, Nb, Pb, Rb, Sr, Y and Zr). Analytical (counting statistics and peak-fitting uncertainties), sampling (separate sampling and analyses at one site within the outcrop) and geochemical variances (within and between outcrops) were determined across eight outcrops, based on a total of 122 measurements. A sampling design of two (neighbouring but independent analyses, 100-200 m apart) measurements at each of a maximal number of locations dispersed over an outcrop was the most effective strategy in indicating the overall chemical variance of that outcrop. This work provides a valuable model to test in determining the chemistry of outcrops, whatever the rock type, and demonstrates the rapid spatial analytical capability of pXRF.

Potts *et al.* (2006) studied the effects of weathering on *in-situ* pXRF analyses of dolerite and rhyolite outcrops. They cautioned that surface measurements by pXRF are influenced by: (1) sampling uncertainty effects (i.e. representivity would be questionable, especially for medium- to coarse-grained rocks); (2) surface irregularity effects (best to have a flat surface in the plane of the instrument); (3) surface coating and weathering effects; and (4) limitations in that the critical penetration depth of X-rays is generally between 0.1 and 2 mm. The objectives of this study were

to quantify the extent to which pXRF results were affected by weathering and hence to determine whether correction factors could be used to then identify the underlying fresh unweathered rock. Little information was presented in this paper as to the pXRF analytical conditions except that a Spectrace TN9000 (radioisotopes as sources) instrument was used with fundamental parameter calibration as supplied by the manufacturer. A depth profile was constructed by successively grinding away, after measuring, layers about 10-15 times until a total of about 10 mm of material had been removed. Analysis by pXRF was made at about five positions per layer. A correction factor (\leq or ≥ 1) was derived for each element (K, Ca, Ti, Mn, Ba, Nb, Pb, Sr, Y, Zr) based on the ratio of the concentration in the weathered surface to that in the fresh underlying rock. However, the authors warned that the use of such factors to correct for weathering effects in surface analysis by pXRF may well not be universal but rather could depend climate as well as rock type.

Houlihan *et al.* (2003) presented three case studies at different Ni, Cu and Cu-Au mines in Australia wherein pXRF was studied for its ability to be used on-site for ore grade control. The instruments were the Niton XL502S and XLi969 models and were used in the fundamental parameter mode, presumably calibrated with a known standard of similar matrix (details not provided). At the Ni Koniambo Mine, results for 175 samples, prepared as pulps to $< 100 \mu\text{m}$, were compared to those by LiBO_2 fusion / XRF at a commercial laboratory: the r^2 values and slopes for Ni (in the ~ 0.5 -5 % concentration range) and Fe (in the ~ 5 -55% range) were 0.9 and 0.98, and 0.88 and 0.90 (pXRF on y-axis), respectively. Comparative analysis of 178 bogger samples at the Mount Lyell Cu operation in Tasmania showed the benefit of crushing and pulverizing samples: the slope and r^2 values for Cu (in the range 0.2-5.5%) in pulp samples for pXRF compared to total digestion AAS were 0.98 and 0.95, respectively, far superior to the values of 0.87 and 0.59, respectively, for the paired crushed samples which were sieved to only 2 mm. In summary, 79% and 53%, respectively, of the results by pXRF for Ni (n=175) and Cu (n=1841) in prepared pulps were within 10% of the referee lab's values and 79% of the results for Cu in unprepared blast hole cuttings were within 20%.

Vanhoof *et al.* (2004) compared the performance of ED-XRF systems, ranging from portable to full laboratory instruments, for the assessment of contaminated soils. They found that the handheld and portable bench-top (as used in this study) models provided similar 'semi-quantitative' results for Zn, Cu, Pb, Ni, As and Cr, useful for locating hot spots and delineating contaminated areas.

In evaluating the performance of pXRF in analysing soils polluted with chromated copper arsenate (CCA)-wood preservatives, Makinen *et al.* (2006) found empirical calibration to be superior (better RSDs) to fundamental parameters for As and Cu. Results for As and Cu by pXRF, measuring the wet soils through plastic bags, were significantly lower than by aqua regia flame atomic absorption spectrometry applied to dried, crushed and sieved ($< 125 \mu\text{m}$) samples, the correlation coefficients being in the order of 0.7. The causes of this disagreement were purported to be the presence of moisture (up to ~ 30 %) and the coarse grain size (< 4 mm) of the bagged samples. Mielke *et al.* (2010) also employed pXRF (Niton 703A) to identify CCA-treated wood in play areas of New Orleans but no details on pXRF methodology were provided and indeed the detection limits quoted were those of the manufacturer and not modified according to the material analysed.

In 2007 the US EPA published their recommended method for the field portable XRF determination of elements in soils and sediments (<http://www.epa.gov/wastes/hazard/testmethods/sw846/pdfs/6200.pdf>). This is a useful document providing not only the procedure recommended for environmental monitoring of soils and sediments but also a background on the principles of the technique. EPA had actually contracted work out to different groups to evaluate the performance of six different instruments equipped with different sources and detectors. The results were only partially summarized but, as an example, the following are the recoveries found by one of the better instruments in up to 13 reference samples: 68-115 % for As (at levels of 105-626 ppm As); 98-199 % for Ba (335-2240 ppm); 61-140 % for Cu (76-4792 ppm); 66-138 % for Pb (161 ppm to 14.4 %); and 41-130 % for Zn (106-6952 ppm). This method calls for the insertion of a calibration control reference check, a standard of similar matrix to the sample, at the rate of 1 in 20. This standard is to be used to adjust the slope and the intercept of the factory calibration for every element to suit the type of sample under investigation.

The efficiency of pXRF determination of Pb in soils in mapping contamination from Pb-based paint or from automobile exhausts has been demonstrated by Binstock *et al.* (2008) and references therein. Seventy-two composite soil samples of ~ 75 g each were dried (in air or using a microwave oven connected to a car battery) and sieved to <250 µm prior to analysis using a Niton XL-309 with a ¹⁰⁹Cd source. Excellent agreement was achieved with laboratory data derived from splits digested in 25 % HNO₃ in an ultrasonic bath and analysed by ICP-AES; Pb levels were in the hundreds to thousands of ppm.

Finding the recommendation of US EPA Method 6200 to dry the soil sample in an oven prior to pXRF measurement to be impractical, Markey *et al.* (2008) tested the feasibility of drying the soil sample between sheets of paper towel, a much faster alternative. They analysed both sieved (<125 µm) and ground soil samples (n=78) for Pb in the field before and after drying and found that the mean Pb value of 816 ppm (range 23-9080 ppm) did not change. The actual extent of drying achieved was not determined; the degree of saturation *in-situ* ranged from 10 to 90 %. At a saturation >65 %, sieving was impossible but drying at levels below this was deemed practical (<10 min) and recommended.

Using a Niton XL3t 500 handheld model, Morris (2009) of the Geological Survey of Western Australia evaluated pXRF in the following areas: count time, detection limit, precision, accuracy, and effects of the sample bag. A basalt CRM pressed pellet was used to optimize count time of the three beams ('Soil Mode'): precision improved progressively from 10, through 20 and 40, to 60 s per beam, as demonstrated by Zr and Sr. A beam time of 40 s (read time of 120 s) was selected as practical. Thompson's 1992 definition of detection limit, unfortunately, was taken to be 3 times the mean of a blank (SiO₂ pressed pellet) measured multiple times (19 in this case) rather than 3 times the standard deviation of those blank values; hence the DLs reported depend upon the level of element contamination in the blank sample and are invalid. Factory calibrations in the soil mode were checked and modified with in-house CRMs (wide range of composition) if necessary; an example of negating a high bias in Zr by amending the calibration was presented. Four in-house CRMs were used to assess accuracy in the soil mode: a basalt, monzogranite, Cu ore, and a REE standard. In examining the tables of data carefully, it is clear

that pXRF did not perform adequately for Co (e.g. 352 vs 37 ppm recommended value, RV, in the basalt), Cs (e.g. 45 vs 2.2 ppm RV in the monzogranite), Ni (234 vs 7 ppm RV in the REE CRM), Sb (e.g. 31 vs 0.3 ppm RV in the basalt), Sn (e.g. 26 vs 1.8 ppm in the monzogranite), Te (e.g. 106 vs <0.1 ppm RV in the basalt), or W (e.g. 648 vs 2 ppm RV in the Cu ore). Elements showing acceptable to good accuracy include Ba, Ca, Pb, Rb, Sr, Th, Ti, Zr and in some but not all samples As, Cr, Cu, Mn, Sc, V and Zn. Elements such as Se, Mo and Cd were too low to be determined. These are diverse matrices and it does not appear that the calibration was modified for specific sample types, rather a range of sample types was used to adjust the factors. Morris tested the Mining Mode, without modifying the factory calibration to suit matrix (i.e. 'as is'), using the four in-house CRMs named above in addition to two laterites and an amphibolite. Accuracy was acceptable for Ca, Fe, Mn and Ti but poor for K (e.g. 2.88 vs 4.53 % RV in the monzogranite). Copper in the ore reported 6.57 % (cf 9.66 % RV) and S was 2.83 % in the amphibolite (cf. 10.15 % RV). Morris indicated that recalibration, presumably matrix-specific, was necessary. Various levels of attenuation, up to as high as 80 %, were measured for a variety of sample bags and some materials showed contamination by As, Cr and Pb. Given the above observations, the statement in the paper's abstract that - "*the XL3t 500 is capable of producing accurate and precise analysis for the majority of the 32 elements available, to levels, for some elements, comparable to those found in crustal rocks and mid-ocean ridge basalts*" - is optimistic and misleading.

The performance of pXRF was evaluated in an extensive survey of arsenic distribution around the Prohibition Mill in the Waiuta area of the south island of New Zealand. Haffert and Craw (2009) employed the InnovX Alpha unit in the soil mode (<10 % As) and the empirical mode (>10 % As) which was based on calibration with six well characterized samples from the site. Substrate types comprised: tailings, wetland sediments, clay-rich subsoil, poorly sorted sediment, silty natural soil and gravelly natural soil. Precision obtained by taking six readings per sample across these different substrates was worse than 20 % RSD for about 50 % of the samples; therefore, several readings per sample were used in the survey. The results of three preparation methods were compared with those obtained by HNO₃-HCl digestion and ICP-MS analysis of the dried and crushed counterpart: *in-situ* and later corrected for moisture content; extracted in the field and analysed through a plastic bag, and later corrected for moisture content; and dried and crushed. There was good overall correlation (coefficient of 0.80) amongst the three methods and indeed with the ICP-MS based method. The scatter around the 1:1 line was considered acceptable for the purpose of this work, i.e. to delineate the scale and distribution of As contamination over a large area. The optimal method selected, because of the need for fast turn-around rather than the best resolution, was the *in-situ* analysis with correction for moisture content (four categories of moisture were outlined for assignment in the field).

Sheppard *et al.* (2010), at the University of Auckland, characterized obsidian samples from four major sites using the InnovX ALPHA pXRF (Si PiN diode detector) and then used these data to source 966 obsidian samples from three Reef/Santa Cruz Lapita sites. They used the results of 14 pXRF analyses of the powdered obsidian standard, NIST SRM 278, to calculate a ratio of certified/mean values to then be used to correct the pXRF data for the unknowns. These ratios varied from 0.94 to 1.41 for the elements reported in this paper, i.e. Mn, K, Ti, Fe, Zn, Rb, Sr, Zr and Pb. Though they were calibrating with powders, the 966 samples were solid flakes, the flattest face of which would be placed against the detector window (the unit was mounted in a

test stand). Therefore an internal solid standard was run over the 17 days of analysis to assess precision which would be affected by surface geometry and sample orientation. The RSD (n=34) for this solid standard varied from 0.98 % for Zr (at 1052 ppm) to 10.8 % for Pb (at 29 ppm). This range in precision was equivalent to that for the NIST SRM 278; clearly obsidian is an ideal medium for pXRF with its high degree of homogeneity and obtainable planar form. They determined 18 elements using the ‘standard analytical package’ and 7 light elements using the ‘LEAP’ mode (light element analytical package), acquiring data for 3 minutes on each mode, but only the aforementioned elements were reported in this paper. Productivity was 60-75 samples analysed per day.

Using the Niton XLt 792 (40 kV tube with Ag anode, Si-PiN diode), Peinado *et al.* (2010) found pXRF to be an excellent screening tool in a study of the spatial distribution of As, Pb, Zn and Cu in soils located in the abandoned mining area of Rodalquilar, SE Spain. The upper 0-10 cm soil layer (moisture content <2 %) was collected and the samples sieved to <2 mm before being analysed through their plastic bags; presumably the manufacturer’s soil mode (Compton normalization) was employed in the calibration (without additional CRMs). Precision and accuracy data were provided only for the CRM analysed.

Berger *et al.* (2010) determined sulphur in sediments from the Copper Basin and Muddy River (Massachusetts) using the Niton XLt with a helium path. ‘Low’ (0-0.3 % S) and ‘high’ (0-3 % S) calibrations were created with six CRMs, though the high calibration had only one point (3.08 % S) above 0.35 % S. Although used in creating the calibration, the result of 0.22 % S for NIST SRM 1646a obtained using the ‘high’ calibration was significantly different from the recommended value of 0.35 % (cf. 0.32 % using the low range). The effect of water on the analysis was tested up to 50 % and as predicted, the fluorescence signal decreased linearly with the dilution. For best results, drying, grinding and sieving to <120 mesh was recommended. With an acquisition time of 4 min, the quantitation limit (10σ of the response for a blank SiO₂ standard) for S was determined to be 237 ppm.

Gonzalez-Fernandez and Queralt (2010) found low-cost ED-XRF (Fischerscope XDAL model with a W tube, operated at up to 50 kV and 1 mA, and a Si-Pin detector of 180 eV resolution) to be very useful in screening sediment cores collected in depositional environments around the long-established mining sites of Cartagena-La Union district of Spain. The analysis was carried out in a lab using a 2-D programmable stage that facilitated the analysis of a split core ~30 cm long and ~7 cm in diameter, with spot sizes of 0.6 mm. Although results were deemed to be semi-quantitative because of the large changes in matrix composition within the core, mapping of the distribution of Ca, Ti, Mn, Fe, Zn, As, Rb, Ar, Zr and Pb was found to provide essential information in understanding the depositional characteristics and fate of the elements studied. From the same Institute of Earth Sciences in Barcelona, Margui *et al.* (2010) investigated the applicability of this technique to testing the use of sunflowers in phyto-remediation around abandoned Pb-Zn mines in Spain. Employing the same instrumentation as Gonzalez-Fernandez and Queralt (2010), they successfully mapped the distribution of Pb and Zn in the pressed leaves, to a limit of detection of 0.08 $\mu\text{g cm}^{-2}$ for Zn and 0.38 $\mu\text{g cm}^{-2}$ for Pb and with a spatial resolution of 0.2-1 mm using different collimators. Sample preparation simply comprised removing surficial dust by rinsing, pressing the sunflower specimens between absorbent paper

with a heavy weight to remove moisture and then placing the various vegetation tissues onto the platform of the ED-XRF instrument.

Kenna *et al.* (2011) devised an interesting calibration method using the InnovX Alpha 4000 series instrument which improved upon the manufacturer's methodology and produced excellent results in the lab for K, Ca, Ti, Cr, Mn, Fe, Co, Cu, Zn, Rb, Zr, Pb and U in siliciclastic soils and sediments of the Hudson River estuary. The scaling factors calculated in the development of the factory calibration for the soil mode were used in the computation. Their approach is based on the use of powdered CRMs as calibration standards, least-squares regression techniques that allow for uncertainty in both x and y data, propagation of error with respect to predicted concentration and a goodness of fit calibration. Although the quality of the data for the above elements was equivalent to that produced by established lab analytical techniques, their method is probably not practical for geochemical exploration as it requires the analysis of a CRM (of similar matrix to the samples) every 2nd or 3rd sample, limiting efficiency, and a suite of CRMs that covers the elemental concentration ranges.

There have been several recent conference presentations of note on the subject of pXRF. Hughes and Rowe (2009, 2010), of the University of Texas, have developed a pXRF-based methodology, using Bruker's handheld Tracer III-V, to delineate shale and mudstone chemostratigraphies in different cores to infer paleodepositional conditions. Recognizing that there were insufficient CRMs to calibrate pXRF for major and trace elements, they selected samples from a multitude of shale and mudrock units spanning Devonian and Cretaceous ages and of variable mineralogy and organic carbon content and established their elemental compositions by fused disc WD-XRF and fusion ICP-MS. They then used this large set of CRMs, as fine powders, to both optimize pXRF conditions and establish excellent calibrations for low (~ 15 kV tube voltage) and high energy (~ 40 kV) elements.

Simandl *et al.* (2011) presented a poster at the Cordilleran Round-up in Vancouver on using a handheld InnovX ALPHA series pXRF analyser to determine Zn, Pb, Fe and Cd in samples from carbonate-hosted non-sulphide deposits of the Kootenay and Cariboo terranes. The mining mode was used without matrix-specific calibration and with a beam time of 60 s. Data for hand specimens and pulps were compared with results by total digestion ICP-MS; precision for the former samples was poor by pXRF (heterogeneity). Agreement between the two analytical methods was reasonable for Fe and Zn but not for Pb and Cd. However, as a tool for distinguishing between barren, moderately mineralized and high-grade samples in exploration for poorly visible 'white Zn-Pb' deposits, pXRF was deemed successful.

3. METHODS

3.1 Instruments Used in This Study

Three manufacturers – InnovX (Olympus), Bruker (Elemental) and Niton (Thermo Scientific) – kindly lent their pXRF instruments for this project. The specifications of the pXRF instruments used are provided in the table below.

Analyzer	Delta-6000	X-5000	XL3t	FXL	Turbo	S2 Ranger
Manufacturer	Olympus Innov-X	Olympus Innov-X	Thermo Niton	Thermo Niton	Bruker Elemental	Bruker Elemental
Type	Handheld (HH)	Field-portable Benchtop (BT)	Handheld (HH)	Field-portable Benchtop (BT)	Handheld (HH)	Lab benchtop
Anode	Rh	Ta	Ag	Ag	Ag	Pd
Tube voltage (kV_{max})	40	50	50	50	45	50
Tube power (W_{max})	4	10	2	10	4	50
Detector area (mm²)	30	25	25	25	10	5
Filter wheel positions	8	6	6	6	5	9
Camera	Yes	No	Yes	Yes	No	No
Method used	Test stand	Closed beam unit only	Test stand	Closed beam unit only	Sample plate and cover	Closed beam unit only
Modes used for study	·3-Beam Soil ·2-Beam Mining	·2-Beam Soil ·3-Beam Soil ·2-Beam Mining	·Soil ·Mining Cu/Zn	·Soil ·Mining Cu/Zn	·Soil ·Mining Light Elements ·Mining Oxides	·Geo

More information on these and other models is available from:

Olympus/InnovX <http://www.olympus-ims.com/en/xrfrd/?gclid=CLjo4uGTnakCFcZ95Qod1xnptQ>

Thermo/Niton
Bruker

<http://www.niton.com/?sflang=en>
<http://www.bruker-axs.com/handheldx-rayspectrometry.html>

Several days of instruction were provided by the appropriate members of these companies; this was followed up by frequent communication between Angelina Buchar and technical staff of each company.

Each handheld instrument was given the designation 'HH' and each benchtop 'BT'; similarly the soil mode was designated 'S' and the mining mode 'M'. Thus, a handheld A used in the soil mode is termed 'HH-A-S' and benchtop B used in the mining mode is 'BT-B-M'. On the next page is a list of elements reported by the various instruments in each mode.

Elements determined by each pXRF analyser; some elements were below detection in all samples and are shown appropriately

Element	HH-A-S	HH-B-S	HH-C-S	BT-A-S	BT-B-S	HH-A-M	HH-B-M	HH-C-M	BT-A-M	BT-B-M
Ag	y		y	y	y	all ND		y	all 'ND'	y
Al						y	y	y	y	y
As	y	y	y	y	y	y	y	y	y	y
Au	y		y	y	y		all '0'	y		y
Ba		y	y	y	y			y		y
Bi	y	y		y		y	y	y	y	y
Br		y								
Ca	y	y	y	y	y	y	y	y	y	y
Cd	y	y	y	y	y	y	y	y	y	y
Ce		y		y			y			
Cl	y			y		all 'ND'		y	y	y
Co	y	y	y	y	y	y	y	y	y	y
Cr	y	y	y	y	y	y	y	y	y	y
Cs			y		y					
Cu	y	y	y	y	y	y	y	y	y	y
Fe	y	y	y	y	y	y	y	y	y	y
Hf		y					y			
Hg	y	all '0'	y	y	y					y
K	y		y	y	y	y	y	y	y	y
La				y						
Mg						y	y	y		y
Mn	y	y	y	y	y	y	y	y	y	y
Mo	y	y	y	y	y	y	y	y	y	y
Nb	y	y		y		y	y	y		y
Nd				y						
Ni	y	y	y	y	y	y	y	y	y	y
P	y			y		y	y	y	y	y
Pb	y	y	y	y	y	y	y	y	y	y
Pd		y	y		y			y		y
Pr				y						
Pt		all '0'								
Rb	y	y	y	y	y		y	y		y
Rh							y			
S	y		y	y	y	y	y	y	y	y
Sb	y		y	y	y	y	all '0'	y	y	y
Sc			y		y					
Se	y	y	y	y	y		all '0'	y		y
Si						y	y	y	y	y
Sm				y						
Sn	y	y	y	y	y	y	y	y	y	
Sr	y	y	y	y	y		y	y		y
Ta		y		y			y			
Te			y		y					
Th	y		y	y	y					
Ti	y	y	y	y	y	y	y	y	y	y

U	y	y	y	y	y		y			
V	y	y	y	y	y	y	y	y	y	y
W	y	y	y	y	y	y	all '0'	y	y	y
Y	y			y						
Zn	y	y	y	y	y	y	y	y	y	y
Zr	y	y	y	y		y	y	y	y	y

3.2 Suite of Samples under Study

The table on the next page lists the wide range of control reference materials (CRMs) used to evaluate accuracy in this project. [The term ‘control’ rather than ‘certified’ is used in this context because not all the samples are *certified* reference materials]. The certifying agencies from which the majority of these samples were obtained comprise:

CCRMP Canadian Certified Reference Materials Project, Canada

<http://www.nrcan.gc.ca/mms-smm/tect-tech/crm-mrc-eng.htm>

IGGE Institute of Geophysical and Geochemical Exploration, China

<http://igge.cags.ac.cn/en/show/view.jsp?id=25>

NIST National Institute of Standards and Technology, USA

<http://www.nist.gov/srm>

GSJ Geological Survey of Japan

<http://www.aist.go.jp/GSJ/dGC/chemtop.htm>

OREAS Ore Assay Standards, Australia

<http://www.oreresearch.com.au/oreas-reports>

Further information on these CRMs can be obtained from the above websites and also from the website (<http://georem.mpch-mainz.gwdg.de>) of the Max Planck Institute where data for > 2300 geological and environmental reference materials are listed.

Other samples in the study suite comprise: three stream sediment samples from the Geological Survey of Canada (GSC) (PF 1002, 1008 and 1010); two samples (GW 28209, GW 799305) containing high concentrations of REEs from Great Western Minerals; and the potash sample (VSP09) provided by Vale. The majority of the CRMs have been crushed, ground, sieved to pass a 74- μm sieve, including the GW samples, and well blended. However, the stream sediments were not milled but sieved to <177 μm . [The sphalerite concentrate, CZn-1, was analysed only by a few instruments as, unlike the other samples, it was in the form of a pellet and was needed by another GSC laboratory].

Bottles containing the CRM powders were shaken in a figure-eight motion for a minimum of 3 minutes to ensure adequate homogeneity. Powders were then transferred in single open-ended sample XRF cups (Chemplex Cat. No.: 1830-SE, Chemplex Industries, Inc., Palm City, FL, USA); although based on our comparison to other cups provided as samples, double-open-ended cups *with caps* (e.g. Chemplex Cat. No.: 1330) provide greater ease for filling and packing while ensuring flat and ridge-free thin-film. Prior to filling, cups were rinsed with deionised water to remove any possible residuals or dust, and dried in an oven for 5 minutes. Most cups were completely filled and packed while some were partially, though adequately, filled, due to limitations in material availability. Powders were supported in cups with 4.0- μm Prolene® thin-film (Chemplex Cat No.: 3018, Chemplex Industries, Inc., Palm City, FL, USA). This thin-film was selected based on a compromise between transmittance and resistance to tearing (in comparison to thinner films or other material).

The suite of CRMs used in this study is shown in the table below.

Suite of control reference materials (CRMs) used in this study

Sample	Type	Classification
CCRMP LKSD-4	lake sediment	stream/lake sediment
CCRMP MRG-1	gabbro	mafic/ultramafic
CCRMP SY-2	syenite	felsic intermediate
CCRMP SY-3	syenite	felsic intermediate
CCRMP TILL-2	till	soil/till
CCRMP WMG-1	gabbro	mafic/ultramafic
	sulphide-bearing ultramafic rock	
CCRMP UM-4	(Ni ore)	mafic/ultramafic
CCRMP MP-1	Zn-Sn-Cu-Pb ore	Ore
CCRMP BL-2a	U ore (pitchblende)	Ore
CCRMP MA-1a	Au ore, siliceous	Ore
CCRMP FeR-1	iron formation, Fe oxide	Ore
CCRMP SU-1	Ni-Cu-Co ore	Ore
CCRMP CZn-1	sphalerite ore	Ore
IGGE GSR-1	granite	felsic intermediate
IGGE GSR-2	andesite	felsic intermediate
IGGE GSR-3	basalt	mafic/ultramafic
IGGE GSR-6	limestone	limestone
NIST SRM2709	soil	soil/till
NIST SRM2710	contaminated soil	soil/till
NIST SRM2711	soil	soil/till
USGS BHVO-1	basalt	mafic/ultramafic
USGS DNC-1	diabase	mafic/ultramafic
USGS GSP-1	granodiorite	felsic intermediate
USGS GXR-5	soil	soil/till
USGS GXR-6	soil	soil/till
USGS PCC-1	peridotite	mafic/ultramafic
USGS RGM-1	rhyolite	felsic intermediate
USGS SCO-1	shale	shale/schist
USGS SDC-1	Mica schist	shale/schist
USGS SGR-1	shale	shale/schist
GSJ JG-1	granodiorite	felsic intermediate
GW-28209	REE-enriched	Other
GW-799305	REE-enriched	Other
PF 1002 SS	stream sed	stream/lake sediment
PF 1008 SS	stream sed	stream/lake sediment
PF 1010 SS	stream sed	stream/lake sediment
OREAS 14p	sulphide Ni-Cu-Pt-Pd-Au	Ore
OREAS 132b	Zn-Pb Sedex	Ore
OREAS 166	Cu ore	Ore
OREAS 76a	NiS ore	Ore
VSP09	potash	Other

These samples were classified into eight groupings for the purpose of plotting the data and identifying any trends in behaviour according to sample type. The groups are: felsic/intermediate; limestone; mafic/ultramafic; ore; shale/schist; soil/till; stream/lake sediment; and ‘other’.

The CRM package was sent to ALS Laboratories in Vancouver and SGS Laboratories in Toronto. The labs were asked to provide *total analysis* for as many elements as possible, using the most sensitive techniques such as ICP-MS in conjunction with lithium metaborate fusion. The sample identities were not hidden as the ranges of elements are very large in light of the ore materials included and these could cause cross-contamination if the lab was not alerted to them.

The methods used and elements determined by ALS in Vancouver are as follows.

ME-ICP06, whole rock $\text{LiBO}_2/\text{LiB}_4\text{O}_7$ fusion + ICP-AES for Al_2O_3 , Fe_2O_3 , CaO, MgO, Na_2O , K_2O , Cr_2O_3 , TiO_2 , MnO, P_2O_5 , SrO, and BaO;

ME-MS81, LiBO_2 fusion + ICP-MS for Ba, Ce, Co, Cr, Cs, Dy, Er, Eu, Ga, Gd, Hf, Ho, La, Lu, Mo, Nb, Nd, Pr, Rb, Sm, Sn, Sr, Ta, Tb, Th, Tl, Tm, U, V, W, Y, Yb, Yb, and Zr;

ME-MS82, (presumably) cold vapour/hydride generation for As, Bi, Hg, Sb, Se, and Te;

ME-4ACD81, ‘four-acid’ HF-based digestion + ICP-AES for Ag, Cd, Co, Cu, Mo, Ni, Pb and Zn;

ME-OG62, ‘four-acid’, for Cu, Pb, Ni and Zn in the four OREAS ores, MP-1 and SU-1;

C-IRO7 and *S-IRO8*, Leco methods, for C and S, respectively;

and LOI at 1000 °C.

SGS Laboratories analysed the suite of samples by sodium peroxide fusion combined with ICP-MS and ICP-AES, known as the *ICM90A* package. The elements determined comprise Ag, Al, As, Ba, Be, Bi, Ca, Cd, Ce, Co, Cr, Cs, Cu, Dy, Er, Eu, Fe, Ga, Gd, Ge, Hf, Ho, In, K, La, Li, Lu, Mg, Mn, Mo, Nb, Nd, Ni, P, Pr, Rb, Sc, Sb, Sm, Sn, Sr, Ta, Tb, Th, Ti, Tl, Tm, U, V, W, Y, Yb, Yb, Zn and Zr. Mercury was also determined by cold vapour AAS (*CVA14C*).

The data, including the ‘certified’ values for the CRMs, are shown in Appendix 3. The ‘certified’ values, shown in the first column (white) are divided into three categories: ‘recommended’ (i.e. well established and accepted, denoted in the text as RV), shown in normal font; ‘provisional’, shown in italics (of less certainty than ‘recommended’); and ‘informational’, shown with a question mark (of less certainty than ‘provisional’). These values are supplied with the CRMs from the various agencies. The data in this column for the two ‘REE’ samples - GW-28209 and GW-799305 – are results provided by Great Western and are based on total analysis for the REEs, the ‘whole rock’ package and the ‘four-acid’ digestion package reported by SRC Geoanalytical laboratories in Saskatoon. The data in this column for the GSC stream sediments – PF 1002, 1008 and 1010 – are based on INAA and the ‘four acid’ package offered by Acme laboratories.

‘Selected’ values (‘SV’ in the table) to be used to evaluate the pXRF data were arrived at by considering all the methods of the individual results (four-acid digestion being the least favourable and used only in the absence of total methods). Recommended numbers were preferentially chosen as the SV but where values were in the ‘provisional’ or ‘informational’ category, averages across the three numbers were often taken. Results for many elements by

ALS and SGS do not agree well for GW-28209 and those for Cu, Pb and Zr in GW-799305 are not in agreement, but otherwise values are generally comparable.

3.3 Optimization of Beam Time

The only parameter that most (geochemical) users of pXRF would optimize is the beam time. Three CRMs were chosen for this study: GXR-6, LKSD-4 and UM-4. Each sample was measured 10 times for each count time. Count times (i.e. seconds per beam/filter of a mode) were randomized as follows: 120s, 30s, 40s, 100s, 60s, 20s, 10s, and 80s per beam/filter. For example, LKSD-4 was placed on the analyser window and analysed 10 times consecutively at 120s per beam without moving the sample, followed by 10 times at 30s per beam, and so on and so forth.

3.4 Evaluation of Accuracy

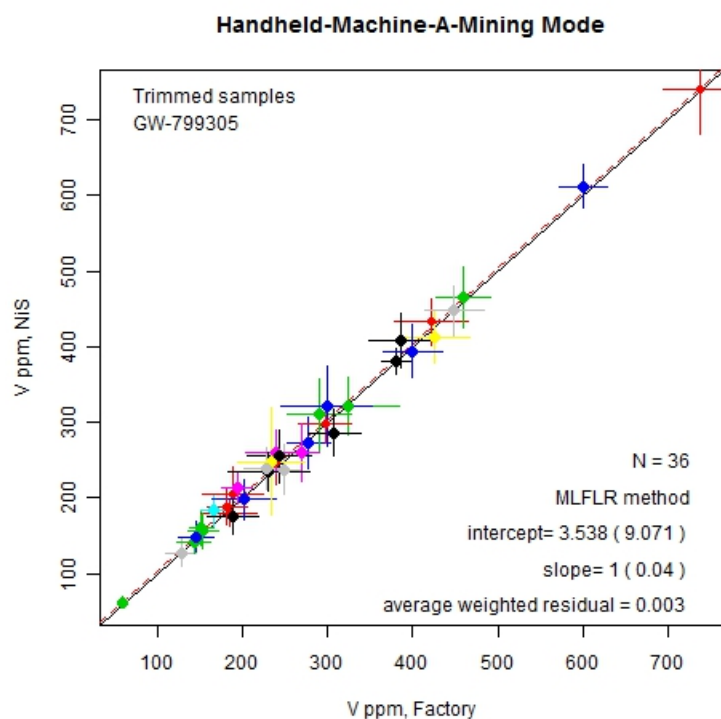
Ten consecutive measurements of each sample at 60 s per beam/filter were used to generate the accuracy data. Each sample was placed on the analyser window and 10 consecutive measurements were taken without moving or lifting the sample between measurements. Note that only factory calibrations (in both modes) have been used throughout this project. Given the wide array of matrices present in the suite of samples under study, it would have been highly impractical to modify calibrations to suit different sample types.

3.5 Evaluation of Precision and Detection Limits

Ten CRMs were used to determine precision and optimum detection limits: BHVO-1, GSR-6, LKSD-4, MRG-1, the NIST SRMs 2709, 2710, 2711, SGR-1, TILL-2 and UM-4. The ore and REE-enriched samples were avoided as some of their elements would suffer from various interferences and hence their precision figures would be compromised. Ten randomized or non-consecutive measurements of each sample at 60 s per beam/filter were used to generate the precision data. In other words, cups were lifted and re-positioned on the analyser window between each measurement. Sample sequence was in most cases randomized or separated to ensure that no two samples were analysed consecutively. The important aspect was ensuring that the cups were removed and replaced on the analyser window prior to each measurement to obtain a more realistic measure of variability.

3.6 Data Analysis

The graphs, included as Appendix 4a (soil mode) and Appendix 4b (mining mode), are designed to show a comparison of the portable XRF results with established (selected) values of the control reference samples (CRMs). The XRF measurements of element concentration come with a standard deviation value for each sample, based on 10 replicated analyses. The CRMs have the published recommended value for most elements: in addition each CRM has been analysed by two labs, so also have a measure of error for each sample, as described in the next section.



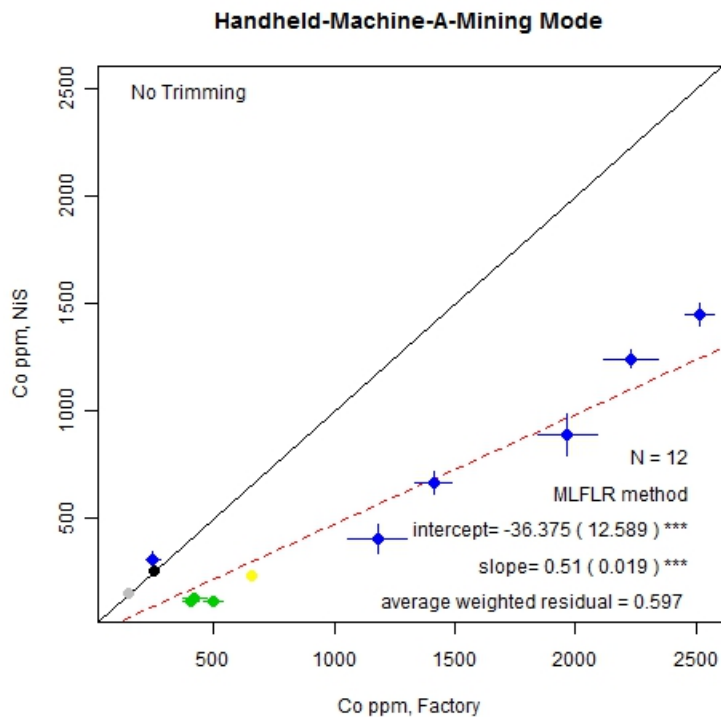
As an illustration, this graph shows vanadium determined in this case by two XRF pre-programmed methods—one with the general factory settings (x axis) and the other using NiS settings (y axis) optimized for this sulphide matrix. Each point is shown as a coloured dot (colour is related to 8 material types used to classify the CRM samples), with the length of the superimposed crossed lines (error bars) being equal to one standard deviation either side of the mean, for each axis. The solid line shows perfect correlation (45°) and the dashed line is a fitted line, which in this example is parallel to the 45° line, but just above it, with an intercept value of 3.5 ppm. In this instance, one sample (GW-799305) is a flier, and has been ‘trimmed’ from the graph, an option in the code.

The method used here for fitting lines was published by Ripley and Thompson (1987) and was later used by Hall and Bonham-Carter (1988) for estimating bias in gold analysis by INAA. An Excel code for the method has been published by the Royal Society of Chemistry (2002). Here we wrote custom code in the R language for automating the fitting process and producing the graphs. We are planning to add the code to the publicly available R library (rgr) developed by Bob Garrett.

In evaluating an analytical method for bias, it is inappropriate to use ordinary linear regression of y on x, which assumes that x is known without error. And fitting x on y will give a different line from y on x—i.e. different results are obtained depending on how the ‘response’ and ‘explanatory’ variables are selected. Furthermore, ordinary regression does not consider the magnitude of the errors that here are known at each point, on each variable. The Ripley-Thompson method, known as a ‘Functional Linear Relationship’ requires a non-linear ‘Maximum Likelihood’ solution (not the normal least squares solution used in linear regression), and is referred to here as the MXFLR method. MXFLR uses the errors on each variable at each point, and choice of y on x or x on y gives the same best fit line. This is better than the ‘reduced

major axis' method which gives the same line independently of how x and y are selected, but it does not use the error measurements at each point. According to Ripley and Thompson (1987), the MXFLR method is also superior to 'weighted' regression, which weights observations inversely by their standard deviations.

Besides the intercept and slope of the MXFLR line shown on the graph, the standard errors of intercept and slope are calculated (shown in parentheses). This allows one to test the null hypotheses that the intercept is zero, and the slope is 1 (perfect correlation, no bias). Rejection of these null hypotheses is shown by asterisks following the standard errors: '*' means rejection at 95 % level of probability, '**' means rejection at the 97.5 % level, and '***' means rejection at the 99 % level. The average squared residual is checked: if this value is greater than 2, the slope and intercept tests are unreliable. In the above vanadium example, there are no asterisks, and the null hypotheses are accepted—i.e. the slope is not different from 1 (no rotational bias) and despite the non-zero intercept value, the difference from zero is not significant (no translational bias).



This cobalt plot illustrates both a rotational and translational bias between the factory (x) and NiS (y) settings. The intercept of -36 is significantly different from zero at the 99 % level (3 asterisks). The slope of 0.5 is significantly different from 1 at the 99 % level (3 asterisks). The blue points are ore samples, the green dots are mafic-ultramafic samples. The average weighted residual (.597) is less than 2, so there is no reason to suspect the reliability of the significance tests on intercept and slope.

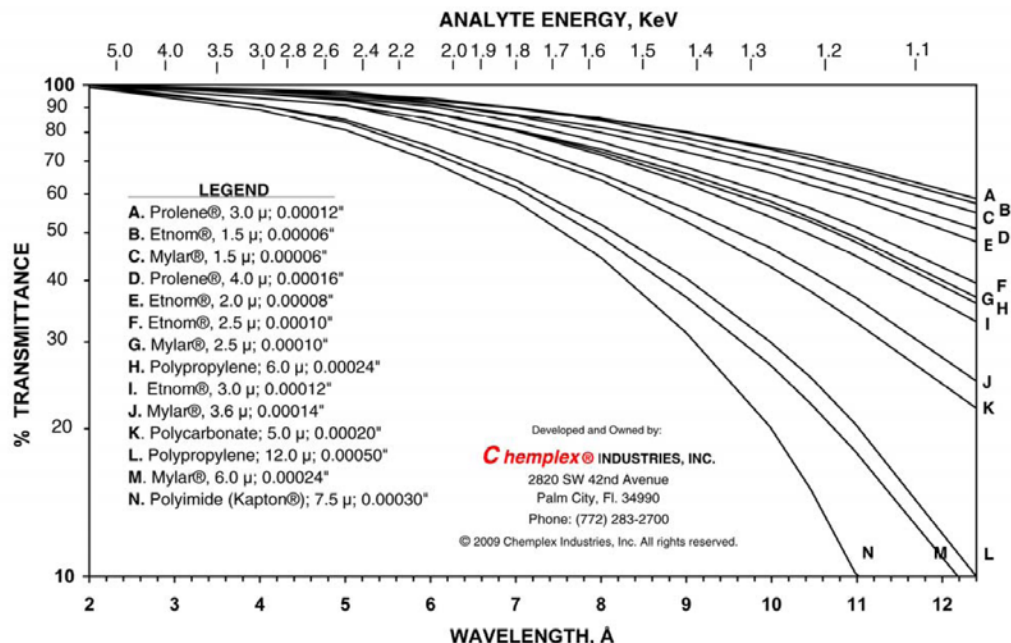
Obtaining mean and standard deviations for each CRM sample

Most of the CRM samples have published values of the recommended element concentration. But some samples, for some elements, have no published values. In this study, each reference sample was sent to two independent laboratories for analysis, so in some cases 3 values were available: the recommended value, and 2 measured lab values. Using these data we built up a table with a 'true' value and an estimate of its standard deviation for each CRM sample using the following method.

1. Where a published recommended value was available, this was used as the 'true' value of the CRM independently of the lab values.
2. If no published data were available, the 'true' value was set to the mean of the 2 laboratory values.
3. Where 2 laboratory values were present and satisfactory, the standard deviation was calculated for that point from the 2 lab values.
4. In some cases, one of the lab values was missing. To fill in the gaps, a linear relationship was fitted to the standard deviation versus 'true' mean value for points where these were known. The predicted standard deviation was then calculated for the unknown values using the fitted line. This worked well, because in general the standard deviation increases with concentration, a well-known situation used in, for example, Thompson-Howarth plots.

3.7 Thin-film Study

The effect of thin-film material, such as Mylar®, Kapton®, Prolene®, and thin-film gauge (i.e. thickness) on element photon transmittance was investigated in a study published in 1985 (Solazzi, 1985). Despite being well-documented, the effects of thin-film on photon transmittance still remain largely unknown to many pXRF users. We chose to investigate this effect to emphasize the importance of thin-film selection for those in the mining industry working with powders and thin-film sample supports. Depending on the element of interest and element concentration, the choice of thin-film can have a major impact on accuracy based on thin-film material, thickness and typical impurities. Low Z elements (e.g. Mg, Al, Si), having K lines in the very low-energy region of the spectrum (1-2 keV), are most susceptible to absorption of their fluorescence photons. The figure below illustrates the difference in % transmittance of various well-known films in use today (Solazzi, 1985). Note that the most transparent film is the 3- μm Prolene® type whereas one of the least is the 6- μm Mylar® type.



Plot of % transmittance vs wavelength for various thin-films, taken from the 2011 Chemplex catalogue.

We compared polyethylene terephthalate (i.e Mylar®) to polypropylene (e.g. the Prolene® brand and others) of various thicknesses, from three thin-film manufacturers (Chemplex, Lab Supply and Spex CertiPrep) using HH-A-M (with test-stand) and BT-A-M as shown in the table below (next page). We prepared pressed pellets (with Licowax ®) of GSR-1, GSR-3, LKSD-4, OREAS 166, and SY-3. Each pellet and thin-film combination was analysed by lining the analyser window with a thin-film sheet and placing the pellet over the thin-film. We opted to use pellets for added ease when changing and handling thin-film as opposed to powders. Also, pellets were selected for added analytical consistency in comparison to powders due to particle losses at the surface for the latter that would introduce undesirable and uncontrolled variability. Each pellet was analysed without thin-film as well as with the following thin-film to establish the % transmittance (concentration of pellet and thin-film/concentration of pellet with no thin-film).

Thin-film material, typical impurities, thickness, manufacturer and ID

Thin-film type	Typical impurities (ppm level) ^a	For CAMIRO Study		
		Thickness (μm)	Thin-film manufacturer	ID
Mylar ($\text{C}_{10}\text{H}_3\text{O}_4$)	Ca, P, Sb, Fe, Zn	2.5	Chemplex	Mylar2.5_X
		3.6	Chemplex	Mylar3.6_X
		6.0	Chemplex	Mylar6.0_X
		6.0	Lab Supply	Mylar6.0_Y
Polypropylene (C_3H_6)	Ca, P, Fe, Zn, Cu, Zr, Ti, Al	3.0	Chemplex	PP3.0_X
		4.0	Chemplex	PP4.0_X
		4.0	Lab Supply	PP4.0_Y
		4.0	Spex CertiPrep	PP4.0_Z

^aAs identified in the Chemplex 2011 Catalogue or on Chemplex product labels.

4. RESULTS

4.1 Silica Blanks

Blank silica samples were run on each instrument consecutively ten times each. Two blanks had been supplied by manufacturers and another was obtained at the GSC. The following table (next page) presents the results reported above the detection limits of the instruments. Running a different silica blank can be useful in identifying whether the ‘contaminant’ is actually in the blank itself or an inherent feature of the instrument (a blank spectrum will show, in addition to Si peaks, the anode lines etc as well as those from components of the instrument). The ‘EC SiO₂’ blank reads 165±5 ppm in Cr by HH-C-M but a different blank (‘SiO₂’) is below detection; this suggests that the Cr reading is specific to *that* particular EC SiO₂ blank. BT-A-M and BT-A-S confirm this value in EC SiO₂. At first glance, the Cl blanks by BT-A-M of 0.49 % in SiO₂ and 1.51 % in EC SiO₂ look worrisome. However, if the samples under study read significantly lower than the blank, as they do in this case, then there should not be a problem and it is a feature of the blank itself. The same is true for the Pb values shown in the table using HH-A-S, HH-C-M and BT-A-M. It is very important to know what to expect from one’s blank spectrum or data.

The blank readings for Cd, Sb and Sn by HH-A-M and for Ag and Sn by BT-B-M and BT-B-S (highlighted in yellow) *do signal a problem* with the background and hence the intercept in the calibration. Such a problem is very evident in the data obtained for the CRM suite. This particular region of the energy spectrum, at ~ 22-26 keV, is one of significant Compton scattering which proves challenging to correct for at trace levels. The reason for the ‘concentrations’ of Ag, Cd and Sn being considerably lower in ‘EC SiO₂’ than in ‘SiO₂’ is unclear, though it could be a reflection of the difference in grain size and density (and hence scatter) of the two samples. One remedy could be to establish an offset (intercept) in the calibration but the magnitude of this is dependent upon the matrix of the sample itself. The manufacturers are currently working to improve this correction which should be available shortly.

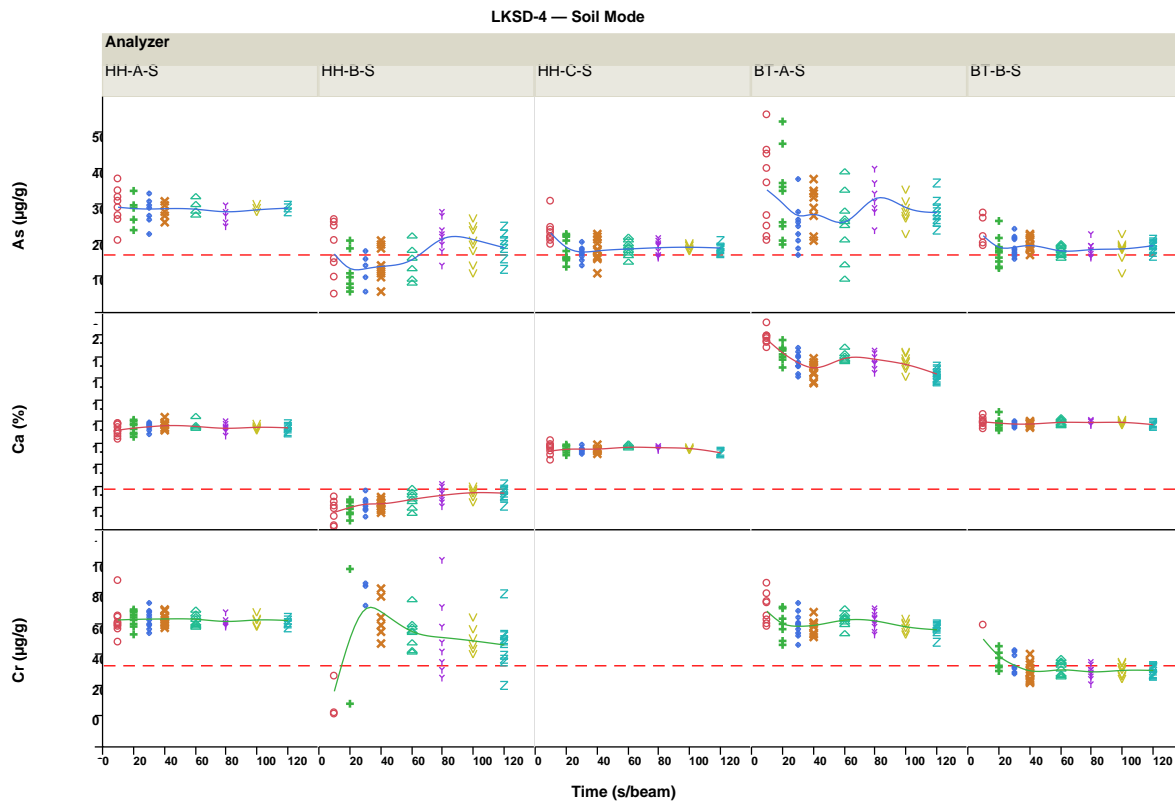
Sulphur and P are reported in some blanks. Sulphur detection at low levels suffers from the shoulder of the Rh (target anode) line and analysis for P (Z 15) in a SiO₂ blank will likely be degraded by its nearness to Si (Z 14), the major constituent.

Elements reported in blank SiO₂ samples, all values in ppm except where noted.

Instrument	Ag	Ba	Ca, %	Cd	Cl	Cr	Mo	P, %
HH-A-M, SiO ₂				253±8				0.394±0.01
HH-A-M, EC SiO ₂				84±5				
HH-A-S, EC SiO ₂							5.5±0.94	0.202±0.04
HH-B-M, SiO ₂			0.041±0.002					0.133±0.007
HH-C-M, SiO ₂					0.032±0.003			
HH-C-M, EC SiO ₂						165±5		
HH-C-S, EC SiO ₂							7.0±0.5	
BT-A-M, SiO ₂					0.494±0.021			0.112±0.015
BT-A-M, EC SiO ₂					1.513±0.044	164±25		
BT-A-S, EC SiO ₂						146±5		0.363±0.058
BT-B-M, SiO ₂ -180	161±3	84±7	0.066±0.001					
BT-B-M, EC SiO ₂	49±3							
BT-B-S, SiO ₂ -180	154±3	55±7	0.071±0.001					
	Pb	S, %	Sb	Sn	Ti, %	V	Zr	
HH-A-M, SiO ₂		0.037±0.003	380±9	246±9	0.029±0.006			
HH-A-M, EC SiO ₂		0.046±0.003	67±9	49±4				
HH-A-S, EC SiO ₂	62±2.9						4.3±0.4	
HH-B-M, SiO ₂								
HH-C-M, SiO ₂								
HH-C-M, EC SiO ₂	61±3							
HH-C-S, EC SiO ₂	71.7±1.9							
BT-A-M, SiO ₂		0.014±0.002			0.068±0.005			
BT-A-M, EC SiO ₂	30±1	0.068±0.007						
BT-A-S, EC SiO ₂			17.7±4.1					
BT-B-M, SiO ₂ -180		0.030±0.002		29±3.1		52±4		
BT-B-M, EC SiO ₂								
BT-B-S, SiO ₂ -180				29±2		24±1.2		

4.2 Optimization of Beam ('Count') Time

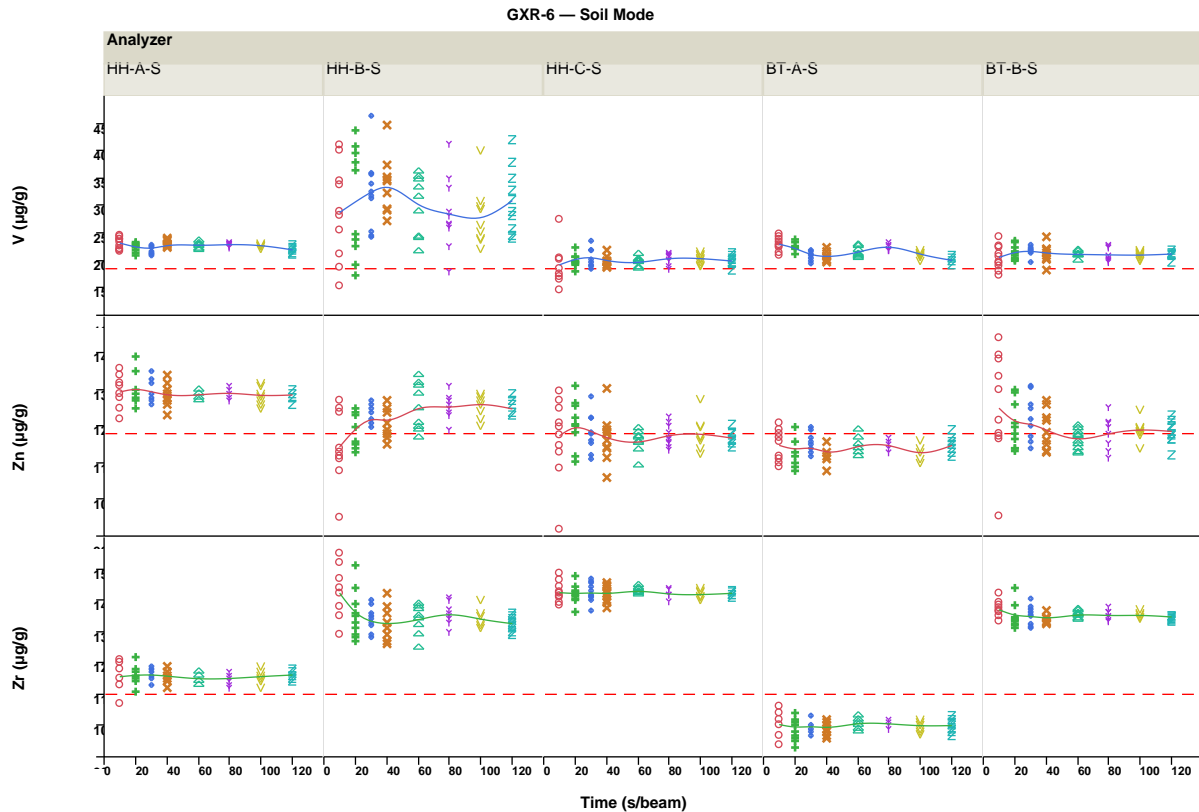
Results of the beam time study are shown graphically in Appendix 5 for the samples GXR-6 (soil), LKSD-4 (lake sediment) and UM-4 (ultramafic rock) analysed by all five instruments. The ten data points for each value of time 't' (20s through to 120 s) are colour-coded for easy viewing and the horizontal red line represents the recommended/established concentration value for that element in that sample, thus providing information on both precision and accuracy. The patterns for As and Cr in LKSD-4 (below) in the soil mode by HH-A-S and H-C-S demonstrate the improvement in precision from 20 s to ~ 60 s, with little change in spread thereafter – a common feature of the data.



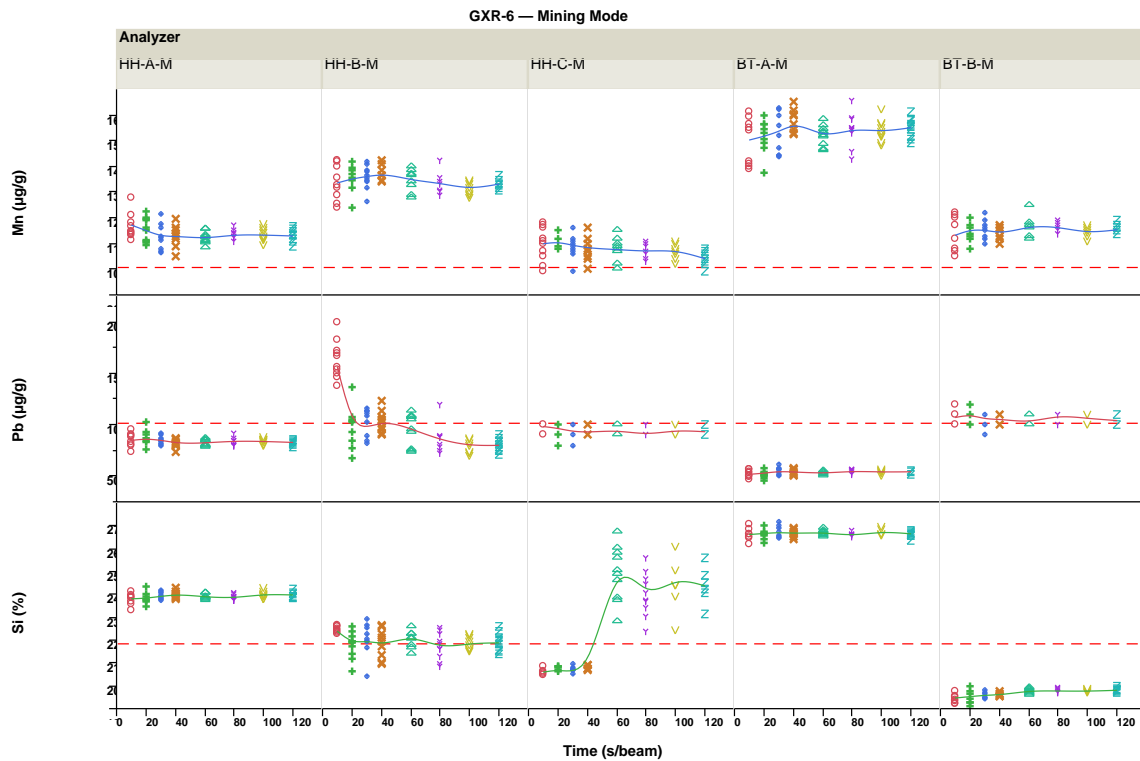
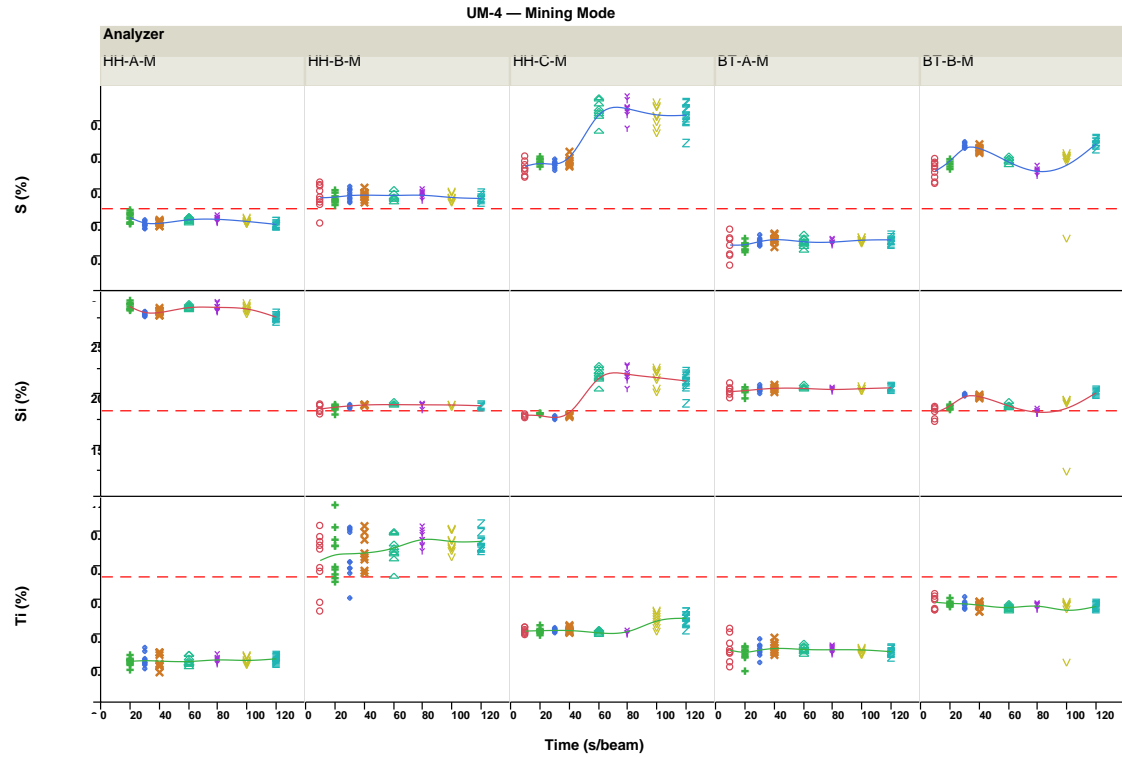
Note above the differences in precision for As between BT-A-S (very poor) and BT-B-S (good) and for Cr between HH-B-S and the others. Also note the considerable drift in Ca by BT-A-S, indicating a significant range in values from ~ 1.8 to ~ 1.95 % Ca. This same pattern is evident for K and Ti in LKSD-4, Ca, Cr and, to a lesser extent, Mn in UM-4 and for Ca, K, Ti and Mn in GXR-6. The good precision associated with this drift for Ca (and other elements) supports the fact that it is 'real': that all three samples show the same shape of drift indicates that it is not related to time of operation of the machine because the samples, at the various values of 't', were analysed in a completely randomized manner. This drift was later demonstrated to be caused by a drift in live-time of the beam, a problem that required resolution by the manufacturer.

The data for GXR-6 in the soil mode (graph below) show that increasing the beam time for V, particularly noisy by HH-B-S, does not improve precision. The spread in results at t=120 s is at

least as large as that for $t=30$ s, not in line with the expected two-fold improvement in precision. This instrument was clearly experiencing a problem with repeatability for the trace elements.



In the mining mode, there is a *huge* jump in absolute values for Al, Mg, Si and S by HH-C-M, followed by a very slight drift downwards. Corresponding to this jump is a much wider spread in the concentrations reported (i.e. much worse precision). This is seen for all three samples; a plot for UM-4 is shown below (Si, S). There should not be a shift in absolute concentration values when the user changes beam time from say 40 s to 60 or 70 s. Clearly this has a major impact on results: in this case, the change in Si concentration is from ~ 18 to 22 %! The lower plot for GXR-6 displays an even sharper jump in Si after 40 s. Another phenomenon for this instrument, perhaps related, is evident in the patterns for Ti, V, Cr and Ca in these samples. The behaviour of Ti in the same plot below for UM-4 is typical: far worse precision at $t=100$ and 120 s, accompanied by an upward drift. The drift is usually upwards but that for Cr in UM-4 is downwards for these last two data points. These drifts in accuracy and precision are not present in the soil mode for this instrument. The instrument BT-B-M also shows a shift in absolute values for Al, S, Mg and Si, but to a lesser degree than that evident in HH-C-M (see UM-4, S and Si by BT-B-M).



In summary, selection of a 60-s beam time, in either the soil or mining mode, seems to be a good compromise between good precision and efficiency. Shorter times of 10-40 s should be avoided. However, this study has highlighted problems with drift and sharp unexpected changes in

precision that the manufacturers need to address. The problem highlighted here for the instrument HH-C was caused by the inter-relation of the various beam time options and was remedied by the manufacturer.

4.3 Accuracy and Precision

4.3.1 Introduction

In this section we look at both accuracy and precision on the full suite of 41 CRM samples, again broken down by soil and mining modes. Precision has been characterized in two different approaches: the first here as ‘noisiness’ around fitted lines (r^2), using the full suite of CRMs; and later as the randomized repeatability (relative standard deviation, RSD or coefficient of variation, CV) on a smaller suite of samples. How accurate are the XRF values? How noisy? Is there an advantage to using benchtop machines over handheld? Which elements give the most reliable results?

All 10 analyses for each sample have been consolidated in this report to the mean and standard deviation of the set (Appendix 6 for the soil mode and Appendices 7a and 7b for the mining mode). When concentrations are very close to the instrument’s detection limit in that matrix, some values will be provided by the instrument. Therefore 10 readings may comprise x ‘non-detects’ and $10-x$ actual values. Rather than eliminate all values for the element, where $n \geq 5$, the mean and standard deviation have been computed and inserted into the data-base with a comment included indicating the value for n . Furthermore, the data have not been truncated at their detection limits and therefore noise at low concentrations is expected to be exceptionally high.

By plotting the recommended value of an element against its XRF measurement (for a particular machine and mode) as an x-y graph, it is easy to visualize both accuracy (how close a best-fit line is to a 1:1 or 45° line) and precision (how closely the points are to a best-fit line). The graphs in Appendices 4a and 4b are grouped 5 to a page, one graph for each machine, with colour coding to show to which of 8 material groups the sample belongs. The layout on the page is always the same: from top-bottom, left to right the machines are BT-A-M, BT-B-M, HH-A-M, HH-B-M and HH-C-M. This allows a comparison of machines. The colour legend is added to each plot for ease of use.

As discussed previously, the best-fit line used here is not an ordinary regression line: it considers errors on both variables, and is the same line irrespective of which variable is considered as ‘dependent’ and which is ‘independent’. In practice we always have plotted the recommended CRM values on the x-axis, and the XRF value on y, so that the intercept, a , and slope, b , are for the line $y' = a + bx$, where y' is the predicted value and a and b are fitted by the non-linear method described previously. This best-fit line is plotted on each graph.

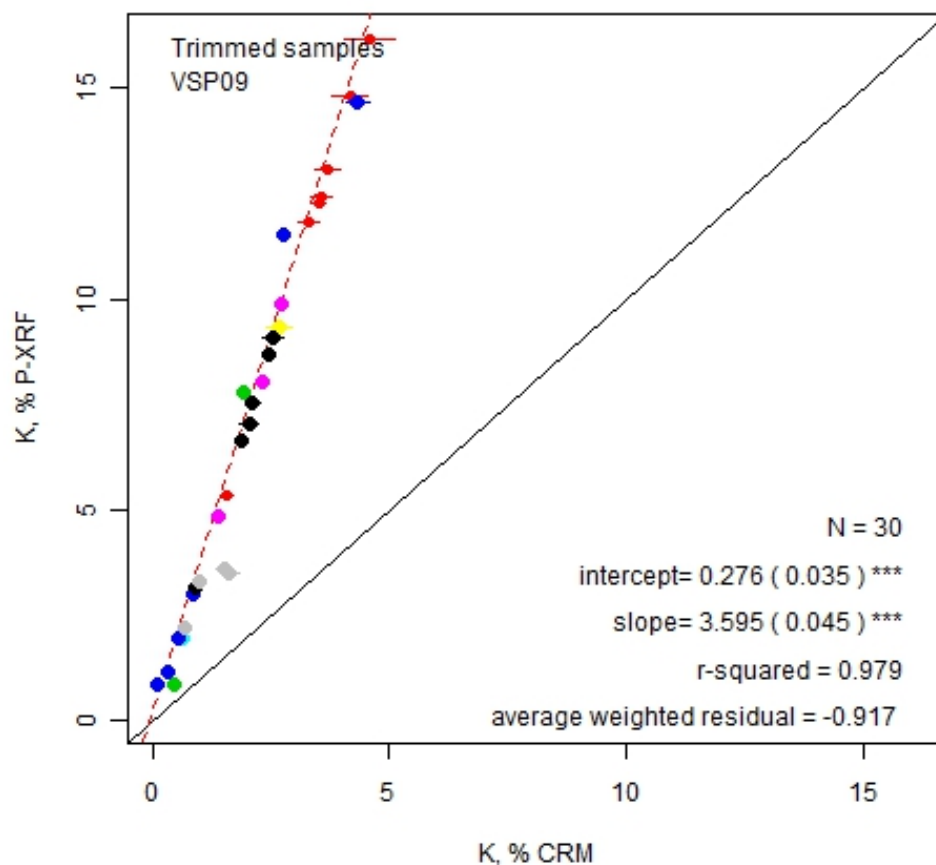
Some statistics are also shown on each graph. N is the number of sample points. The intercept, a , with its standard error (se) in brackets with asterisks to indicate whether the null hypothesis “intercept=0” can be rejected (one * for 5 %, ** for 2.5 %, and *** for 1 %). In general, the rule

of thumb is that the hypothesis is rejected if $a/\text{se}(a)$ is greater than 2. The larger the ratio, the greater is the probability of rejection. The slope, b , is provided with its standard error. Here the null hypothesis “slope=1” is tested by the ratio $\text{abs}(b - 1)/\text{se}(b)$, and the asterisks are again used to indicate significance. The coefficient of determination, r^2 , is provided as a measure of goodness of fit. It is simply the square of the correlation coefficient between x and y and provides a scale between 1 (perfect fit) and 0 (very poor fit). One may say that r^2 describes “the proportion of the y variation explained by the relationship with x ”, so that $r^2 = 0.8$ implies that 80% of the variation can be explained. In addition, the average residual from the best fit line is given, also as a measure of noise.

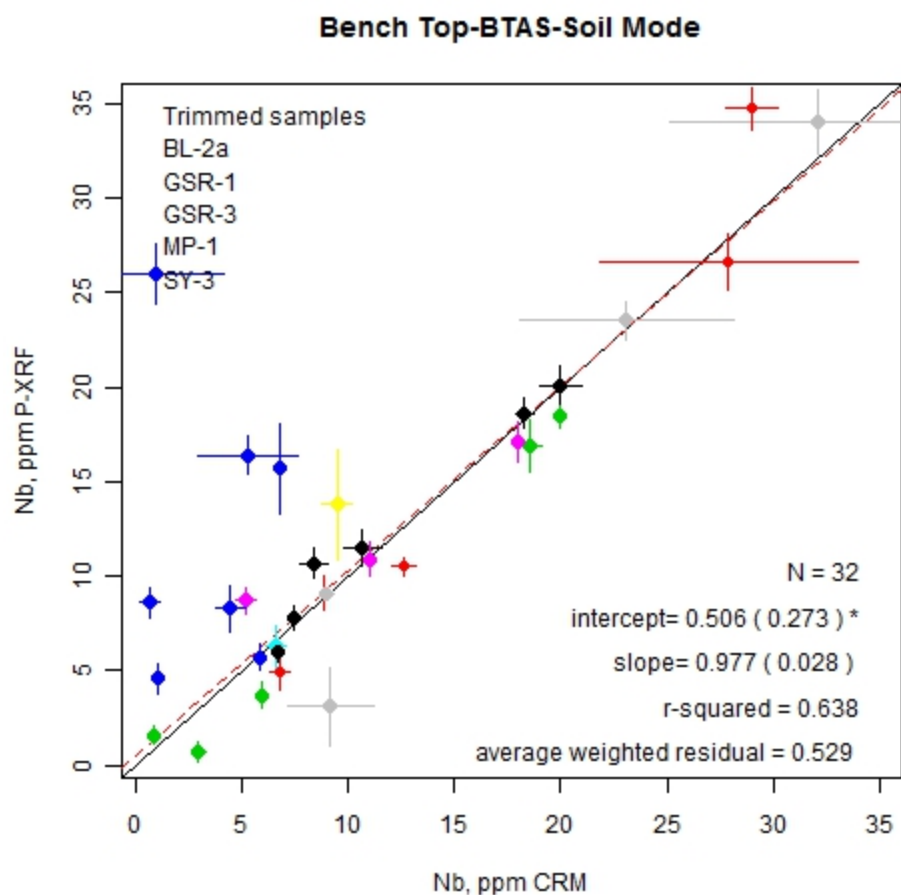
In general, the formal tests of significance of a and b in this study are not particularly useful, because in almost every case the null hypotheses of $a=0$ and $b=1$ are confidently rejected. However, the intercept and slope (particularly the slope) are very useful to see the degree of rotational bias (slope greater or less than 1), and translational bias (intercept greater or less than 0). Thus a value of $b=1.2$ immediately tells us that the XRF values are 20 % too high on average, or $b=0.9$, they are 10 % too low, providing a measure of what is usually obvious on the graph. We have found that the r^2 value seems to work well as a measure of goodness of fit, whereas the average residual is sometimes difficult to interpret.

As an example of using the graphs, consider the example of K measured in mining mode by HH-A-M, shown below (next page). We see that the slope is nearly 3.5, so that the XRF values are 3.5 times too large, But $r^2 = \sim .98$, indicating that only 2 % of the variation is not explained, a very good fit. Neither is the intercept=0, nor the slope=1, statistically (3 asterisks). Clearly this is a case where recalibration is in order! And it is not a situation where different matrices are causing the problem, because one line fits a wide variety of sample types.

Handheld-Machine A-Mining Mode



On the other hand, consider a case where the slope is close to 1, but the data are noisy. Nb on a benchtop machine in soil mode (BT-A-S) provides an example (see below, next page). Here we see that the slope is very close to 1 and the hypothesis $b=1$ is not rejected, although the slope $a=0$ is rejected at 5 %. However, $r^2=.64$ indicates a noisy fit, as can be readily seen visually. Some of the damage is coming from ore samples (blue dots) that are being over-predicted at low levels.



Two types of plots are shown for each element by each machine mode. One is for ‘untrimmed’ data (essentially all samples). The other ‘trimmed’ plot removes samples greater than a cutoff value. The purpose here is to remove high ‘fliers’ so that we can see better what is going on at low levels without the extreme values affecting the best-fit line. As an example, on the BT-A-S plot of Nb, we can see that 5 samples were excluded because they exceeded a threshold of 35 ppm (either on the recommended value, or the XRF value). The sample names are shown in upper left of the graph, so that the detailed analyses can be checked in the data tables in the Appendices 6 and 7 if needed. The cutoff values applied were determined by inspection of probability plots of recommended values of CRMs, and are listed in the accompanying table below.

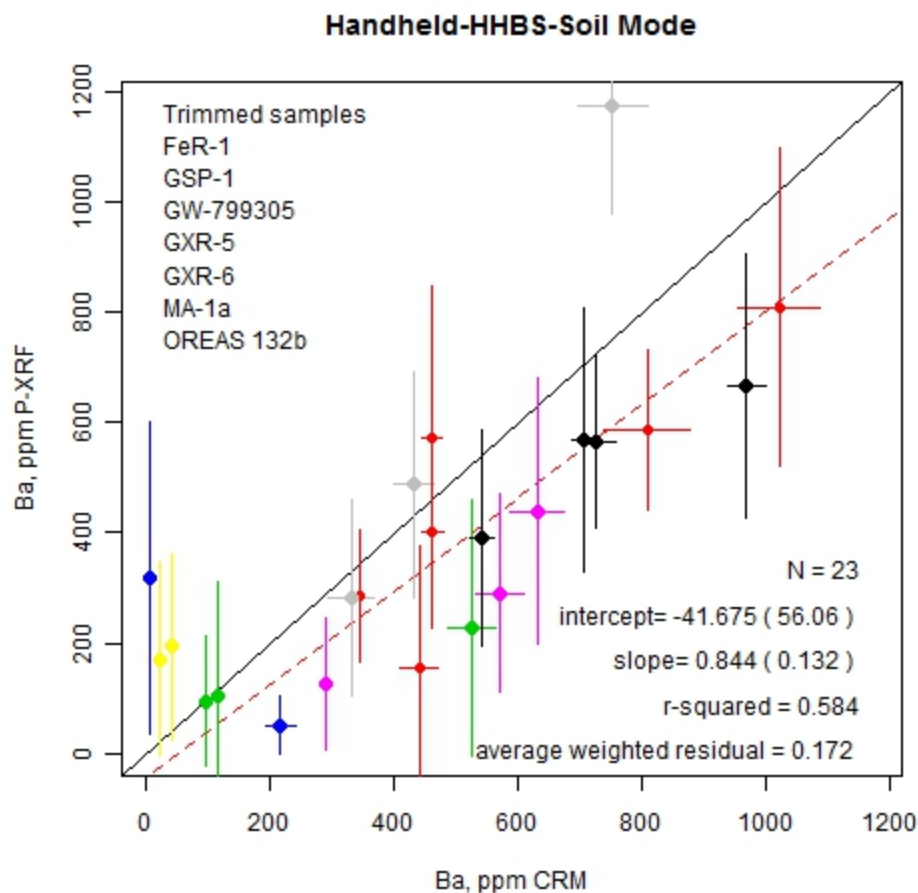
Cutoff values used for trimming in soil and mining mode graphs

Threshold determined from probability plots of recommended values

Units in ppm unless otherwise noted

Element	Value	Element	Value
Ag	10	Nd	500
Al	9%	Ni	500
As	1000	P	0.50%
Au	2.5	Pb	200
Ba	1300	Rb	250
Bi	15	S	2.50%
Br	100	Sb	60
Ca	7.50%	Sc	20
Cd	100	Se	7
Ce	300	Si	35%
Cl	160	Sm	150
Co	250	Sn	70
Cr	1000	Sr	500
Cs	20	Ta	2.5
Cu	600	Te	2
Fe	15%	Th	100
Hf	12.5	Ti	0.75%
Hg	5	U	200
K	5%	V	200
La	300	W	25
Mg	12.5	Y	1000
Mn	3000	Zn	400
Mo	20	Zr	400
Nb	35		

Many of the plots show a problem with both accuracy (bias) and precision, as measured by the goodness of fit, r^2 . For example, consider Ba (soil mode, trimmed) by HH-B-S in the next graph. Here we see that on average, the XRF values are biased downwards (16 % too low) and that the goodness of fit is only 58 %. Also notice that the standard deviations of the XRF values are large, as indicated by the length of the error bars on the y-axis. Here 7 samples have been trimmed for having concentration values >1300 ppm. Also notice that N=23, so only 23+7=30 samples gave results reported by this machine, leaving 41-30=11 samples without a reported value. This is usually because the XRF values were below detection limit, or there were problems with interferences detected in the built-in correction algorithms.



4.3.2 Discussion of results by element

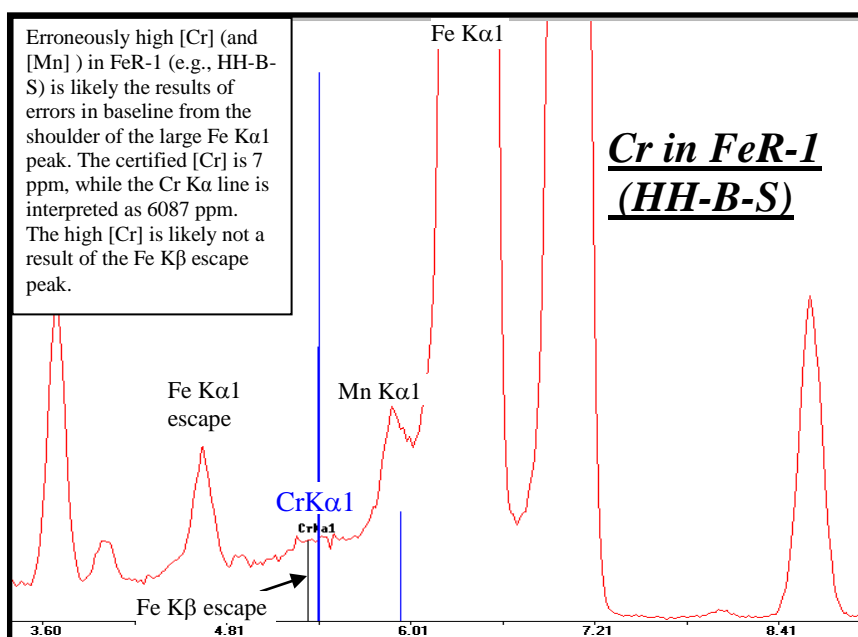
It should be kept in mind that calibrations according to matrix type were not carried out in the mining FP or soil mode, i.e. the factory calibrations were used without change to the slope or intercept. However, if a particular sample grouping (e.g. mafic, shale, soil) shows a distinct and coherent behaviour in a plot of pXRF vs the selected value then it is clear that a recalibration using CRMs of that matrix would lead to more accurate analysis. Results are discussed with reference to the mining and soil mode data files (Appendices 6, 7) and to the corresponding files containing all the graphs of pXRF results vs selected values (Appendices 4a, 4b). Many of these graphs in the mining and soil mode (across the full range of concentrations or ‘trimmed’ to view the performance at lower concentrations) are used to illustrate the discussion and are inserted at the end of Section 4.3.2. In the data files, some elements have a column showing ‘recovery’; this is simply the average of the means divided by the recommended or selected value for that sample, expressed as a percentage.

The manufacturer’s *optimum* detection limit quoted in the discussion is that provided by InnovX for their Delta premium series fitted with a Rh anode; this limit will vary slightly for the model

used, particularly according to the tube's anode but all instruments in this study are more or less 'on an equal footing' (e.g. all fitted with SDDs).

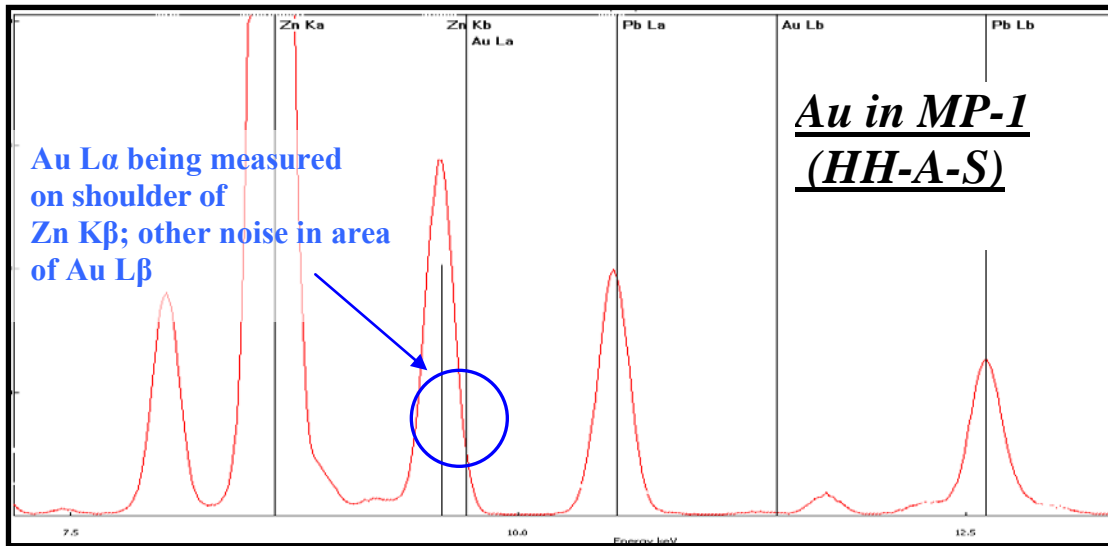
The mining mode (denoted by 'M', e.g. instrument HH-A-M) is the focus of discussion for the major elements whereas it is the soil mode (denoted by 'S', e.g. HH-A-S), with Compton normalization, for the trace elements.

Spectral interferences are cited in this text; the following spectra provide examples of serious overlap. The first (below) illustrates the interference of Fe on Cr in FeR-1 which contains 52.96 % Fe. The Cr K α line at 5.41 keV is being read on the shoulder of the massive Fe K α line at 6.4 keV.



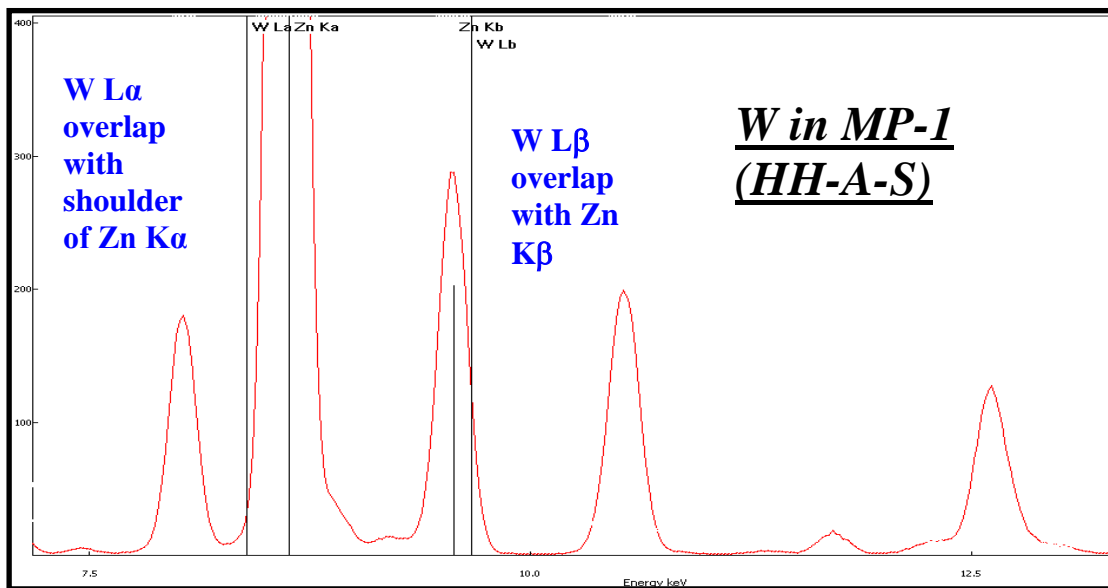
Spectrum of FeR-1 showing the interference of Fe on Cr.

On the next page there is a spectrum of MP-1 (Zn at 15.9 %) showing that the Au L α peak at 9.71 keV is being measured on the large shoulder of the Zn K β peak at 9.57 keV. Gold was erroneously reported as 104 ppm in MP-1. The second spectrum shows the interference of Zn on W in MP-1. The W L α line at 8.4 keV and the W L β line at 9.67 keV are measured on the shoulders of the large Zn peaks at the Zn K α line (8.64 keV) and Zn K β line (9.57 keV), respectively. Tungsten was reported as 1796 ppm in MP-1 where, in fact, the recommended concentration is 180.7 ppm.



Above: spectrum of MP-1 showing interference of Zn on Au.

Below: spectrum of MP-1 showing interference of Zn on W.



Some of the erroneous data we encountered, such as those for Ti, Mn, Cr and Ni, may be caused by poor de-convolution of the spectra (Keith McIntosh, Anglo Research, pers. comm.). Both the $K\alpha$ and $K\beta$ peaks are normally used in analysis because this provides a better fit as there are two positions to fix and the ratio of the two peaks. However, the ratio of $K\alpha$ and $K\beta$ peaks can change depending on the matrix and other major analytes in the sample. If a K absorption edge falls between the $K\alpha$ and $K\beta$ peaks, this can have a marked change in the ratio of these two peaks. However, the differences in these ratios are often then used to identify other analytes that

may overlap. The ‘unaccounted’ intensity may then be incorrectly assigned to another analyte and errors occur. This effect becomes much worse when you move to analytes that are determined with their L lines – the REE and PGEs. Firstly, the sensitivity of these lines is ~20 times lower than analytes determined with the K lines in the same energy range. Secondly, the spectrum is more complex with up to 5 or 6 major peaks spread over a much wider range and changing ratios. To make things even more difficult, if there is a large problem with a particular element, for example Sc, then the neighbouring elements, for example Ca and Ti, may be affected. In this manner Fundamental Parameters can actually cause severe problems: neighbouring analytes which are the most affected, are either under- or over-corrected. If the major errors are addressed, many of the others will automatically improve (Keith McIntosh, Anglo Research, pers. comm.).

4.3.2.1 Major and minor elements

Mg, magnesium (Figs. 1a, b, available at the end of Section 4.3.2)

The pXRF industry detection limit for Mg is better than or equal to ~ 1 %, too high for the accurate analysis of many geological samples. With $K\alpha$ and $K\beta$ lines at the very low energy region of the spectrum (~1.3 keV), Mg is very poorly determined by pXRF in the absence of a vacuum or He atmosphere. This is borne out in the five sets of mining mode results shown in Figs. 1a and 1b (trimmed data). Only 6 and 8 results (at > 4 % Mg) are above detection limits by HH-A-M and HH-C-M, respectively; Mg was not reported by BT-A-M. Note that in the data-set there are numerous missing values (i.e. <DL) for many low-level Mg samples. Before viewing the SD associated with the mean value of 10 results for a sample, one should examine the counting statistics error for Mg (or any light element). For example, at levels of ~ 3-4 % Mg, this error is comparable to the result itself and is sometimes higher, a good indication to ignore the data.

The best fit, with a slope of 0.96, is shown by HH-B-M (Fig. 1a), even though the SDs can be very large (e.g. MRG-1 at 7.46 ± 2.78 %) and $n \leq 10$ for numerous samples. The results for the REE-enriched sample, GW 799305, and the Cu ore, OREAS 14p, are extremely inaccurate, at 6.05 ± 0.73 % (cf SV, selected value, of 1.89 %) and 7.47 ± 2.74 % (cf SV of 0.28 %). Taking the mean of the 10 values actually can be misleading in the case of Mg as the SD of 10 readings, for example for OREAS 14p, can be considerably less than the counting statistics error on just one reading (e.g. 8.86 ± 6.27 % for 1 reading; cf the SD of 2.74 % across 10 readings).

Much less individual variation is shown by BT-B-M ($n=23$) but a substantial negative bias is evident (slope of 0.45) and the scatter about the line is high (even more so for the trimmed graph; Fig. 1b). The instruments HH-A-M and HH-C-M will detect Mg when it is greater than ~ 4 % but the plots indicate the inaccuracies present would not benefit a great deal from recalibration.

The range in recovery by the mining mode for Mg at concentrations >2 % is 59-175 %. Thus, the performance in analysis for Mg differs remarkably amongst the instruments and only two report for most of the samples, albeit with high SDs but a good slope or the reverse.

Al, aluminium (Figs. 2a, b)

The industry detection limit for Al is better than or equal to ~ 0.5 %. Although Al is also a light element, the data are certainly an improvement over those for Mg, the counting statistics errors are much less significant, and a majority of the samples are reported across the instruments. The best fit is shown for HH-B-M, with an r^2 of 0.86 and a slope of 1.05 (Fig. 2a). One sample that shows very poor agreement is the potash, VSP09, where the pXRF value by the HH-B-M is 7.89 ± 0.37 % and the selected value is only 0.41 %. The counting statistics error for this sample is ~ 0.4 % Al, not indicative that there could be a problem with the accuracy. The cause of this high result is undoubtedly the Br $L\alpha$ line (1.48 keV) on the Al $K\alpha$ line (1.49 keV). Typical RSDs are in the range 4-6 % but the variation for OREAS 14p (3.2 ± 1.14 % Al) is unusually high at 36% RSD; this noise was suggested by a counting statistics error of ~ 0.8 % Al, proportionately higher than that for other samples.

Although there is a small translational bias in the results for BT-A-M, with a slope of 0.97, there is a good fit to the line (r^2 of 0.96). At concentrations of Al < ~8 %, this instrument shows slightly more noise in the 10 readings per sample than the others (Fig. 2b). There is a fair amount of scatter in the plots for HH-A-M; they suggest that separate calibrations for the mafic and ore grouping vs the other sample types would improve accuracy. The scatter about the best fit lines for BT-B-M (r^2 of 0.85 and 0.74 trimmed) and HH-C-M (r^2 of 0.87 and 0.63 trimmed) is much greater than that of the other instruments, with the former under-reporting Al concentrations (e.g. 4.1 ± 0.05 % in SRM 2711; cf 6.53 % RV) and the latter over-reporting (e.g. 7.42 ± 0.35 % in SRM 2711).

It is interesting that *all instruments* are low in Al for the lake and stream sediments. For example, results are in the range 1.9-3.5 % for PF1002 (cf SV of 5.44 %), 3.3-4.4 % for PF1010 (cf SV of 6.09 %) and 1.5-2.4 % for LKSD-4 (cf 3.12 % RV). Their random scatter does not suggest recalibration to this matrix would completely correct these recoveries.

The range in recovery for Al by the mining mode is 51-132 % at Al concentrations >0.4 %.

Si, silicon (Fig. 3)

The industry detection limit for Si is better than or equal to ~ 0.5 % so that is more than adequate for geological materials! Silicon, with $K\alpha$ and $K\beta$ lines at 1.74 and 1.84 keV, is generally well determined by all instruments, although the slopes of most lines do differ from 1.0. The best fit to the 45°-line appears to be for HH-B-M as instruments BT-A-M, HH-A-M and HH-C-M have slopes of up to 1.2 and BT-B-M a negative slope of 0.8 (Fig. 3). Deviations from these lines in all cases are seen for the stream sediments PF1002 and 1010 which are significantly under-reported and, not surprisingly for the iron formation, FeR-1 (7.91 % Si), which averages a high recovery of 165 %.

Most spread is evident in the graph for BT-B-M, and this is accompanied by curiously high SDs for several high-Si samples such as the granite GSR-1 (29.02 ± 6.14 % Si). Most instruments (e.g. HH-B-M) handle the ores well but there are some fliers such as in BL-2a, the U-Th ore, by BT-B-M (17.00 % vs 27.63 % RV) and in MP-1, the Zn-Sn-Cu-Pb ore, by BT-A-M and HH-A-M (at ~ 28 % vs 19.41 % RV). The limestone, GSR-6, is well analysed by all instruments except HH-C-M where it is reported at 16.55 ± 0.79 % (7.29 % RV).

Eliminating the fliers mentioned above, the range in mean recovery for Si by the mining mode is 83-111 %.

K, potassium (Figs. 4a, b, c)

The optimal industry detection limit for K is ~ 0.005 % which should be adequate for most geological materials. Results for K cluster tightly around the best-fit lines, though the slopes of these lines can dramatically differ from 1 (e.g. 1.4 for HH-B-M and 0.8 for HH-C-M), most astonishingly for HH-A-M where the slope of the line is 3.6 (Fig. 4a)! Clearly this instrument needs to be recalibrated for K; these results were not used in computing the average recovery! Results would improve also for HH-B-M and HH-C-M by recalibrating. The potash VSP09, at 14.8 % K, is poorly determined across the instruments, registering 1.4, 7.7, 11.2 and 13.3 %, ignoring the HH-A-M result.

Looking at the trimmed graphs (Fig. 4b, $K < \sim 4.5$ %), SDs for the high-K felsic/intermediate group again are high for BT-B-M, as is seen for Si. For example, for the granodiorite GSP-1 (4.57 % K), BT-B-M reports 4.15 ± 0.57 % whereas the value by BT-A-M is 5.37 ± 0.02 %. This unexpected noise in BT-B-M data was investigated further by examining the 'raw' data: the cause for these high SDs is universally due one sporadic lower reading amongst the 10 individual readings. It was evident in samples GSP-1, GSR-1, GSR-3, LKSD-4, MRG-1, RGM-1, and WMG-1 and for the elements Ba, Ca, Al, K, P, Cl, S, Si, Ti, V, and Cr, not elements that are determined in one particular beam. This problem was specific to the mining mode. Later, severe problems were encountered with this instrument and it was sent back to the manufacturer for a replacement of the tube. If a user was not taking multiple readings as is the case in this project, this phenomenon would probably not have been noticed. Insufficient time was available to repeat these particular samples; others were run on the replacement machine.

The stream sediments PF1002 and 1010 are again showing low average recoveries of 62-66 %, very distinct behaviour compared to any other samples. Eliminating results for the two stream sediments, BL-2a (U-Th ore) and VSP09, the average recovery for K by the mining mode at levels >0.10 % is in the range 71-117 %. These ranges in recoveries evident for elements in the mining mode strongly suggest that recalibration by the user is necessary to obtain accurate data.

In the soil mode (Fig. 4c), the data are: (1) much the same for BT-B-S (as BT-B-M) except that the noise for the group of samples discussed above has disappeared; (2) more accurate for HH-C-S (i.e. close to the 45°-line); (3) slightly less accurate for BT-A-S; and (4) far more accurate for HH-A-S and lacking that huge positive rotational bias seen for HH-A-M. [K was not reported in the soil mode by HH-B]. Clearly the best data in the soil mode are provided by HH-C-S and BT-B-S. The limestone, GSR-6, shows a large range in concentration, at 0.960 to 1.723 % K (cf 0.648 % RV). Calcium and K are neighbours in the Periodic Table (K lines of 3.69 and 3.31 keV, respectively) and hence a very high concentration of one will cause an interference on the other. This interference, perhaps surprisingly, was much better handled in the mining mode in the cases of HH-C-M, BT-A-M and BT-B-M.

Ca, calcium (Figs. 5a, b, c)

The industry detection limit for Ca is ~ 0.003 %, well above expected concentrations and thus Ca should be more than adequately well determined by pXRF. BT-B-M shows excellent agreement

between the results and selected values while the other instruments have a positive bias, from a slope of 1.07 for HH-C-M to 1.26 for BT-A-M, each goodness-of-fit being acceptable (Fig. 5a). The one sample that is in poor agreement with the recommended value across the instruments is the limestone GSR-6 (25.49 %) where as high a value as 35 % is being reported, suggesting that the top end of the calibration needs attention. The graphs for BT-A-M and HH-A-M of the trimmed data (Fig. 5b) show erroneously high concentrations for numerous ore samples, indicating a separate calibration is in order. Stream sediment PF1008, at 2.28 % Ca, reports high by all instruments, to as much as 4.47 ± 0.01 % by BT-A-M. The other two stream sediments report low, with recoveries in the range 83-88 %.

Again BT-B-M reports some high SDs for some samples, namely in GSR-3 (6.32 ± 0.71 %), MRG-1 (10.93 ± 1.07 %) and WMG-1 (11.05 ± 0.9 %). If the sole erroneous readings were ignored and the mean and SD based on 9 rather than 10 readings, the precision would be as good as that provided by the other instruments. With the exceptions of results for GW28209 (0.20 % Ca) and PF1008, the average recovery by the mining mode for Ca is 80-123 % across this wide range of matrices.

To be expected, the results (see Appendix) for the limestone, GSR-6, are more inaccurate in the soil mode, with an average recovery of 182%. This medium would clearly be analysed in the mining mode after a matrix-specific calibration has been created. Two further 'fliers' are seen in the soil mode data (Fig. 5c), not in evidence in the mining mode and these are for FeR-1 and GW799305 by HH-B-S. They are both erroneously high, at 13.84 % for the former (cf 2.37 % RV) and 26.12 % for the latter (cf 16.44 % SV). The rotational bias of ~ 1.3 present in the BT-A-M and HH-A-M data is more exaggerated in the soil mode, with slopes of 1.4-1.5. In general, the data across elements for the soil mode (Fig. 5c, trimmed data, $< \sim 6$ % Ca) are slightly noisier for the other instruments but still usable. With the exceptions of FeR-1 and GSR-6, the range in recovery by the soil mode is 71-151%. Comparison of the graphs in the two modes at Ca concentrations below < 6 % suggests that results by the soil mode would only be slightly inferior.

Fe, iron (Figs. 6a, b)

The results for Fe in the mining mode are excellent over a wide range in concentrations (up to ~ 53 % for FeR-1; Fig. 6a). Slopes range from 0.8 for HH-A-M to 1.0 for BT-B-M and the fit is tight (Fig. 6a). The only fliers are: by HH-B-M, OREAS 14p (21.93 % Fe vs 37.10 % RV), OREAS 76a (19.13 % vs 24.60 % RV) and SU-1 (18.63 % vs 22.90 % RV); by HH-C-M and BT-A-M, OREAS 14p (32.28 % and 29.80 %, respectively); and by HH-A-M, FeR-1 (61.26 % vs 52.96 % RV). The plot for HH-A-M suggests that a separate calibration for the non-ores would be beneficial and this is borne out by plot of the trimmed data (Fe $< \sim 12$ %; Fig. 6b). However, the other instruments do not show this divergence. The sediments PF1002, PF1008 and LKSD-4 again display anomalous behaviour, with average recoveries of 126, 134 and 128 %, respectively. With these exceptions, the average recovery ranges from 84 to 107% at concentrations of Fe > 0.2 %.

The soil mode data suggest that it could be used up to a concentration of 5 % Fe, though with a bias of 1.4 by HH-A-S and 0.9 by HH-C-S. There is a large positive interference on MP-1 (Zn-Sn-Cu-Pb ore), with values in the soil mode ranging from 13 to 21 % Fe (cf 5.68 % RV). The

untrimmed graphs for Fe and the average recoveries in this mode demonstrate the dangers of analyzing for Fe above ~5 % in the soil mode.

Ti, titanium (Figs. 7a, b, c)

The industry detection limit for Ti is ~ 0.005 %. Results across the full concentration range by HH-B-M for Ti are good, with a slope of 0.94 and an r^2 of 0.97 (Fig. 7a); only FeR-1 shows an obviously inaccurate value at 0.345 % (cf 0.02% RV). Data for BT-B-M are a close second but showing slightly low results at high Ti concentrations (in BHV0-1, GSR-3, MRG-1; the last two suffered from one low result amongst the 10). The slopes of the other graphs are significantly lower than 1 (0.47-0.73) but the fit appears to be good, suggesting that a recalibration would lead to accurate data. The trimmed data (Fig. 7b) illustrate well the noise in Ti below a concentration of ~0.7%. The slopes of the lines are about the same (trimmed vs untrimmed), in the range 0.53-0.80, all indicating an under-evaluation of values. The sample that does show erroneously high results across all instruments is the REE-enriched GW799305, at 0.385-0.568 % Ti (cf 0.167 % SV); it was not reported by BT-B-M. This sample contains 3880 ppm La which is probably the cause of the interference: the La $L\alpha$ line (4.65 keV) overlaps with the Ti $K\alpha$ line (4.51 keV). The other REE sample, GW28209 also reports high by BT-A-M (0.171±0.012 %; cf 0.02 % SV) and HH-A-M (0.118 %). [The counting statistics noise for these samples is very low]. With the exceptions of these two REE samples, the range in recoveries in the mining mode is 58-113% at concentrations of Ti >0.03 %.

The soil mode data look much the same as those for the mining mode for BT-B-S, HH-B-S and HH-C-S (not reported by BT-A-S). However, the rotational bias shown by HH-A-S is much less, with a slope of 1.12 vs 0.49 in the mining mode (Fig. 7c). As in the mining mode, Ti in FeR-1 is high by HH-B-S, at 0.781 % (cf. 0.02 % RV). Generally the trimmed soil mode data show similar slopes to the untrimmed. Overall, the results by the soil mode appear slightly superior to those by the mining mode over the entire concentration range (up to ~ 2.5 % Ti). With the exception of GW799305, the average recoveries in the soil mode are in the range 68-125 % for Ti >0.03 %.

Mn, manganese (Figs. 8a, b)

Results for the two stream sediments, PF1002 and 1010, across the instruments are erroneously high: in the range 1.88 % (BT-B-M) to 2.43 % (HH-A-M) for PF1010 (1.41 % SV) and 1.37 % (HH-A-M) to 1.74 % (BT-A-M) for PF1008 (0.79 %, SV). Viewing the trimmed data (Fig. 8a; Mn <2500 ppm), the responses for instruments BT-B-M, HH-A-M and HH-C-M are similar, with best fit lines close to unity and r^2 values of 0.7. There are a few more fliers and a slope of 1.12 for HH-B-M, and large rotational bias for BT-A-M of 1.5, though the fit is good (r^2 of 0.89). Most of data for the ores do not fall on the lines but the worst results by far are for the two REE-enriched samples. Manganese in the heavy REE-enriched GW28209 is extremely low, at <10 ppm, but pXRF results range from 398 to 1067 ppm; the SV for the light REE-enriched GW799305 is 697 ppm but the range in results is 1789-3458 ppm. This is hardly surprising as the L lines of these high concentrations of REEs play havoc on the K lines of the first row transition elements. For example, the $L\alpha$ line of Dy, at 6.5 keV, directly overlaps with the Mn $K\beta$ line (6.49 keV) and the $L\alpha$ line of Gd, at 6.06 keV, overlaps with the Mn $K\alpha$ line (5.90 keV). GW28209 contains 2450 ppm of Dy and 680 ppm of Gd. Thus more positive interferences on other transition elements can be expected for these samples. The Fe $K\alpha$ line (6.4 keV) overlaps

with the Mn K β line and thus it is not surprising that the average recovery for Mn in FeR-1 is 150 % (Appendix 7a).

In the soil mode, the slope of the data for BT-A-S (1.09) is far better than in the mining mode (1.47) and the fit as good (Fig. 8b), but the good results obtained by BT-B-M disappear in the soil mode as the mafic group and the ores diverge dramatically from the line. Results for the remaining three instruments are comparable in the soil and mining modes.

4.3.2.2 Anions P, S, Cl

P, phosphorus (Fig. 9)

The industry detection limit for P is ~ 0.1 %, much too high for most geological materials. Hence there are numerous non-detects in the data-sets for P, except for that of BT-B-M where n=34. Two samples contain >1 % P: FeR-1, at 1.065 % P (RV), averages a 200 % recovery across the instruments; and GW799305, at 7.590 % P (SV), averages a recovery of 110% but the range of values is wide (6.5-12.4 % P). The trimmed plots (Fig. 9, at <~0.4% P, mining mode) show that the best response is by HH-A-M, with a slope of 1.14 and r^2 of 0.90 but there are many values <DL (n=14). Results by BT-A-M are more scattered, with much higher individual SDs and a slope of 1.41 (n=15). There is a lot of scatter in the 27 results (trimmed) by BT-B-M, with an r^2 of 0.36, and the slope is 2.1: with better calibration, this instrument would provide adequate data. The noise and lack of results for HH-B-M and HH-C-M indicate very poor performance (Fig. 9).

Only HH-A-S and BT-A-S reported P in the soil mode; there are many non-detects and samples with <10 positive readings (Appendix 6). These instruments are reporting P at 3.59 and 3.90 % P in the ore MP-1 (0.027 % P, RV). This may be due to Zn sum peaks (L α and L β energies of 1.01 and 1.03 keV) on the P K α line (2.01 keV; 2.14 keV, K β); MP-1 contains 15.9 % Zn. It is hardly surprising that P is not determined well by pXRF: its neighbour is the major element Si, with K α and K β energies of 1.74 and 1.84 keV so P, at much lower concentrations, would be on the shoulder of the Si peak.

S, sulphur (Figs. 10a, b)

The industry detection limit for S is ~ 0.03 %, borderline for many geological matrices. Given the wide range in S concentration in the suite (up to 23.8 % in OREAS 14p) and not specifically calibrating for the ores, the agreement with accepted values for HH-B-M and BT-B-M is remarkably good (Fig. 10a). The slopes are unity and the r^2 values are 0.98 and 0.96. Data points for SU-1 and MP-1 are below the line in both cases and so results are low. For example, by HH-B-M, SU-1 reports 9.437 \pm 0.152 % (12.1 % S, RV) and MP-1 9.902 \pm 0.041 % (11.8 % S, RV). Although slopes are 0.80 and 1.43 for BT-A-M and HH-C-M, the fit is good and recalibration would improve accuracy immensely. Results for HH-A-M are more scattered and the slope is 0.65.

Trimming out the ore results reveals the noise at levels of S <2 % (Fig. 10b); r^2 values range from 0.45 (HH-B-M) to 0.87 (HH-C-M) and slopes are in the range 0.82 (HH-A-M) to 1.74 (HH-C-M). There are numerous fliers but consistently, across the instruments, results are high for stream sediment PF1008 (up to 3.073 % S; cf 1.12 % SV), lake sediment LKSD-4 (up to

2.299 %; cf 0.99 % RV), the potash VSP09 (up to 1.868 %; cf 0.005 % SV), and GW28209 (up to 0.328 %; cf 0.05 % SV).

In the soil mode, the slopes all differ significantly from unity, from 0.42 (HH-C-S) to 1.68 (HH-A-S) (Fig. 10c) and hence the values for the average recoveries are highly variable (Appendix 6). However, the fit to the lines for the ores is good for BT-B-S, HH-A-S (n=11 only) and HH-C-S; considerable scatter is evident for BT-A-S (HH-B-S did not report S in the soil mode). The fit for the trimmed graphs (S <2 %; not shown here) is very poor except for BT-A-S where r^2 is 0.85 and the slope is 1.43.

There are clearly significant differences in performance for S across the instruments. This element is not determined well with an Rh target anode as it would suffer from the scatter of its L lines (Rh $L\beta$ line at 2.83 keV; S $K\alpha$ line at 2.31 keV and $K\beta$ at 2.46 keV).

Cl, chlorine (Fig. 11)

The industry detection limit for Cl is ~ 0.02 %, much too high for most sample types. Unfortunately many of the CRMs lack reference values for Cl and this analysis was not carried out by the sponsoring laboratories (too little sample). The only complete data-set in the mining mode is by HH-C-M; only 5 analyses were >DL for BT-A-M and 12 by BT-B-M (Appendix 7a). However, the results for HH-C-M are nonsense: there is a huge background of hundreds of ppm Cl. The following results provide examples: 545 ppm for SCo-1 (cf 51 ppm RV); 535 ppm for SDC-1 (cf 32 ppm); 455 ppm for JG-1 (cf 60 ppm); 986 ppm for BHVO-1 (cf 92 ppm); and 1025 ppm for GSR-3 (cf 114 ppm). However, the graph (Fig. 11) of the results by HH-C-M shows the mafic/ultra-mafic group and the felsic/intermediate group forming two separate linear steep trends and this begs the question as to whether careful matrix-specific calibration and optimization would make this analysis workable.

The results for the potash VSP09 (46.9 % Cl from Vale, reflecting soluble Cl) are: 63.4 % by HH-C-M; 51.3 % by BT-A-M; and 37.9 % by BT-B-M. It is hard to say whether the other few values by these last two instruments are anywhere near accurate but for one of the several samples where Cl was detected this seems dubious, this being GSR-6 where 488 ppm is reported vs a provisional value of 80 ppm. It must be kept in mind that such values are at the detection limit of the instrument, though some of the SDs belie this (e.g. 408 ± 9.2 ppm in UM-4 by BT-B-M).

In the soil mode, HH-A-S and BT-A-S report some Cl values and of these, the following three are in agreement: 5350 (HH-A-S) and 5790 ppm (BT-A-S) for MP-1; 4798 and 4588 ppm (cf 1.63 % in mining mode) in OREAS 132b; and 83.2 and 86.3 % (cf 51.3 % in mining mode) in VSP09 (46.9 % SV, soluble Cl). It is interesting that in the mining mode Cl in MP-1 is <DL for BT-A-M.

4.3.2.3 Trace elements

Optimal detection limits (based only on counting statistics using pure elements) quoted by the manufacturing industry for the trace elements are in the range 1~30 ppm. Clearly real detection limits are influenced by the sample matrix. Furthermore, some elements are affected by the scatter lines from the target anode, such as Ag by the Rh anode.

Ag, silver

Given the expected concentration of Ag in most geological samples, at <1 ppm, this element will be poorly determined, if at all, by pXRF. The performance of the four instruments reporting Ag in the soil mode varies enormously. Only 2 results are reported by HH-A-S and these are reasonable: 44.5 ppm Ag in the soil NIST 2710 (35.3 ppm RV) and 67.8 ppm in OREAS 132b (61 ppm RV). HH-C-S reports 14 results and, while that for NIST 2710 is good at 32.8 ppm, the ores read high and misleading values of 6.8, 9.0 and 13.3 ppm are reported in DNC-1 (dolerite), MRG-1 and WMG-1 (gabbros), respectively, which contain only 0.03, 0.11 and 2.70 ppm. Data for the 11 samples above DL by BT-A-S are good, even for FeR-1 reported at 4.2 ppm (5.60 ppm RV; cf 45.4 ppm by HH-C-S). Results by BT-B-S for Ag are absolute nonsense, the vast majority at the hundreds of ppm level. There is clearly a background or intercept problem; the SD associated with the mean values are low and the counting statistic errors are similarly low. This same problem exists for the mining mode data for BT-B. The only other results in the mining mode are by HH-C-M and they are good: 44 ppm for MP-1 (57.97 ppm RV), 30 ppm for NIST 2710 (cf 35.3 ppm), and 60 ppm for OREAS 132b (cf 61.0 ppm).

As, arsenic (Figs. 12a, b, c)

The range in As concentrations in the suite is huge, from 0.1 to 7700 ppm. The slopes of the best-fit lines for BT-B-S, HH-B-S, BT-A-S and HH-C-S are all at 0.90 or above (Fig. 12a) whereas that for HH-A-S is high, at 1.37, and consequently the results are significantly higher than the rest. An example of the good agreement is seen in the data for NIST 2709 soil: the first four instruments are reporting 16.7-19.8 ppm Ag (17.7 ppm RV), and HH-A-S is reporting 34.3 ppm. There are two obvious fliers in the data: values for the Zn-Pb massive sulphide OREAS 132b and those for FeR-1 by HH-C-S and BT-C-S (note that they were not reported by the other two instruments, eliminated by the software program). The results for OREAS 132b are 924 and 1064 ppm (cf 155 ppm RV) and for FeR-1 294 and 213 ppm (cf 7.0 ppm RV); note the RSDs for these values are fairly high, at 8-10%. The interference of Pb on As is well known (Pb L α at 10.55 keV on As K α at 10.54 keV). The trimmed graph (Fig. 12b) shows the low results across the instruments for the REE GW799305 (4-29 ppm; cf 88 ppm SV) and for SU-1 across the four instruments (230-331 ppm; cf 588 ppm RV). Otherwise the agreement is good for the four instruments.

In the mining mode recalibration is obviously necessary for BT-A-M and HH-C-M (slopes of 0.48 and 0.62) but there appears to be a curvature (saturation?) above ~ 4000 ppm As for all instruments (Fig. 12c). Thus values for the As-rich MP-1 ore are low at 2300-5290 ppm (cf 7700 ppm RV).

Au, gold

The industry optimal detection limit for Au is ~ 5 ppm, orders of magnitude too high for most geological applications. The results for Au are, for the most part, nonsense (Appendix 6). For example, BT-A-S reports 21.6 \pm 3.7 ppm for OREAS 14p (0.051 ppm RV) and 7.7 \pm 1.1 ppm for GXR-6 (0.095 ppm provisional); in NIST 2710 (0.6 ppm provisional), HH-A-S reports 26.0 ppm and BT-A-S 5.0 ppm. The values for the Au ore, MA-1a, certified at 21.4 ppm are in the range 10.1-15.1 ppm which is fairly good but it is extremely hard for the user to know *when the number is valid* (except that the SD *may* be high). Results for the Zn-Sn ore, MP-1, are in the

range 36-129 ppm: this is due to the interference from Zn (Zn K β line at 9.57 keV on Au L α line at 9.71 keV). These random results for Au strongly suggest that the manufacturer's optimal detection limit of 5 ppm is an *extremely dangerous guide* for those in exploration and mining.

Ba, barium (Figs. 13a, b)

With two exceptions, the data for Ba in the soil mode by BT-A-S are *superb* (Figs. 13a, b). The exceptions are two samples containing unusually high concentrations of light REEs: GW799305 reporting only 1302 ppm Ba (cf 5478 ppm SV); and SY-3 reporting 83 ppm (cf 440 ppm RV). The K and L lines of Ba are very close to those of the light REEs; these low results suggest absorption of Ba fluorescence by the light REEs which is not compensated for by the software program. These samples report low by the other instruments too but not as distinctly. The trimmed graph (Fig. 13b) for BT-B-S is really poor, showing a large degree of noise with erroneously high values for the mafic and ore group (e.g. 336 ppm for the Ni ore OREAS 76a; cf 29 ppm RV) and low for soils (e.g. 621 ppm for NIST 2709; cf 968 ppm RV) and others. HH-C-S behaves very similarly to BT-B-S. The huge SDs (RSDs ~ 25-200%!) associated with essentially all the results by HH-B-S are puzzling; clearly this instrument in its present form is unusable for Ba.

Only the instruments BT-B and HH-C report Ba in the mining mode: results are very similar to those by the soil mode but the SDs are in general significantly greater for BT-B-M (cf BT-B-S).

Bi, bismuth

Bismuth is reported in some samples (many non-detects) by HH-A-S, HH-B-S and BT-A-S but for the most part the data are highly erroneous. Most samples contain Bi at levels well below 1 ppm but, for example, HH-B-S reports Bi in GSP-1 and GSR-1 in the hundreds of ppm. The Bi L β line (13.02 keV) suffers from interference by the Th L α line (12.97 keV). This interference from Th is very evident in the following results: 1257 and 110 ppm in SY-3 (cf 0.29 ppm RV; SY-3 contains 1003 ppm Th) by HH-B-S and HH-A-S, respectively; 147 and 319 ppm in PF1008 (cf 0.21 ppm SV; contains 185 ppm Th) by HH-B-S and HH-A-S, and 207 ppm in PF1002 (cf 0.11 ppm, contains 148 ppm Th) by HH-B-S. Most samples by BT-A-S are reported below detection but it does give a value of 12.8 ± 5.7 ppm Bi for NIST 2710 (cf 19.1 ppm RV) and 220 ± 27.2 ppm for MP-1 (cf 240 ppm RV); unfortunately it reports very high values for OREAS 76a, 14p and PF1008.

Cd, cadmium

The optimal detection limits provided by the manufacturer, of 12-15 ppm for a Rh anode and 6-8 ppm for a Ta anode, are far too high for most geological materials. This is borne out by the soil mode data (Appendix 6). The only samples containing Cd at high enough concentrations to measure are as follows: MP-1, with a range by the pXRF instruments of 403-789 ppm (cf 700 ppm RV); NIST 2710, with a range of 16-29 ppm (cf 21.8 RV); NIST 2711, with a range of 38-60 ppm (cf 41.7 ppm RV); and OREAS 132b, with a range of 158-267 ppm (cf 174 ppm RV). Clearly there are interferences creating erroneously high values by HH-C-S and BT-B-S in the OREAS CRMs and FeR-1. Really in the soil mode only BT-A-S is usable.

The mining mode data are worse, not surprisingly, but of particular concern is the background of several hundred ppm 'Cd' seen for all samples by HH-A-M (Appendix 7a). This was also

evident in the Sb and Sn data-sets for this instrument and was discussed recently with the manufacturer. The reason for this background is that there is significant Compton scattering in this region of the spectrum, common to these three elements, and it is not being corrected for properly at these trace levels. This problem is being addressed currently.

Ce, cerium

The K lines of the first row transition elements play havoc on the REE L lines, those used in measurement, and that is evident in the pXRF data. Cerium was reported for some samples only by HH-B-S (n=7) and BT-A-S (n=24 but for most n <10). The SDs associated with these results are very high (Appendix 6), for example: in GW799305, at 9250 ppm Ce (SV), 15850±417 and 9952±280 ppm are reported by these instruments; and in stream sediment PF1002, at 533 ppm (SV), the reported values are 1515±295 and 523±158 ppm. The precision is better for SY-3 (2230 ppm RV), with results of 2275±106 and 2587±202 ppm, perhaps because of finer particle size and homogeneity. Clearly HH-B-S has a problem with accuracy for the few samples analysed, including the value of 3002 ppm for FeR-1 (cf 7.5 ppm RV!) but the RSD of ~ 50% indicates further investigation is required. This inaccuracy is also evident in the mining mode for BT-A-M in the samples FeR-1, GW799305, PF1002 and SY-3 (Appendix 7a). The results, in addition to those above, reported by BT-A-S where all 10 readings are above detection are: 502±62 ppm in GSP-1 (cf 399 ppm RV); 316±129 in MP-1 (cf 164 ppm RV); 262±93 ppm in PF1008 (cf 211 ppm SV); and 202±96 ppm in SY-2 (cf 175 ppm RV).

Co, cobalt (Figs. 14a, b, c)

The trace element Co sits immediately to the right of the major element Fe in the Periodic Table and therefore suffers considerable interference. The optimal detection limit is ~ 10-20 ppm but in 'real' geological samples it is much higher. This is demonstrated in Figures 14a (full CRM range, dominated by the ores) and 14b (trimmed data, <200 ppm Co). Data for the ores are: much too high (BT-B-S, HH-C-S with slopes of 1.9); much too low (BT-A-S, HH-A-S with slopes of 0.2-0.4); or a bit of both (HH-B-S). For example, the range of results for SU-1 (630 ppm RV) is 138-1430 ppm Co and for OREAS 14p (754 ppm RV) it is 250-1918 ppm. The untrimmed plots for BT-B-S and HH-C-S suggest that a recalibration in the soil mode could lead to decent accuracy in the ores (Fig. 14a). The trimmed graphs show the large positive bias for BT-B-S and HH-C-S, illustrating that these instruments, as programmed, are essentially useless for Co at this concentration range. The performance of HH-B-S is somewhat better but the best results are by HH-A-S and BT-A-S. Some examples of results from these two instruments are: in GXR-5 (29.9 ppm, RV) 22.3±1.3 and 13.1±0.9 ppm; in GSR-3 (46.5 ppm Co, RV; 9.37% Fe) 52.5±2.3 and 34.5±1.4 ppm; and in MRG-1 (87 ppm, RV; 12.55% Fe) 76.6±3.2 and 52.1±1.5 ppm. The results for the mafic group by BT-A-M are low (Fig. 14b), as they are for the ores. It is interesting that two instruments seem to over-correct for Fe whereas a correction by another two instruments is woefully inadequate.

All five mining mode plots (Fig. 14c) for the ore samples containing high concentrations of Co show that a line could be fitted quite well to these data for each instrument so recalibration would bring the results much closer to the truth than they are currently (the ranges for these samples are more or less those evident in the soil mode).

Cr, chromium (Figs. 15a, b, c)

The range in Cr in the suite of CRMs is large, from 5 ppm to 17.7% (UM-4). The best-fit lines in the soil mode over this range are quite good, with slopes mainly of 0.9 and r^2 of 0.98 (Fig. 15a). The ultramafic, UM-4 with an RV of 17.7 % Cr, reports 13.9-19.5 % Cr across the 5 instruments. The peridotite PCC-1, at 2730 ppm (RV) Cr, is reported in the range 2187-2746 ppm. Only HH-B-S reports a value of Cr for FeR-1 (7.0 ppm, RV) and this is highly erroneous, at 6087 ppm. This is likely due to the shoulder of Fe $K\alpha$ 6.4 keV line on Cr $K\beta$ line 5.95 keV) if that is the line being read (see spectra at the beginning of Section 4.3.2). The light REE-enriched samples GW799305 and SY-3 exhibit interference on Cr, with high results of 1117-2934 ppm (30.0 ppm SV) and 245-551 ppm (11.0 ppm RV), respectively. This is caused by the L lines of the light REEs on the K lines of Cr (e.g. Pr $L\beta$ and Nd $L\alpha$ lines on Cr $K\alpha$ at 5.41 keV).

The best-fit lines change considerably for the trimmed plots, up to ~800 ppm Cr and the scatter increases significantly (Fig. 15b). The values for the slope and r^2 are in the range 0.51-1.15 and 0.69-0.76, respectively. The SDs associated with the results by HH-B-S are exceptionally high; only about half the samples are above detection by this instrument. The performances of BT-A-S and HH-A-S are similar and moderately good; however, those of BT-B-S, HH-B-S and especially HH-C-S are poor. Examples of the range in results are: 24-110 ppm for TILL-2 (74 ppm RV); 79-181 ppm for NIST 2709 (130 ppm RV); and 488-833 ppm for WMG-1 (770 ppm RV).

In the mining mode it is quite apparent that the Ni ores and mafic groups form two separate calibrations (Fig. 15c) which would lead to much better accuracy. *This supports the absolute necessity to adjust the slope and intercept according to one's own sample matrix under study.*

Cs, caesium

Instruments HH-C-S and BT-B-S report Cs but the data are unacceptable for the vast majority of samples. The OREAS ores are reported in the hundreds of ppm whereas they contain less than 2.4 ppm Cs. Even in a presumably 'benign' matrix such as a granite, JG-1, Cs is reported at 52 ppm whereas its recommended value is 4.2 ppm Cs. Similarly, high values of 79 and 77 ppm are obtained for the dolerite, DNC-1 (cf 0.21 ppm RV), and 49 and 36 ppm for the basalt, GSR-3 (cf 0.5 ppm RV), by HH-C-S and BT-B-S, respectively.

Cu, copper (Figs. 16a, b)

The trimmed plots (<~500 ppm) for Cu in the soil mode have slopes that are close to unity and are of good fit with only a few exceptions (Fig. 16a); thus most of the data above ~ 10 ppm Cu are excellent. One flier is the result for the heavy REE-enriched GW28209 where four instruments are reporting several hundred ppm Cu whereas the selected value is 0.7 ppm. The Au ore MA-1a, at 248 ppm Cu, is reported low by all instruments, down to a low of 175 ppm, but by and large the agreement is very good. For example, the range for NIST 2709, at 34.6 ppm (RV), is 29-40 ppm (like that for the shale SCo-1, at 29.0 ppm Cu) and that for TILL-2, at 150 ppm, is 140-160 ppm Cu.

There are numerous Cu-rich samples in this CRM suite that would best be analysed by the mining mode. In this mode (Fig. 16b), the best-fit lines are good except for BT-A-M where the slope is 0.57, indicating a recalibration is necessary. Omitting the BT-A-M data, the range in results for the following samples is: 7.00-8.28 % (cf 10.66-13.36 % by soil mode) for OREAS

166 (8.75 % RV); 1.67-1.85 % (cf 3.81-5.29 % by soil mode) for MP-1 (2.09 % RV); and 0.78-0.91 % (cf 0.93-1.09 % by soil mode) for SU-1 (0.87 % RV). It appears that the soil mode could be used to a reasonably high concentration of Cu, certainly to ~3-4000 ppm Cu. For example, the range in results for NIST 2710, at 0.295 % Cu (RV), is 0.305-0.351 % in the soil mode and 0.251-0.311 % in the mining mode, with similar SDs.

Hf, hafnium

Only HH-B-S reports Hf and only in 7 samples. These results are either high or very suspect. In non-ore samples such as the granodiorite, GSP-1, which contains a significant amount of Hf at 15.5 ppm, no value is reported.

Hg, mercury

The manufacturer's optimum detection limit for Hg is 2-4 ppm. All but HH-B-S report Hg, with many non-detects as indeed there should be given Hg's natural abundance in the ppb range. However, there are many reported values in the low ppm to tens of ppm range when the actual CRM concentrations are well below 1 ppm (Appendix 6)! For example, in supposedly non-problematic matrices, Hg is reported at: 8-12.2 ppm in the basalt BHVO-1 (<0.01 ppm SV) and 18.9-25.6 ppm in the gabbro MRG-1 (0.14 ppm SV). The few results (in ores) reported by HH-C-S are wild, for example: 751 ppm in MP-1 (0.06 ppm Hg SV) and 250 ppm in OREAS 132b (0.74 ppm SV), probably due to the shoulder of the Zn L β line (9.57 keV) on the Hg L α line (9.99 keV). BT-A-S reports Hg in the vast majority of samples, from 2 to 40 ppm! The only result that stands out in this sea of inaccuracy is that for NIST 2711 (6.25 ppm RV), in the range 8.4-15.1 ppm. But how would the user identify this sole value as being acceptable given the rest? The manufacturers have much work yet to do on this element, as was evident for Au: not reporting values below reasonable (i.e. *much higher*) detection limits would benefit users enormously.

La, lanthanum

Only BT-A-S reports La. Readings for much of the data at levels of La in the low tens of ppm are below 10, indicating a problem with detection. However, given that the RSDs are mostly in the range 23-100 %, the mean values agree *remarkably well* with the CRM RV or selected values. For example, note the following results: 53.1 vs 54 (RV) ppm in GSR-1; 24.2 vs 22.4 ppm in JG-1; 36.8 vs 23 ppm in NIST 2709; and 26.6 vs 24 ppm in RGM-1. This suggests that multiple readings would compensate for the poor precision. The precision and accuracy in the two light REE-enriched samples are excellent: 3912 \pm 107 (3 % RSD) in GW799305 (3880 ppm SV); and 1523 \pm 62 ppm in SY-3 (1340 ppm RV).

Mo, molybdenum (Fig. 17)

The manufacturer's optimum detection limit for Mo is in the 1-3 ppm range. All instruments report Mo but HH-B-S provides data for only 4 samples and HH-A-S for about half the suite; the highest concentration of Mo in the CRMs is only 140 ppm. With two fliers eliminated (BL-2a and PF1008), the slopes for BT-A-S (n=31) and BT-B-S are ~1.02, with r^2 values of 0.87 and 0.97, respectively (Fig. 17). These instruments are reporting 103-272 ppm Mo in BL-2a (15.0 ppm RV) and 107-270 ppm (63.0 ppm SV) in PF1008; both these samples are very high in U (BL-2a, 4260 ppm U and PF1008, 2730 ppm U), and the U L β line (17.22 keV) is close to the Mo K α line (17.48 keV). A few other less dramatic fliers are seen in these instruments' data for

SY-2, SY-3 (also high in U) and GW28209, all containing Mo below 2 ppm but reporting in the range 17-34 ppm.

The results for HH-C-S are good except for the above mentioned problematic samples but the values for these are not so erroneously high (e.g. 74 ppm for BL-2a) as reported for the former two instruments. HH-A-S suffers from a positive bias, with a slope of 1.47, and thus all results are high except, strangely, for PF1008 which is under-reported at 31.2 ppm (cf 63.0 ppm SV and the other high results above). Ignoring the data by HH-A-S and HH-B-S, the following results show the performance that can be obtained in the soil mode by pXRF: 115-135 ppm in MA-1a (124 ppm RV); 105-149 ppm in MP-1 (140 ppm RV); 35-40 ppm in GXR-5 (31 ppm RV); and 16-20 ppm in TILL-2 (14.0 ppm RV).

Nb, niobium (Figs. 18a, b)

There are only two complete data-sets for Nb, by BT-A-S and HH-A-S; HH-B-S reports the elements in only 9 samples. The best performance is definitely given by BT-A-S, with a slope of 1.0 and an r^2 of 0.91 (Fig. 18a). Examples of such accuracy are 26.6 vs 27.9 ppm (RV) in GSP-1, 40.5 vs 40.0 (RV) in GSR-1 and 6.0 vs 6.7 ppm in GXR-5. The fliers in this data-set are: 233 ppm in SY-3 (148 ppm RV); 26.0 ppm in FeR-1 (1.0 ppm RV) and 51.1 ppm in BL-2a (10.7 ppm RV). The results by HH-A-S are somewhat high, the slope of the best-fit line being 1.26 (r^2 0.96). The trimmed plots, with Nb <35 ppm, show the good results by BT-A-S at low Nb concentrations and the moderately high bias of values obtained by HH-A-S (Fig. 18b).

The very poor mining mode data for Nb illustrate interferences in U- and Y-enriched samples. For example, the range of values reported in GW28209 (1.35 % Y) is 1280-1372 ppm Nb (cf 2.5 ppm SV) and in SY-3 (718 ppm Y) it is 305-362 ppm (cf 148 ppm SV). The Y $K\beta$ line (16.74 keV) overlaps with the Nb $K\alpha$ line (16.62 keV).

Nd, neodymium

Only BT-A-S reported Nd: the data, in the hundreds of ppm, are nonsense, as indicted by the very high SDs and the number of times not all 10 readings report values (Appendix 6). This would have been a good suite to test pXRF for Nd as the range in concentrations is large.

Ni, nickel (Figs. 19a, b, c)

The optimum detection limit stated by a manufacturer for Ni is 10-20 ppm, inadequate for many geological samples and hence there are numerous non-detects in the CRM data. The range in Ni concentrations in the CRM suite is 2 ppm in the granite GSR-1 to 7.6 % in the NiS ore OREAS 76a. In the soil mode, BT-A-S, BT-B-S and HH-C-S do surprisingly well at high concentrations of Ni (Fig. 19a). For example, they report 1.87-2.06 % (cf 2.10 % RV) for OREAS 14p, with very low SDs. Although the value of 7.39 % Ni in OREAS 76a by BT-B-S is accurate (7.40 % RV), it would be unwise to use the soil mode to such high concentrations and certainly not beyond ~ 1 % for HH-A-S and HH-B-S. At more moderate Ni levels, the range in values for all instruments except HH-A-S is acceptable, at: 0.19-0.23 % (cf 0.25 % RV; 0.33 % by HH-A-S) in UM-4; and 0.19-0.25 % (cf 0.27 % RV; 0.34 % by HH-A-S) in WMG-1. Again, the RSDs at these levels across the 10 readings is very low, at ~ 1 %. There is an obvious interference from Yb ($L\alpha$ line at 7.42 keV) on Ni ($K\alpha$ line at 7.48 keV) in the heavy REE-enriched sample GW28209: it contains only 9 ppm Ni but Ni is reported by these instruments from 328 ppm (HH-

B-S) to 1202 ppm (HH-A-S). This is also in evidence for: GW799305 (range of 64-217 ppm; cf 10.5 ppm SV); PF1002 (range of 119-320 ppm; cf 28 ppm SV); and SY-3 (range of 27-109 ppm; cf 11 ppm RV). As expected, the Cu ore OREAS 166 suffers from huge interference in the determination of Ni, its neighbour in the Periodic Table, and is (wisely) not reported by most instruments but it is by HH-B-S at 937 ppm (cf 94.5 ppm RV).

Linearity and noise are problematic at levels of Ni under ~ 300 ppm for BT-A-S and HH-A-S (Fig. 19b). What data there are (n=19 and 10, respectively) cannot be relied upon. BT-B-S and HH-C-S behave similarly, with slopes of 0.75 and 0.88 but poor r^2 values (0.33, 0.13); the performance of HH-B-S is certainly superior (r^2 of 0.96) but it reports fewer samples (n=12). The four samples in the mafic group are quite well determined by these three instruments at this low level.

Linearity over the large range is good by the mining mode, though less so for HH-B-M (Fig. 19c). Recalibration is required in order to obtain accurate results, especially for the instruments BT-A-M (slope of 0.47) and HH-C-M (slope of 0.77). Linearity at the low levels for the mafic group is also good.

Pb, lead (Figs. 20a, b, c)

The general pXRF optimal detection limit for Pb is 2-5 ppm, and like Ni, too high for many samples. The range of Pb concentration in the CRM suite is from 2 ppm to 3.88 % in OREAS 132b. The untrimmed graphs for Pb by the soil mode for BT-A-S, BT-B-S, HH-B-S and HH-C-S indicate that a fairly good linear relationship exists to ~ 4 % Pb, with slopes close to unity (Fig. 20a). Results for OREAS 132b are in the range 3.79-4.69 % whereas those for MP-1 report a little low at 1.42-1.73 % (cf 1.88 % RV). Data for NIST 2710, in the range 0.532-0.574 % (cf 0.553 % Pb RV) and for FeR-1, in the range 0.527-0.574 % (0.52 % RV), are excellent. HH-A-S, however, shows a strong positive bias, with a slope of 1.57 and r^2 of 0.99.

Results at low Pb levels (<~150 ppm; Fig. 20b) are excellent by BT-B-S and HH-C-S, for example: 93 and 97 ppm in SY-2 (cf 85 ppm RV); 86 and 96 ppm in LKSD-4 (cf 91 ppm RV); and 46 and 56 ppm in GSP-1 (cf 55 ppm RV). The data by BT-A-S are almost as good but there are two fliers: 385 ppm in OREAS 14p (cf 20 ppm RV) and 192 ppm in OREAS 76a (cf 13 ppm RV). A high bias is shown by HH-A-S (slope of 1.26). Results by HH-B-S at low Pb levels are poor, the precision is not that of the other instruments (which is excellent) and only about half the samples are reported.

The mining mode data do not appear to be quite as good as the soil mode at high concentrations, though precision is about the same; recalibrations would be required for BT-A-M and HH-A-M (Fig. 20c). Linearity compared to the soil mode at high Pb levels is not as good for HH-A-M and HH-B-M.

Pd, palladium

Instruments HH-B-S, HH-C-S and BT-B-S report Pd, all at highly erroneous values. HH-B-S is by far the worst, with a background problem in the tens of ppm Pd! For the one sample that is known to contain more than 0.01 ppm Pd, that is WMG-1 at 0.382 ppm Pd, HH-C-S reports 12.6 ± 1.1 ppm, BT-B-S reports 4.9 ± 1.2 ppm and HH-B-S gives below detection.

Rb, rubidium (Fig. 21)

Rubidium is extremely well measured by pXRF, as illustrated by the untrimmed soil mode plots with slopes of 0.86 to 1.15 and r^2 values better than 0.90 (Fig. 21). The few fliers that degrade the best-fit lines comprise: BL-2a at 21-315 ppm Rb (cf 19.8 ppm RV); FeR-1 at 15-163 ppm (cf 0.6 ppm RV); and PF1008 at 35-307 ppm (cf 43.3 ppm SV). The high U concentrations in BL-2a (4260 ppm U) and PF1008 (2730 ppm U) are the cause of their erroneously high Rb values (U $L\alpha$ line at 13.61 keV overlapping on Rb $K\alpha$ line at 13.4 keV). HH-C-S actually handles this interference from U completely, reporting values of 20.8 ± 2.5 ppm for BL-2a and 35.1 ± 2.5 ppm for PF1008. Examples of good data across the instruments are: 90-114 ppm (cf 114 ppm SV) in GW799305; 81-95 ppm (cf 96 ppm RV) in NIST 2709; 26-32 ppm (cf 25.8 ppm RV) in SU-1; and 409-477 ppm (cf 466 ppm RV) in GSR-1.

Sb, antimony (Fig. 22)

The manufacturers' optimum detection limit for Sb is ~15-20 ppm, too high for most geological samples. All instruments except HH-B-S report Sb in the soil mode but naturally there are many non-detects (Appendix 6). BT-A-S does remarkably well, even though SDs at these low levels are high and not all 10 readings were >DL. Some examples are: 8 ± 2.8 ppm (cf 7.9 ppm RV) in NIST 2709; 39 ± 3 ppm (cf 38.4 ppm RV) in NIST 2710; and 21 ± 3.9 ppm (cf 17.48 ppm RV) in OREAS 166. A longer beam time (currently at 60 s) might well improve the results at levels of a few ppm Sb. The data reported by the other instruments are very poor and erroneously high.

The instrument HH-A in the mining mode reports a background of about several hundred ppm Sb in all samples, as is the case for Cd and Sn (Appendix 7b). The cause of this is an inadequate correction for the Compton scatter in this region of the spectrum.

Sc, scandium

Only BT-B-S and HH-C-S report Sc and the results are nonsense. Most samples are < 20 ppm in Sc but most of the values reported are in the tens to several hundred ppm (Appendix 6).

Se, selenium

The manufacturer's optimum detection limit for Se is 1-3 ppm, much too high for most geological samples. All five instruments report Se in the soil mode but the vast majority of data are below detection and many of those reported by HH-B-S are at 10 ppm, obviously the detection limit for that instrument. Where Se is high enough in the samples, it is reported at: 51-56 ppm (HH-C-S, BT-A-S, BT-B-S) in OREAS 14p (cf 41.5 ppm RV); 17-34 ppm (all but HH-C-S) in SU-1 (cf 21 ppm RV); and 13-22 ppm (all instruments) in WMG-1 (cf 15 ppm RV). HH-B-S is not dealing with interferences well as it reports values over 10 ppm for samples such as GSR-6, SY-2, SY-3 and VSP09, all of which contain < 0.1 ppm Se; the other instruments do not report values for these samples.

Sm, samarium

Only BT-A-S reports Sm, in 8 samples and in half of these not all 10 readings are above detection. Standard deviations are very high. Even though GW28209 contains 70 ppm Sm, it is not detected and the value reported for GW799305 is 322 ± 66 ppm, much lower than its accepted value of 790 ppm Sm. The two other examples (n=10) are: 52 ± 19 ppm (cf 14.4 ppm SV) in

PF1010; and 94 ± 30 ppm (cf 112 ppm RV) in SY-3. Samarium is not adequately determined by tube-based pXRF.

Sn, tin

The manufacturer's optimum detection limit for Sn is 20-25 ppm. All samples except FeR-1 (59 ppm Sn) and MP-1 (2.43 % Sn) contain Sn at levels below 13 ppm. All instruments report Sn but most values are <DL. However, BT-B-S clearly has a background problem for Sn as tens of ppm are reported in almost all samples (Appendix 6). Unlike the other instruments, BT-A-S reports remarkably accurate, though imprecise, data at low Sn levels, for example: 12 ± 3 ppm in NIST 2710 (cf 7.5 ppm RV); 14 ± 2 ppm in GSR-1 (cf 12.5 ppm RV); 8 ± 1 ppm in GSP-1 (cf 6.6 ppm RV); and 9 ± 2 ppm in MA-1a. This suggests that longer beam times may improve precision for this element and it would be the only instrument in this group capable of determining Sn at these low levels. HH-C-S shows sporadic highs in the tens of ppm (e.g. in DNC-1, MRG-1, WMG-1, VSP09, UM-4 and OREAS CRMs). Values range across the instruments from 73 to 221 ppm in FeR-1 (59 ppm RV) and from 2.13 to 7.69 % in MP-1 (2.43 % RV).

In the mining mode the same troublesome background in the tens of ppm is present for BT-B-M. The problem of poor correction for Compton scatter that is evident for Cd and Sb is also present for Sn by HH-A-M (and hence all samples show a huge background of several hundred ppm Sn). Values for the two CRMs highest in Sn concentration, FeR-1 (59 ppm Sn RV) and MP-1 (2.43% Sn RV), are in the ranges 11-177 ppm and 0.71-3.03 %, respectively. A recalibration, with more standards at high Sn concentrations, would be required to improve accuracy.

Sr, strontium (Figs. 23a, b)

Strontium is very well determined by pXRF, with slopes essentially unity and most r^2 values of >0.98 for the range from 1 to 5180 ppm Sr (Fig. 23a). The r^2 value for BT-A-S is degraded principally because of its odd very low value for the highest CRM, GW799305, reporting at only 1458 ppm. It is the two GW REE samples that tend to deviate from the best-fit lines; their values by the two commercial labs were not in the excellent agreement evident for other elements. Examples of good data amongst the instruments at high Sr concentrations are for: GSR-2 (790 ppm RV), in the range 773-847 ppm; GSR-3 (1100 ppm RV), in the range 960-1185 ppm; and MA-1a (650 ppm RV), in the range 564-643 ppm. The trimmed plots show slopes close to unity for all instruments, with excellent values of r^2 , 0.97-0.99, except for BT-A-S where there are a few fliers (Fig. 23b). These comprise the stream and lake sediments which are handled better by the other instruments. BL-2a tends to under-report by BT-B-S, HH-B-S and HH-C-S (195-228 vs 275 ppm RV), as does SGR-1 in most instruments (353-377 vvs 420 ppm RV). However, the agreement overall is excellent.

The mining mode, reported by BT-B-M, HH-B-M and HH-C-M, shows equally good data BUT recalibration is necessary, especially for HH-C-M with a slope of < 0.6 . HH-B-M reports a strangely high value of 1474 ppm in GSR-6, certified at 913 ppm.

Ta, tantalum

Tantalum in the CRM suite is below 7 ppm and at this level pXRF is hopeless, as shown by the results for HH-B-S and BT-A-S (Appendix 6). A background of tens of ppm Ta is evident in all results by BT-A-S (and in the mining mode), rising to 206 ppm in FeR-1 (0.05 ppm Ta RV).

Te, tellurium

In the CRM suite the vast majority of the samples contain Te at levels well below 0.1 ppm, several at a few ppm and MA-1a at 26 ppm. Thus one would not expect Te to be offered for geological materials by pXRF but it is reported by BT-B-S and HH-C-S. As expected, results are nonsense by both instruments, in the tens if not hundreds of ppm Te (Appendix 6). For MA-1a (26 ppm RV), Te is reported at 113 ppm and 37 ppm by HH-C-S and BT-B-S, respectively, but one can hardly rely on 37 ppm as being an accurate number when other samples with <0.1 ppm Te also give similar or higher numbers.

Th, thorium (Figs. 24a, b)

The manufacturer's optimum detection limit for Th is 2-4 ppm. The range in Th concentration in the CRM suite is from <1 to 1003 ppm in SY-3. Performance varies considerably amongst the four instruments reporting (Fig. 24a). Over the entire concentration range, the slopes for BT-A-S, BT-B-S and HH-C-S range from 0.83 to 1.19, with r^2 values of 0.80 to 0.99. There is a *huge* positive bias for HH-A-S, with a slope of 5.1! Eliminating the latter's data, the range in results for some samples is as follows: 88-112 (cf 106 ppm RV) in GSP-1; 53-63 ppm (cf 54 ppm RV) in GSR-1; and 84-282 ppm (cf 50.1 ppm RV) in MP-1, clearly a problematic matrix. REE-enriched samples are highly variable; BT-A-S reports 158 ppm in GW28209 (cf 4.0 ppm SV) and only 153 ppm in GW799305 (cf 637 ppm SV). At low levels of Th (<~55 ppm): HH-A-S continues to be useless; HH-C-S shows a high bias for the ores; BT-B-S shows a somewhat lower bias for the ores and a small translational bias; and BT-A-S performs the best but with a small translational bias (Fig. 24b). For example, some of the low-level data for BT-A-S are: 6.8 vs 5.6 ppm (RV) in GXR-5; 5.8 vs 5.3 ppm in GXR-6; 14.5 vs 13.5 ppm in JG-1; 15.4 vs 15.1 ppm in RGM-1; and 17.3 vs 18.4 ppm in TILL-2.

U, uranium (Figs. 25a, b)

The manufacturer's optimum detection limit for U is 2-4 ppm. The CRMs range in U concentration from <1 to 4260 ppm in BL-2a. The slopes of the best-fit lines (untrimmed data) vary from 1.00 for BT-A-S to 1.25 for HH-A-S (Fig. 25a). HH-A-S reports results down to only ~ 10 ppm and hence there are many non-detects. The results for U ore BL-2a fall well below these lines for BT-A-S, BT-B-S and HH-B-S, and hence its values are generally low, in the range 2860 to 5577 ppm. Results for SY-3 are much better, at 639 to 773 ppm (cf 650 ppm RV), with excellent RSDs of ~1 %.

The trimmed plots, at levels of U <~130 ppm, show that the various ores are not well handled and report high by all four instruments, especially by BT-A-S and the data by HH-B-S are essentially unusable (Fig. 25b). 'Benign' samples show good agreement between BT-A-S and BT-B-S, the best performers being: 18.0 and 15.4 ppm in GSR-1 (18.8 ppm RV); 39 and 34 ppm in LKSD-4 (31 ppm RV); 27.9 and 29.1 ppm in NIST 2710 (25 ppm RV); 5.1 and 7.1 ppm in RGM-1 (5.1 ppm RV); and, 6.7 and 8.2 ppm in SGR-1 (5.4 ppm RV).

V, vanadium (Fig. 26)

The manufacturer's optimum detection limit for V is 7-15 ppm. The range in concentration in the suite is 7 to 678 ppm in BL-2a. The untrimmed graphs show: unusable results by HH-B-S; a high degree of scatter in results by BT-A-S and HH-A-S with slopes of ~ 0.4 from unity; quite good

data by BT-B-S and HH-C-S but with a fair amount of noise (r^2 of ~ 0.6) and some curvature towards low results above ~ 300 ppm V (Fig. 26). Some examples of the data by these last two instruments are: 93 and 108 ppm in GSR-2 (cf 96 ppm RV); 120 and 124 ppm in NIST 2709 (cf 112 ppm RV); 159 and 151 ppm in UM-4 (105 ppm RV); 552 and 494 ppm (i.e. low) in BL-2a (cf 678 ppm RV); and 72 and 72 ppm in LKSD-4 (cf 49 ppm RV). These instruments report high for GW799305 and SY-3, at 546 and 518 ppm for the former (cf 73 ppm RV) and 179 and 190 ppm for the latter (cf 50 ppm RV). This is caused by Ce concentrations of 0.92% and 0.22% in these two samples: the $L\alpha$ line of Ce (4.84 keV) overlaps with the $K\alpha$ line of V (4.95 keV).

The mining mode graphs for V show: a huge positive bias for BT-A-M and HH-C-M (slopes of 2.7, 2.1 and r^2 of <0.1) and much scatter; a slope of 1.78 for BT-B-M but much less scatter (r^2 of ~ 0.6); a slope of 1.2 for HH-A-M but again a lot of scatter; and unusable data by HH-B-M. Thus a recalibration for BT-B-M would provide the best chance of some degree of accuracy at high V levels.

W, tungsten

The manufacturer's optimum detection limit for W is 3-5 ppm. The vast majority of the samples contain W below 12 ppm and hence there are many non-detects in the results by the five instruments. The data are deplorable. The ores are reported in the tens to hundreds of ppm (even thousands, in SU-1 and OREAS 76 and 14p) when in fact W is <10 ppm. MP-1, containing the highest concentration of W at 181 ppm, is reported to have 874-2703 ppm. Even NIST 2710, at 93 ppm W, has a range in results of 206-429 ppm. A few decent results (hard to find), by the BT instruments, are for GSR-1 (18-20 ppm; cf 8.4 ppm RV), MA-1a (27-38 ppm; cf 20 ppm RV), and NIST 2711 (10-23 ppm; cf 3 ppm RV).

Y, yttrium (Fig. 27)

Only BT-A-S and HH-A-S report Y. Over the whole concentration range, up to 1.35 % Y, the slopes and r^2 values are essentially unity. Some examples of results at the higher levels comprise: 1.41 and 1.45 % in GW28209 (cf 1.35 % SV); 476 and 479 ppm in GW799305 (cf 514 ppm SV); 492 and 378 ppm in PF1002 (cf 460 ppm SV); 603 and 667 ppm in SY-3 (cf 718 ppm RV); and, not quite as good, 209 and 356 ppm in MP-1 (cf 209 ppm RV).

The trimmed plot (at $Y < \sim 120$ ppm) shows excellent results by HH-A-S, with a slope of 0.97 and r^2 of 0.91 (Fig. 27). The only fliers are a few ore samples (OREAS 132b, 166 and BL-2a), and their lack of agreement is not that serious; otherwise the data are superb. Results by BT-A-S are not as good, with more noise created essentially by the ore samples reporting high.

Zn, zinc (Figs. 28a, b)

The manufacturer's optimum detection limit for Zn is 3-5 ppm, more than adequate for geological materials. The range in Zn concentration in the CRM suite is from 2 ppm to 15.9 % in MP-1. Not surprisingly, the untrimmed graphs in the soil mode show a deviation from linearity above ~ 1 % Zn. With the exception of HH-A-S, the instruments report Zn in NIST 2710 in the range of 0.65-0.72 %, in good agreement with the RV of 0.69 %. Viewing the trimmed soil mode graphs ($Zn < \sim 350$ ppm), the best performance appears to be that by BT-B-S and HH-C-S with slopes of 0.91-0.93 and r^2 of ~ 0.90 (Fig. 28a). The other three instruments seem to have a small rotational bias. At these levels, with a few exceptions, the recoveries are excellent, in the

90-110 % range (Appendix 6). As expected, the Cu ore OREAS 166 suffers from interference on Zn from Cu (neighbours in the Periodic Table) and Zn is reported high by HH-A-S and BT-A-S; however, this correction seems to be well handled by HH-B-S. The few remaining inaccuracies comprise: 55-169 ppm in the GW28209 (cf 2 ppm SV); 924 ppm in PF1008 (cf 673 ppm SV) by HH-A-S; and by BT-B-S, 125 ppm in OREAS 76a (cf 49 ppm RV) and 353 ppm in SU-1 (cf 300 ppm RV).

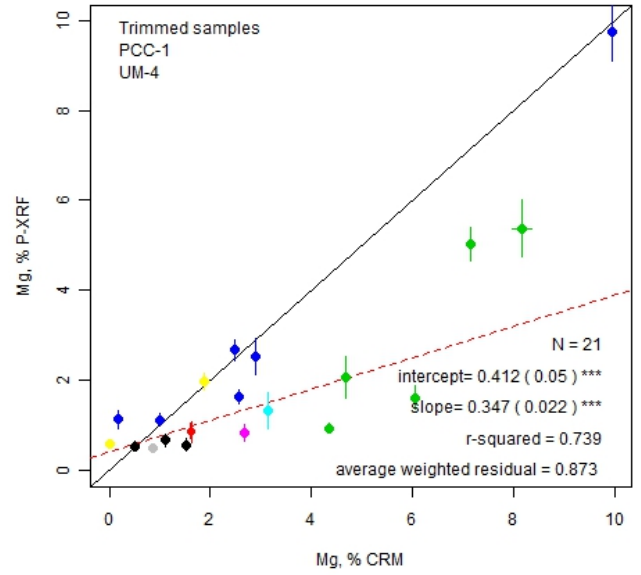
In the mining mode, with the exception of that for BT-A-M, the slopes of the four best-fit lines across the concentration range vary from 0.92 to 1.14 with r^2 values essentially of 1 (Fig. 28b). Results for Zn (except those by BT-A-M) at these high levels are: 13.2-16.6 % in MP-1 (15.9 % Zn); 4.64-5.92 % in OREAS 132b (5.19 % RV); and 0.41-0.51 % in FeR-1 (0.36 % RV).

Zr, zirconium (Figs. 29a, b)

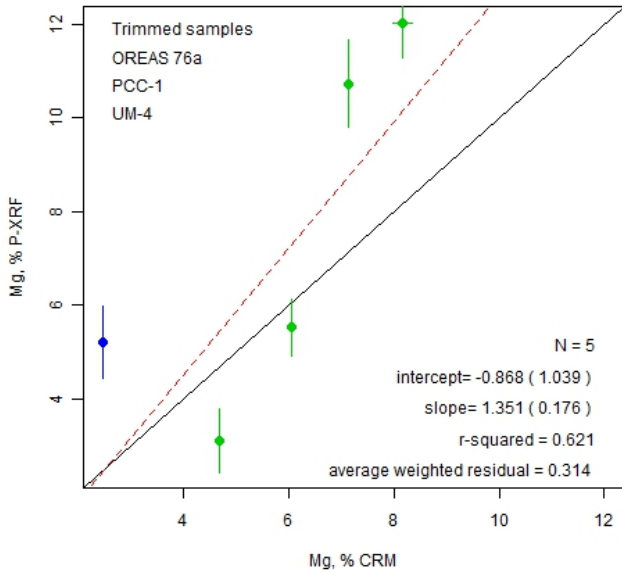
The manufacturer's optimum detection limit for Zr is 1-3 ppm so it should be well determined in geological materials by pXRF. The range in Zr concentrations in the CRM suite is 6-1000 ppm. Over this range the slopes in the soil mode vary from 0.71 (BT-A-S) to 1.18 (HH-B-S) and the r^2 values from 0.84 (HH-B-S) to 0.95 (BT-A-S) (Fig. 29a). BT-B-S did not report Zr. The three stream sediments consistently fall off these lines and report at: 382-590 ppm for PF1002 (cf 650 ppm SV); 201-338 ppm for PF1008 (cf 113 ppm SV); and 618-900 ppm for PF1010 (cf 1000 ppm SV). Viewing the trimmed graphs (Zr <~400 ppm), HH-B-S and HH-C-S perform very well, with slopes close to unity and r^2 values of ~0.86 (Fig. 29b). [The SD bars on the x-axis for the two GW samples are particularly wide because the ALS and SGS lab results do not agree]. There are a few fliers for these two data-sets but by and large the results are very good, for example: 33 and 38 ppm vs 41 ppm (RV) in DNC-1; 173 and 189 ppm vs 174 ppm in BHVO-1; 167 and 185 ppm vs 167 ppm in GSR-1. Neither instrument reports results for FeR-1 (25 ppm Zr) or PCC-1 (16 ppm). Though the data are slightly tighter, the slopes of the best-fit lines for BT-A-S and HH-A-S are inferior to those of the former instruments, at 0.71 and 0.79, respectively. Recoveries across the instruments are low for SU-1 (140 ppm Zr RV), at 58 %, and for UM-4 (27 ppm Zr), at 47 %. As seen for other elements, the REE-enriched samples – GW799305, GW28209, SY-2 and SY-3 – are problematic, with much more noise associated with their results, below and above the RV value (e.g. 168-467 ppm in SY-3; 320 ppm RV).

The data in the mining mode are very noisy for all instruments except HH-C-M and the results for the difficult sample types mentioned above are worse (e.g. by BT-B-M, 1669 ppm for SY-3!). The results by BT-B-M for the two U-enriched samples, BL-2a (4260 ppm U) and PF1008 (2730 ppm U), are hugely erroneous, at 8432 ppm Zr (cf 227 ppm RV) and 6833 ppm (cf 362 ppm SV). [Could these be caused by U escape peaks from the U $L\beta$ line on Zr $K\alpha$?]. The soil mode and Compton normalization compensates nicely by BT-B-S, producing results of 195 ppm in BL-2a and 245 ppm in PF1008.

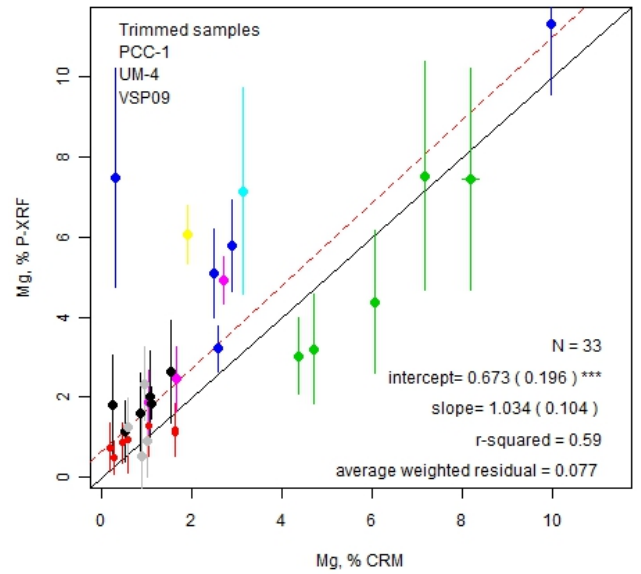
Benchtop-BTBM-Mining Mode



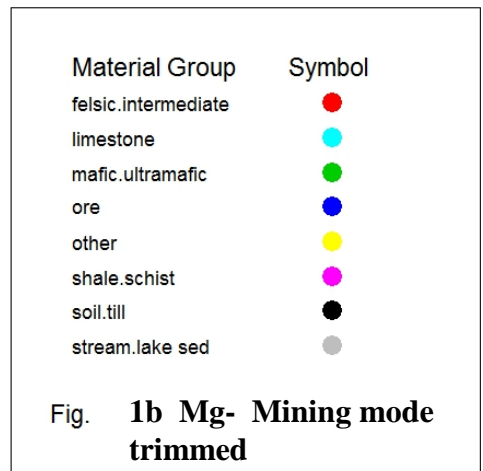
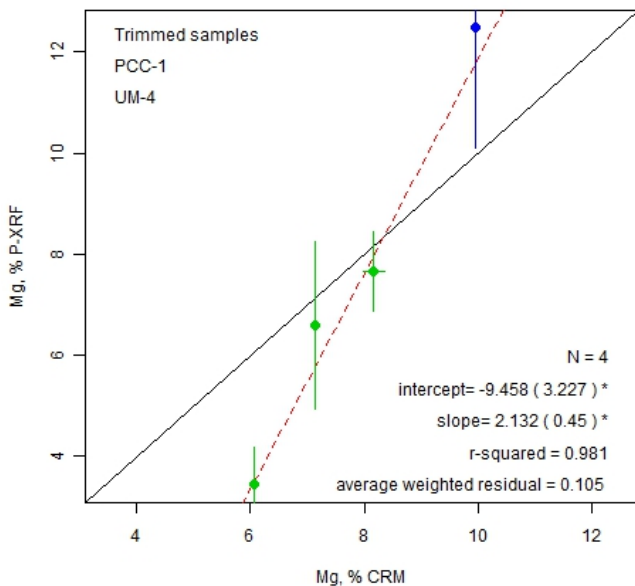
Handheld-HHAM-Mining Mode



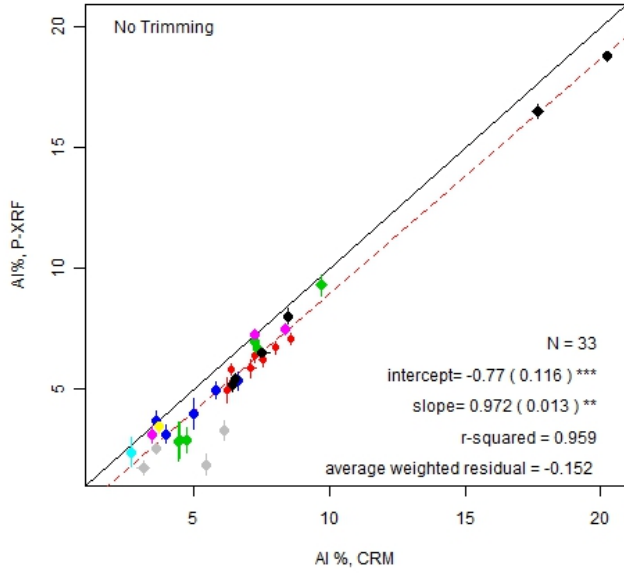
Handheld-HHBM-Mining Mode



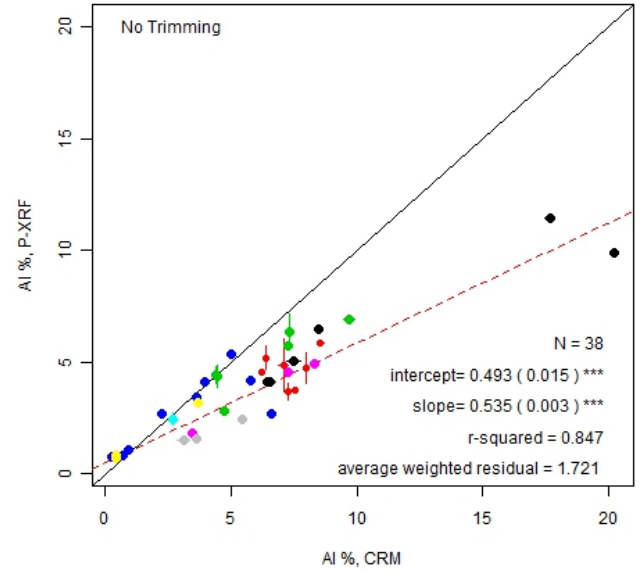
Handheld-HHCM-Mining Mode



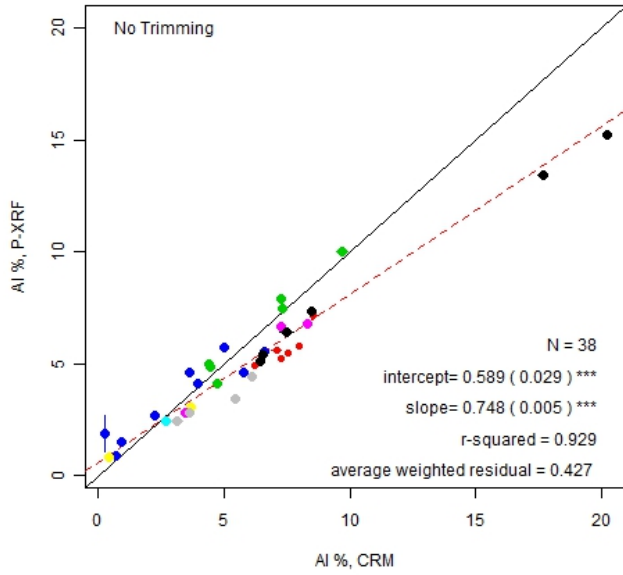
Benchtop-BTAM-Mining Mode



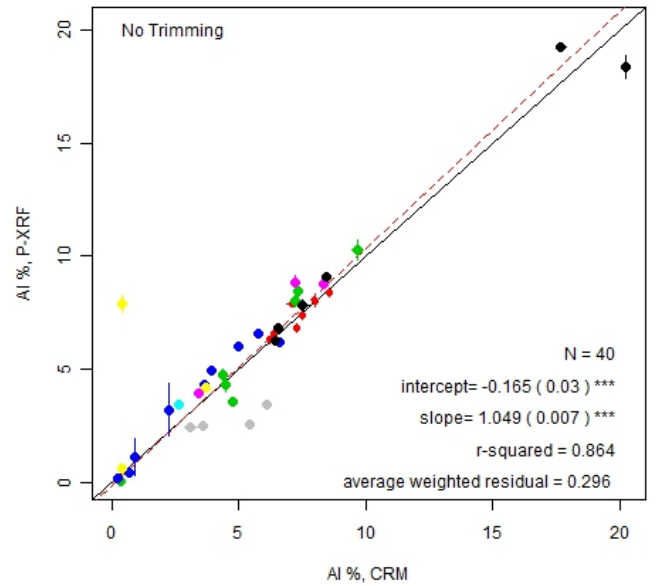
Benchtop-BTBM-Mining Mode



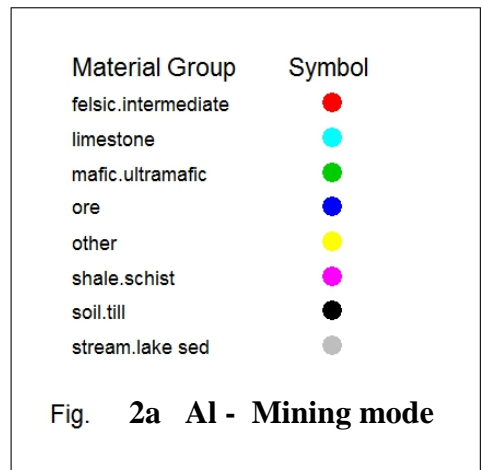
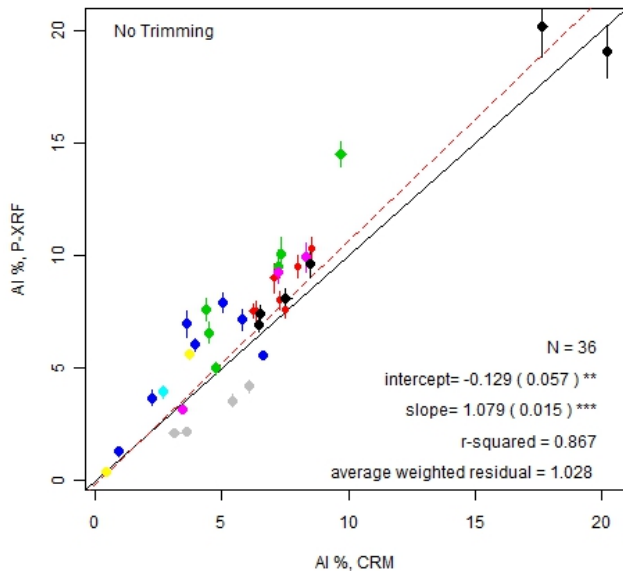
Handheld-Machine A-Mining Mode



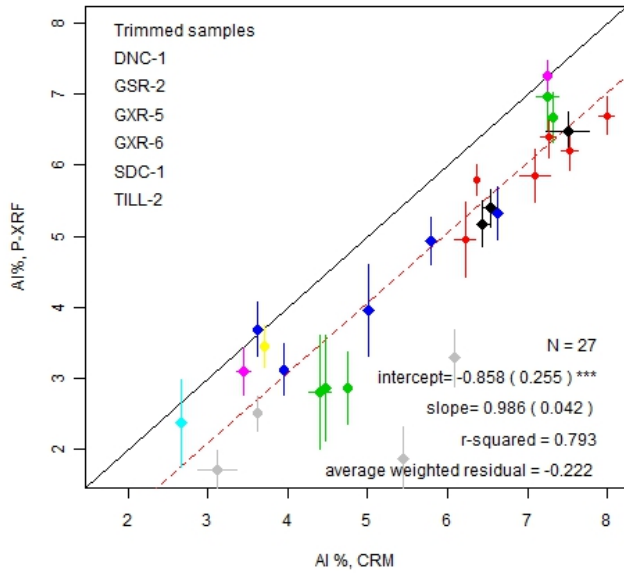
Handheld-HHBM-Mining Mode



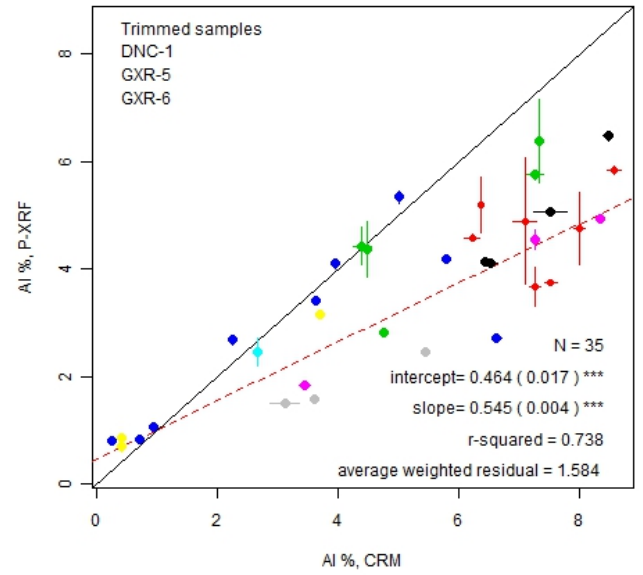
Handheld-HHCM-Mining Mode



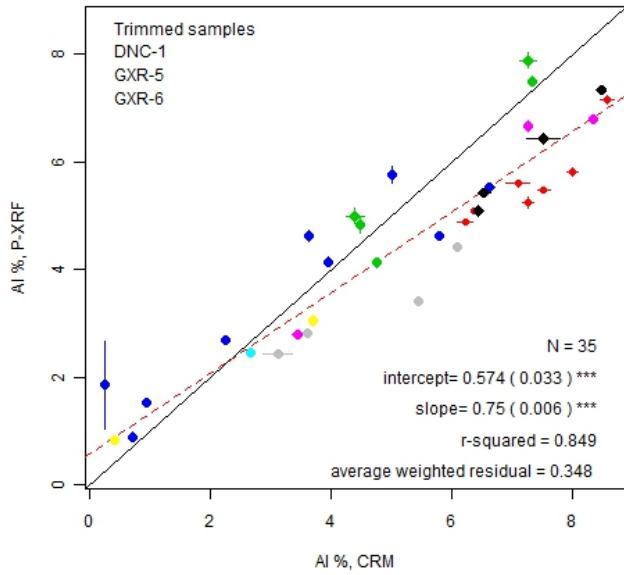
Benchtop-BTAM-Mining Mode



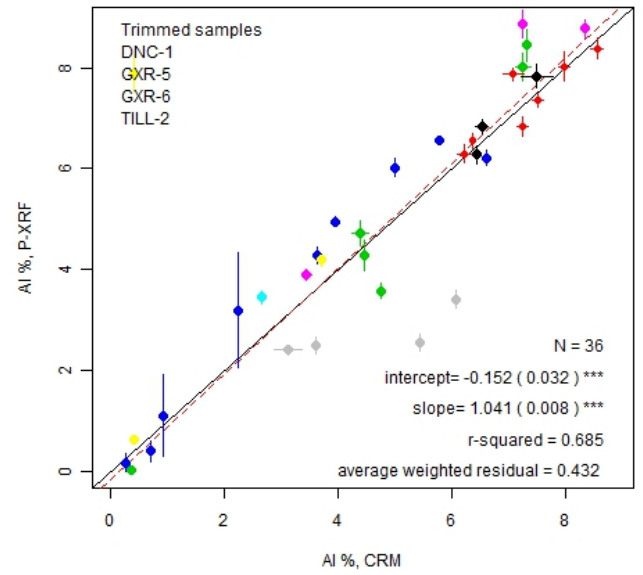
Benchtop-BTBM-Mining Mode



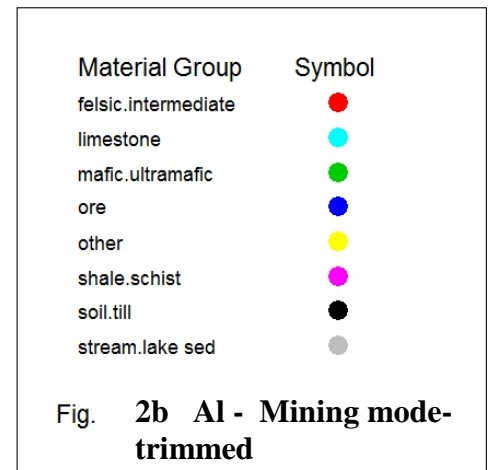
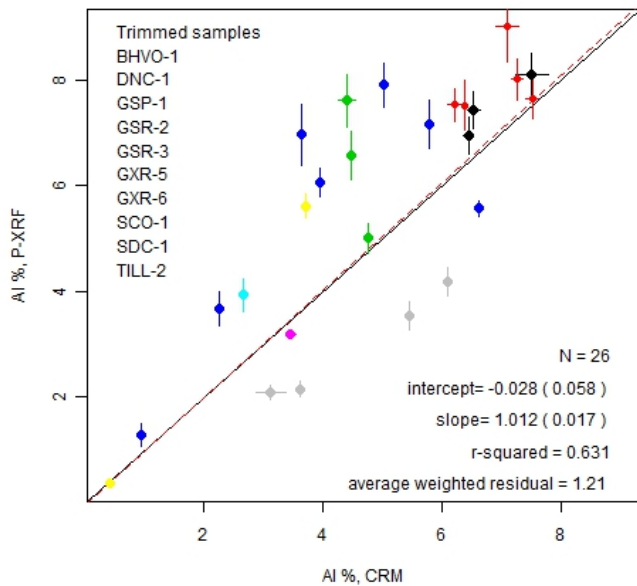
Handheld-Machine A-Mining Mode



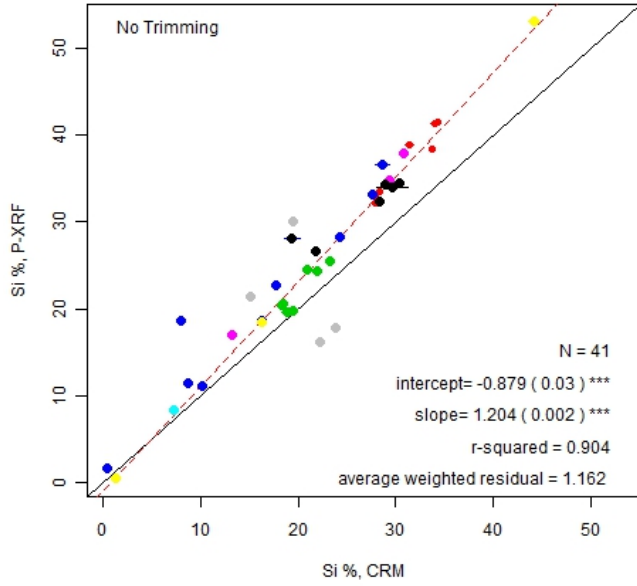
Handheld-HHBM-Mining Mode



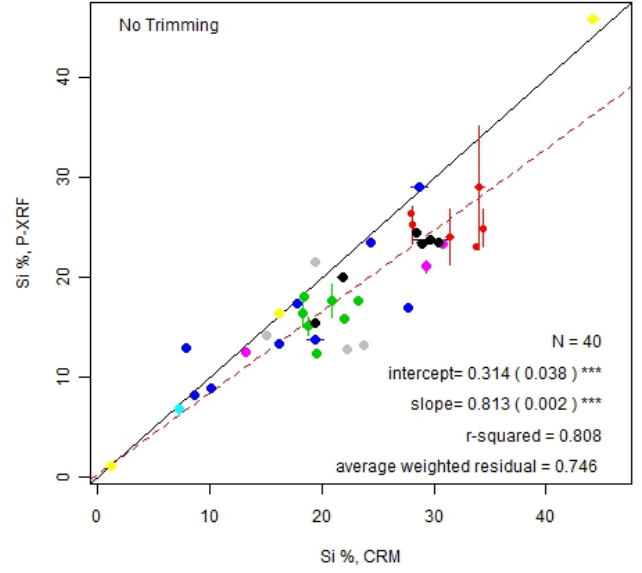
Handheld-HHCM-Mining Mode



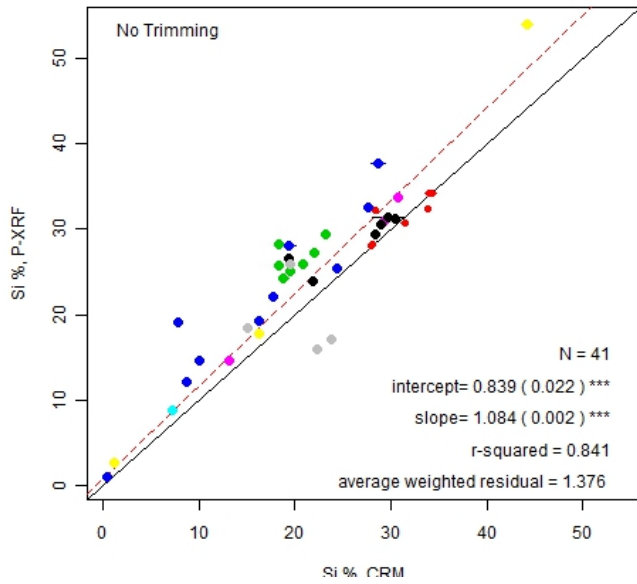
Benchtop-BTAM-Mining Mode



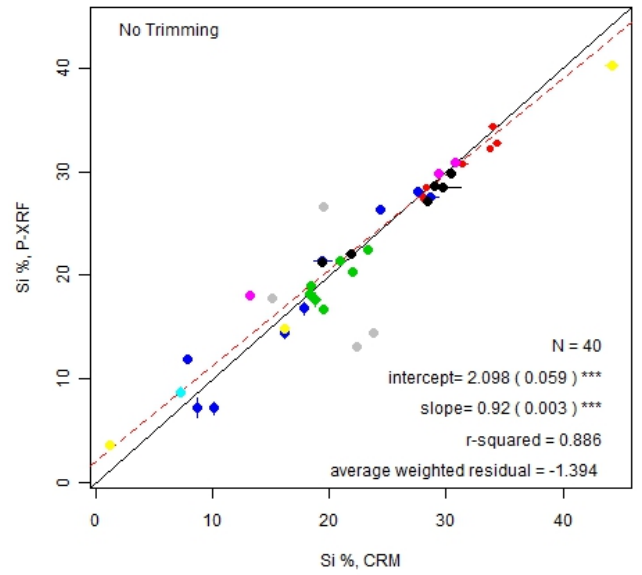
Handheld-BTBM-Mining Mode



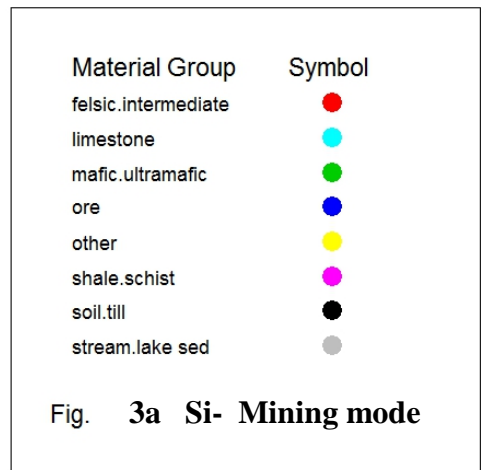
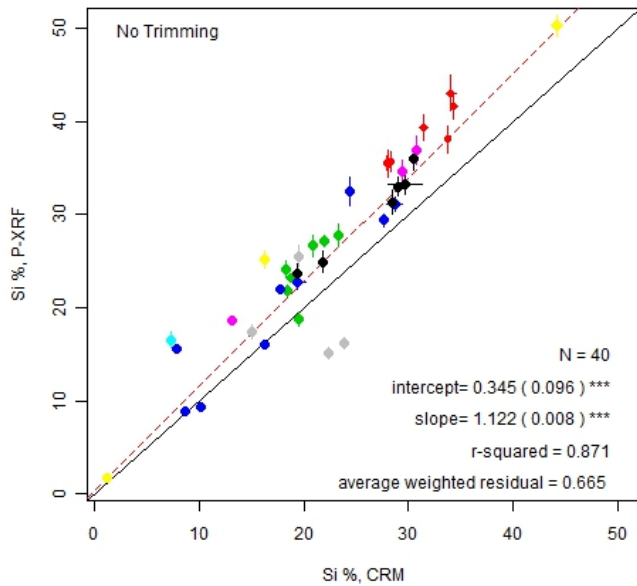
Handheld-HHAM-Mining Mode



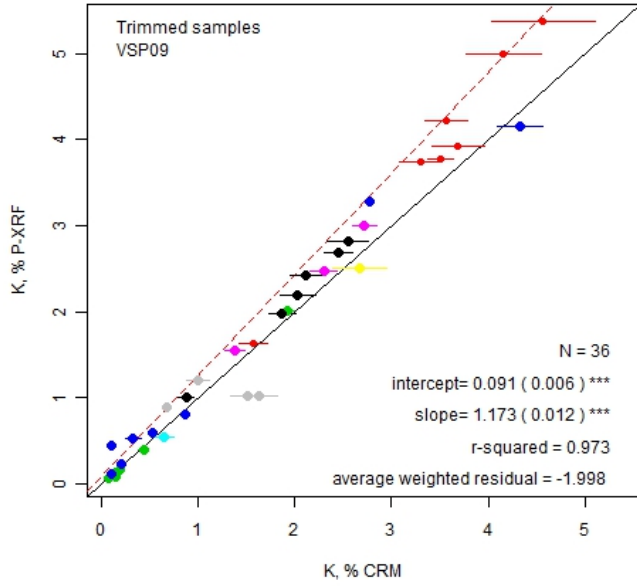
Handheld-HHBM-Mining Mode



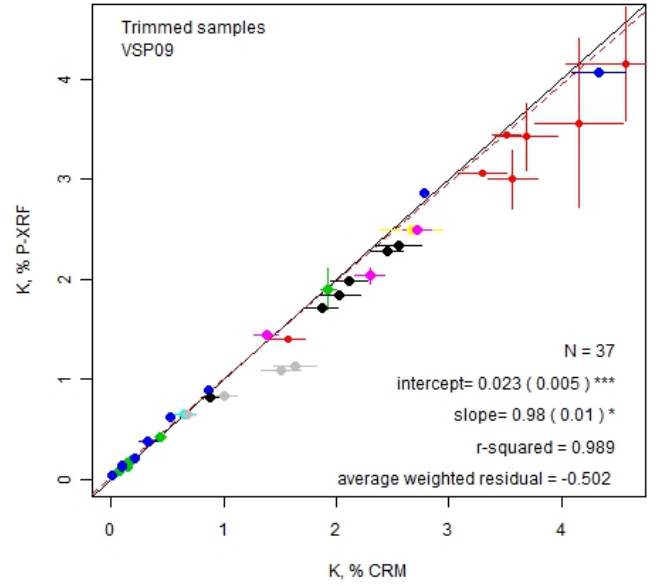
Handheld-HHCM-Mining Mode



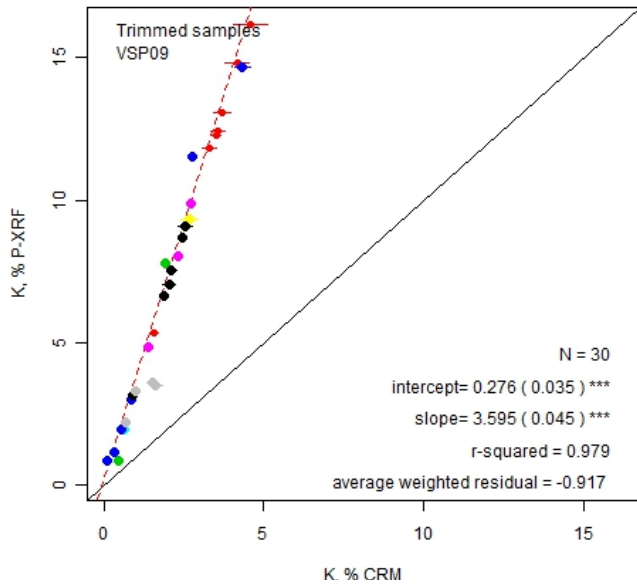
Benchtop-BTAM-Mining Mode



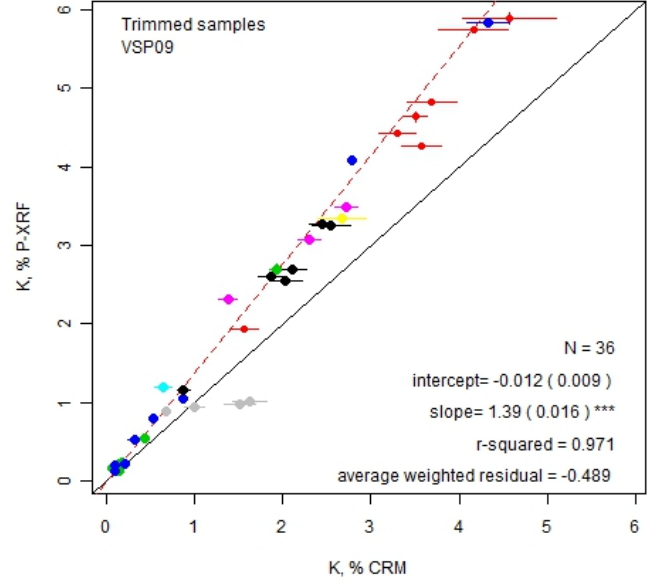
Benchtop-BTBM-Mining Mode



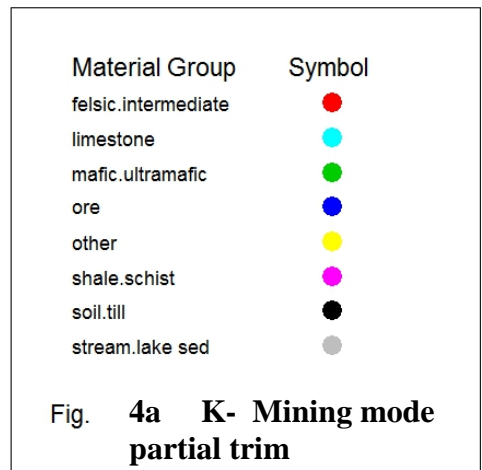
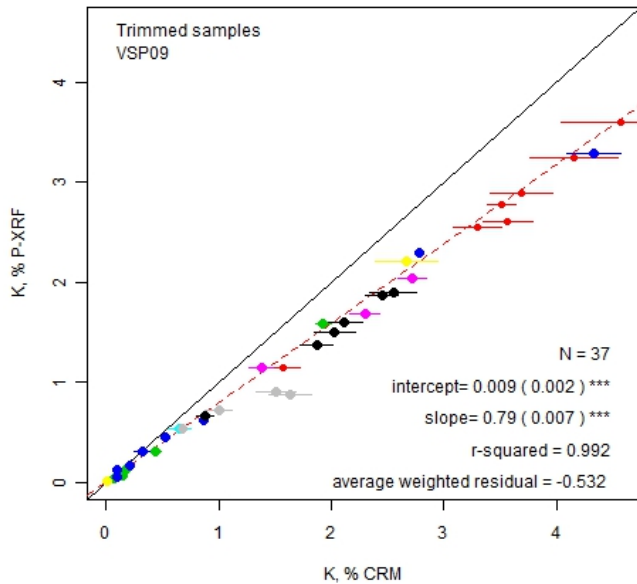
Handheld-Machine A-Mining Mode



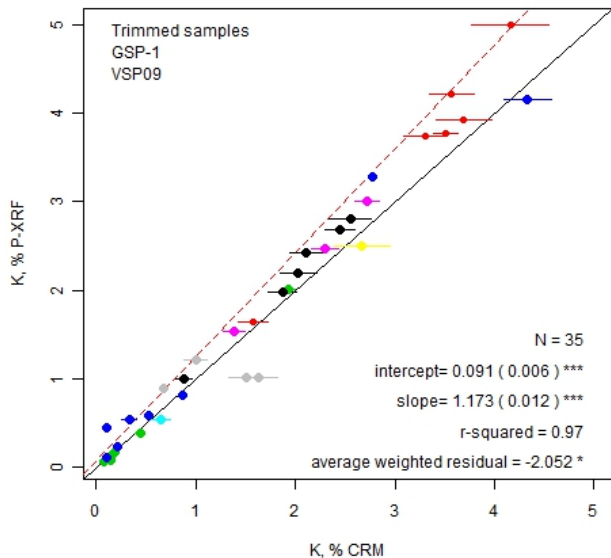
Handheld-HHBM-Mining Mode



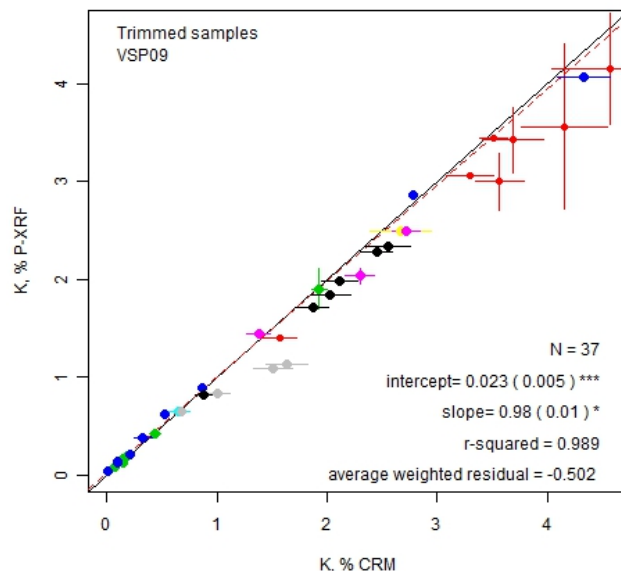
Handheld-HHCM-Mining Mode



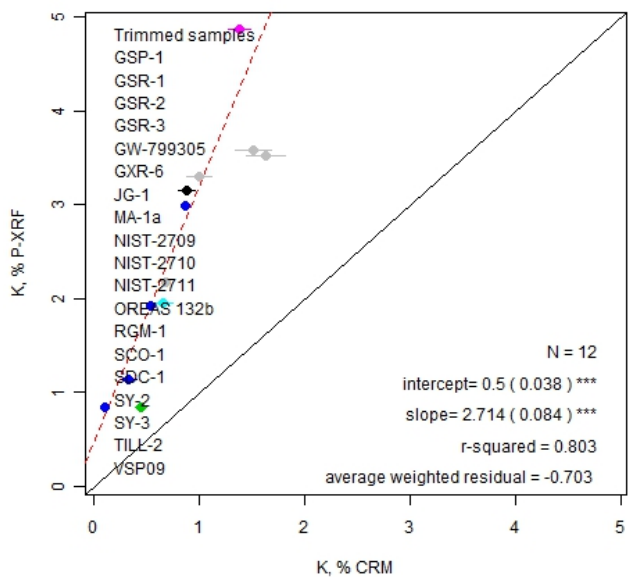
Benchtop-BTAM-Mining Mode



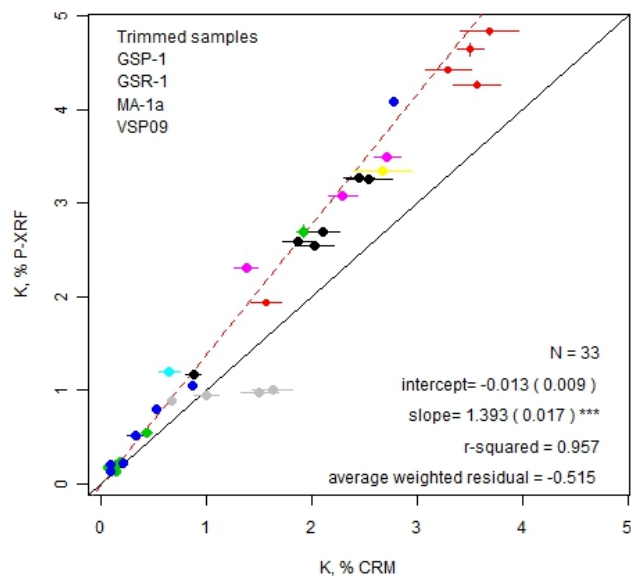
Benchtop-BTBM-Mining Mode



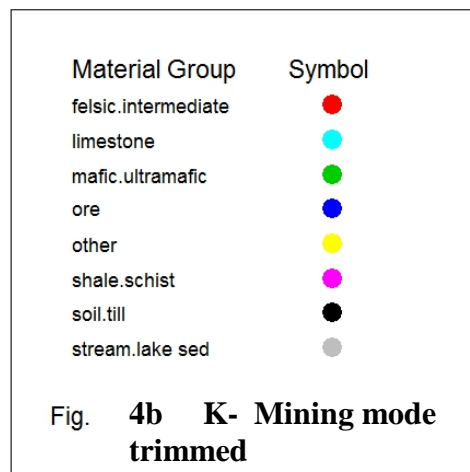
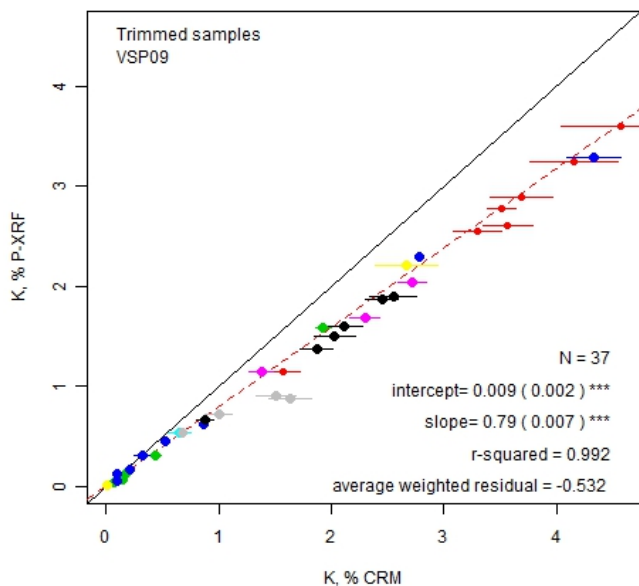
Handheld-HHAM-Mining Mode



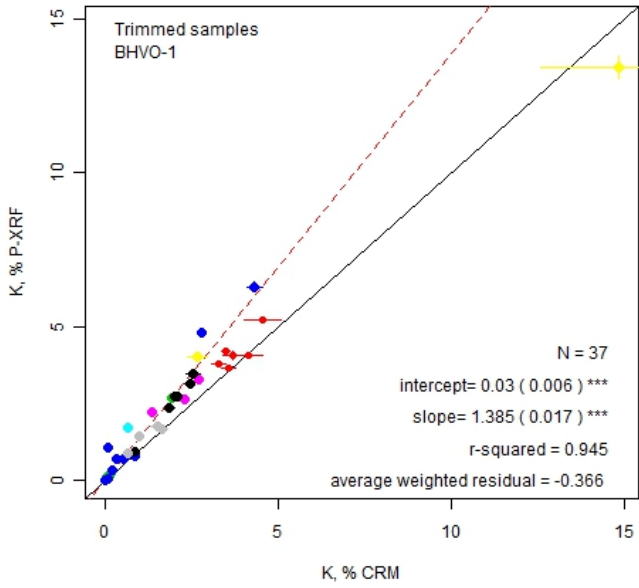
Handheld-HHBM-Mining Mode



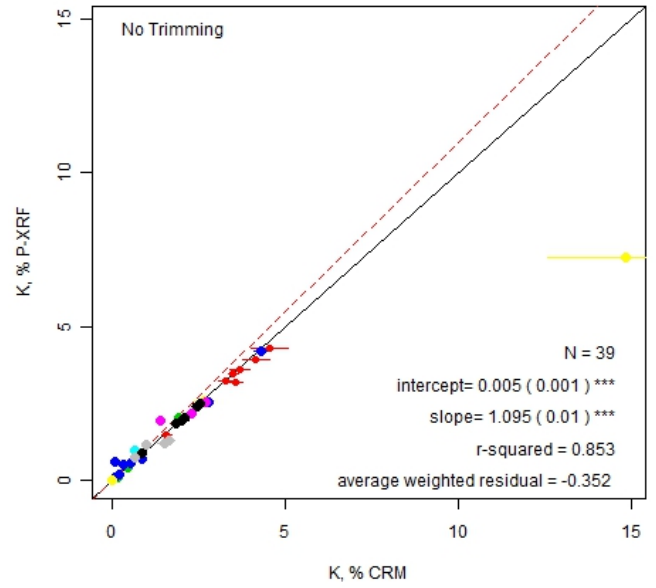
Handheld-HHCM-Mining Mode



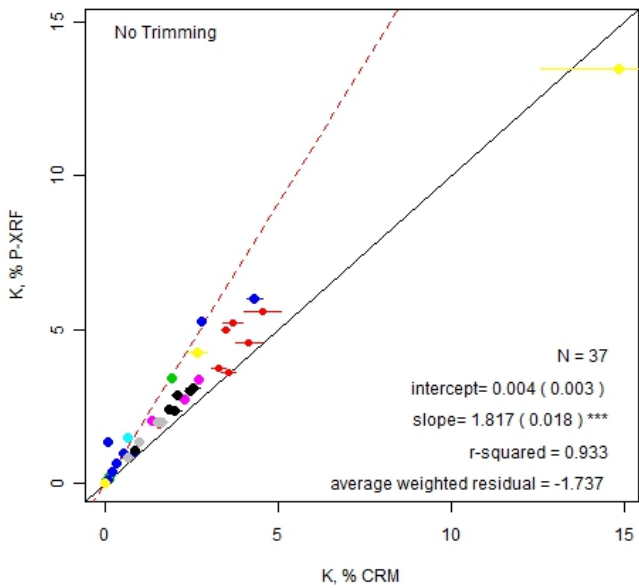
Bench Top-BTAS-Soil Mode



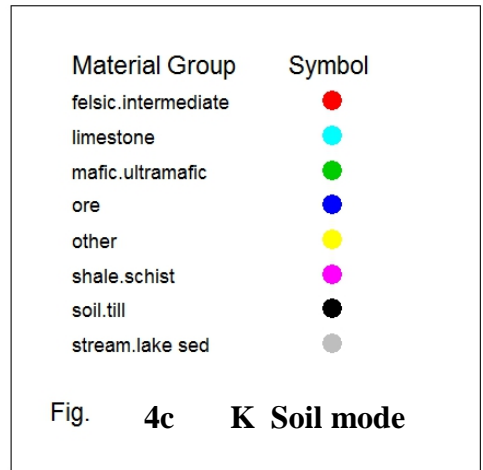
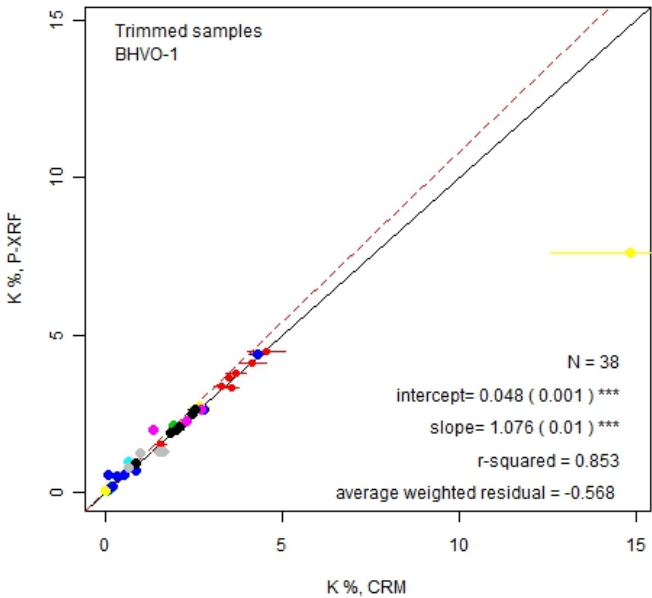
Bench Top-BTBS-Soil Mode



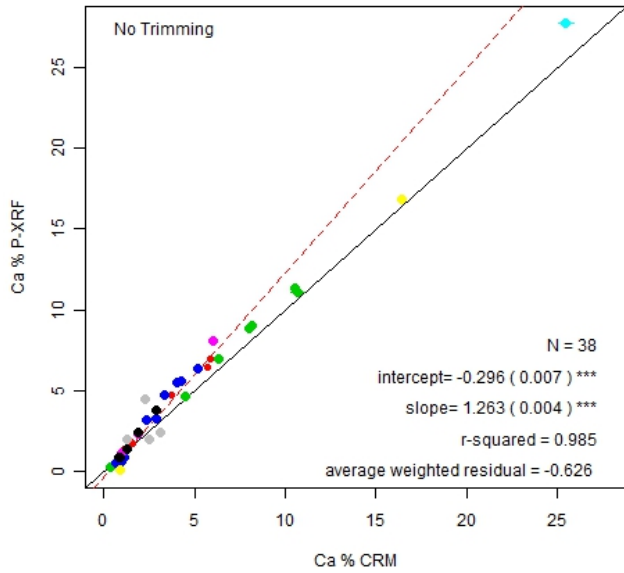
Handheld-HHAS-Soil Mode



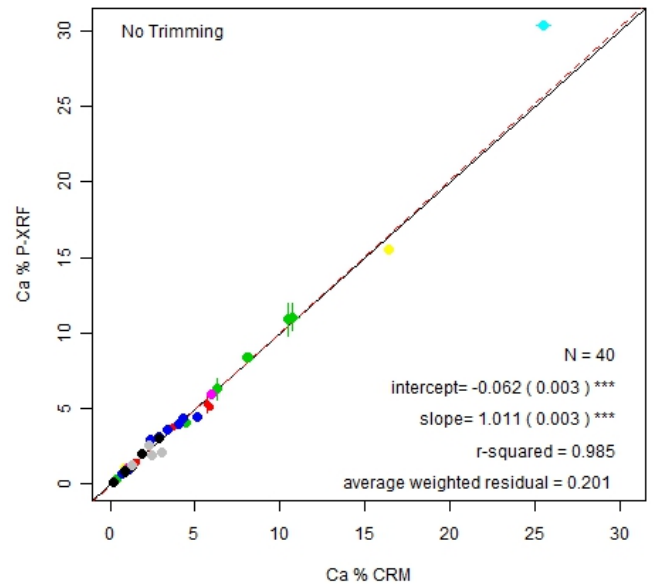
Handheld-HHCS-Soil Mode



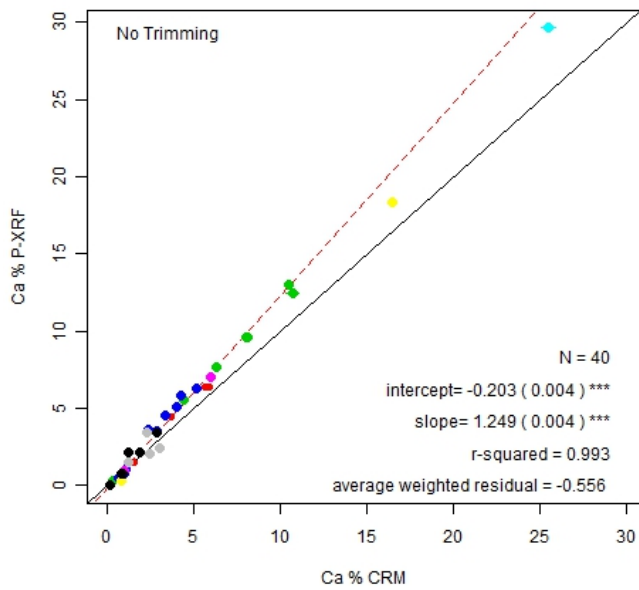
Benchtop-BTAM-Mining Mode



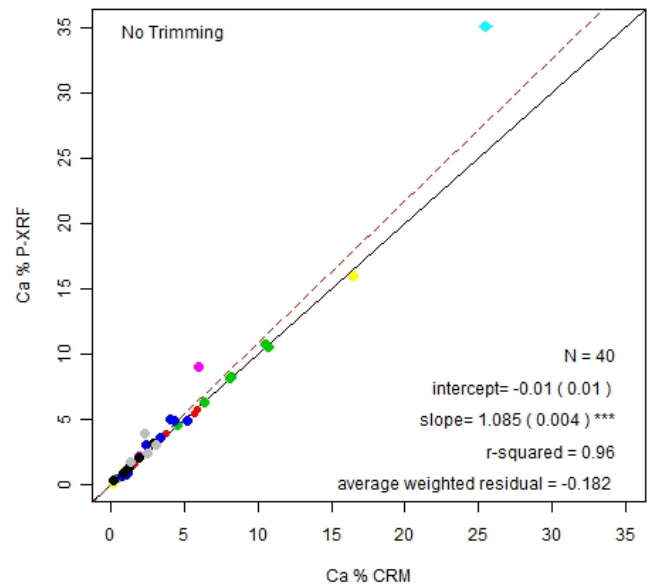
Benchtop-BTBM-Mining Mode



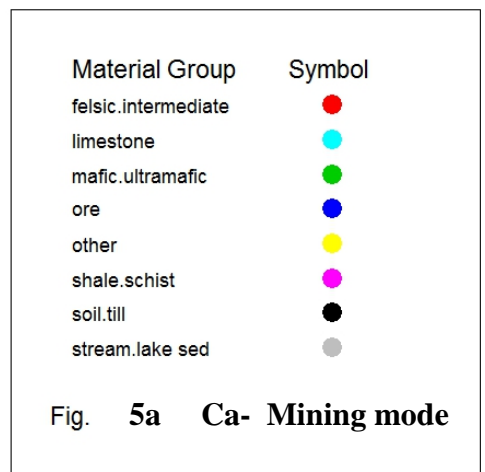
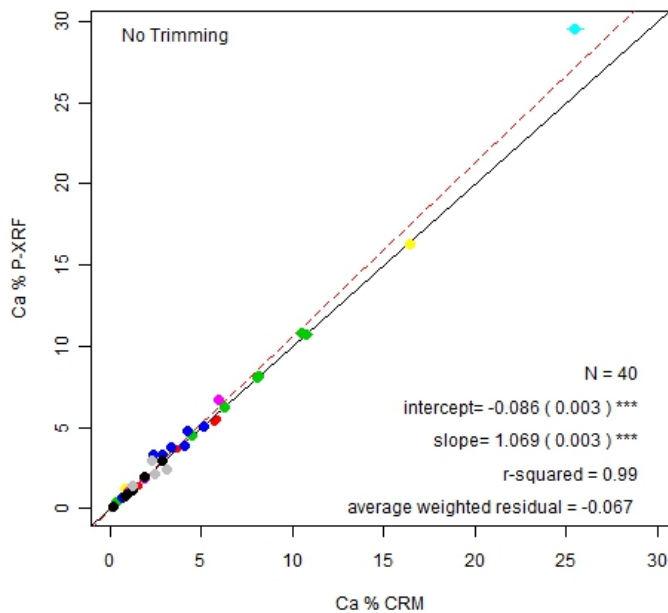
Handheld-Machine A-Mining Mode



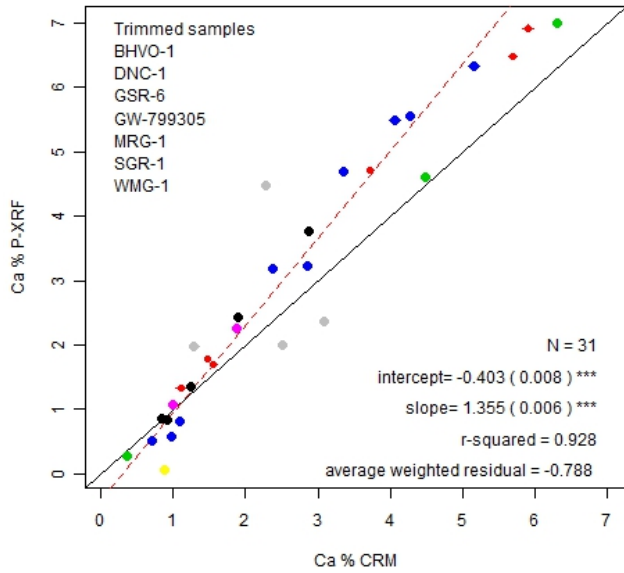
Handheld-HHBM-Mining Mode



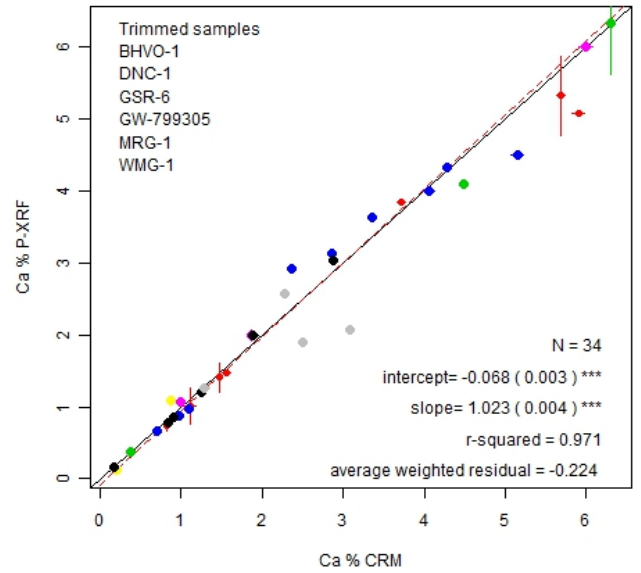
Handheld-HHCM-Mining Mode



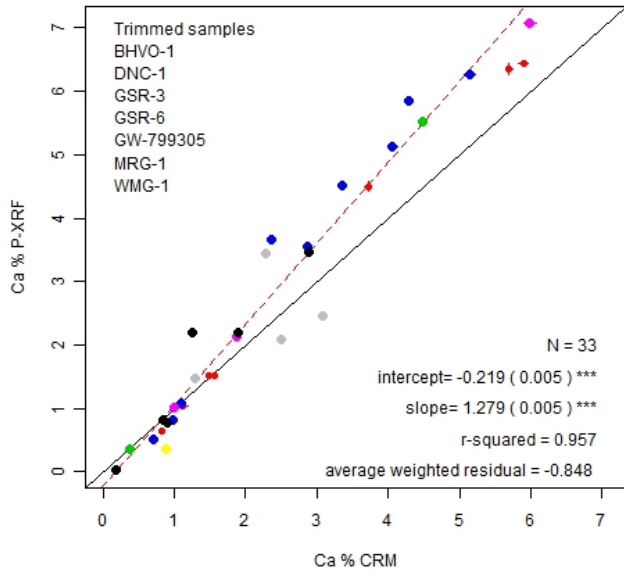
Benchtop-BTAM-Mining Mode



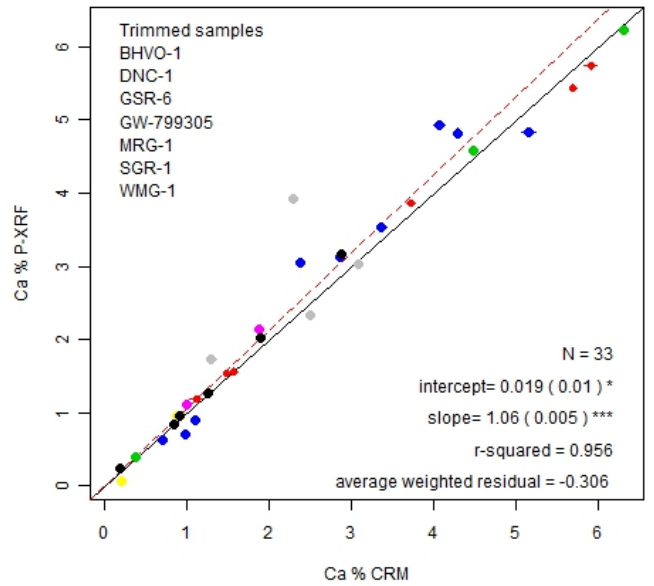
Benchtop-BTBM-Mining Mode



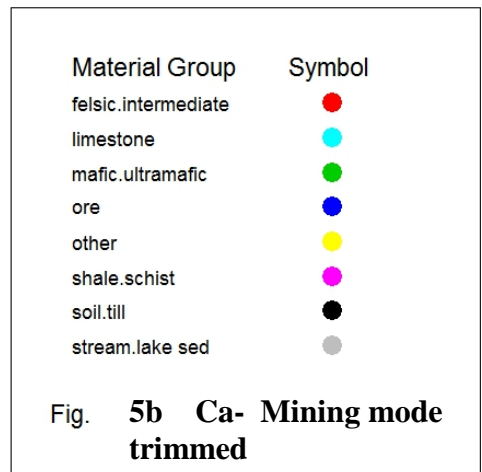
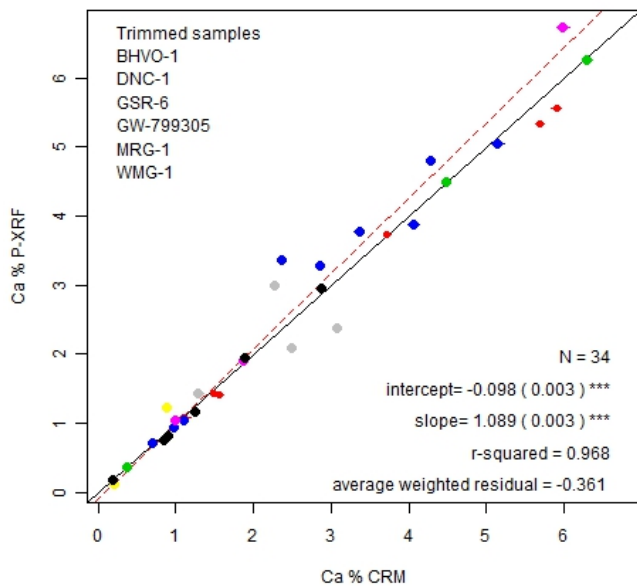
Handheld-HHAM-Mining Mode



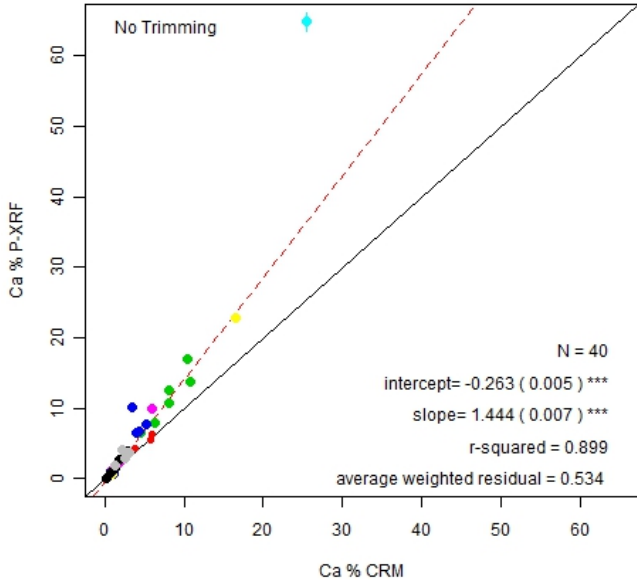
Handheld-HHBM-Mining Mode



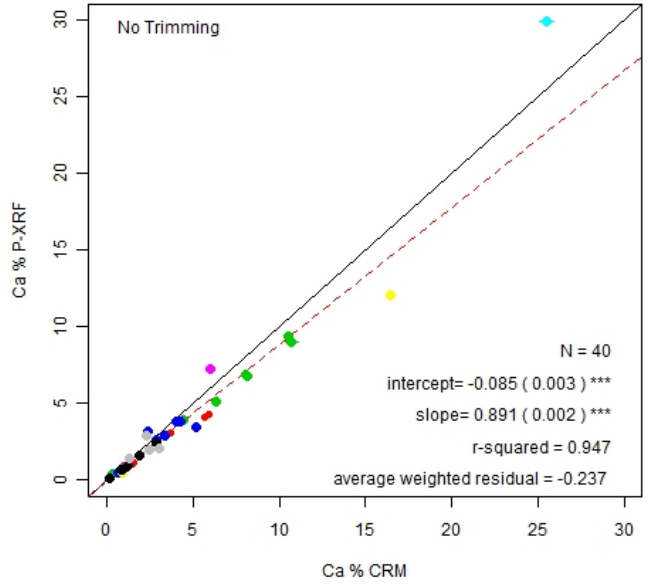
Handheld-HHCM-Mining Mode



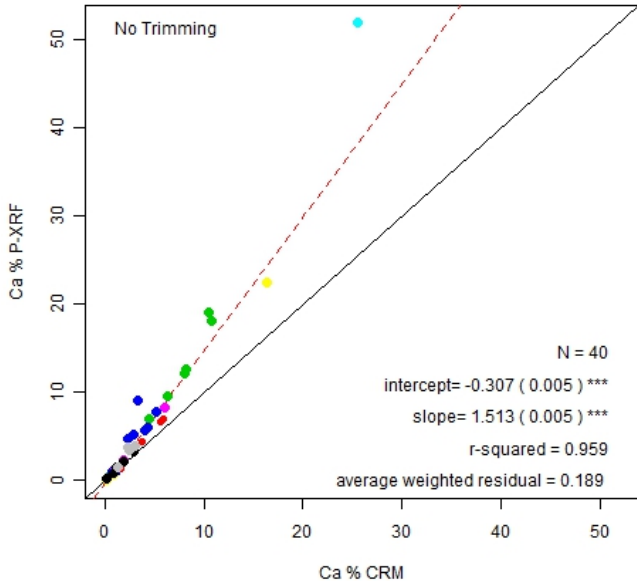
Bench Top-BTAS-Soil Mode



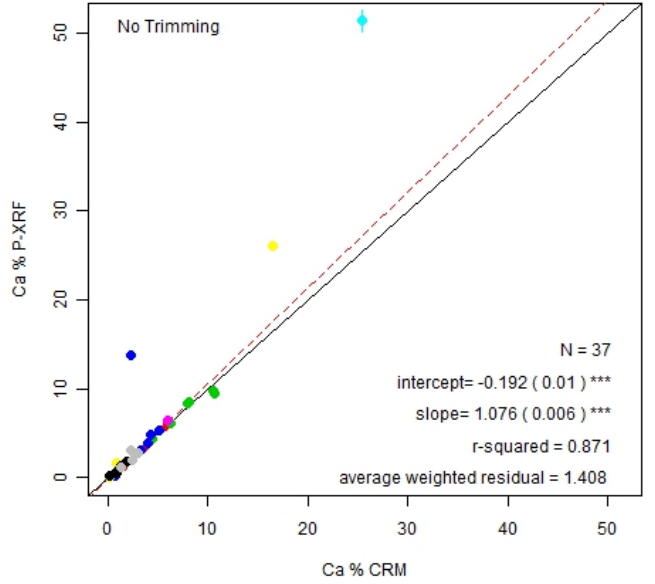
Bench Top-BTBS-Soil Mode



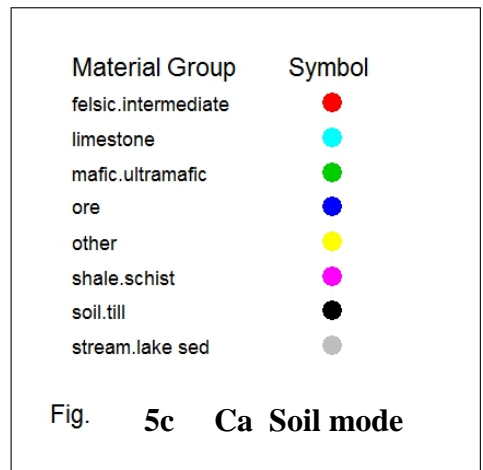
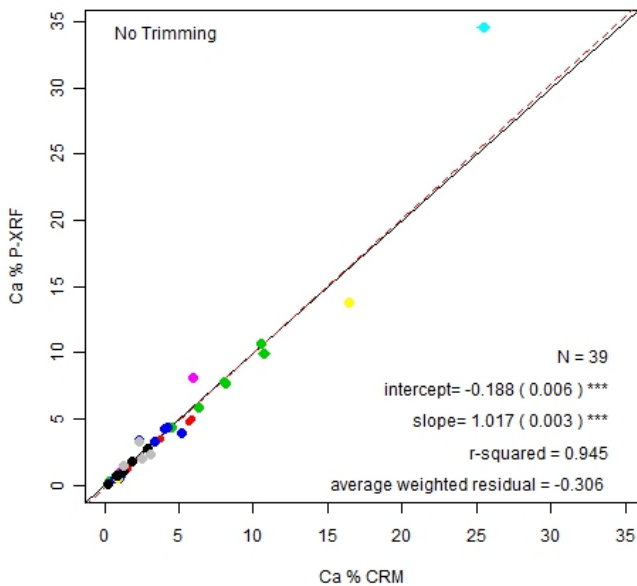
Handheld-HHAS-Soil Mode



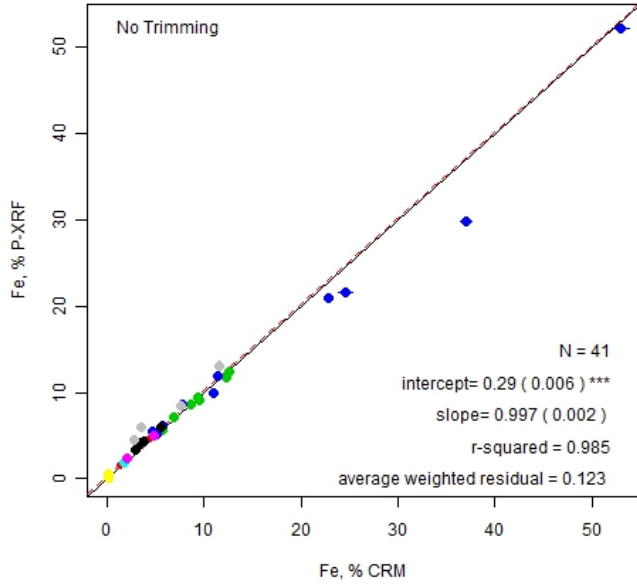
Handheld-HHBS-Soil Mode



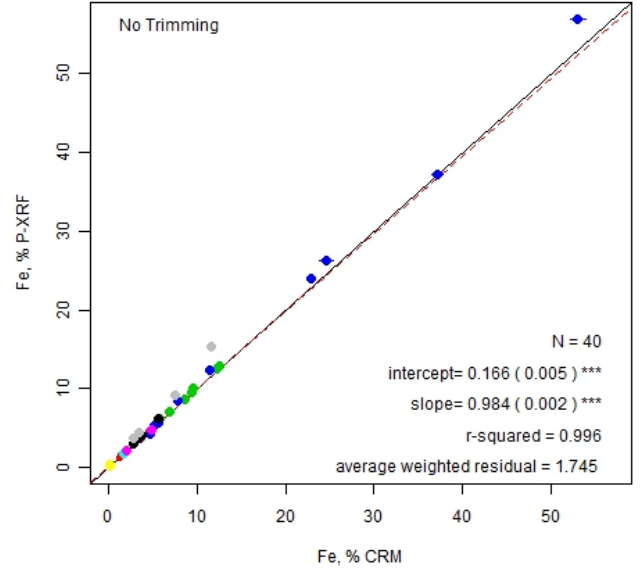
Handheld-HHCS-Soil Mode



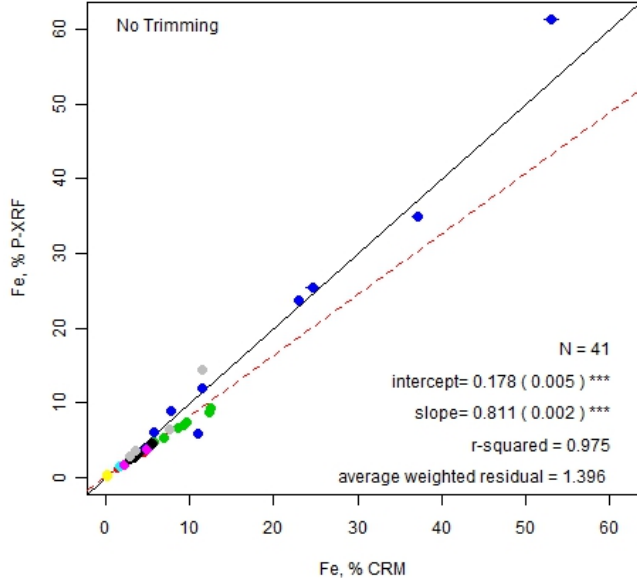
Benchtop-BTAM-Mining Mode



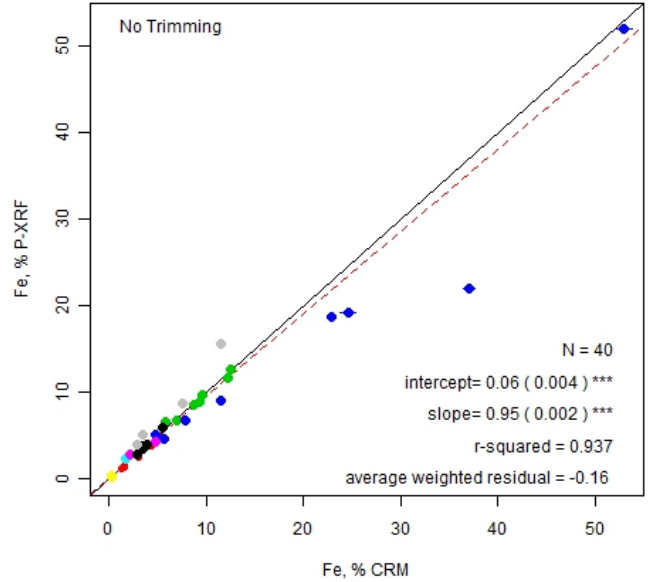
Benchtop-BTBM-Mining Mode



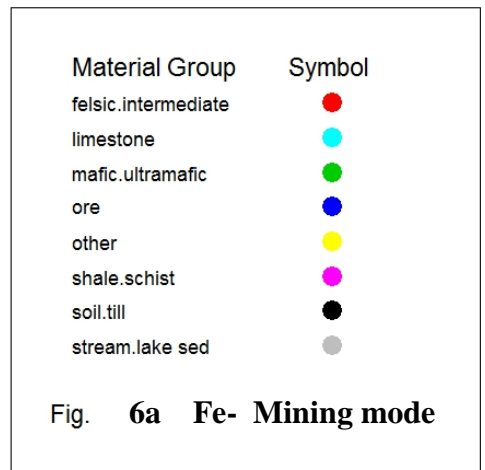
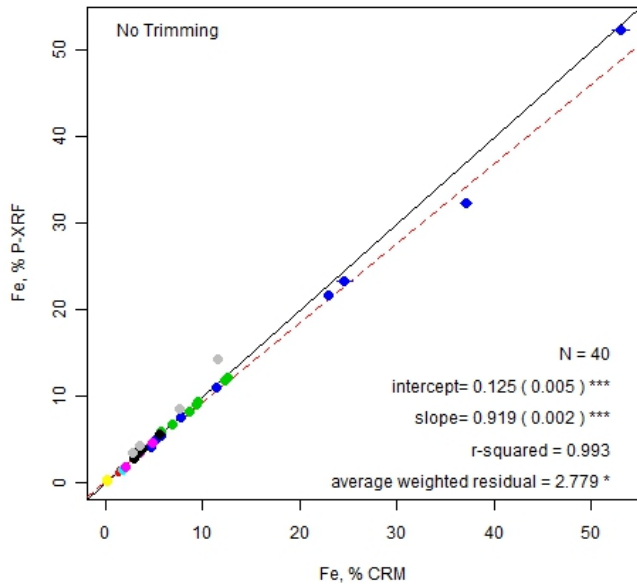
Handheld-Machine A-Mining Mode



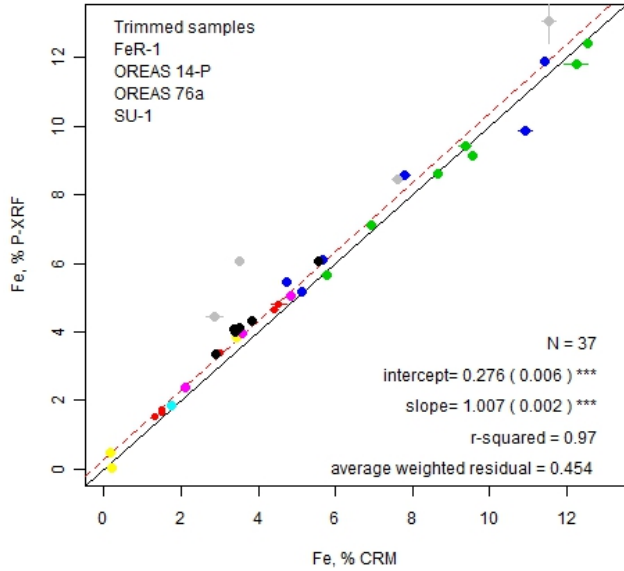
Handheld-HHBM-Mining Mode



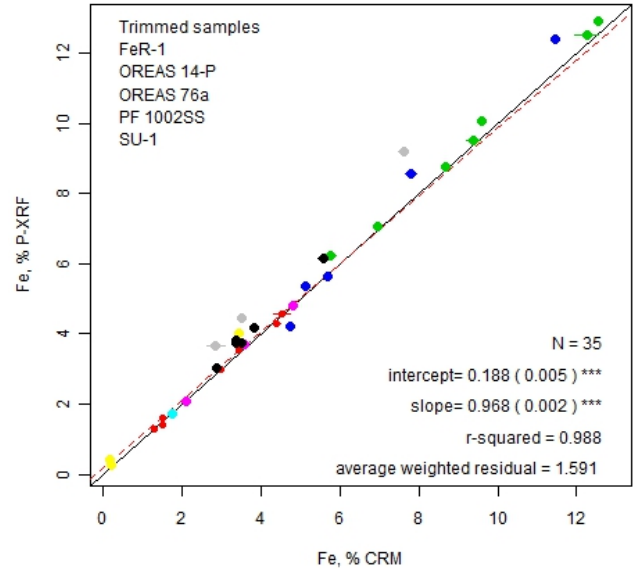
Handheld-HHCM-Mining Mode



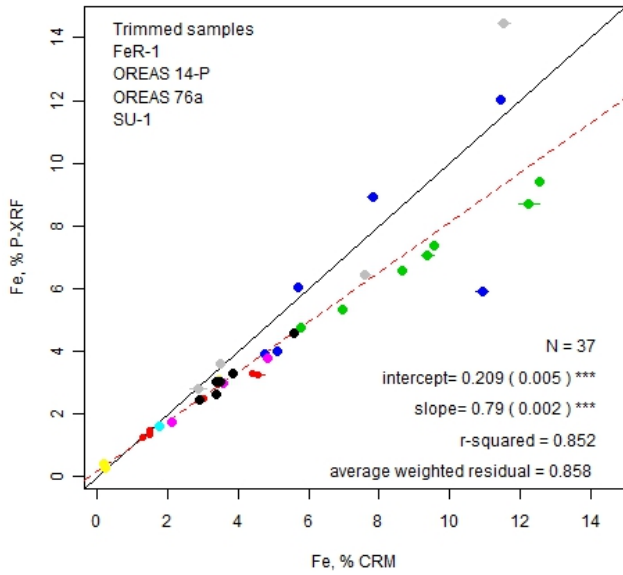
Benchtop-BTAM-Mining Mode



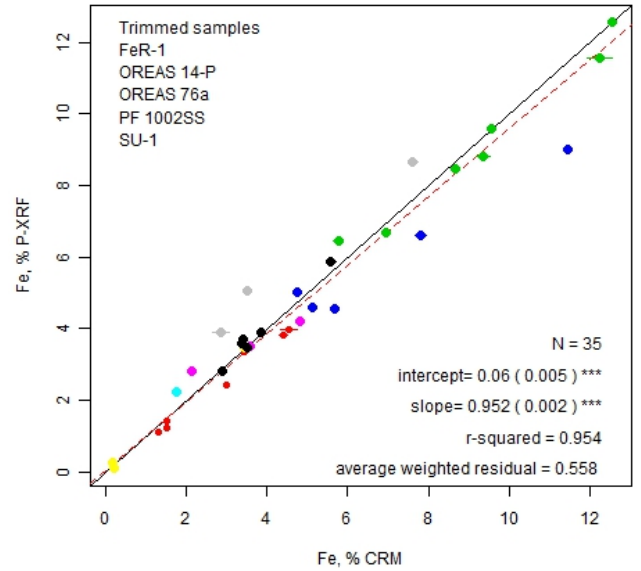
Benchtop-BTBM-Mining Mode



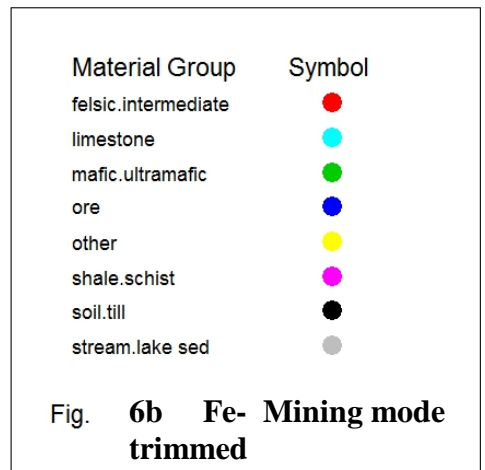
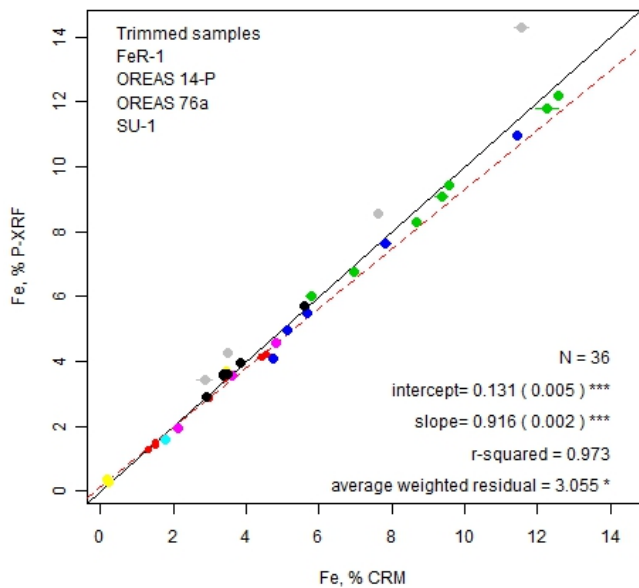
Handheld-Machine A-Mining Mode



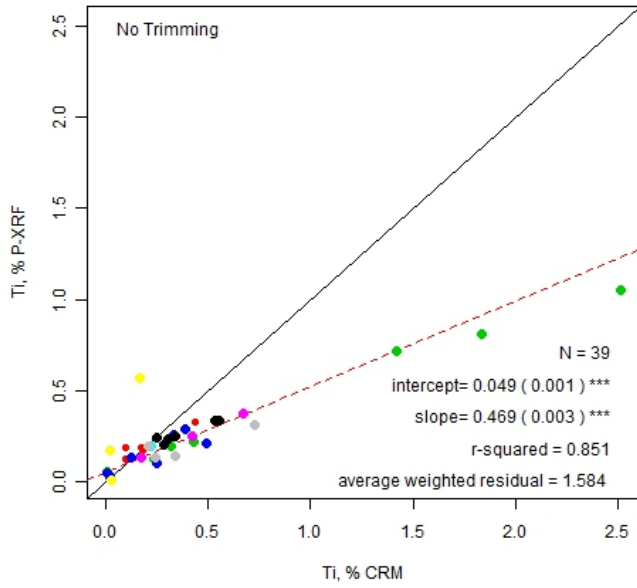
Handheld-HHBM-Mining Mode



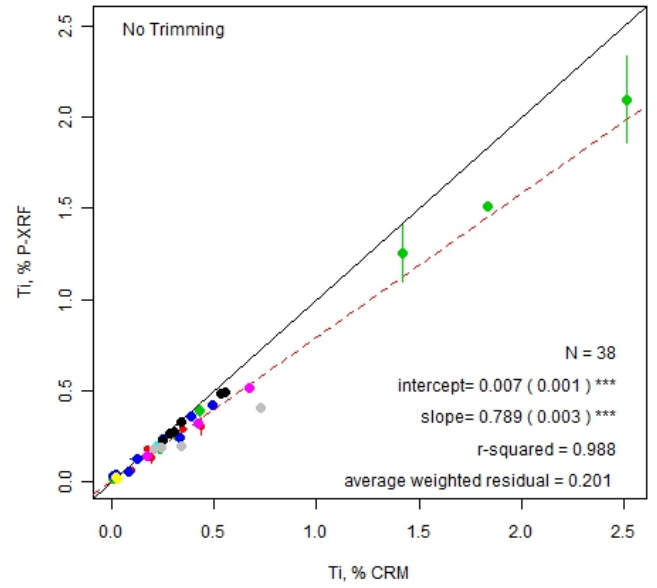
Handheld-HHCM-Mining Mode



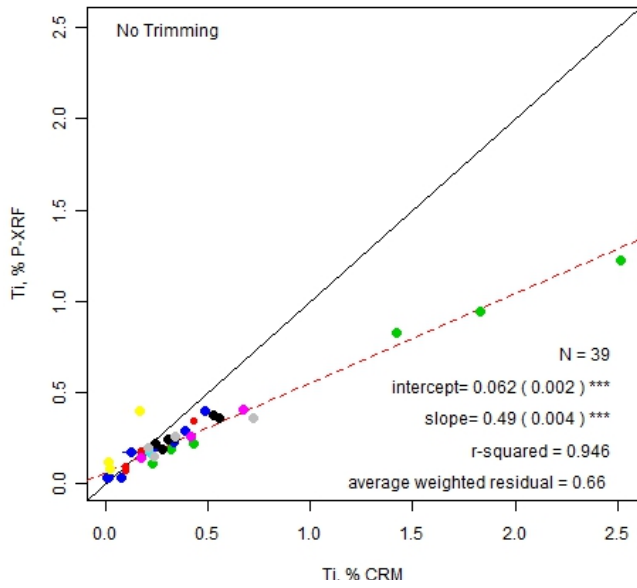
Benchtop-BTAM-Mining Mode



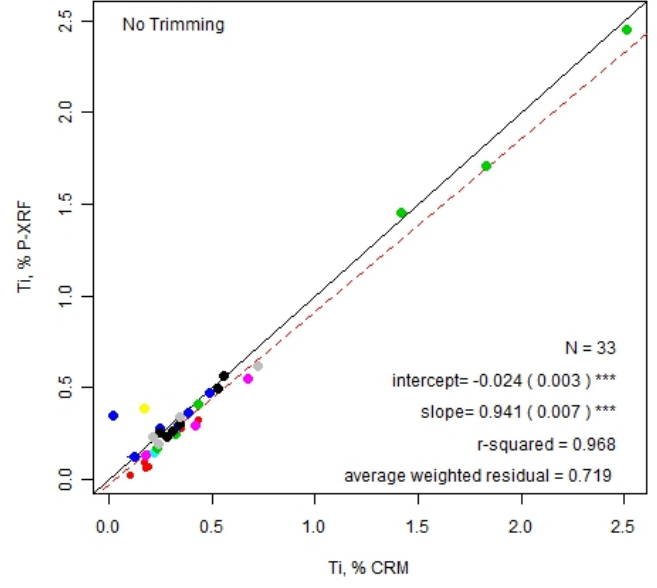
Handheld-BTBM-Mining Mode



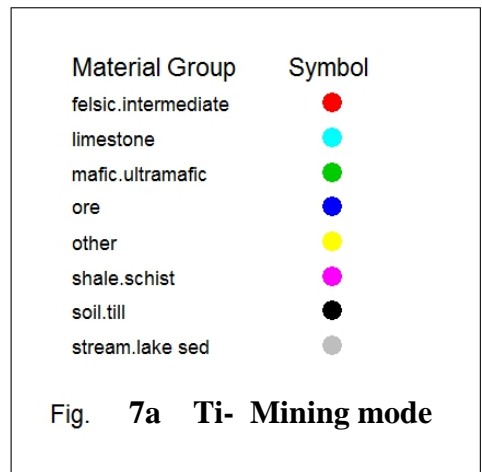
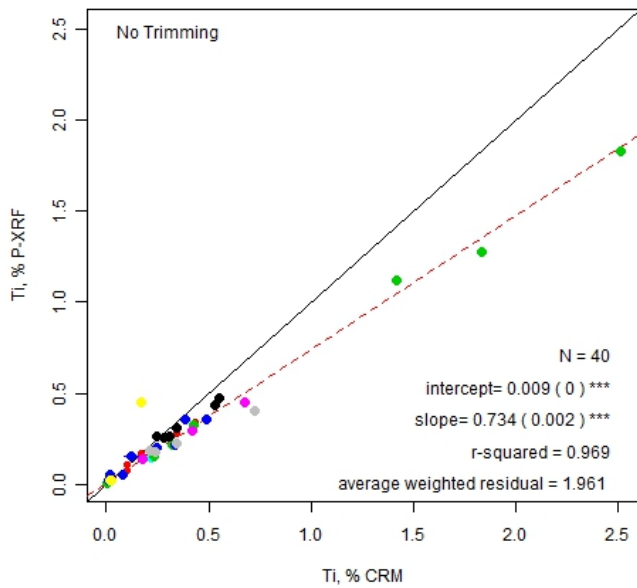
Handheld-HHAM-Mining Mode



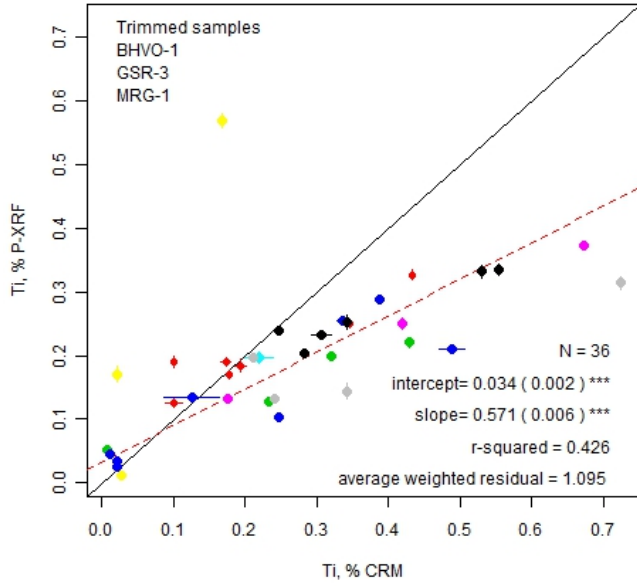
Handheld-HHBM-Mining Mode



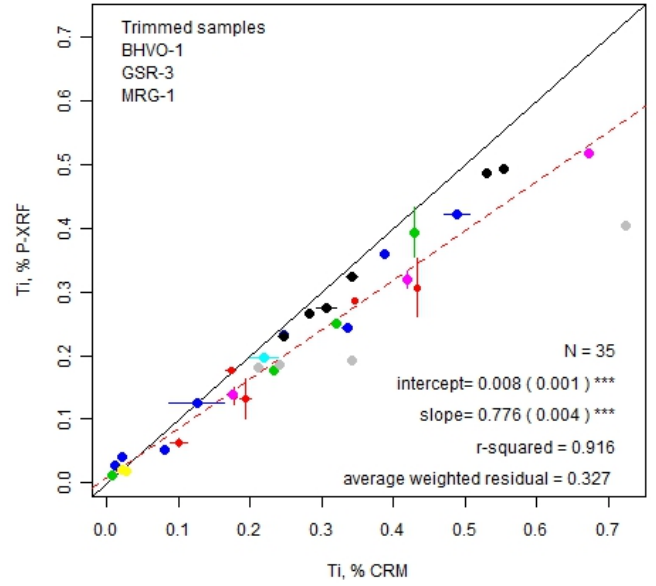
Handheld-HHCM-Mining Mode



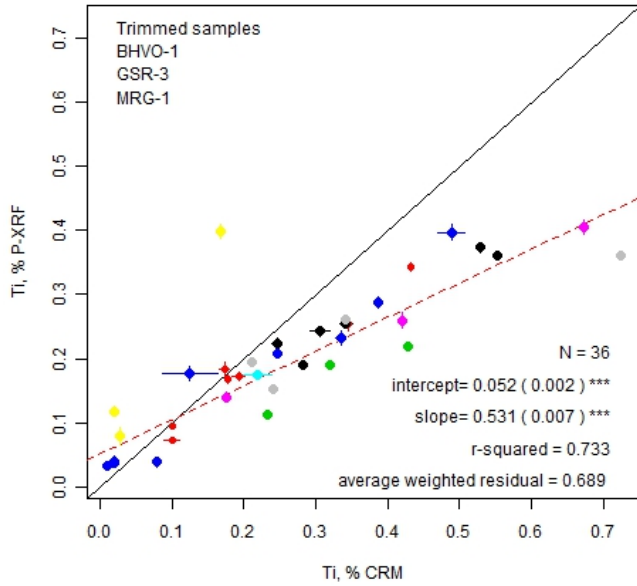
Benchtop-BTAM-Mining Mode



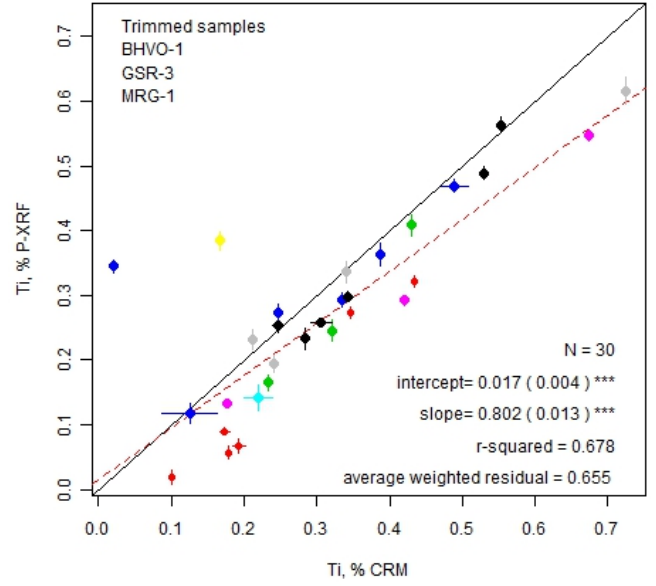
Handheld-BTBM-Mining Mode



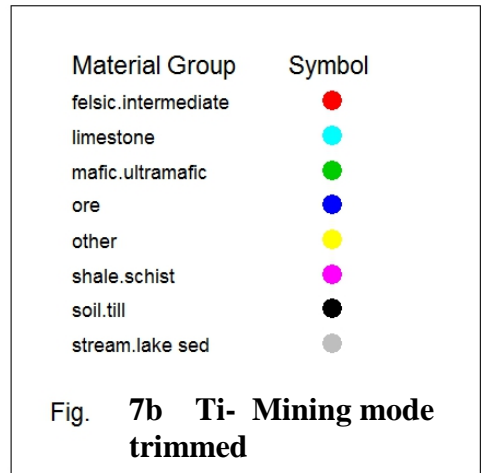
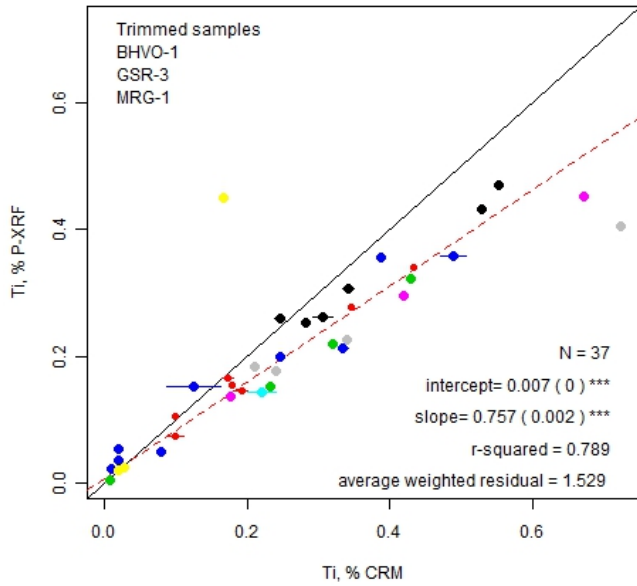
Handheld-HHAM-Mining Mode



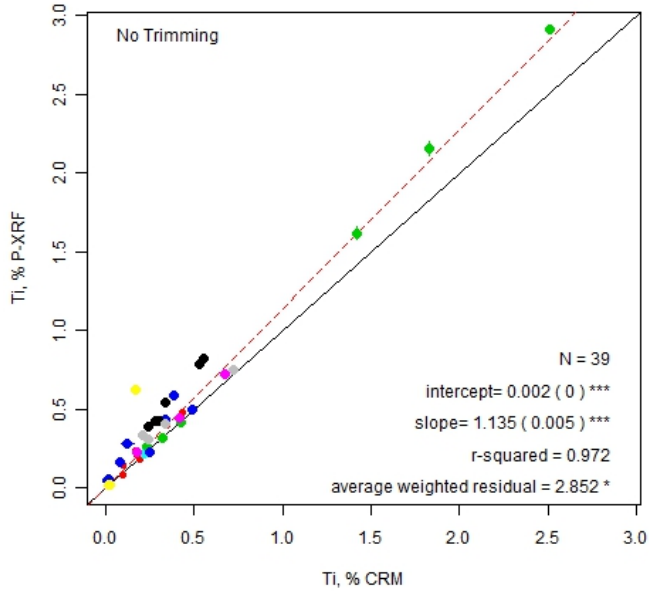
Handheld-HHBM-Mining Mode



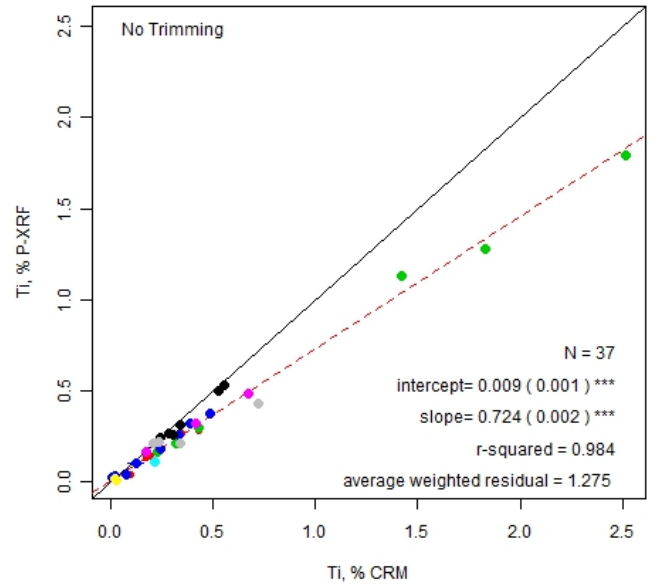
Handheld-HHCM-Mining Mode



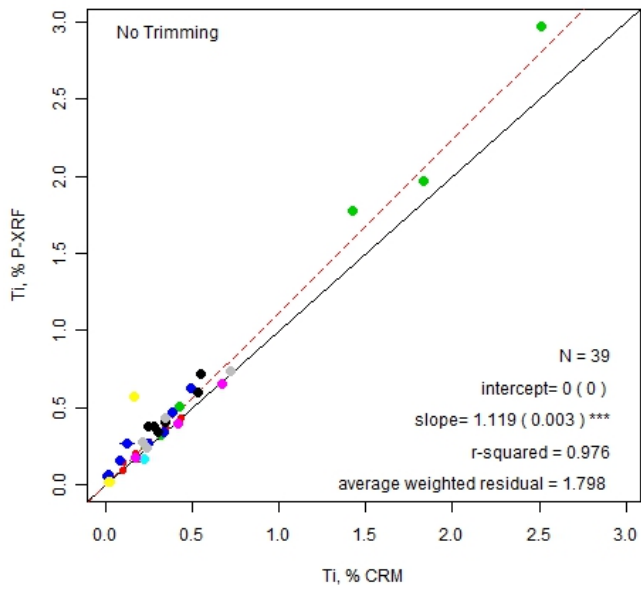
Bench Top-BTAS-Soil Mode



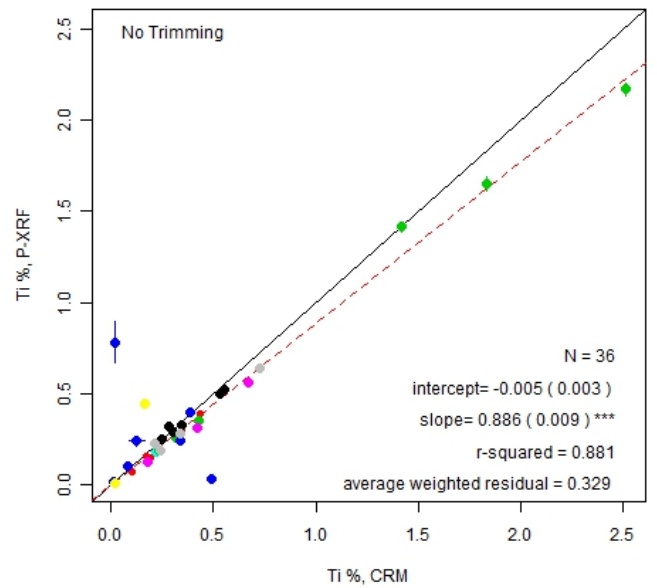
Bench Top-BTBS-Soil Mode



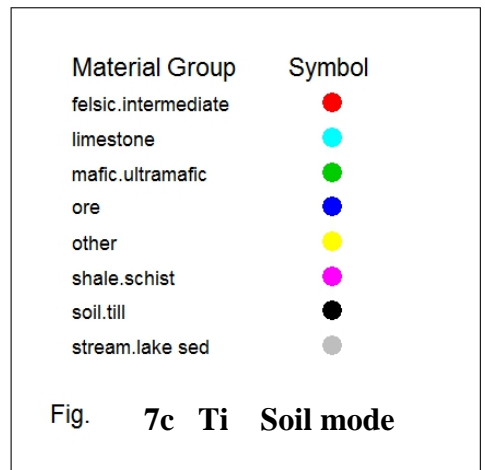
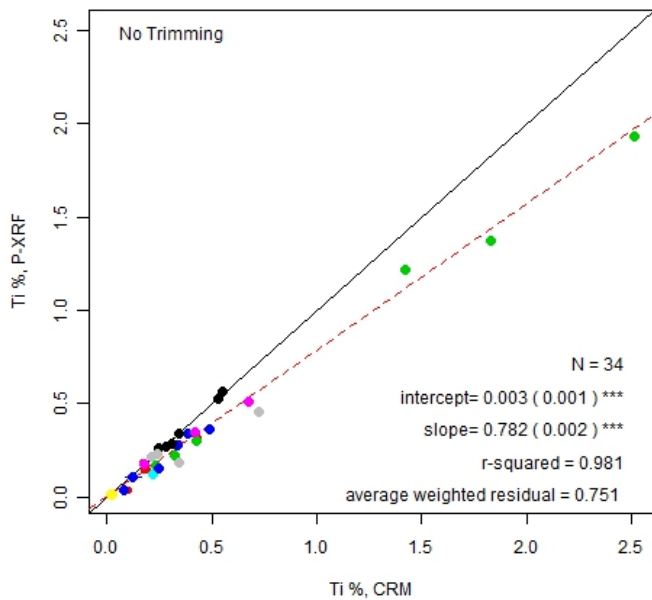
Handheld-HHAS-Soil Mode



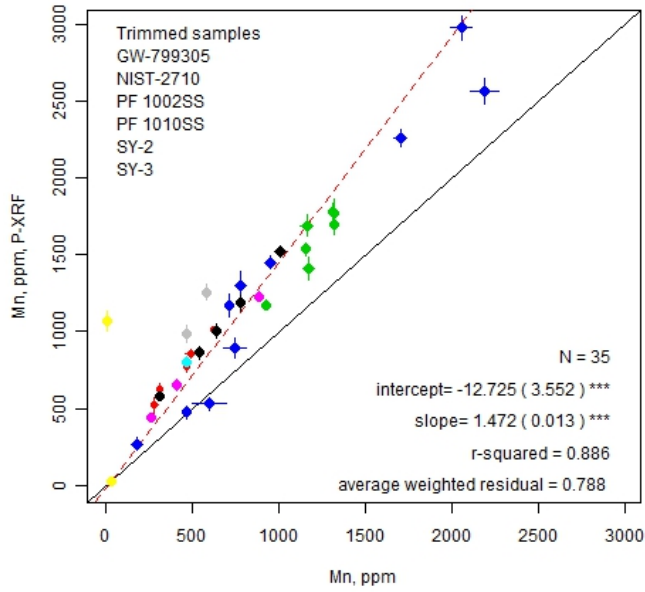
Handheld-HHBS-Soil Mode



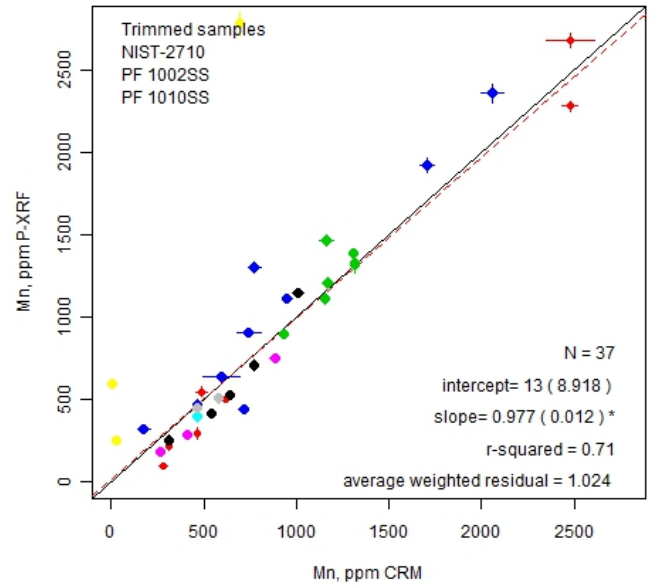
Handheld-HHCS-Soil Mode



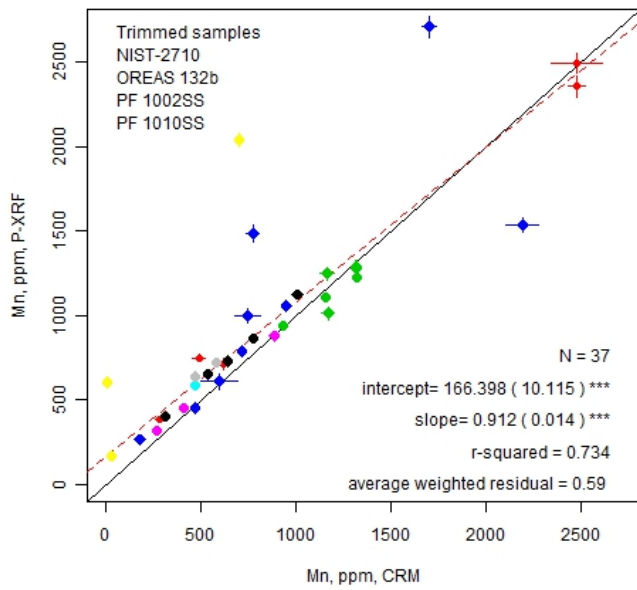
Benchtop-BTAM-Mining Mode



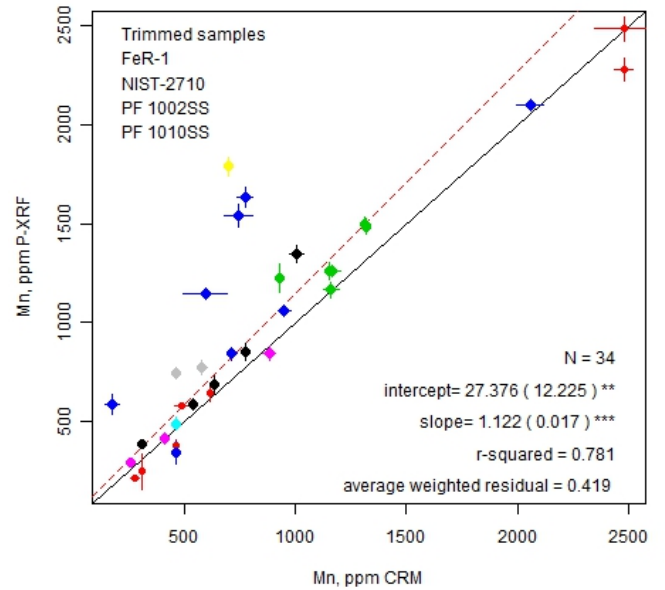
Benchtop-BTBM-Mining Mode



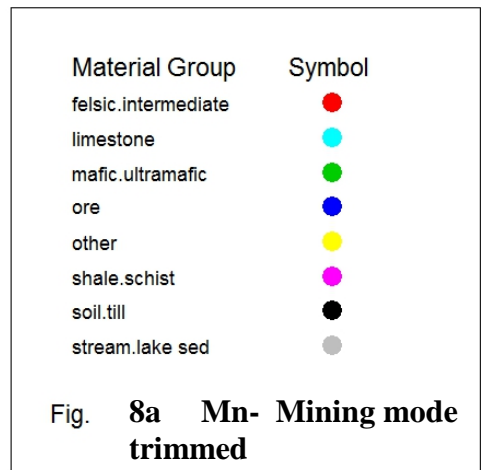
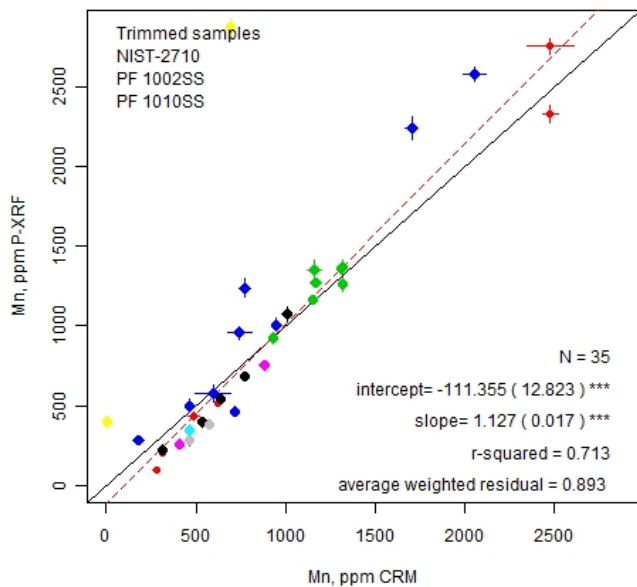
Handheld-HHAM-Mining Mode



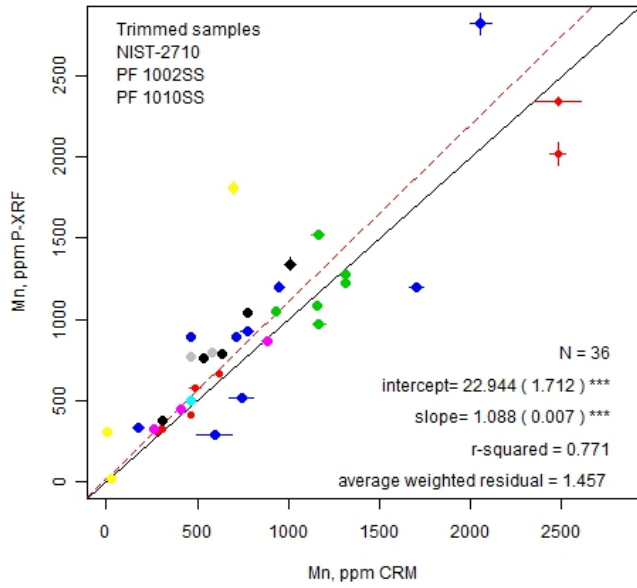
Handheld-HHBM-Mining Mode



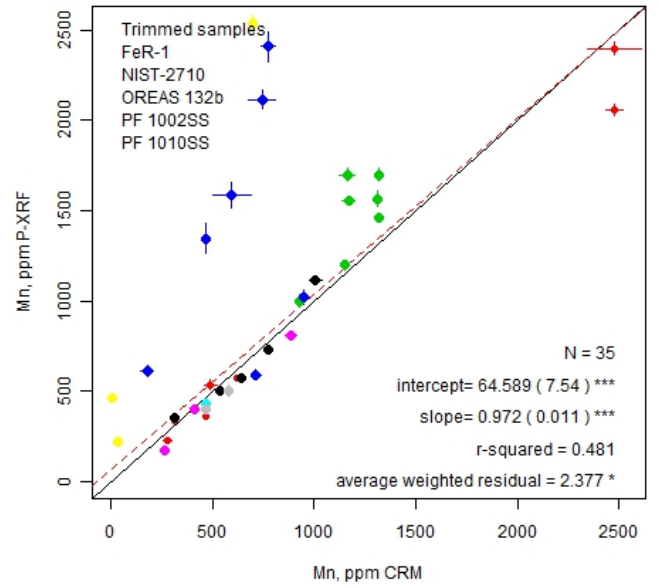
Handheld-HHCM-Mining Mode



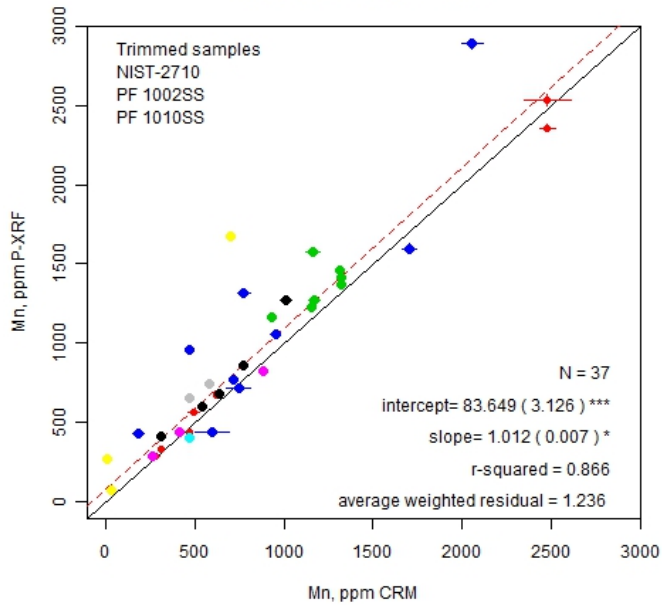
Bench Top-Machine A-Soil Mode



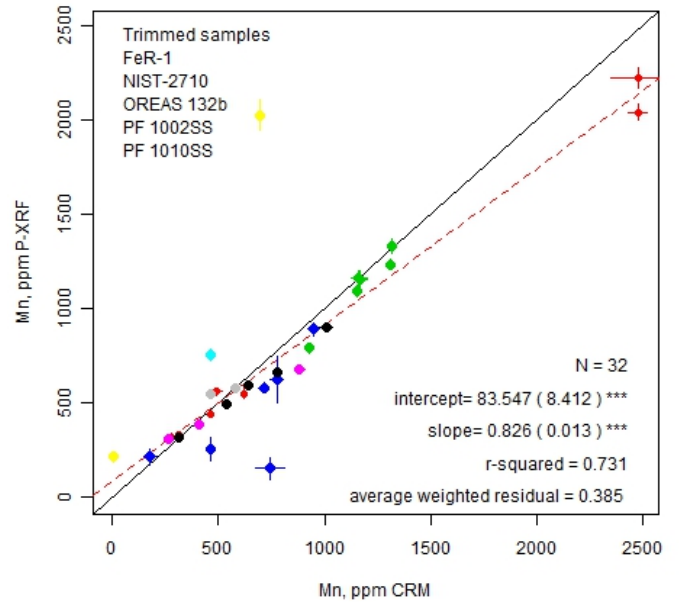
Bench Top-BTBS-Soil Mode



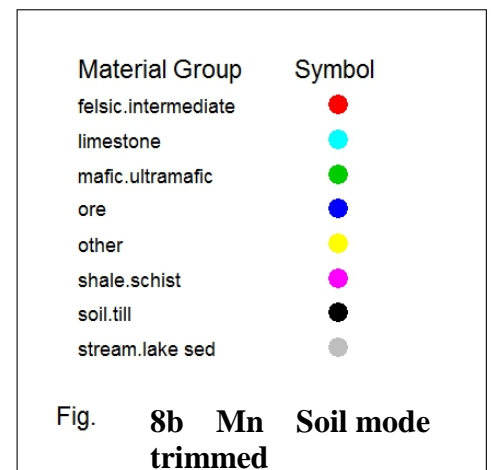
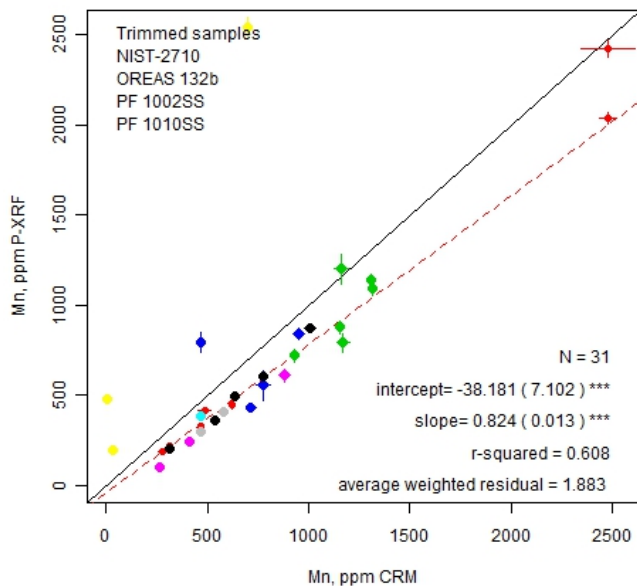
Handheld-HHAS-Soil Mode



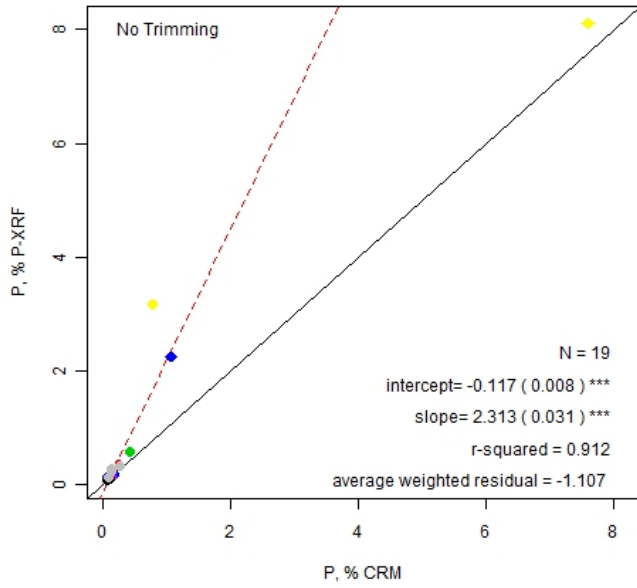
Handheld-HHBS-Soil Mode



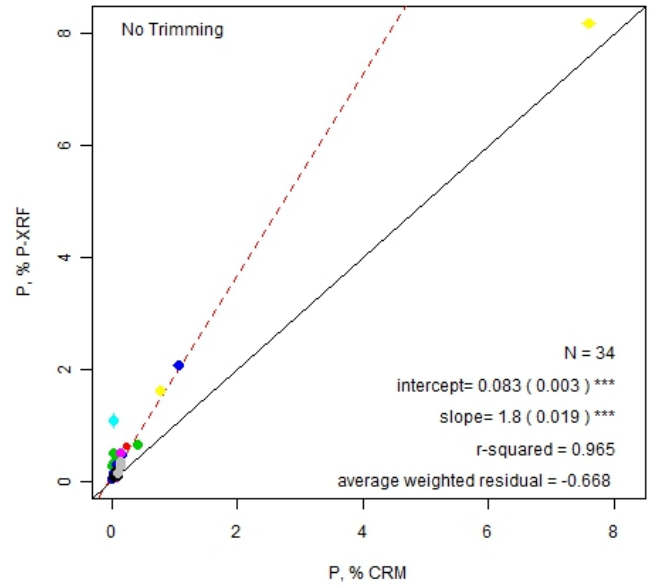
Handheld-HHCS-Soil Mode



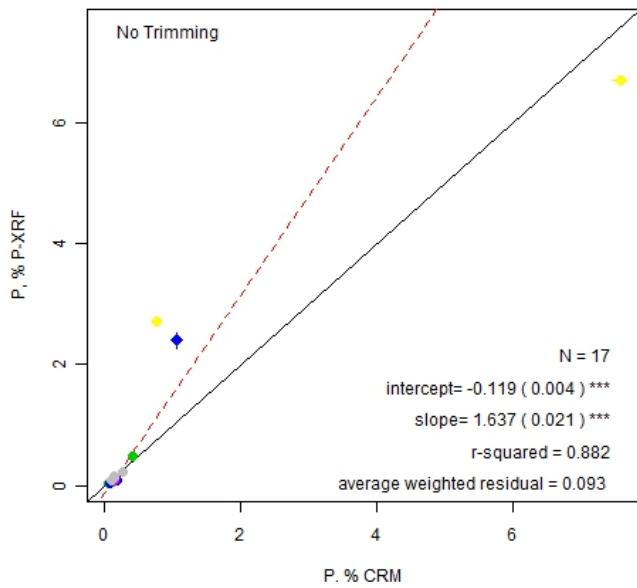
Benchtop-BTAM-Mining Mode



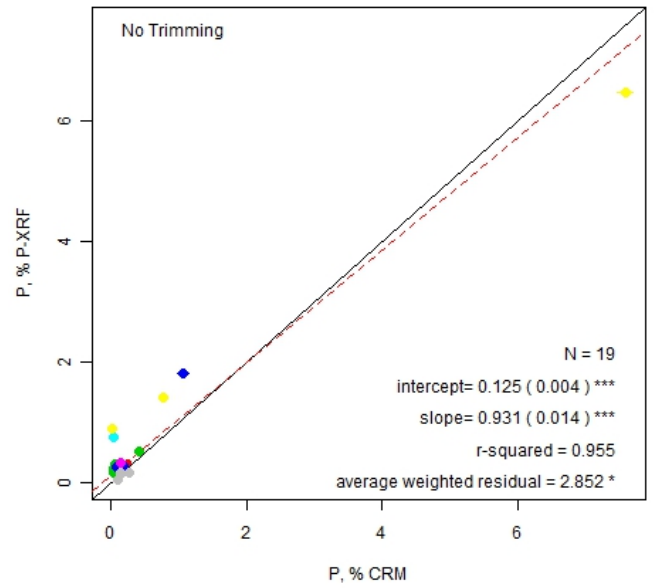
Handheld-BTBM-Mining Mode



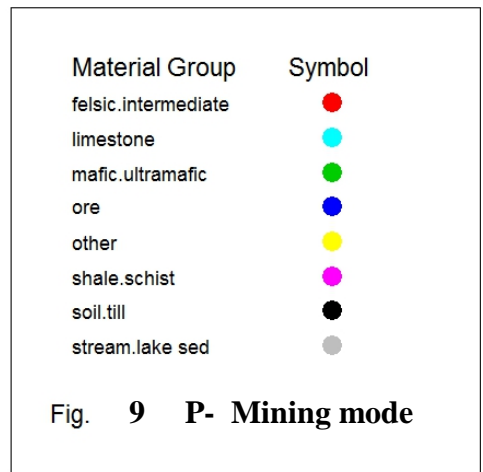
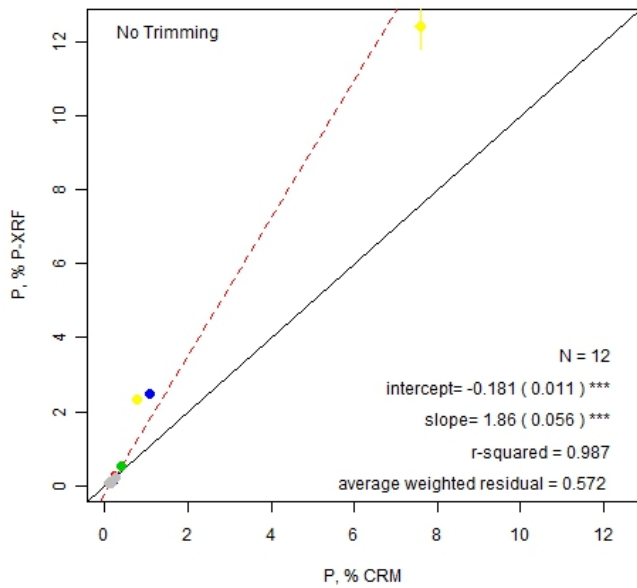
Handheld-HHAM-Mining Mode



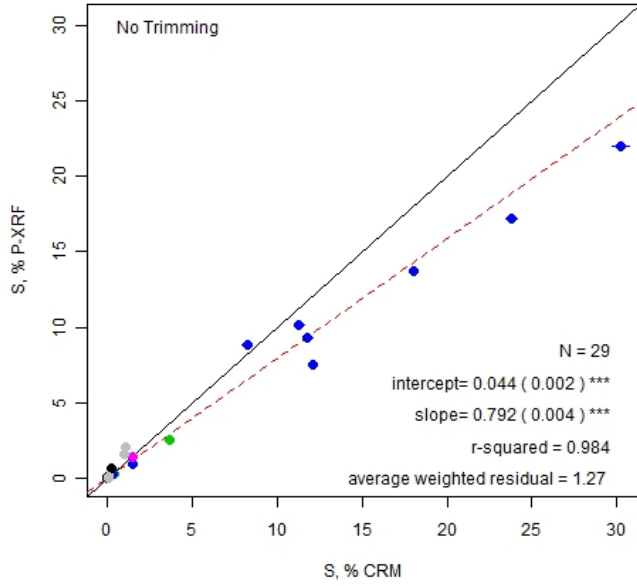
Handheld-HHBM-Mining Mode



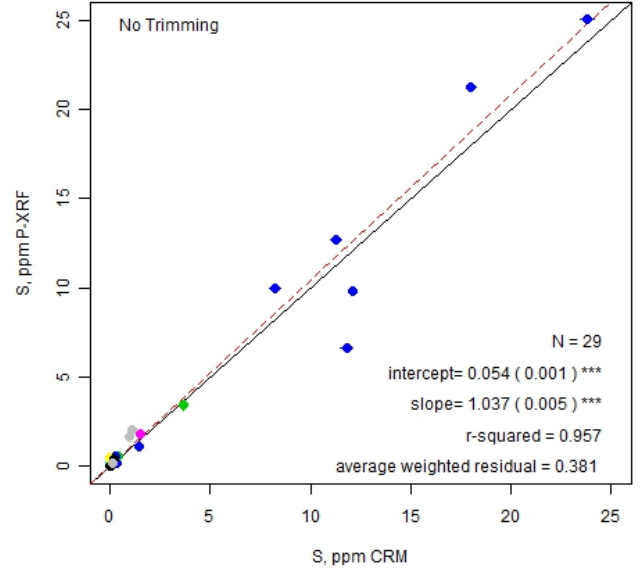
Handheld-HHCM-Mining Mode



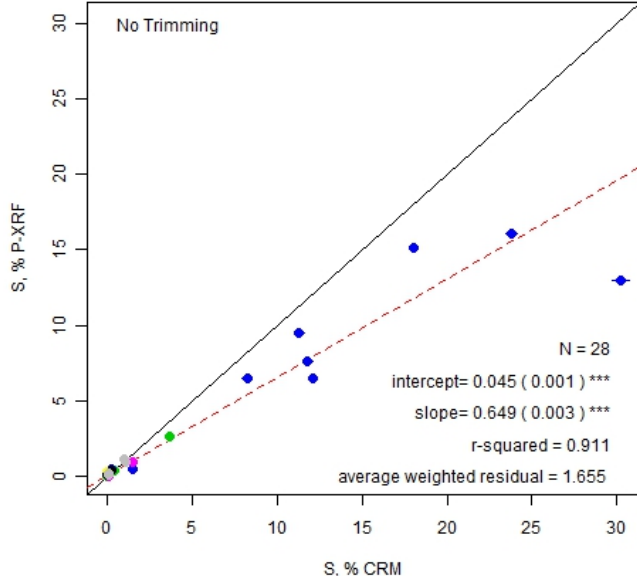
Benchtop-BTAM-Mining Mode



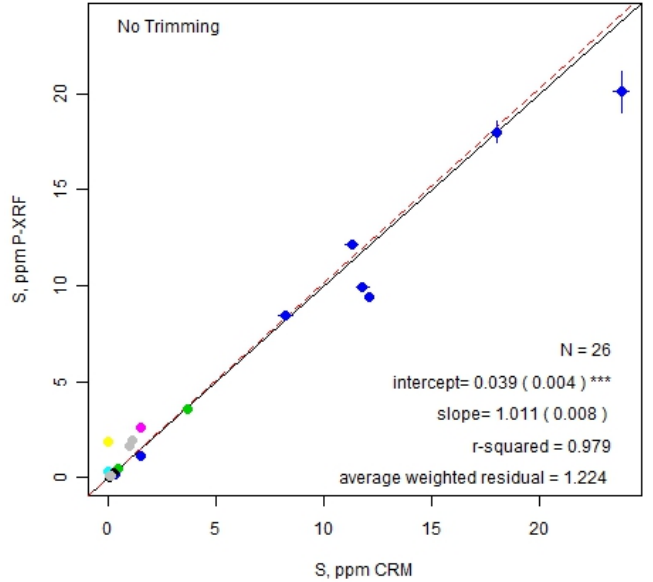
Handheld-BTBM-Mining Mode



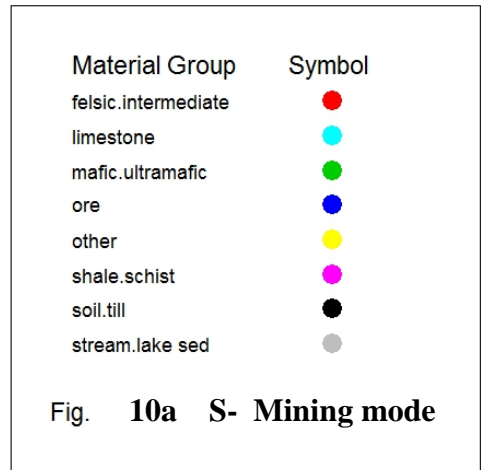
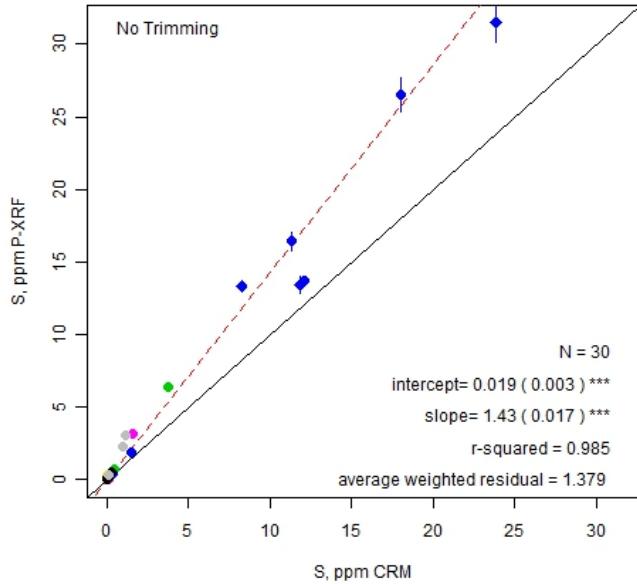
Handheld-HHAM-Mining Mode



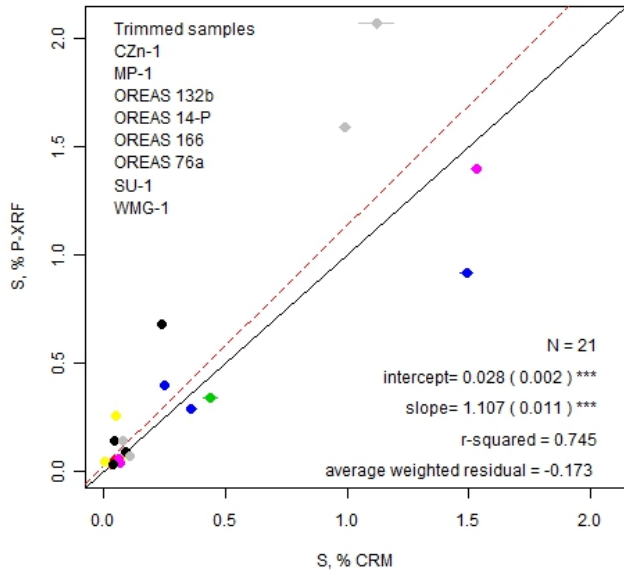
Handheld-HHBM-Mining Mode



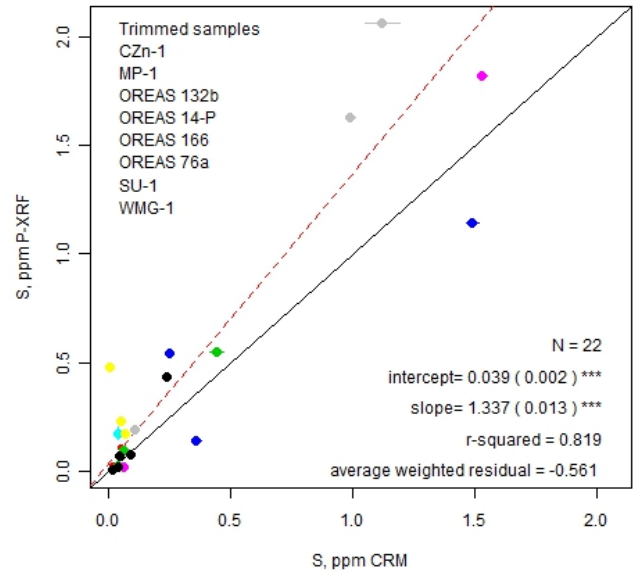
Handheld-HHCM-Mining Mode



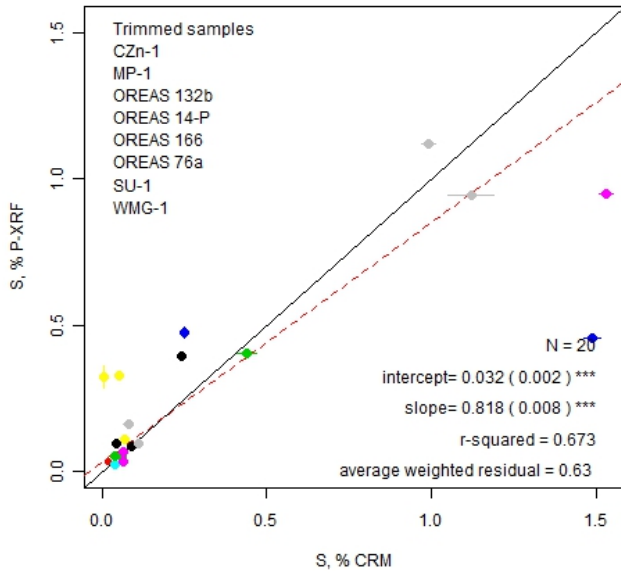
Benchtop-BTAM-Mining Mode



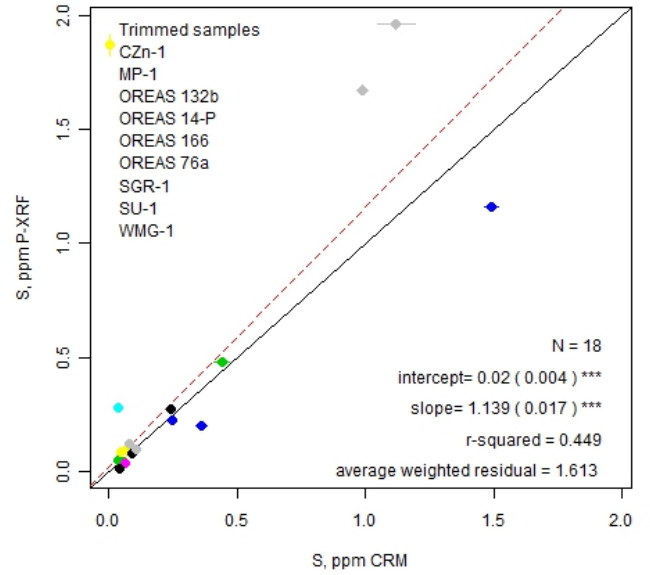
Handheld-BTBM-Mining Mode



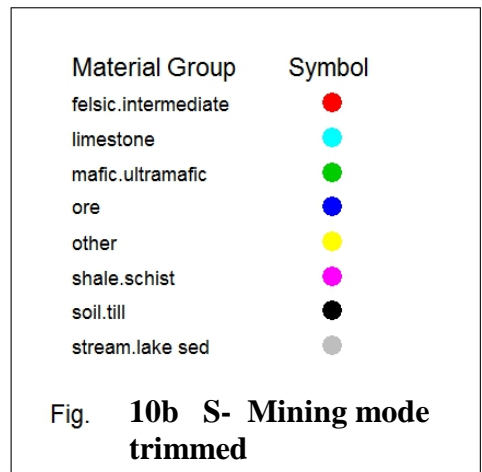
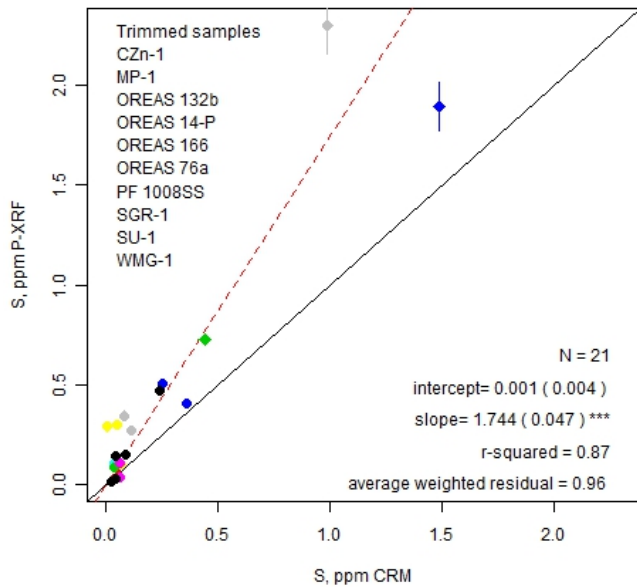
Handheld-HHAM-Mining Mode



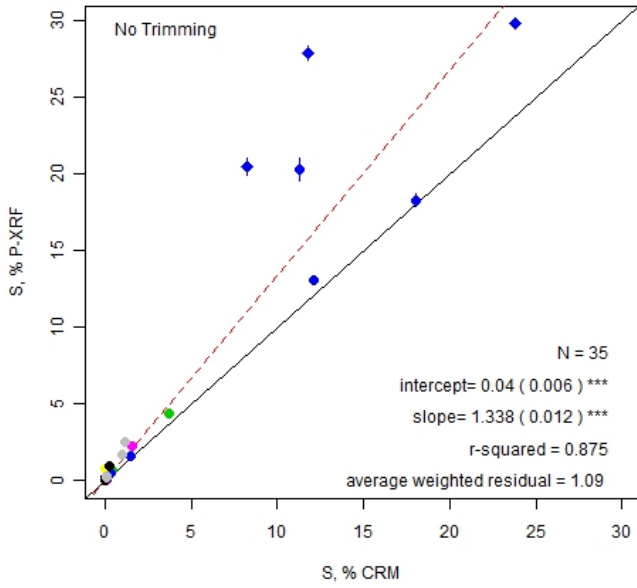
Handheld-HHBM-Mining Mode



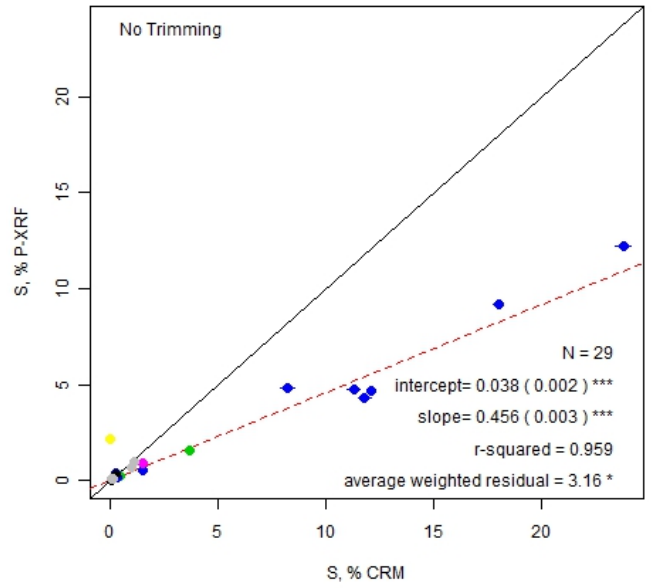
Handheld-HHCM-Mining Mode



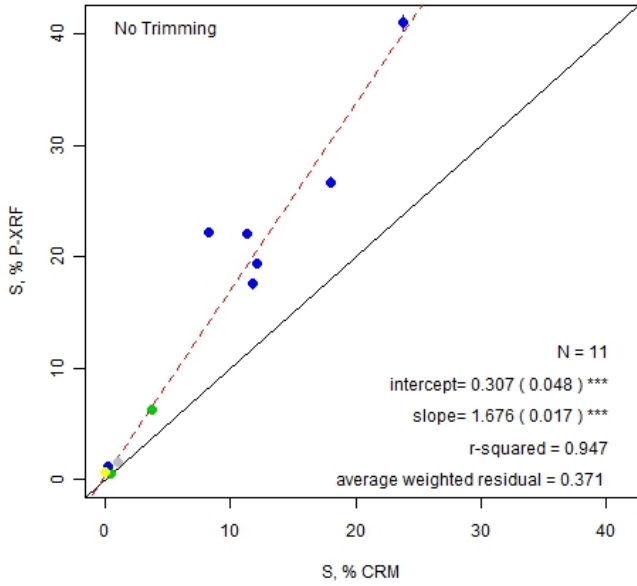
Bench Top-BTAS-Soil Mode



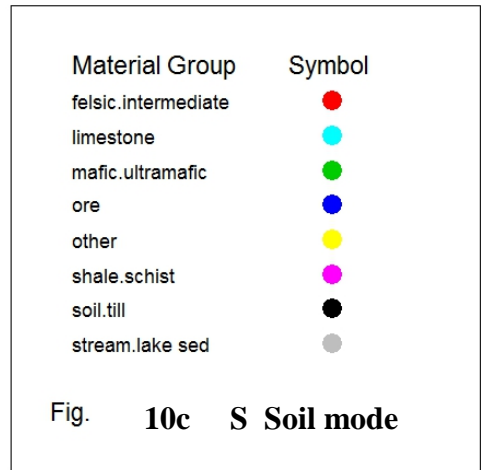
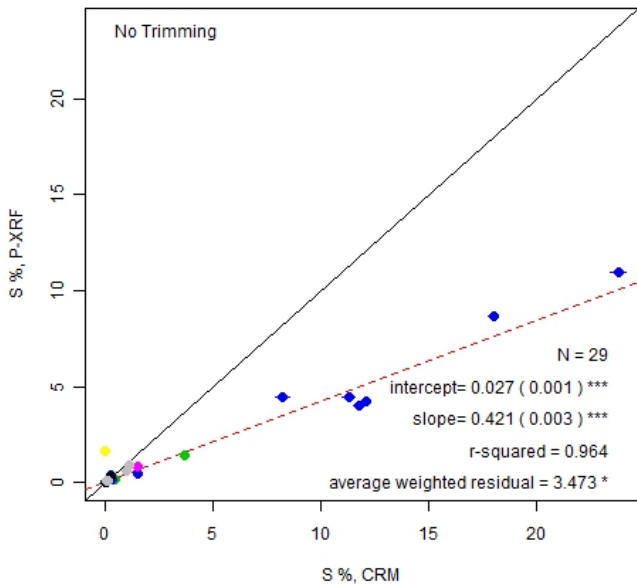
Bench Top-BTBS-Soil Mode



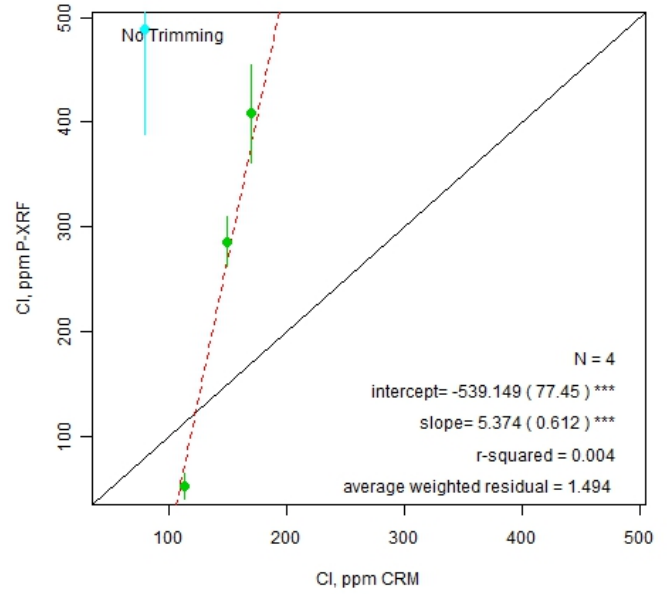
Handheld-HHAS-Soil Mode



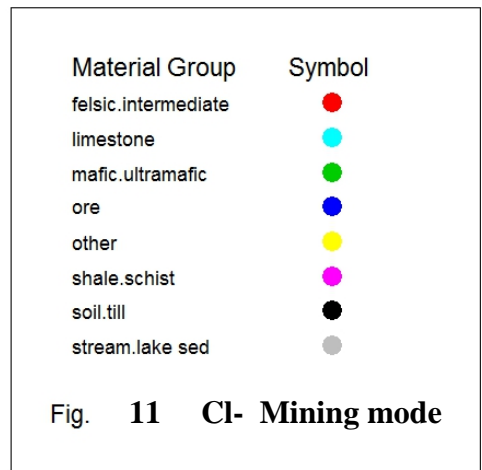
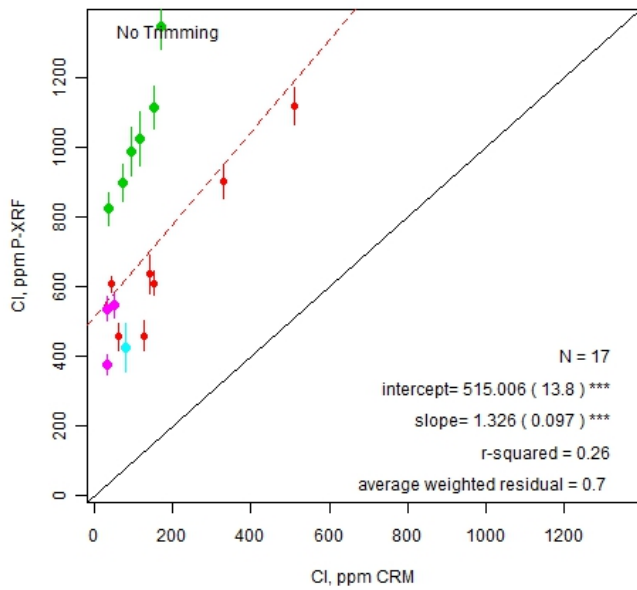
Handheld-HHCS-Soil Mode

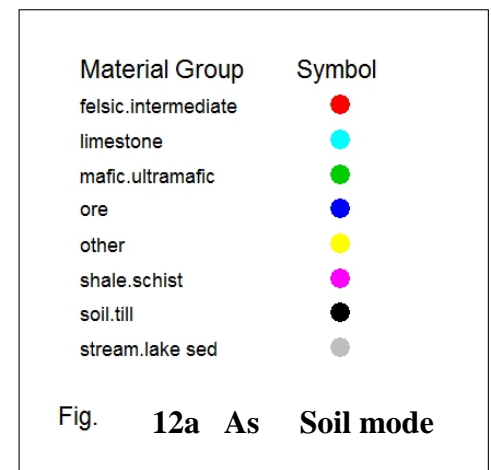
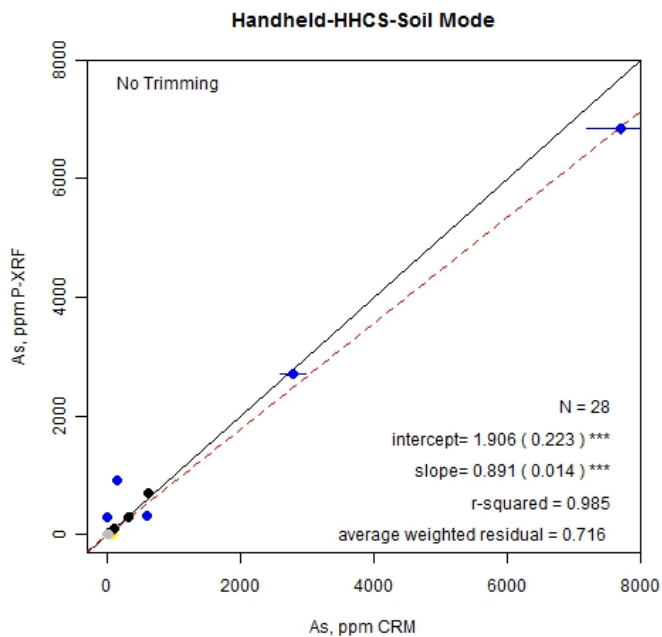
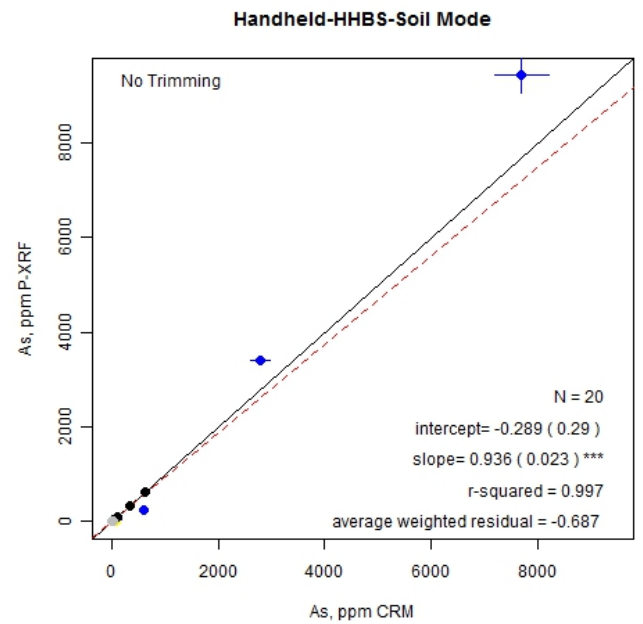
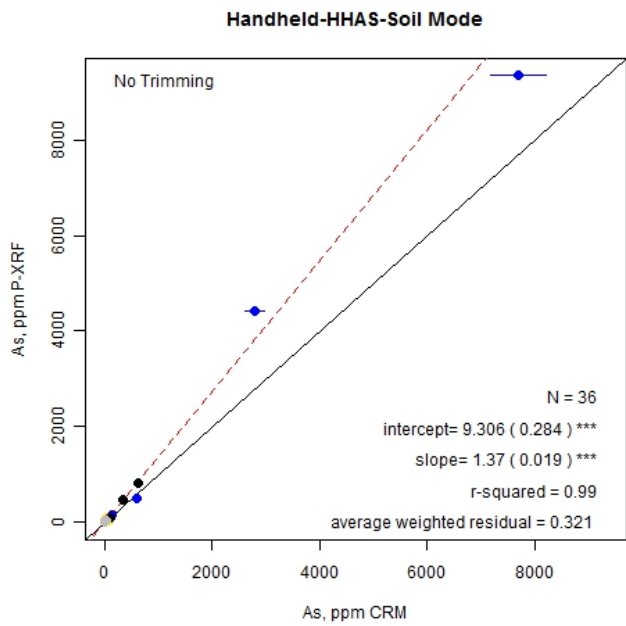
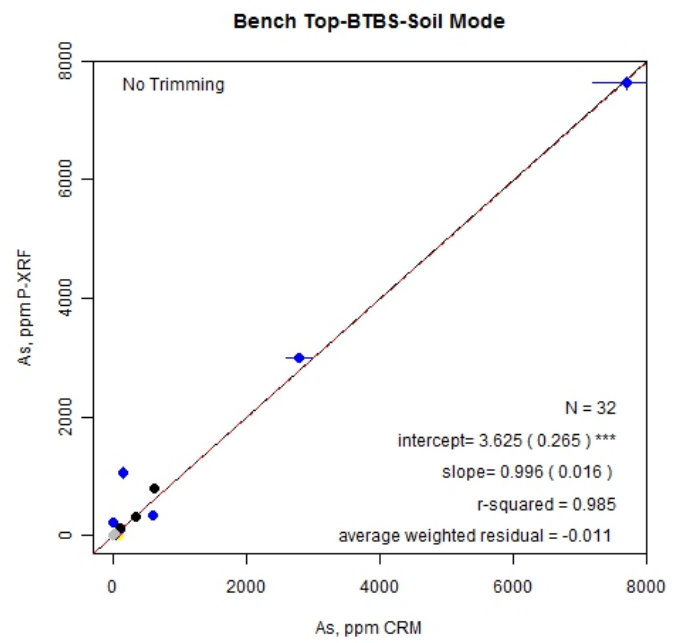
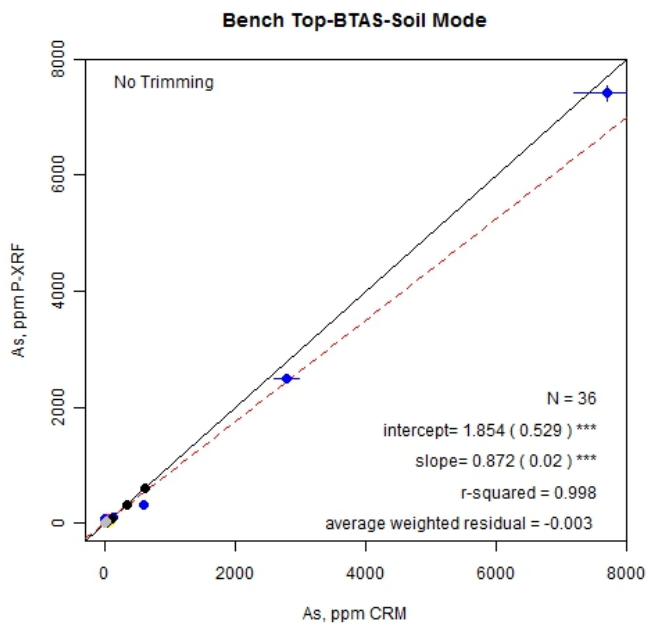


Benchtop-BTBM-Mining Mode

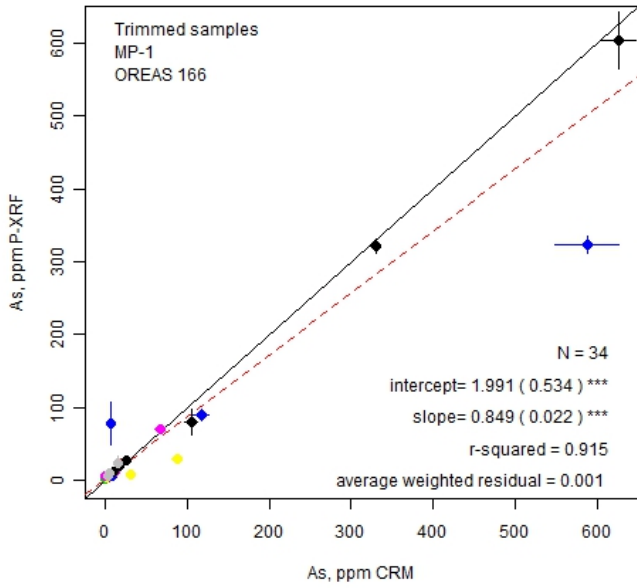


Handheld-HHCM-Mining Mode

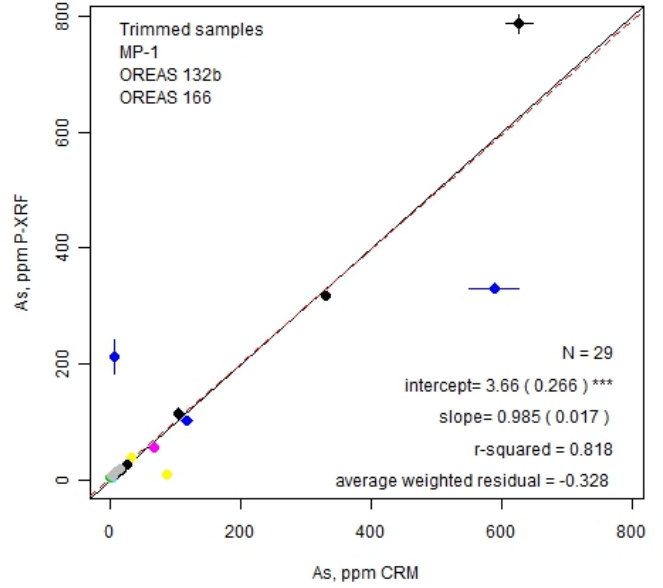




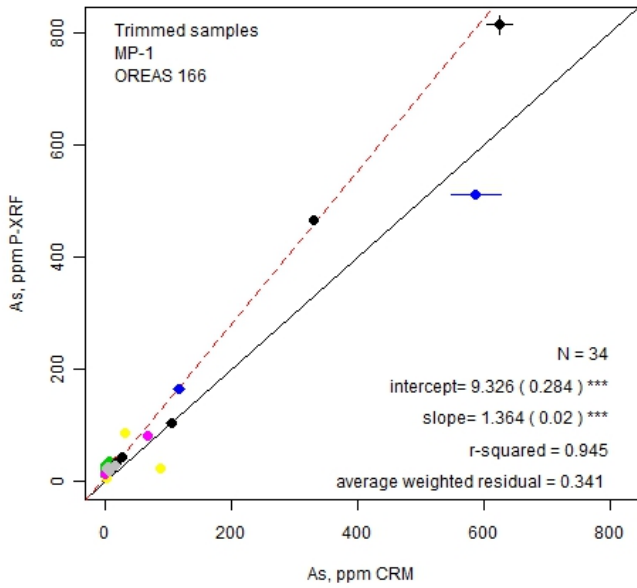
Bench Top-Machine A-Soil Mode



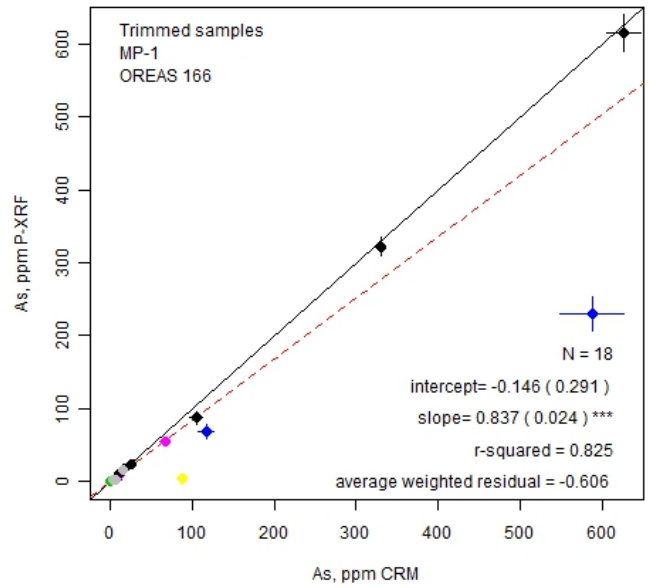
Bench Top-BTBS-Soil Mode



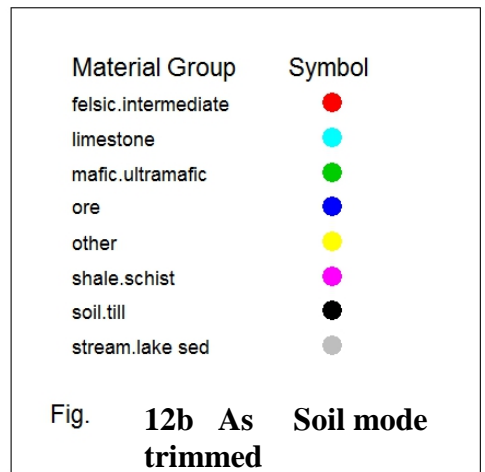
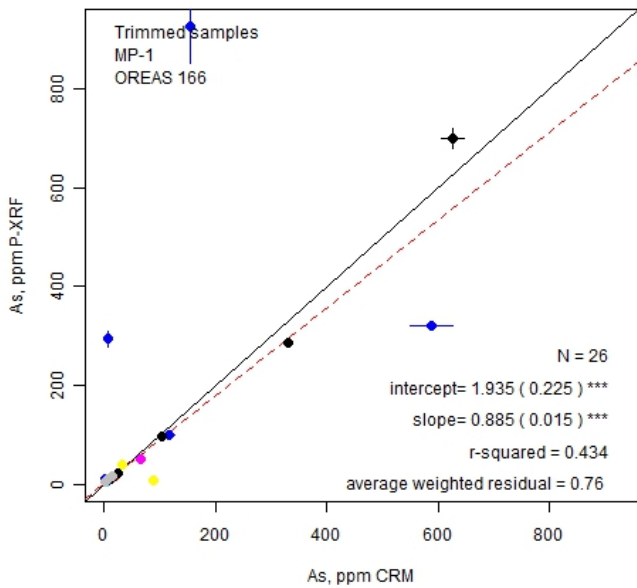
Handheld-HHAS-Soil Mode

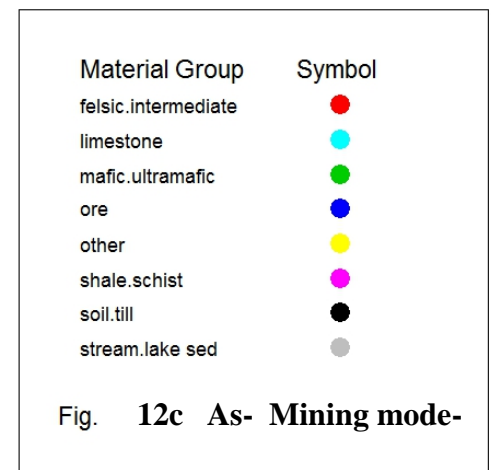
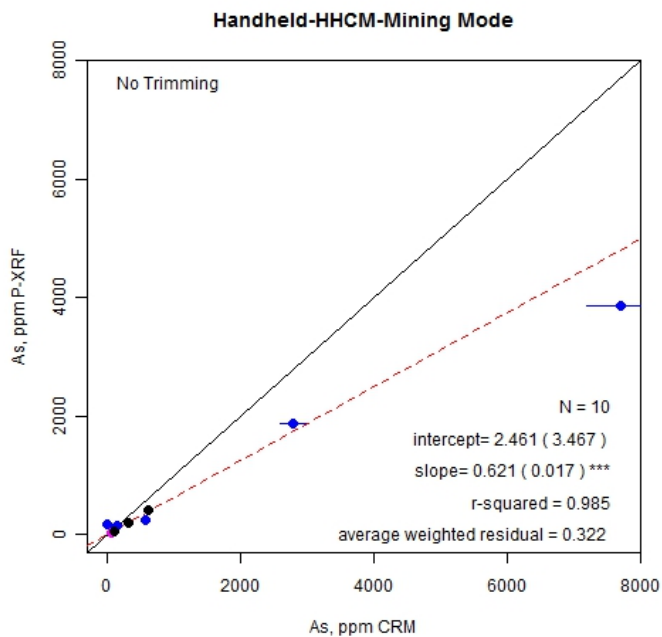
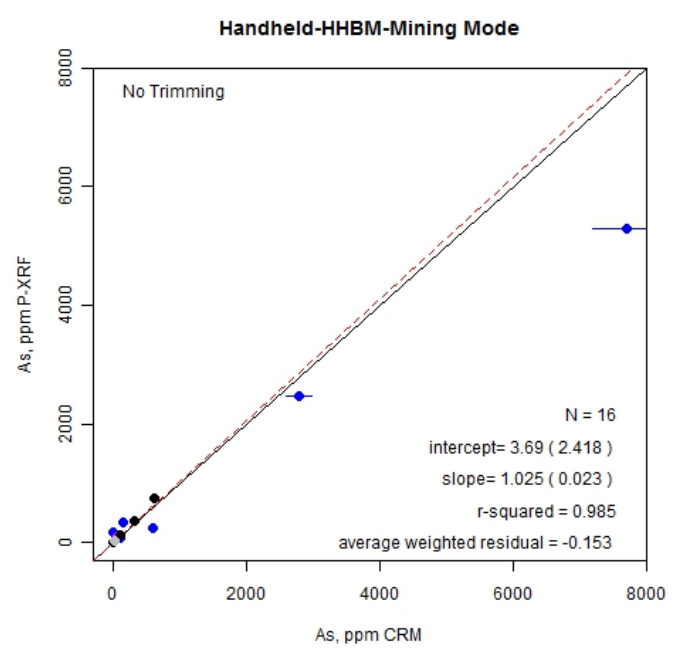
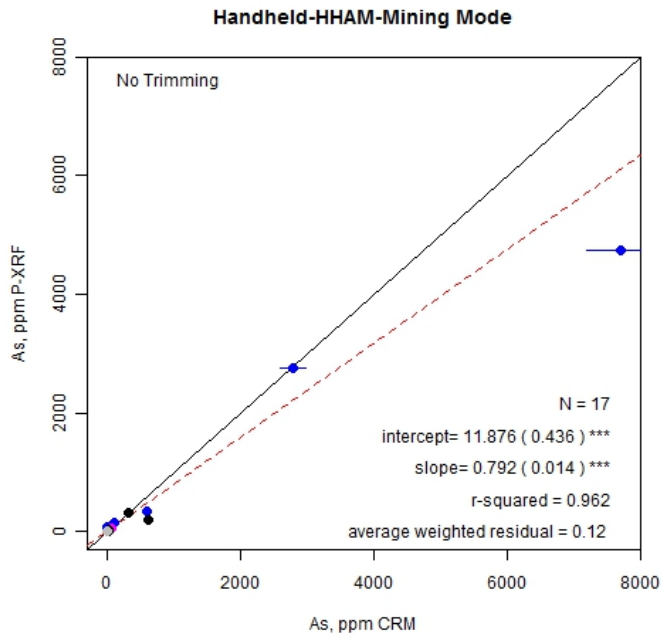
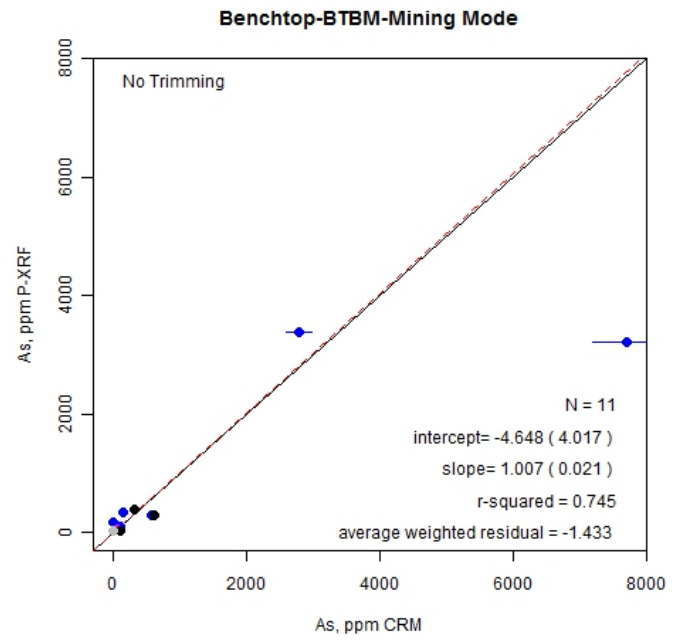
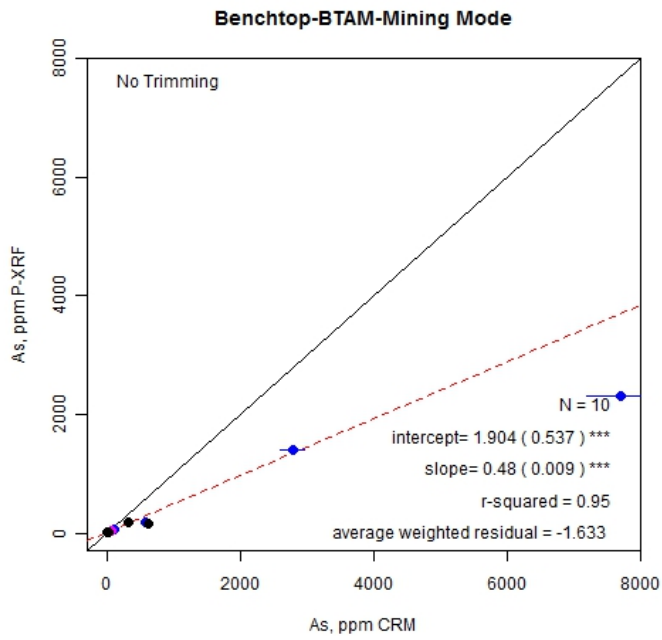


Handheld-HHBS-Soil Mode

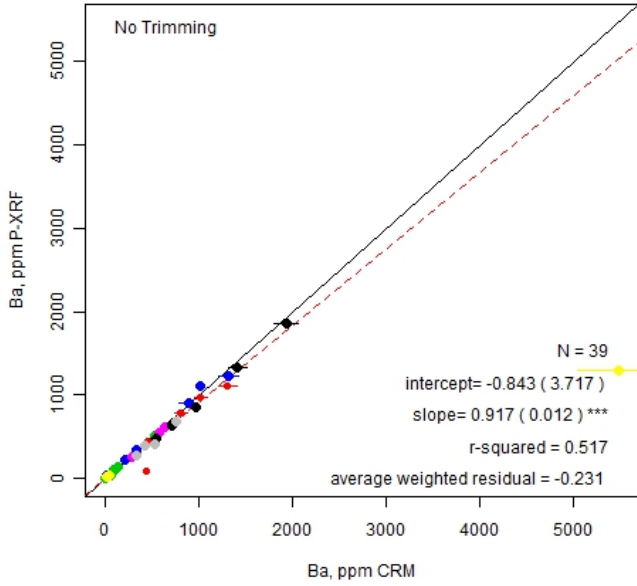


Handheld-HHCS-Soil Mode

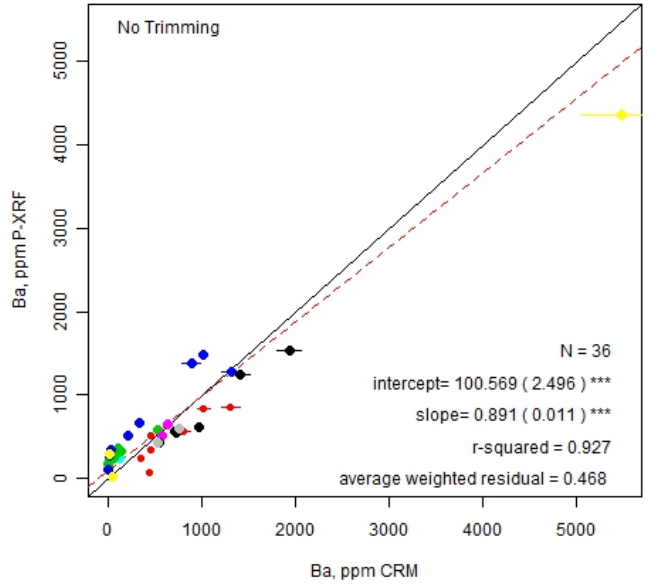




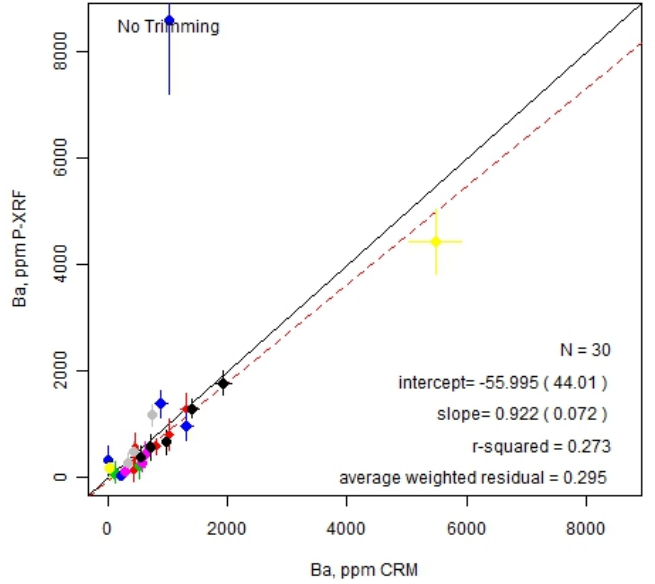
Bench Top-BTAS-Soil Mode



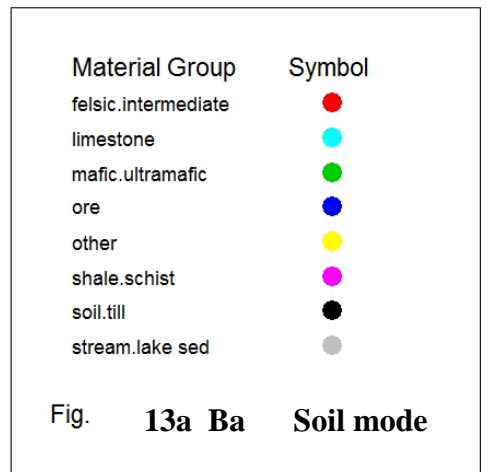
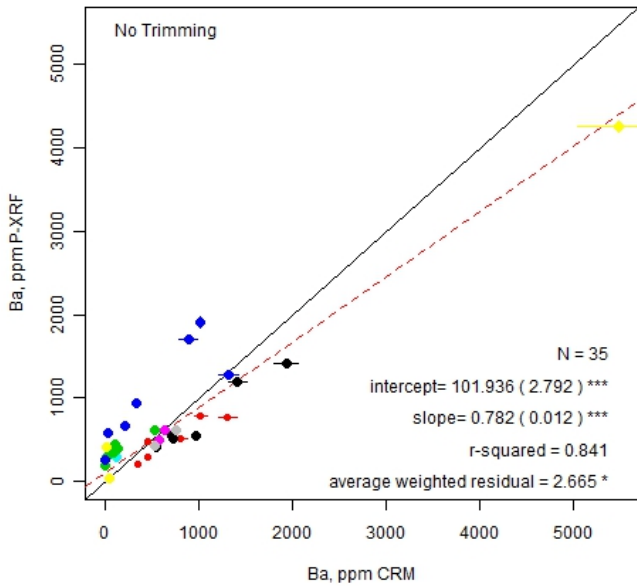
Bench Top-BTBS-Soil Mode



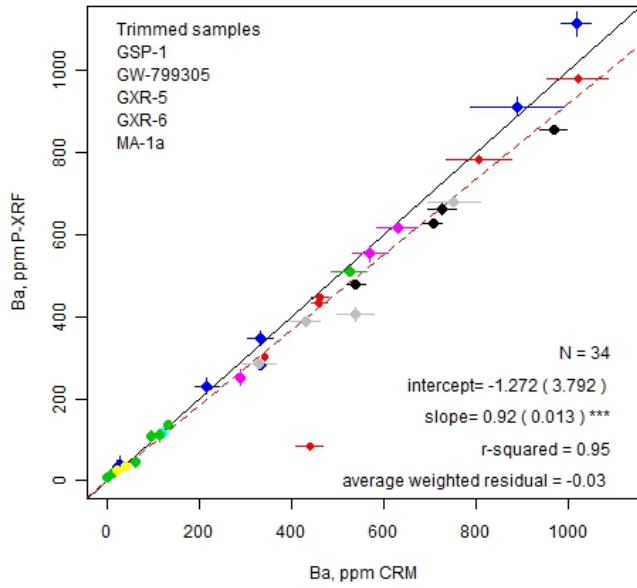
Handheld-HHBS-Soil Mode



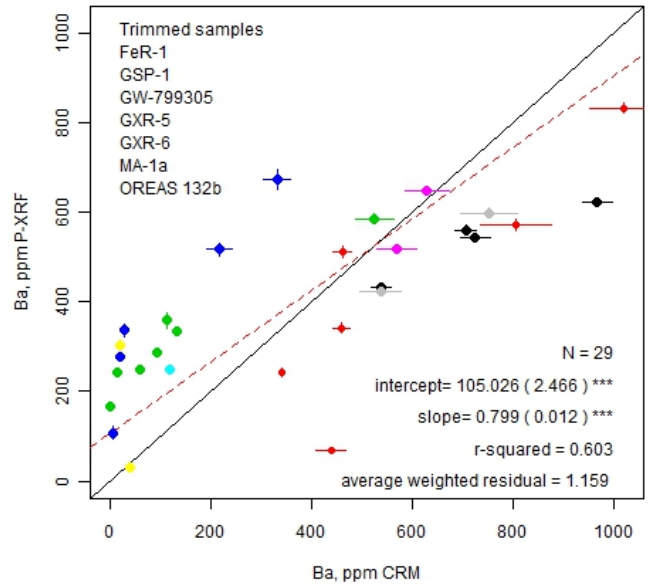
Handheld-HHCS-Soil Mode



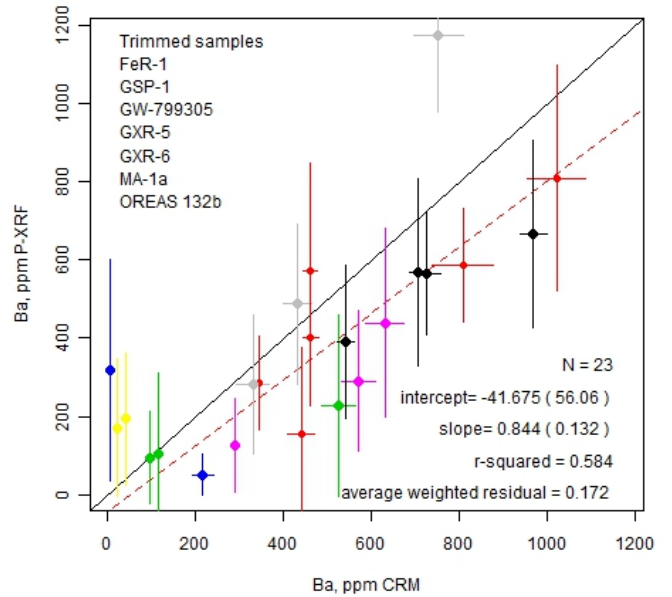
Bench Top-Machine A-Soil Mode



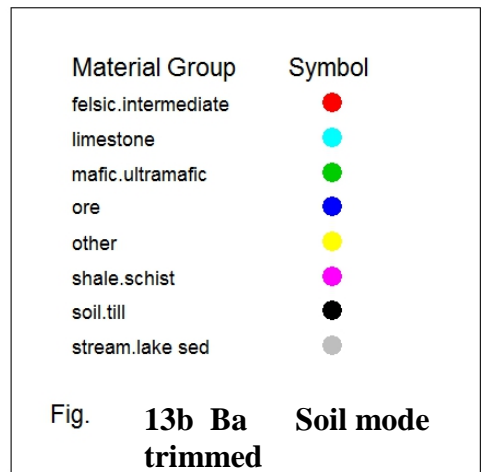
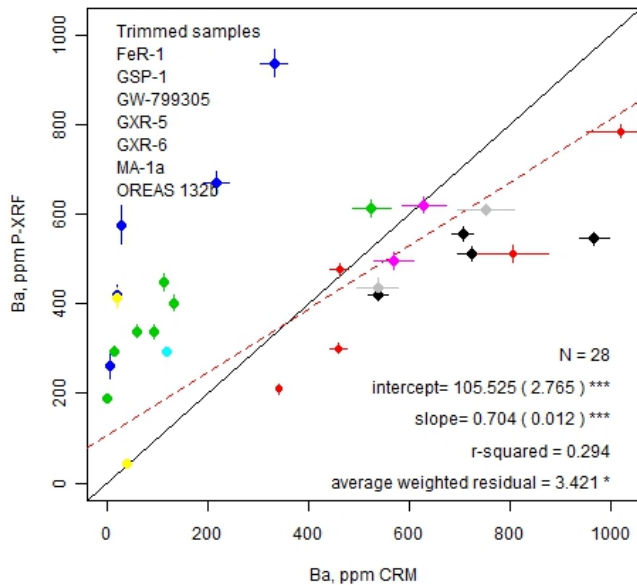
Bench Top-BTBS-Soil Mode

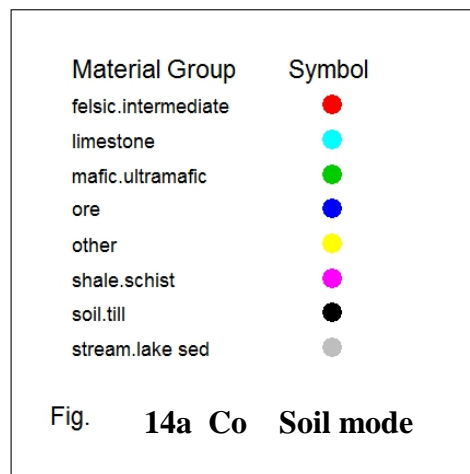
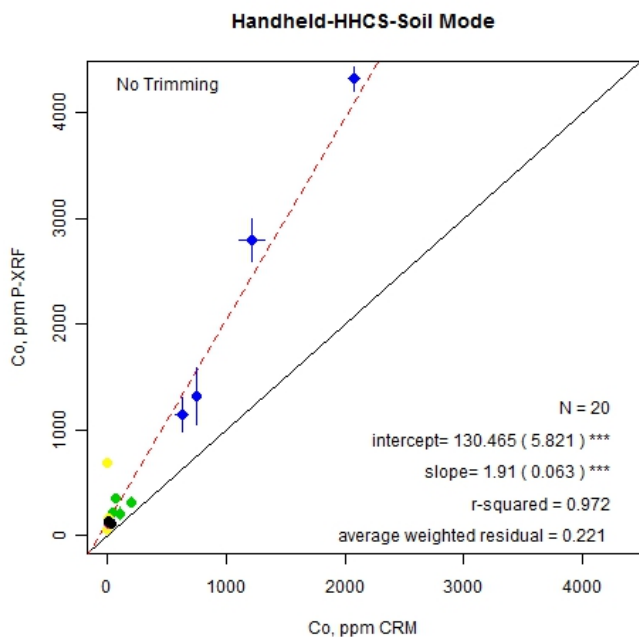
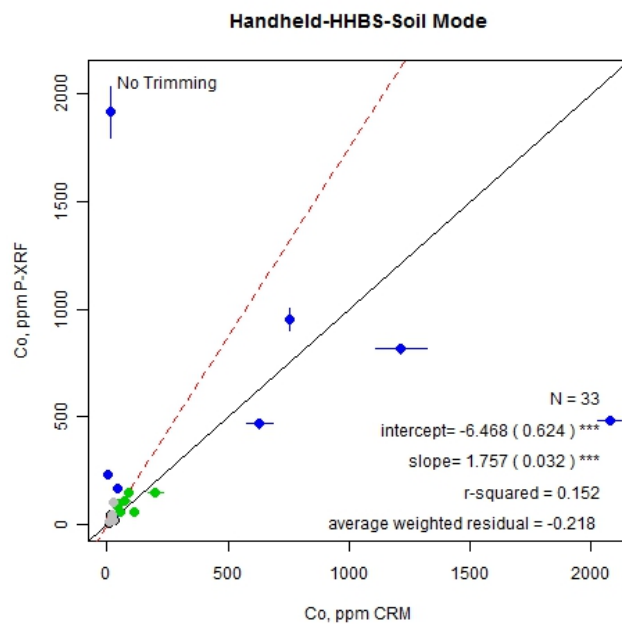
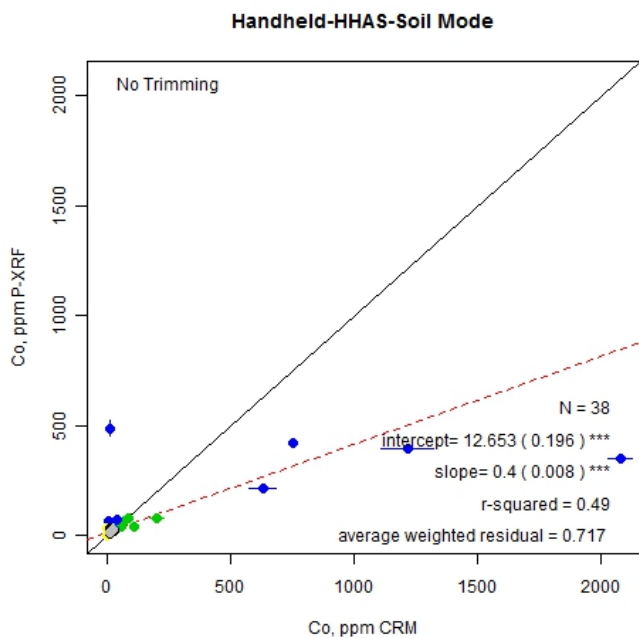
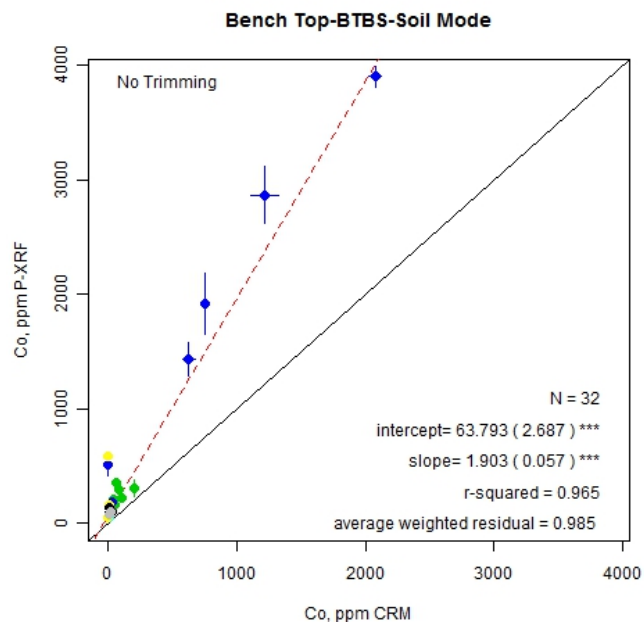
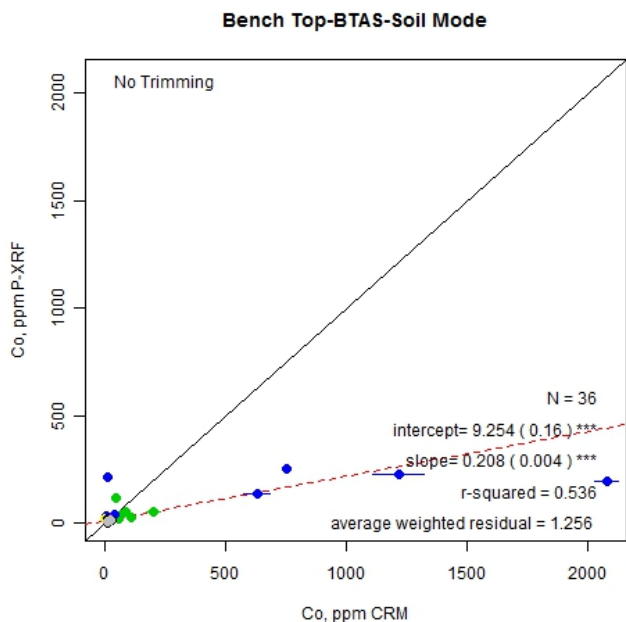


Handheld-HHBS-Soil Mode

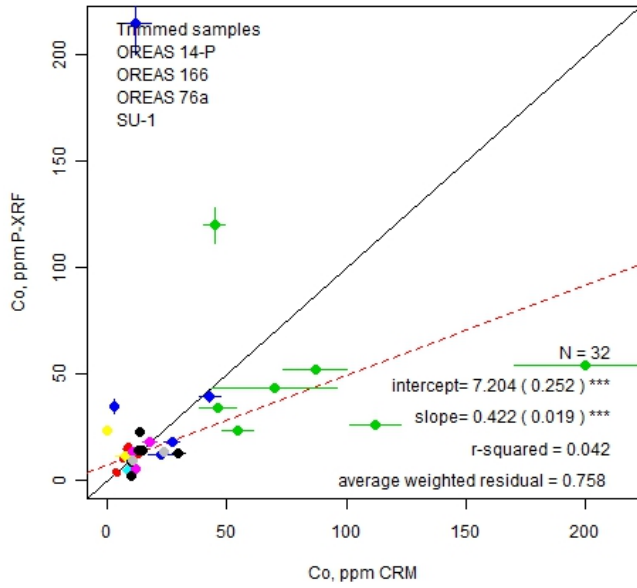


Handheld-HHCS-Soil Mode

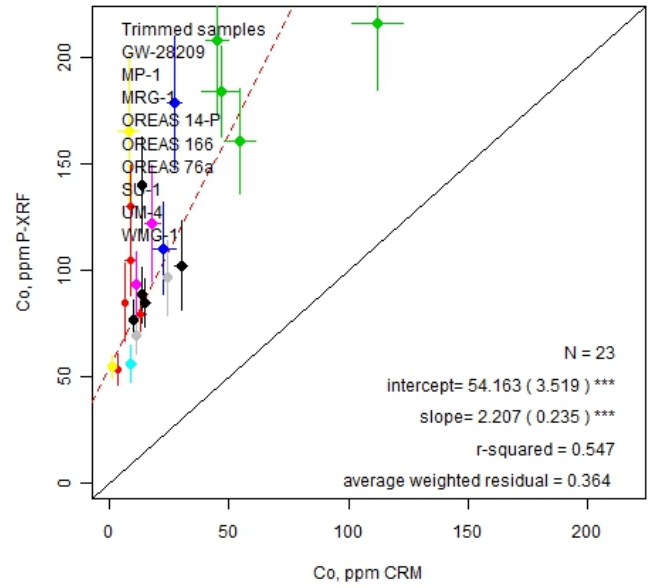




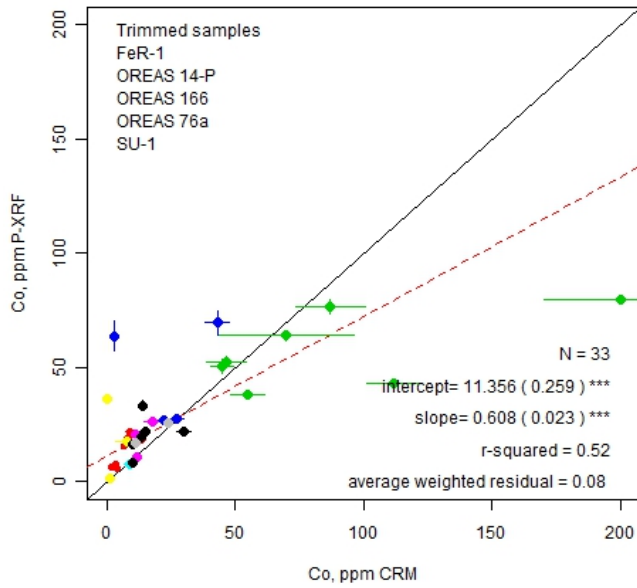
Bench Top-Machine A-Soil Mode



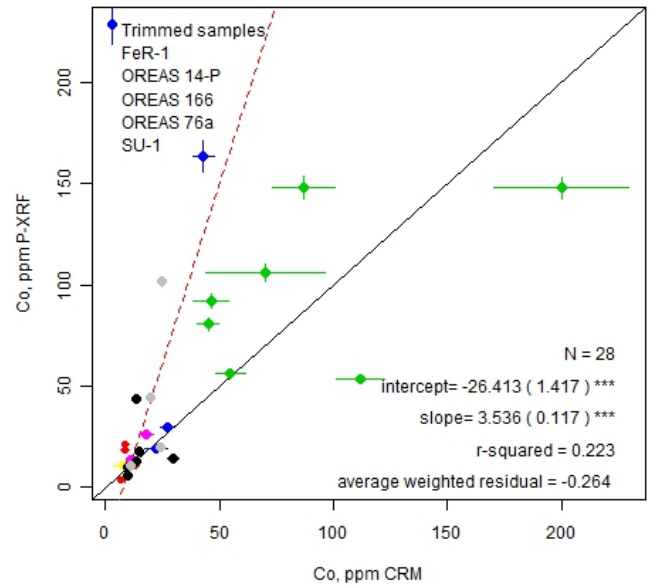
Bench Top-BTBS-Soil Mode



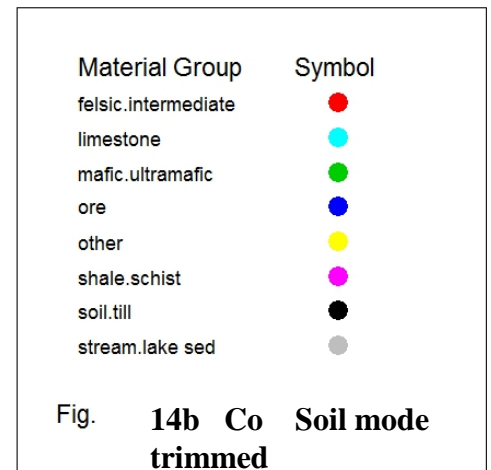
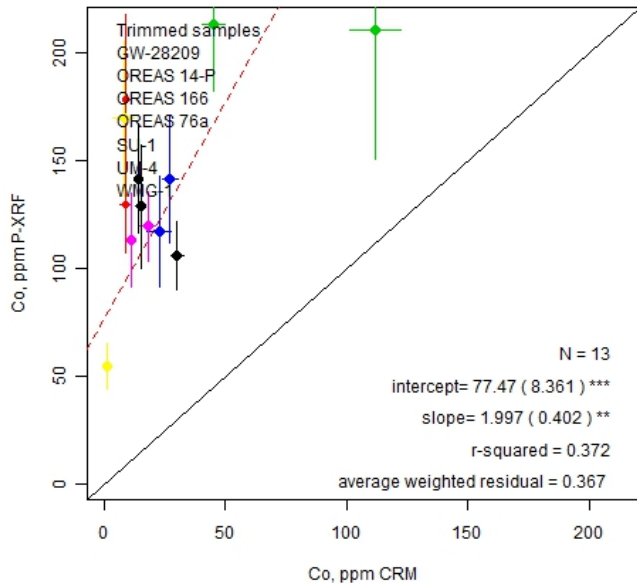
Handheld-HHAS-Soil Mode



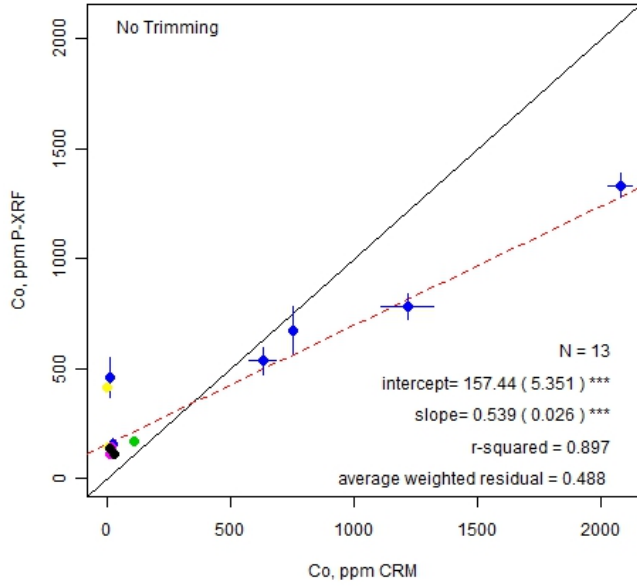
Handheld-HHBS-Soil Mode



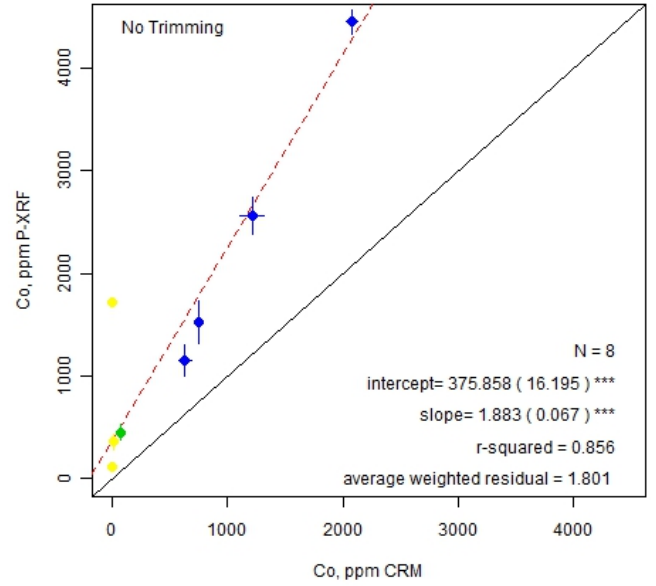
Handheld-HHCS-Soil Mode



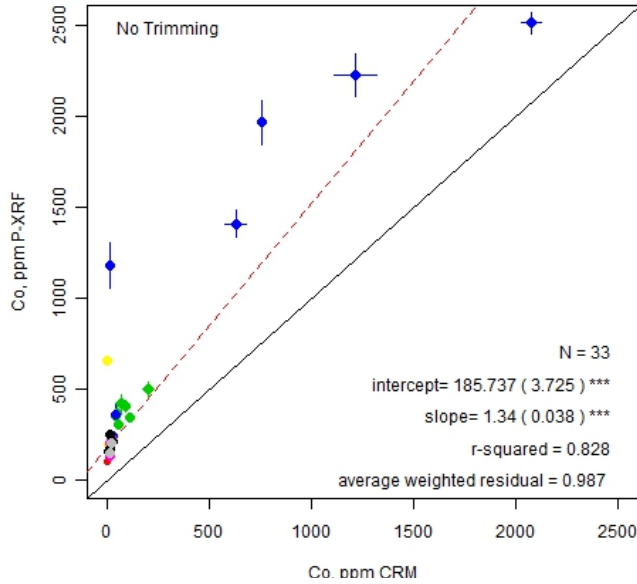
Benchtop-BTAM-Mining Mode



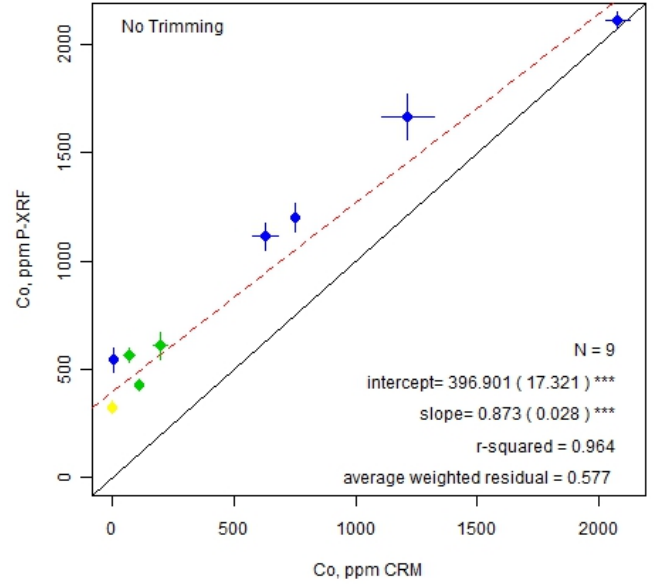
Benchtop-BTBM-Mining Mode



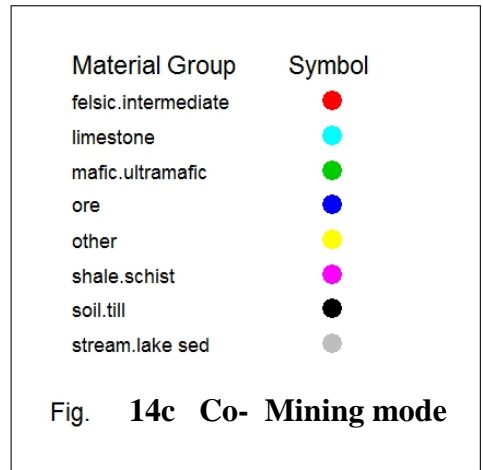
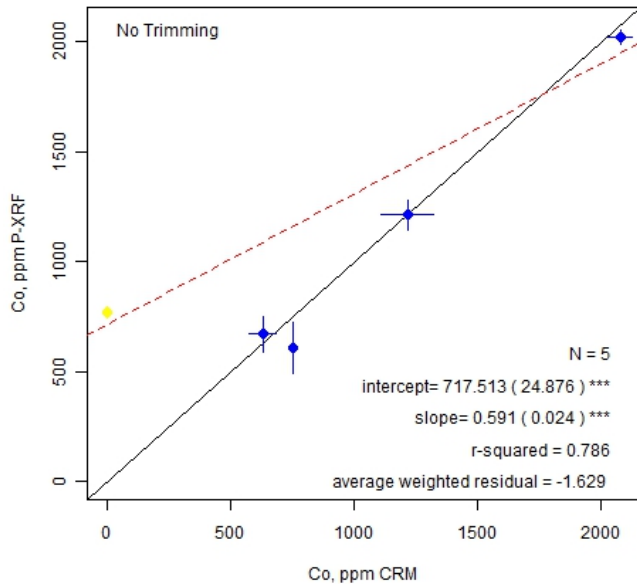
Handheld-HHAM-Mining Mode

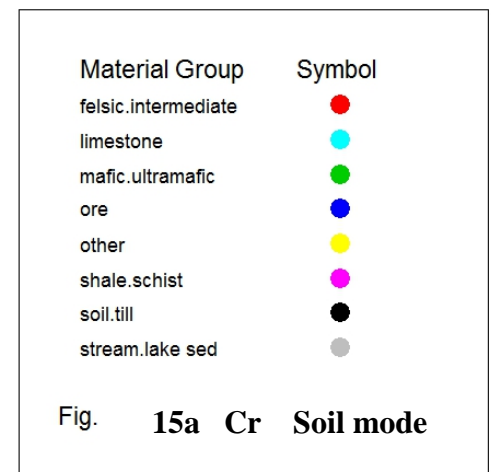
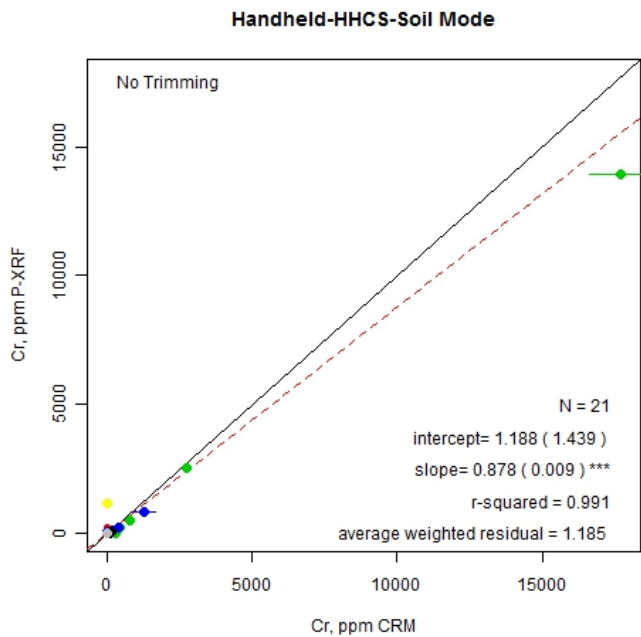
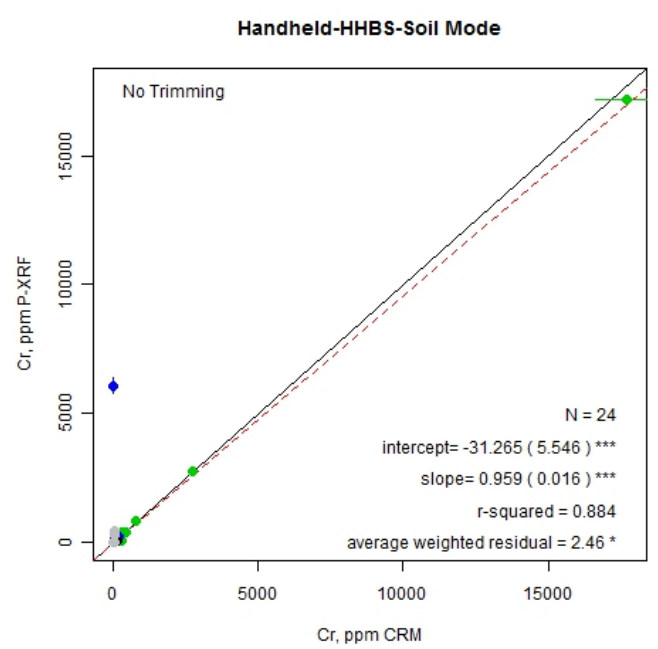
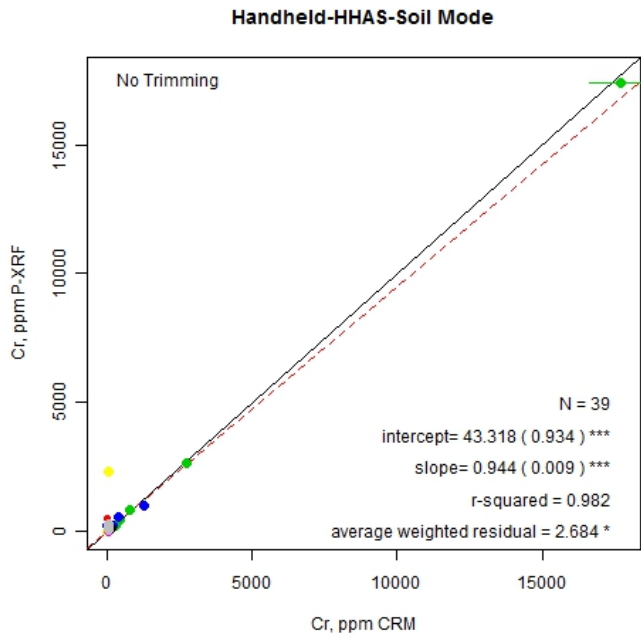
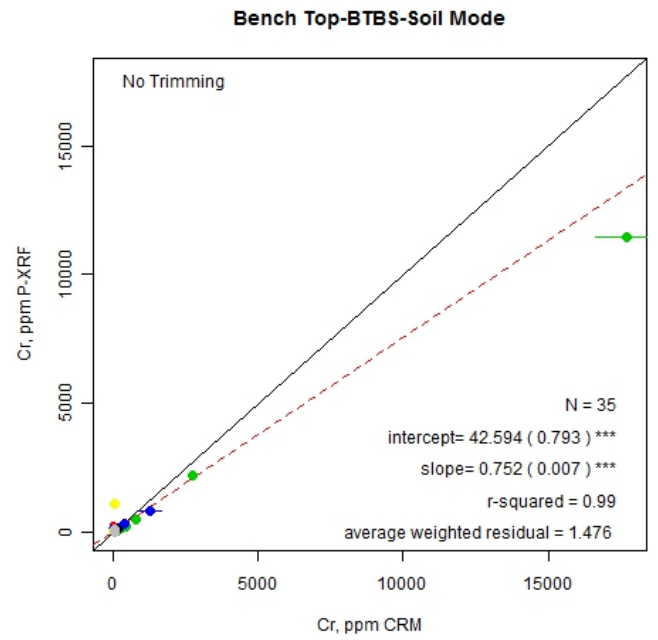
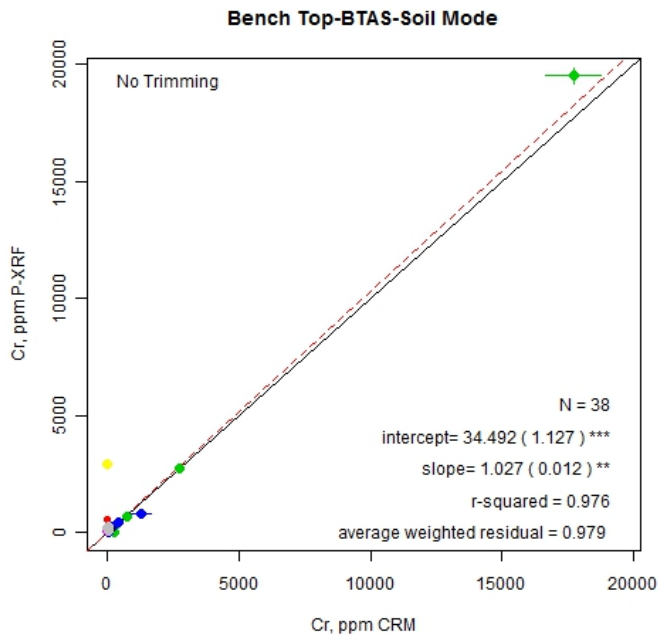


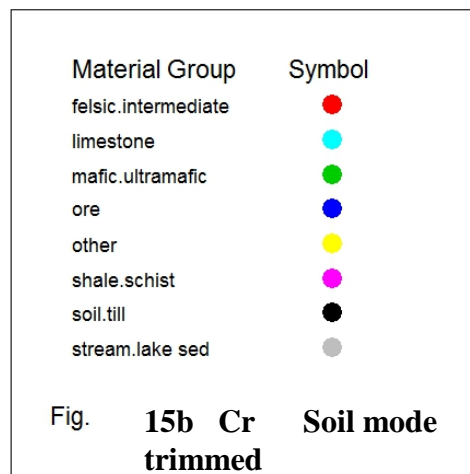
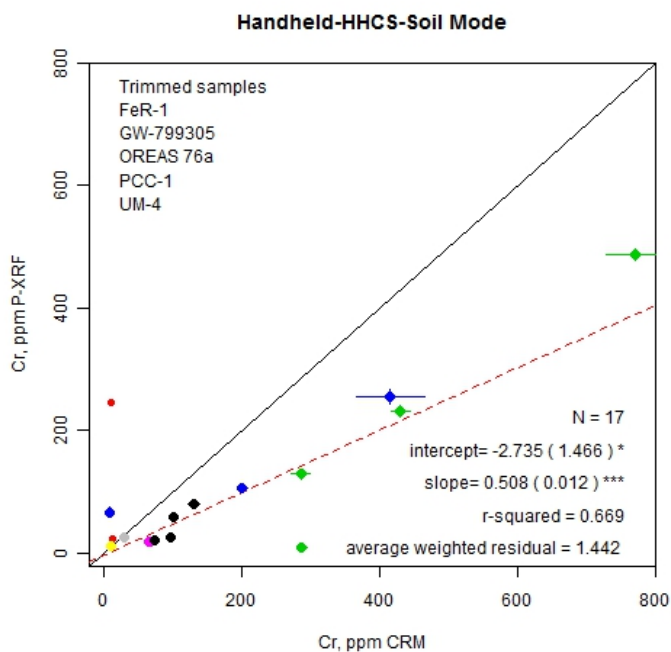
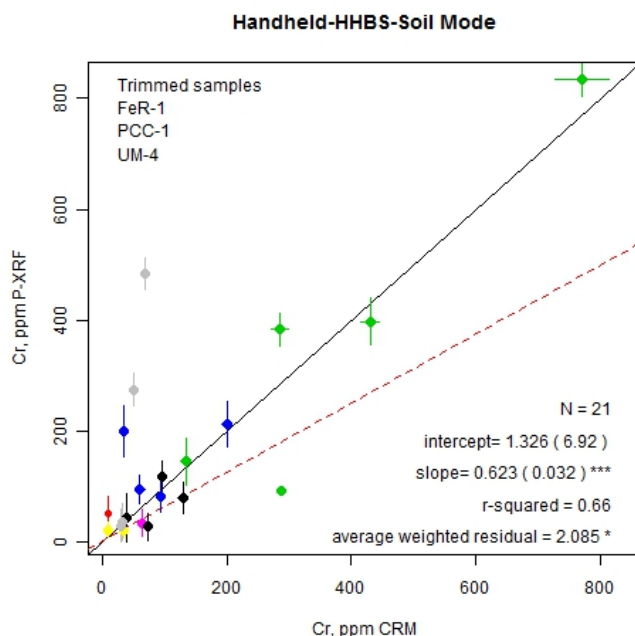
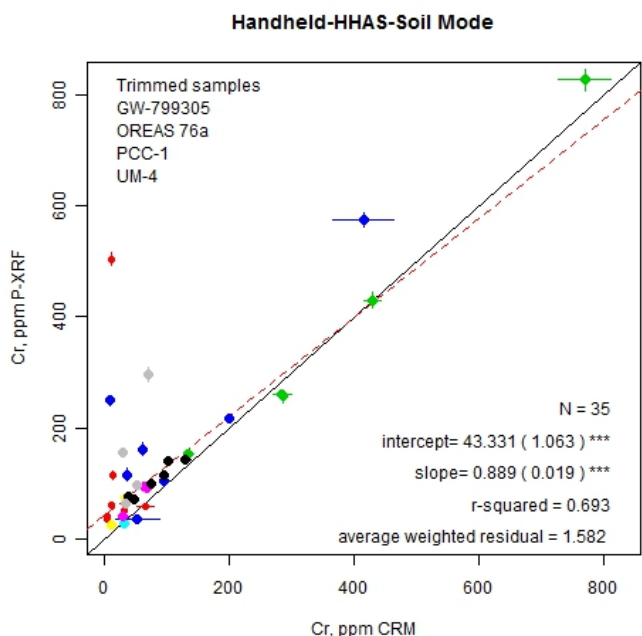
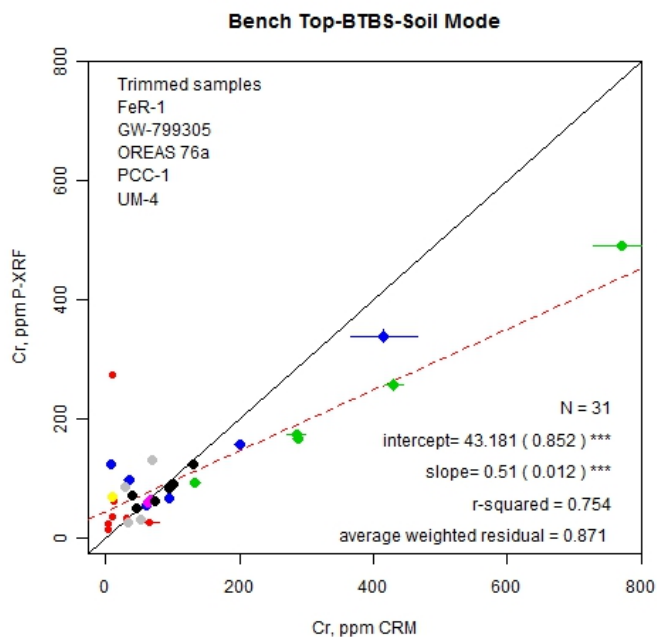
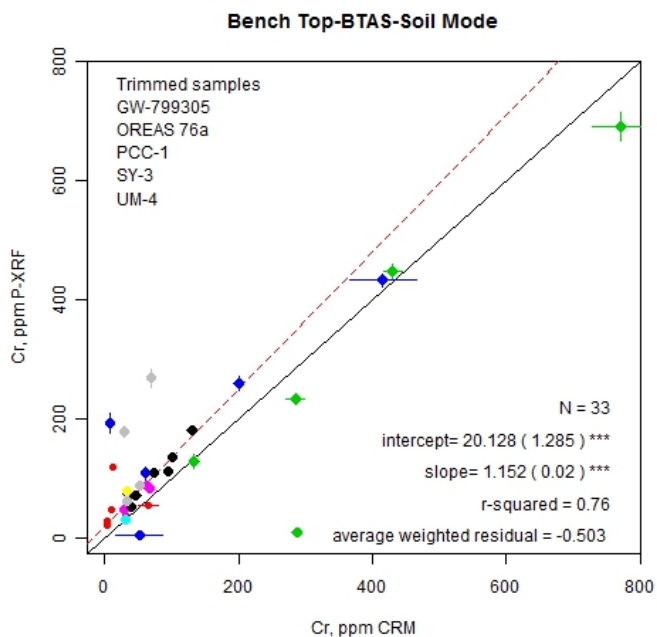
Handheld-HHBM-Mining Mode



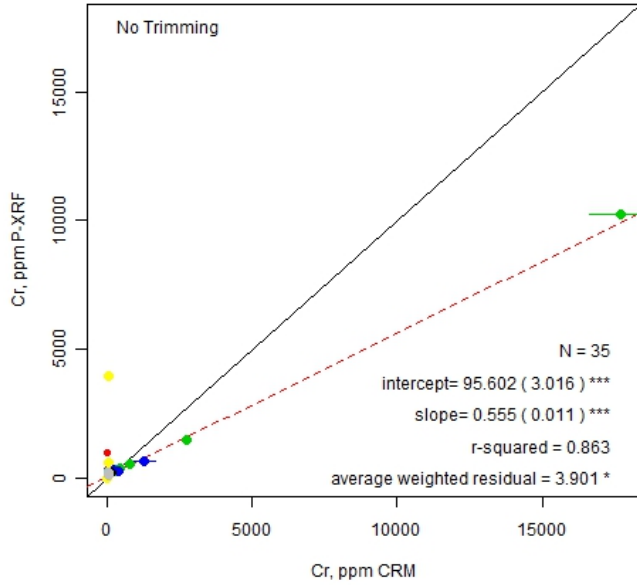
Handheld-HHCM-Mining Mode



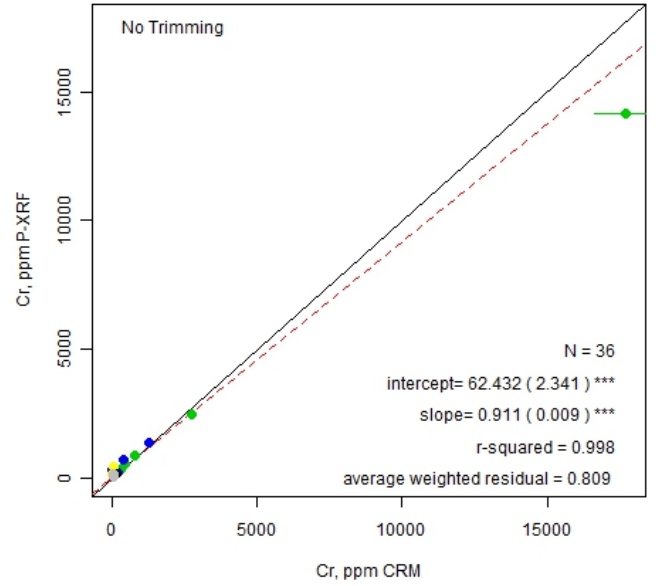




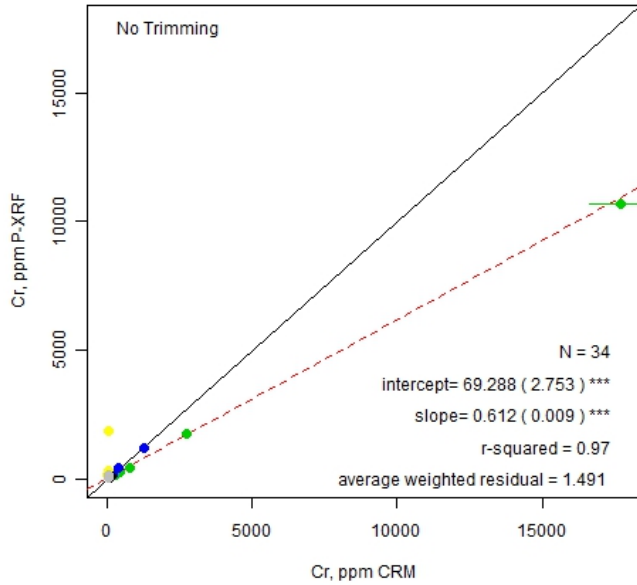
Benchtop-BTAM-Mining Mode



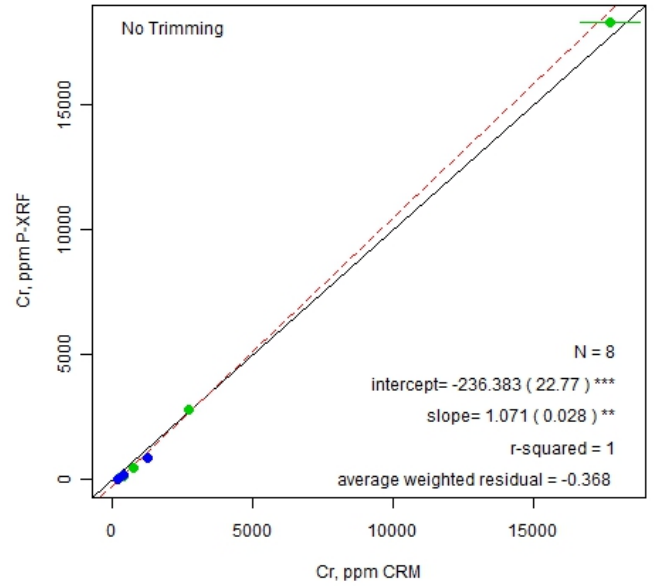
Benchtop-BTBM-Mining Mode



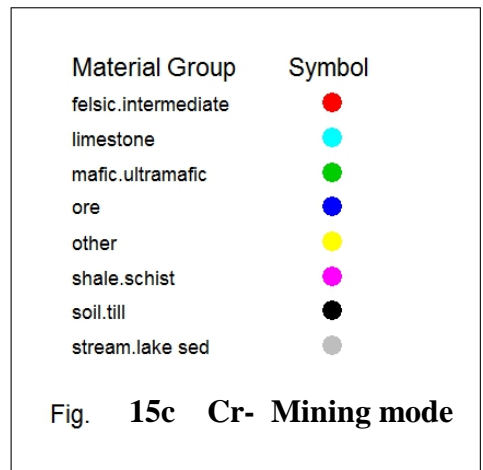
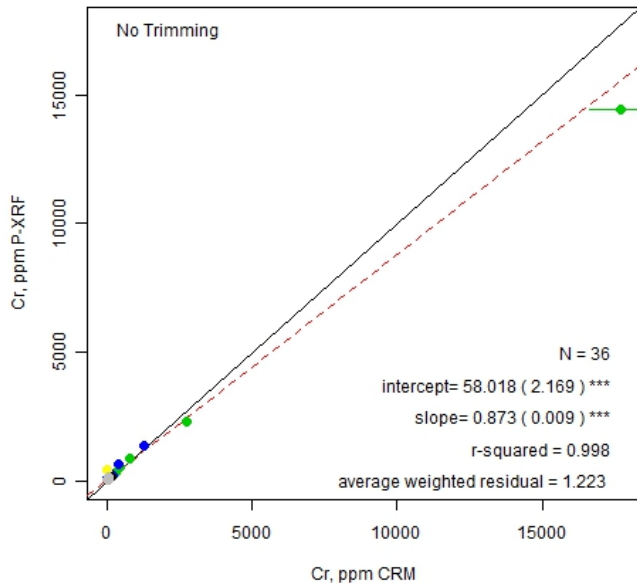
Handheld-HHAM-Mining Mode

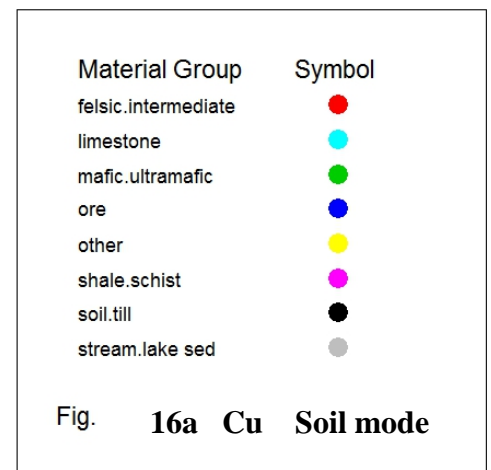
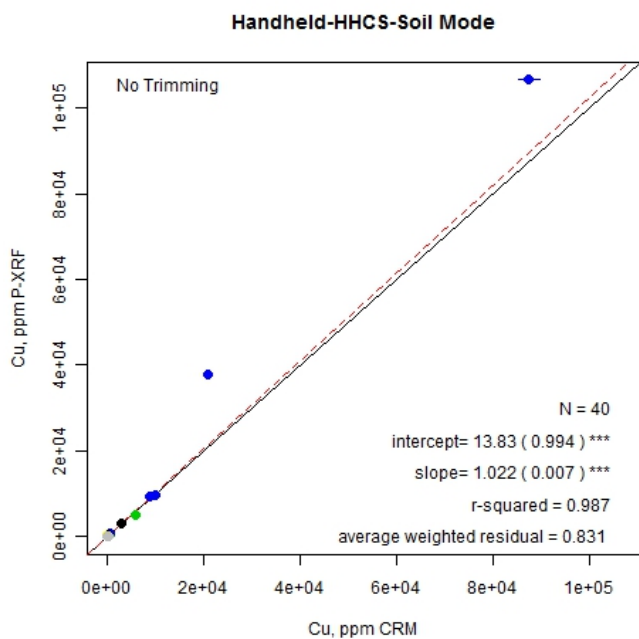
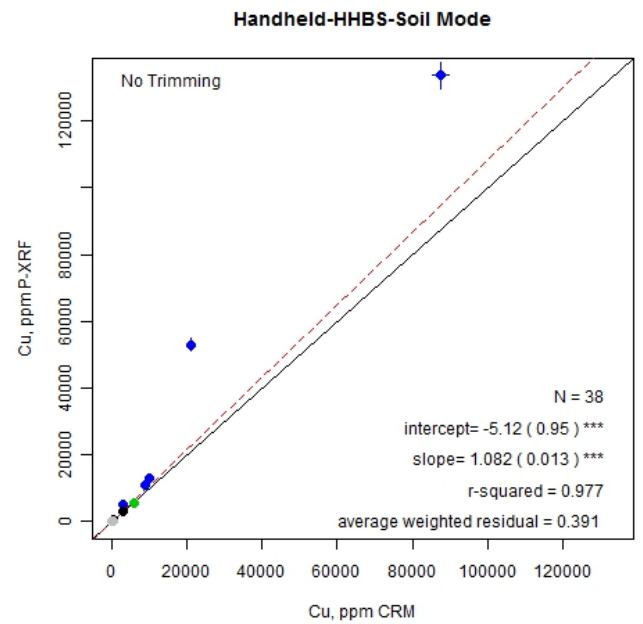
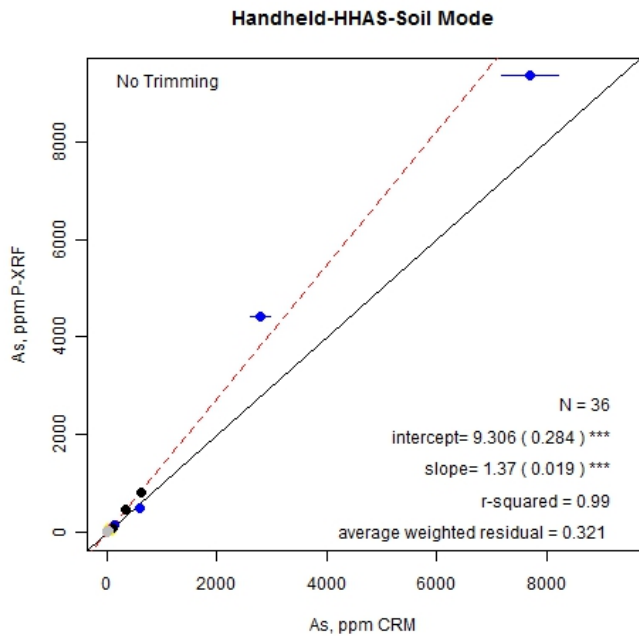
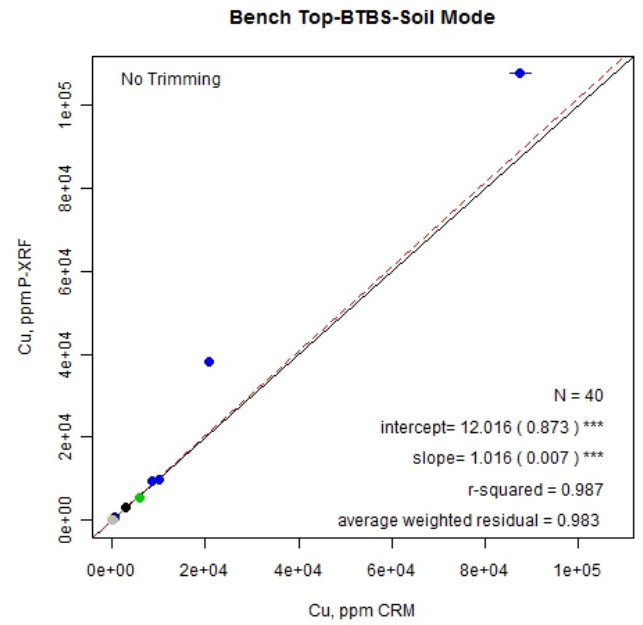
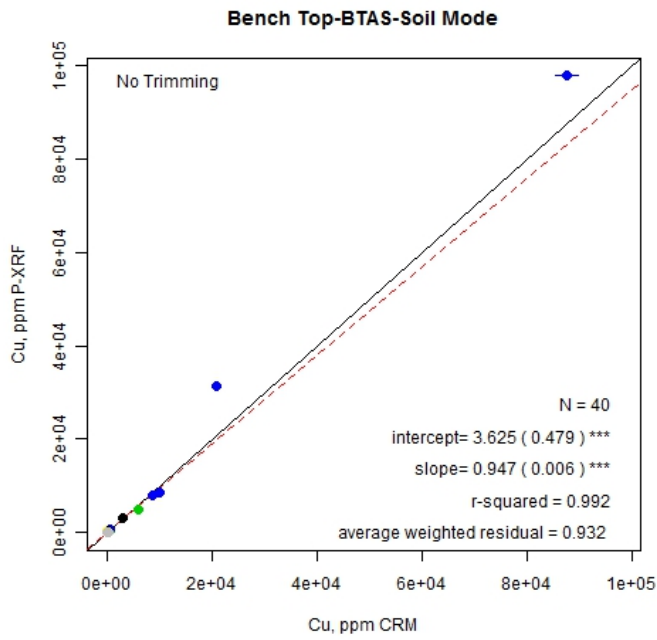


Handheld-HHBM-Mining Mode

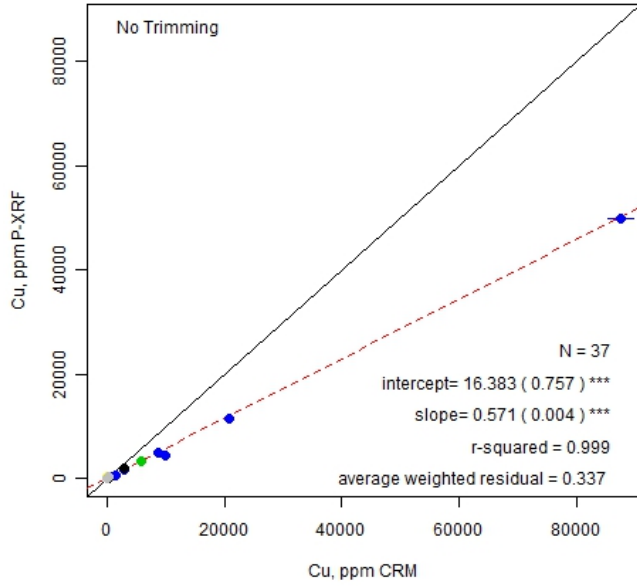


Handheld-HHCM-Mining Mode

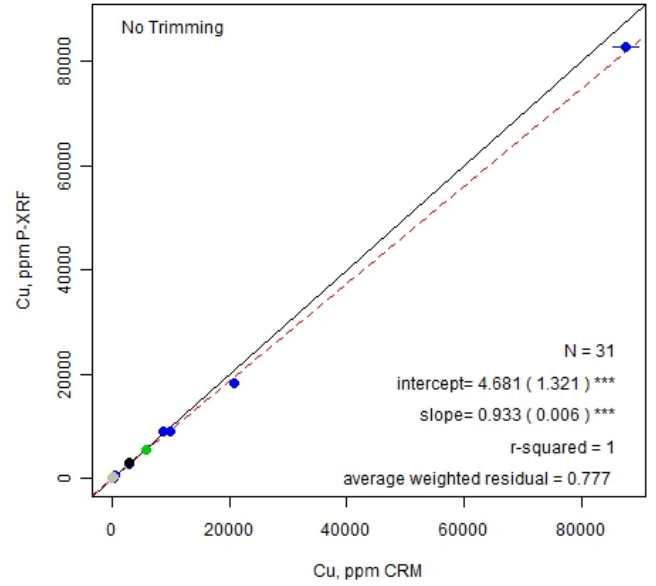




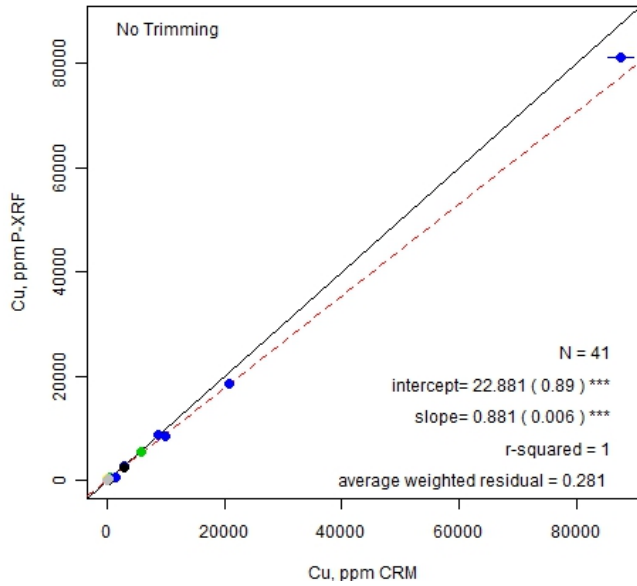
Benchtop-BTAM-Mining Mode



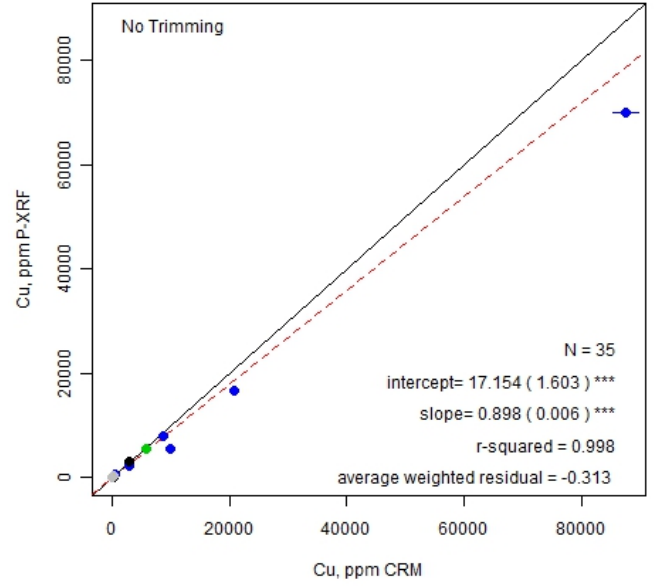
Benchtop-BTBM-Mining Mode



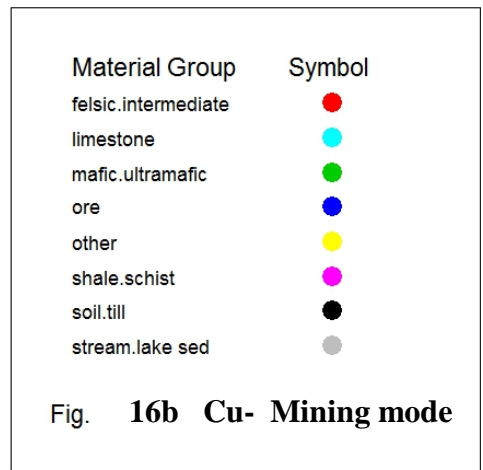
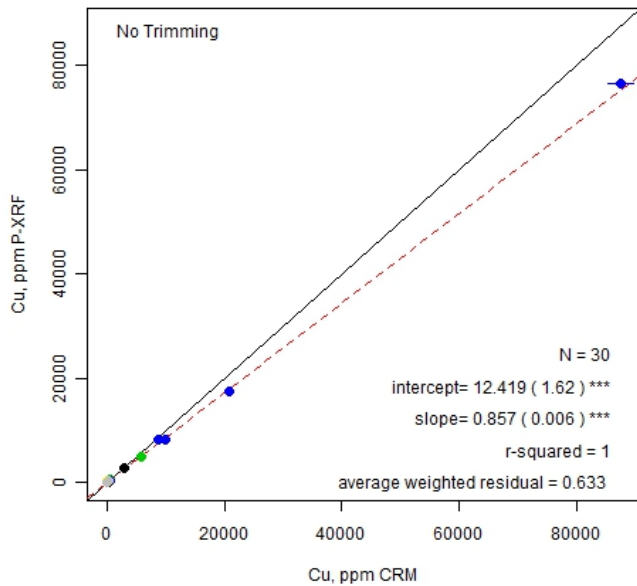
Handheld-HHAM-Mining Mode



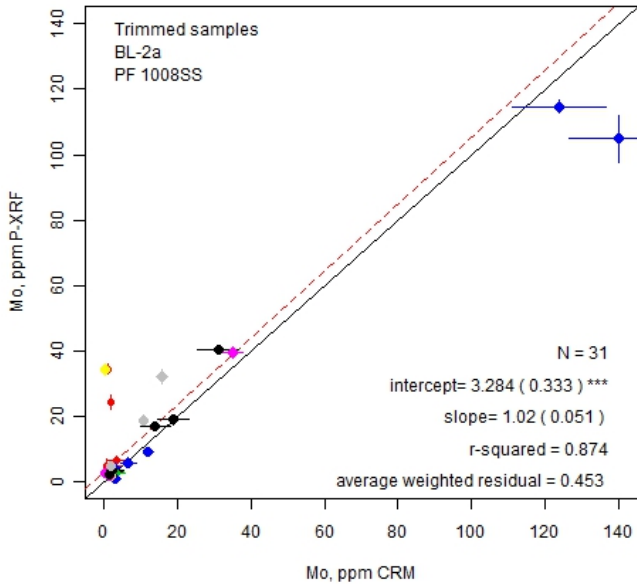
Handheld-HHBM-Mining Mode



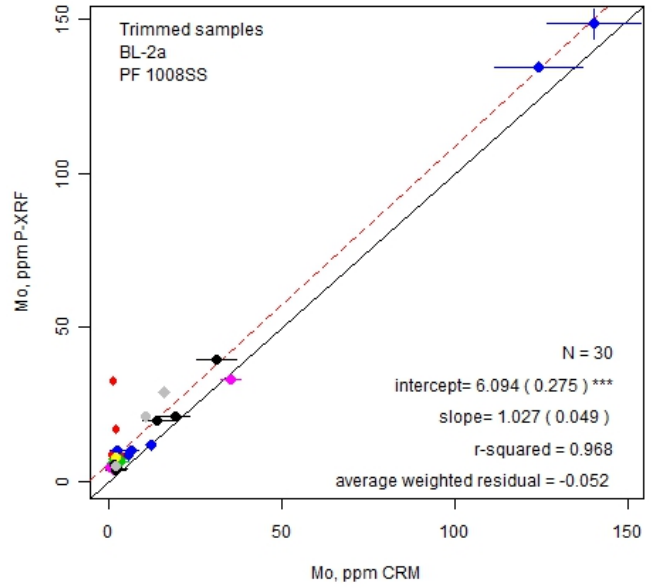
Handheld-HHCM-Mining Mode



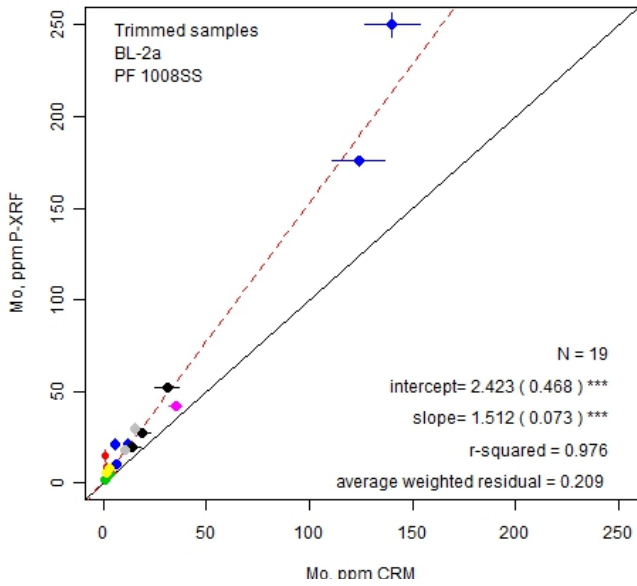
Bench Top-BTAS-Soil Mode



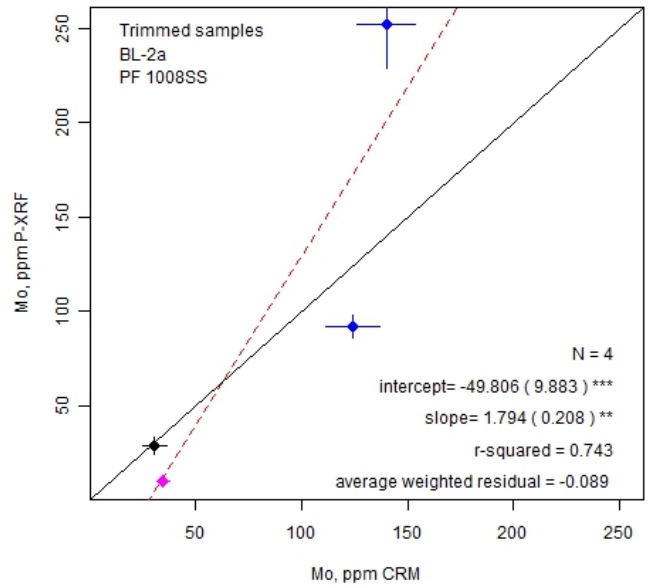
Bench Top-BTBS-Soil Mode



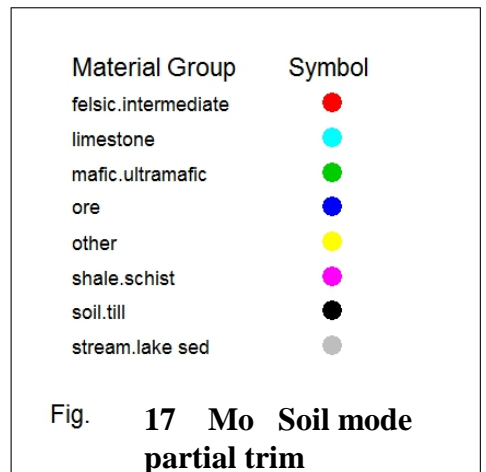
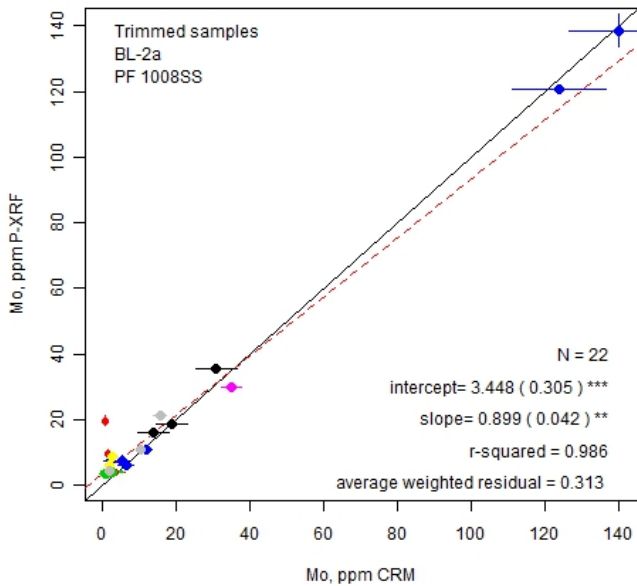
Handheld-HHAS-Soil Mode



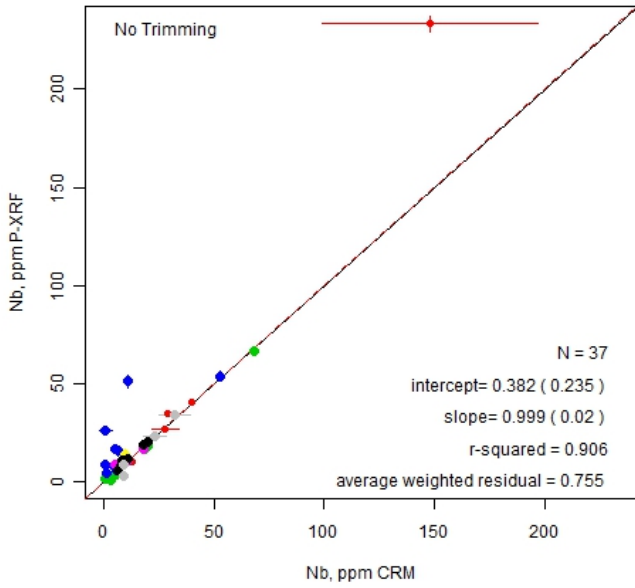
Handheld-HHBS-Soil Mode



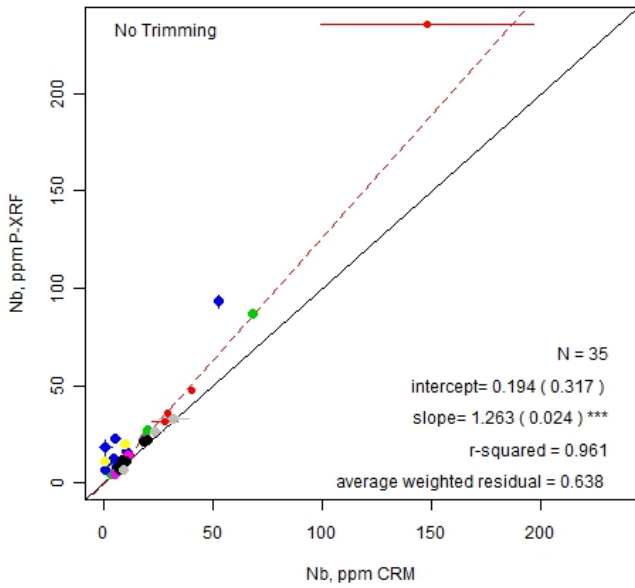
Handheld-HHCS-Soil Mode



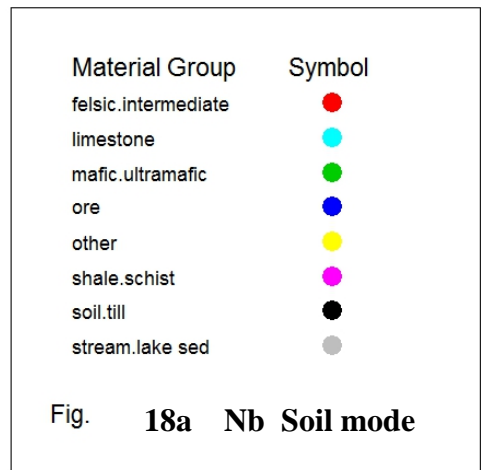
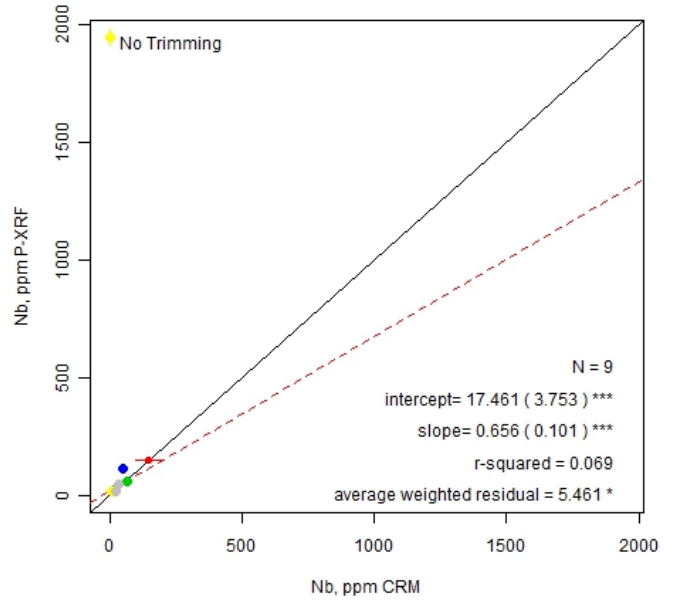
Bench Top-BTAS-Soil Mode



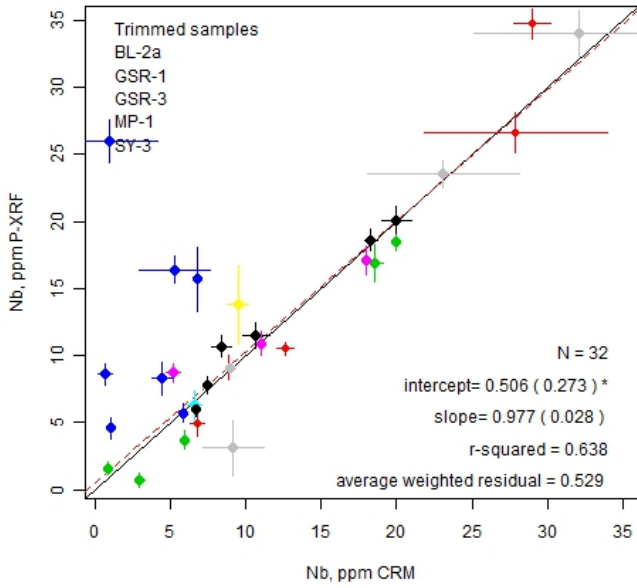
Handheld-HHAS-Soil Mode



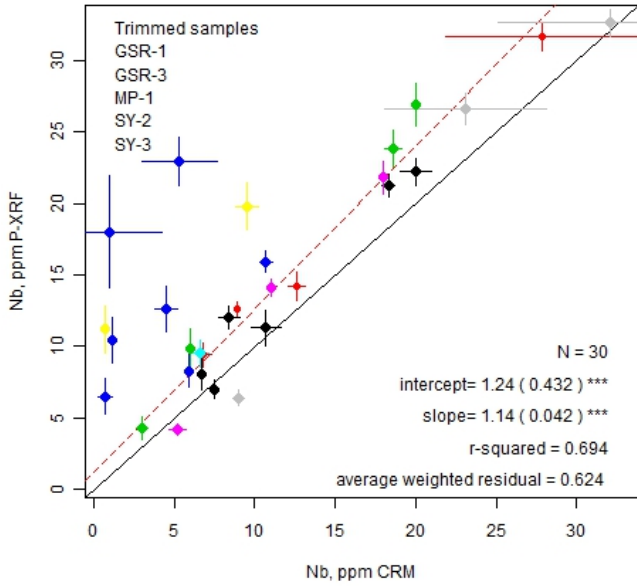
Handheld-HHBS-Soil Mode



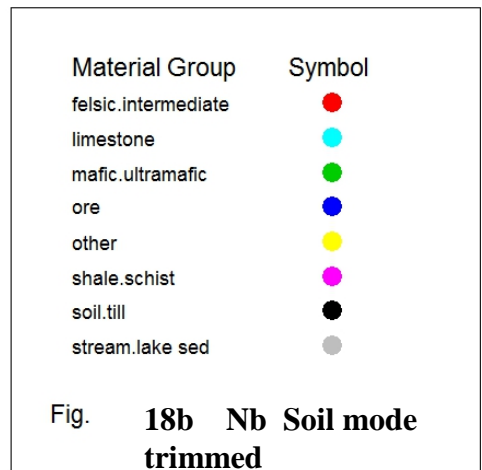
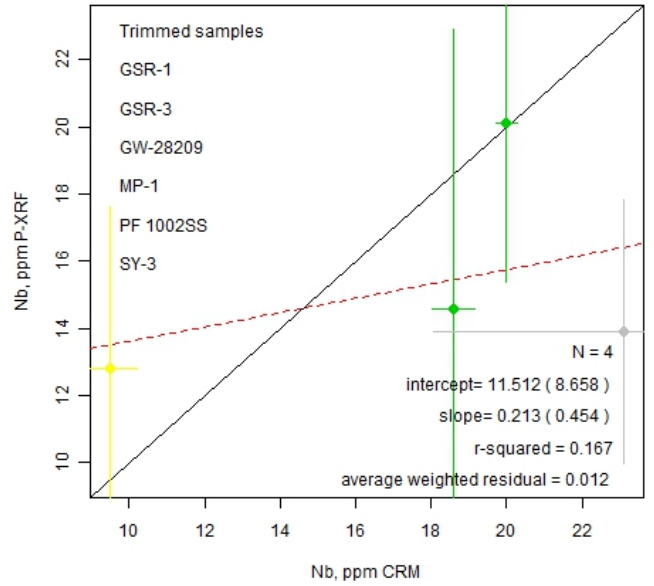
Bench Top-Machine A-Soil Mode



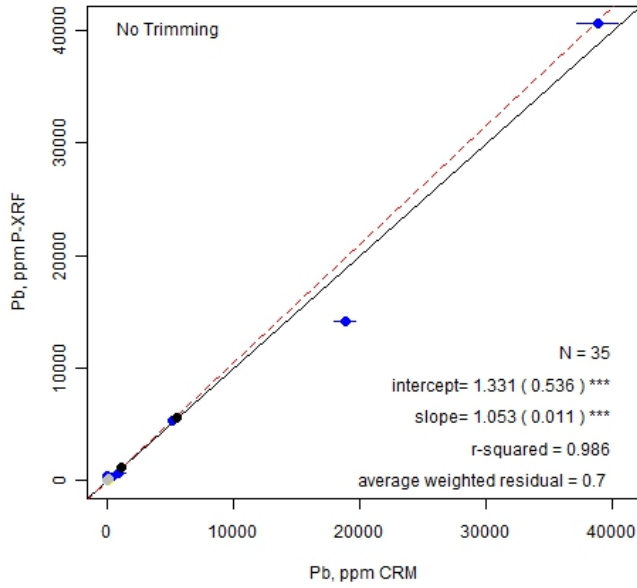
Handheld-HHAS-Soil Mode



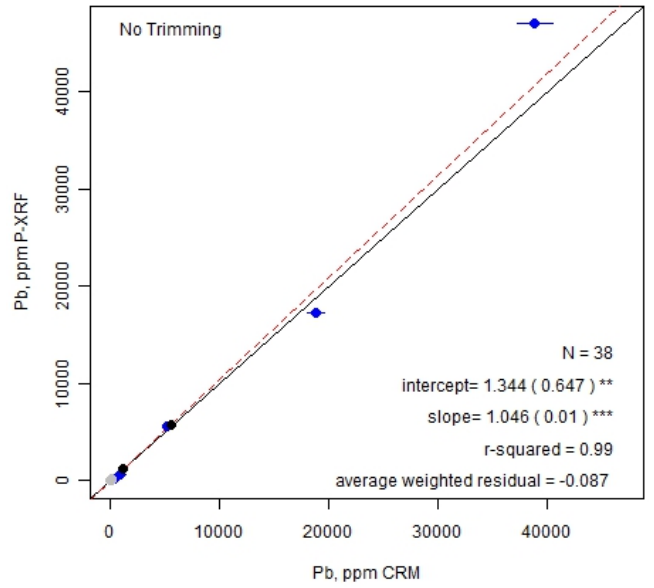
Handheld-HHBS-Soil Mode



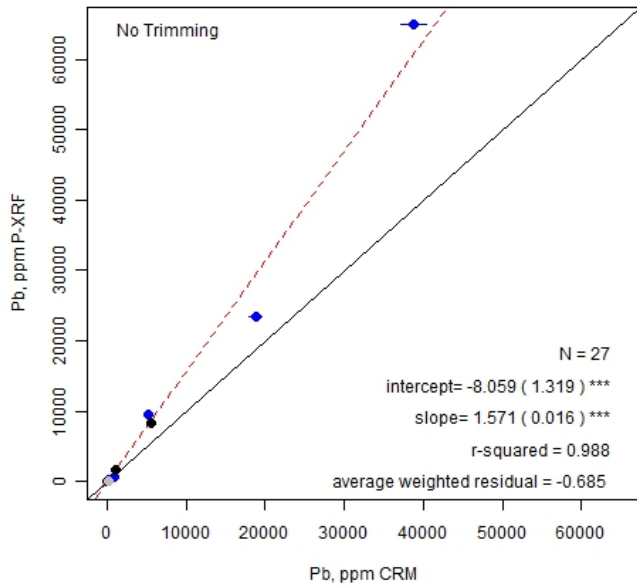
Bench Top-BTAS-Soil Mode



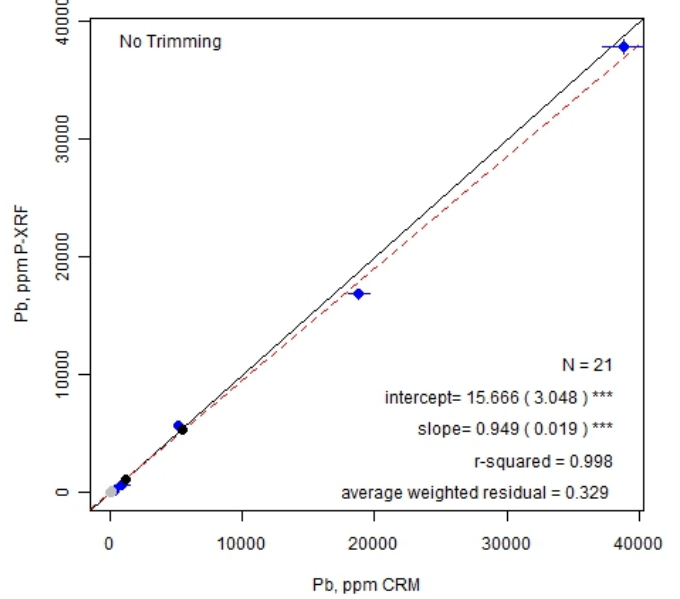
Bench Top-BTBS-Soil Mode



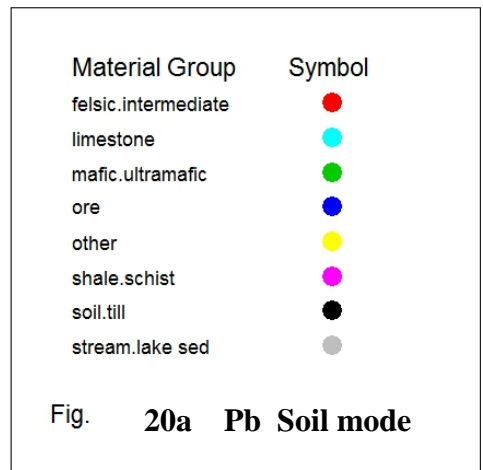
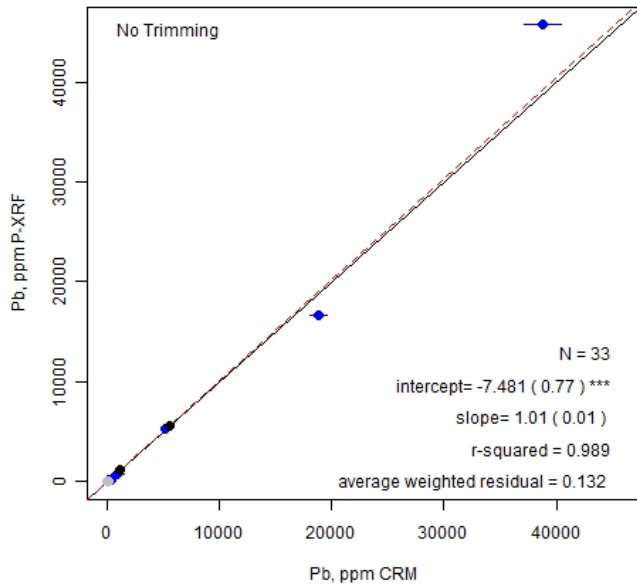
Handheld-HHAS-Soil Mode



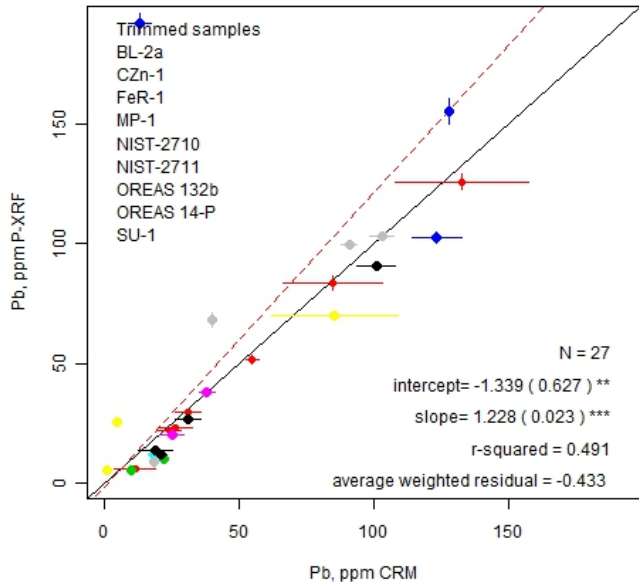
Handheld-HHBS-Soil Mode



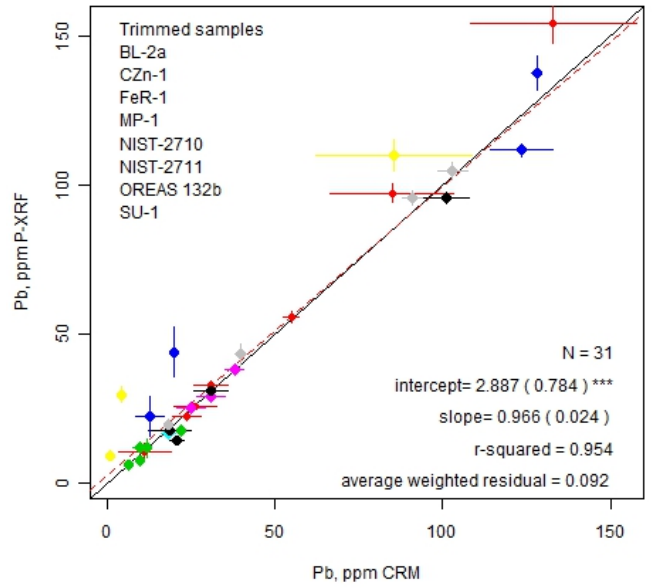
Handheld-HHCS-Soil Mode



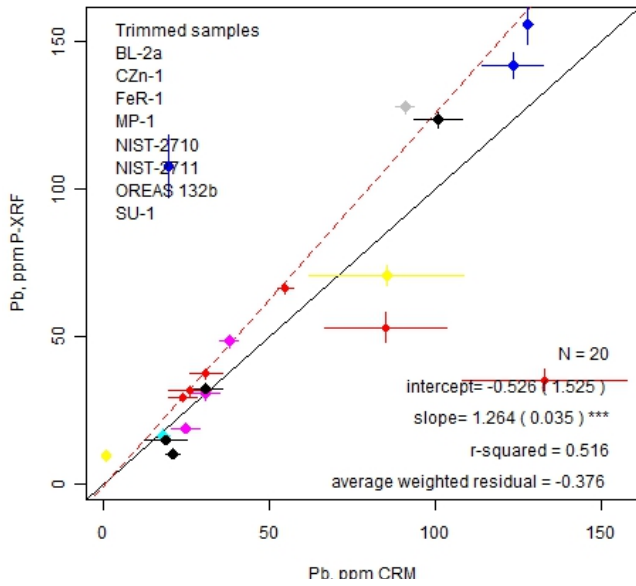
Bench Top-Machine A-Soil Mode



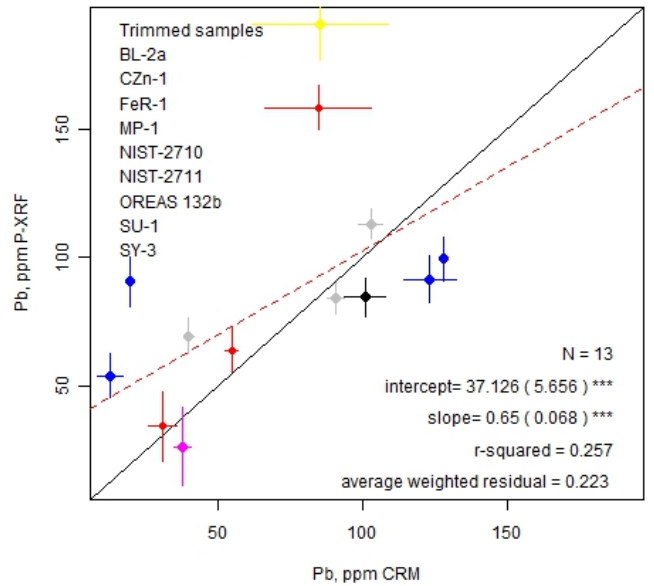
Bench Top-BTBS-Soil Mode



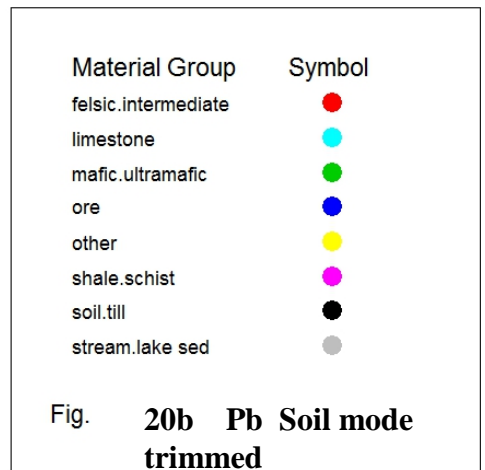
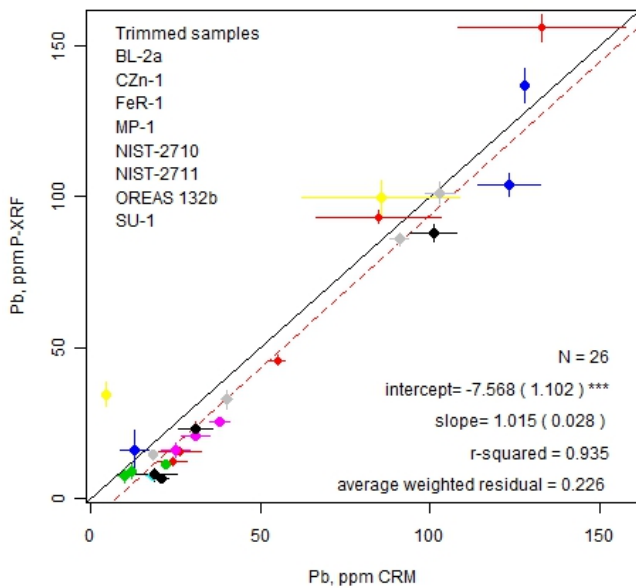
Handheld-HHAS-Soil Mode



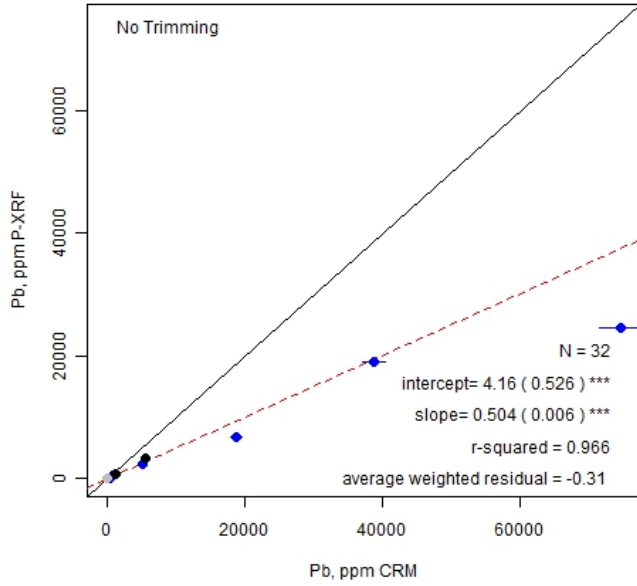
Handheld-HHBS-Soil Mode



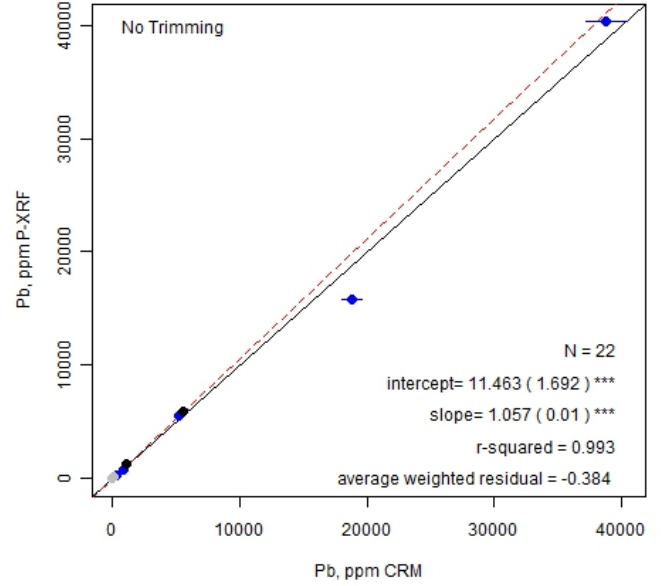
Handheld-HHCS-Soil Mode



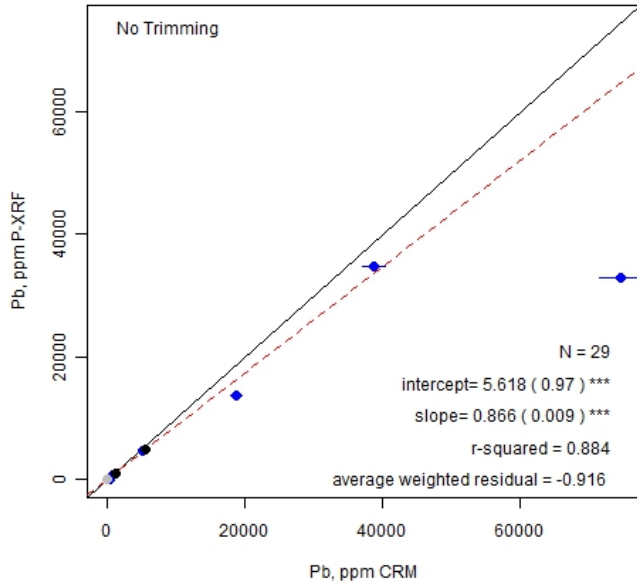
Benchtop-BTAM-Mining Mode



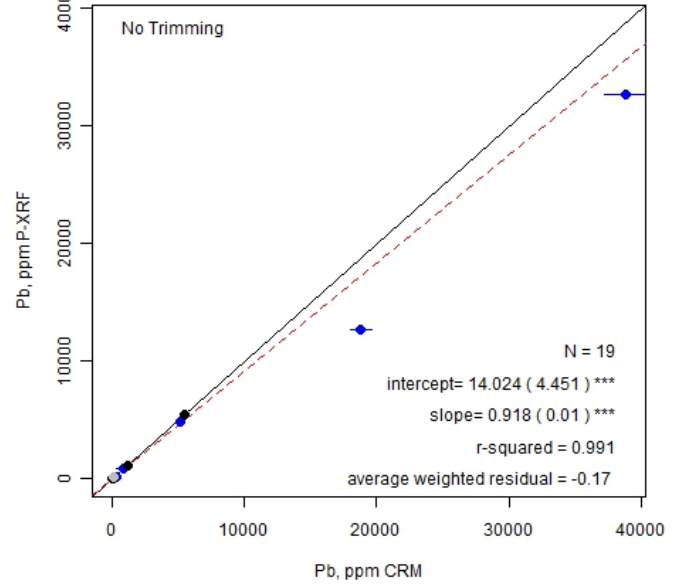
Handheld-BTBM-Mining Mode



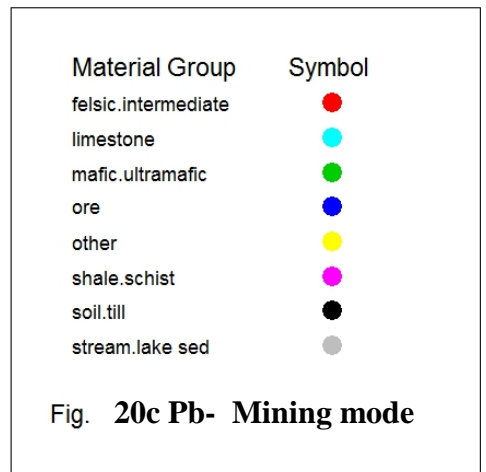
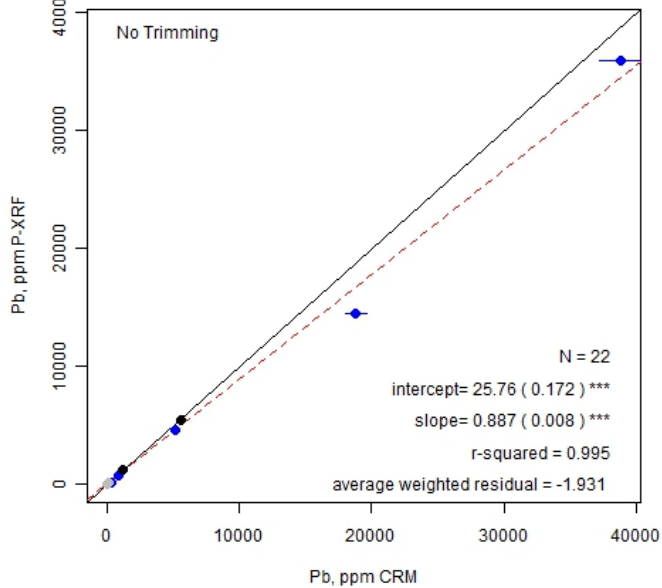
Handheld-HHAM-Mining Mode

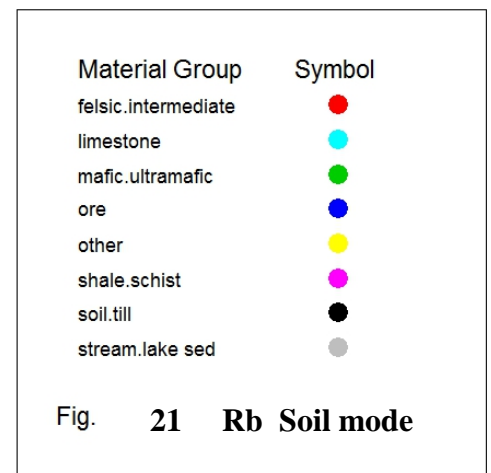
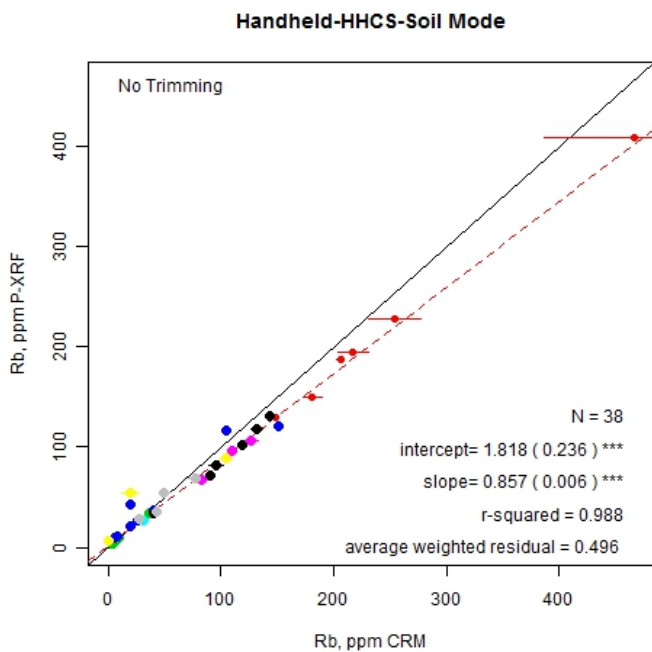
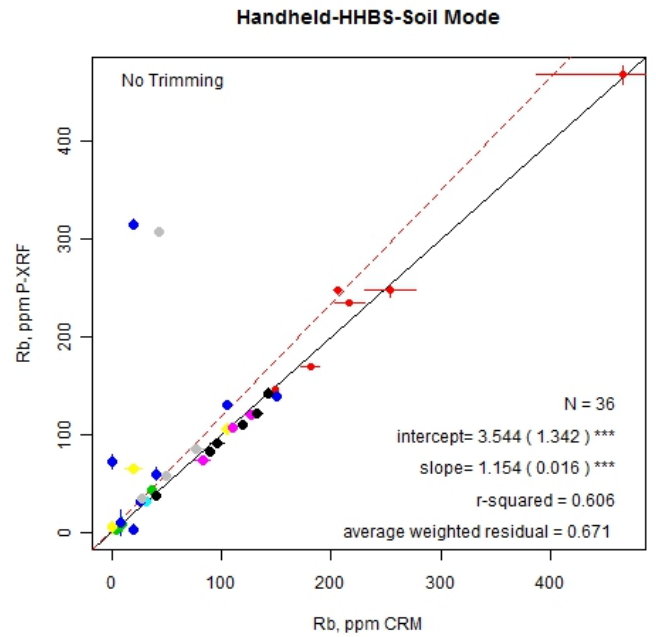
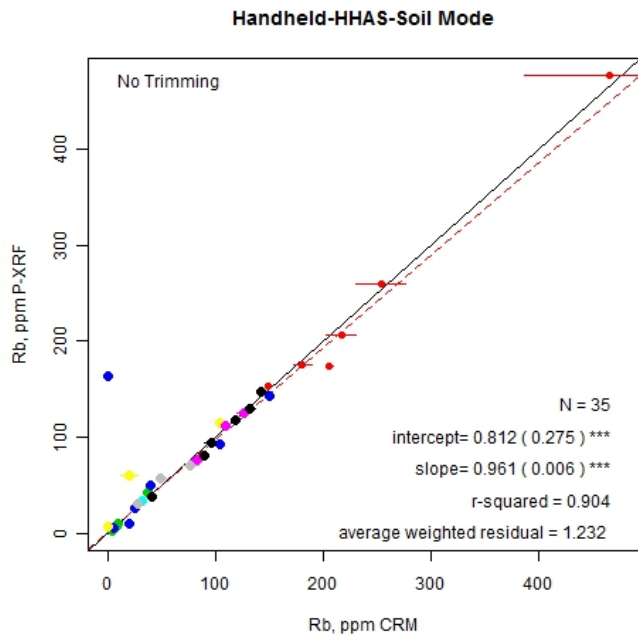
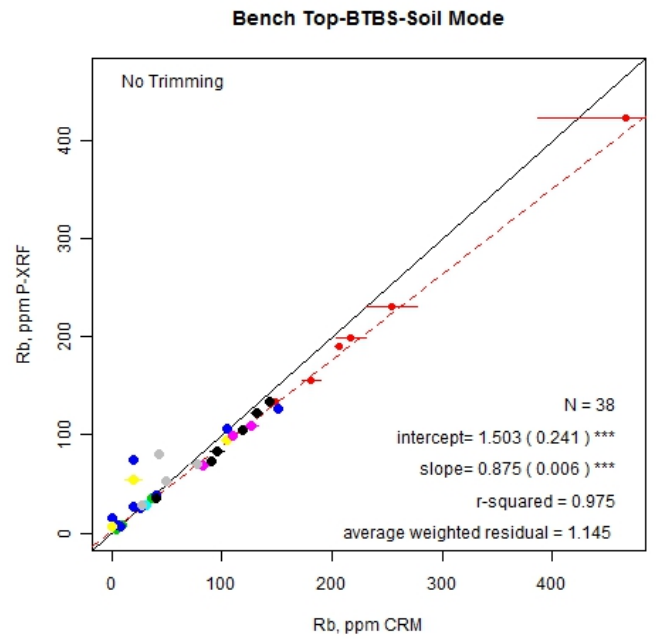
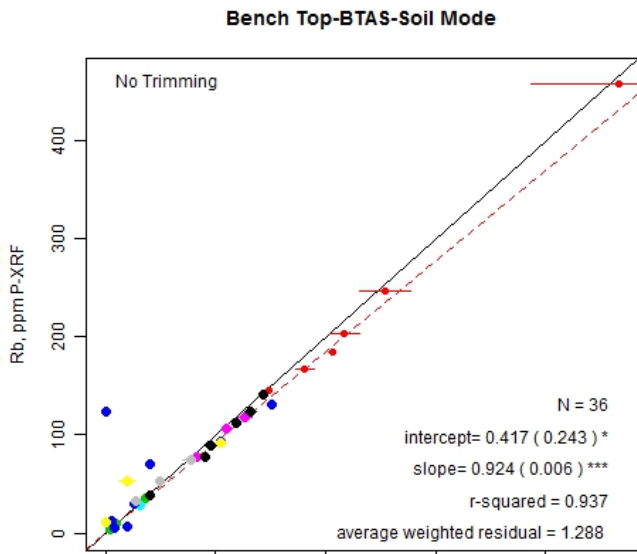


Handheld-HHBM-Mining Mode

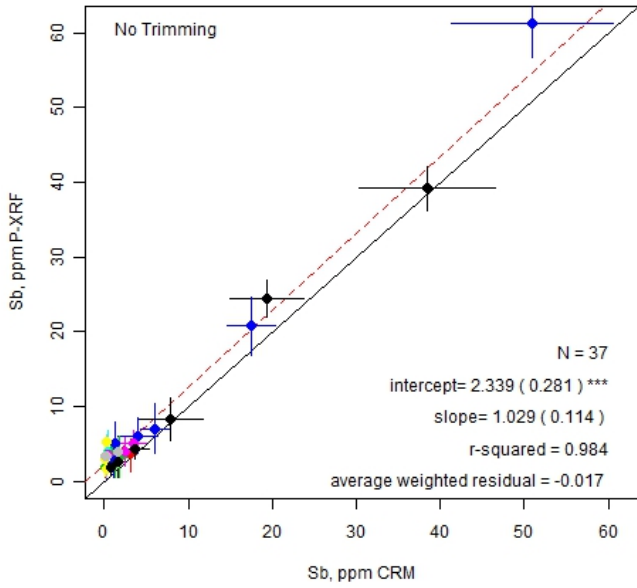


Handheld-HHCM-Mining Mode

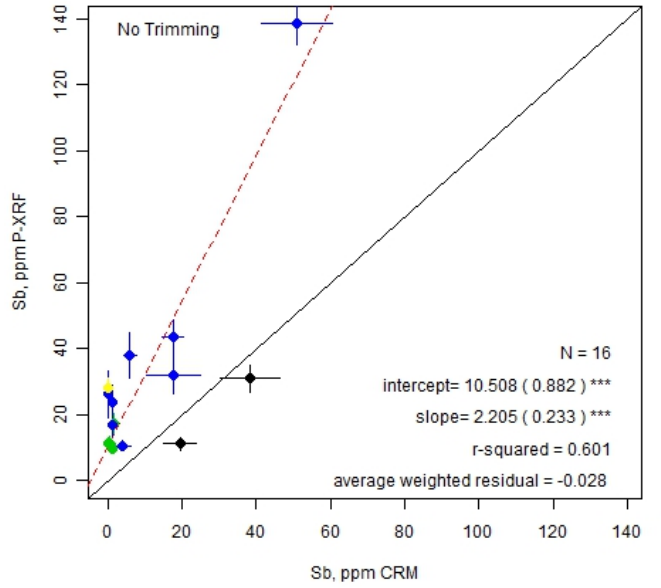




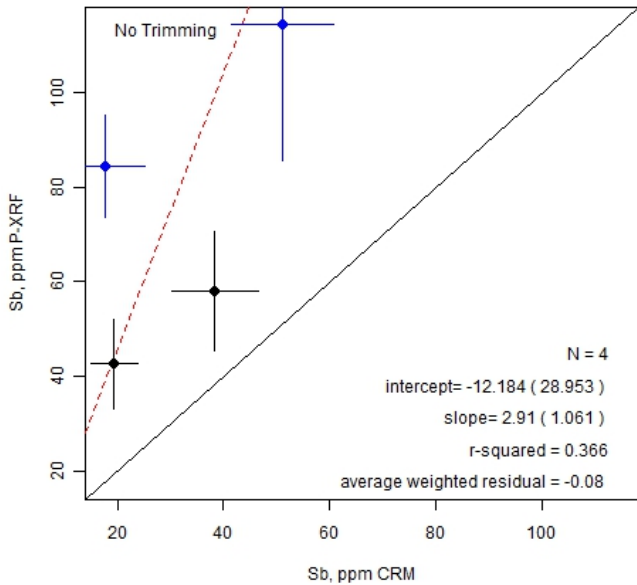
Bench Top-BTAS-Soil Mode



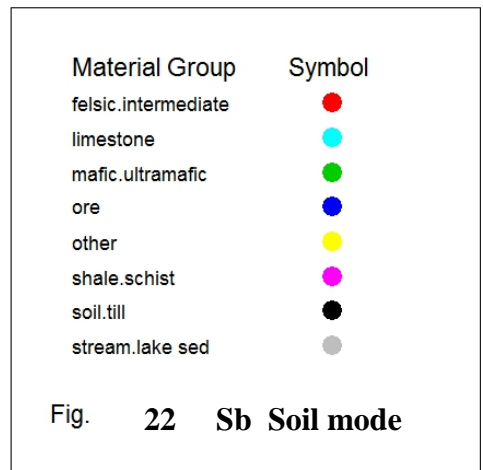
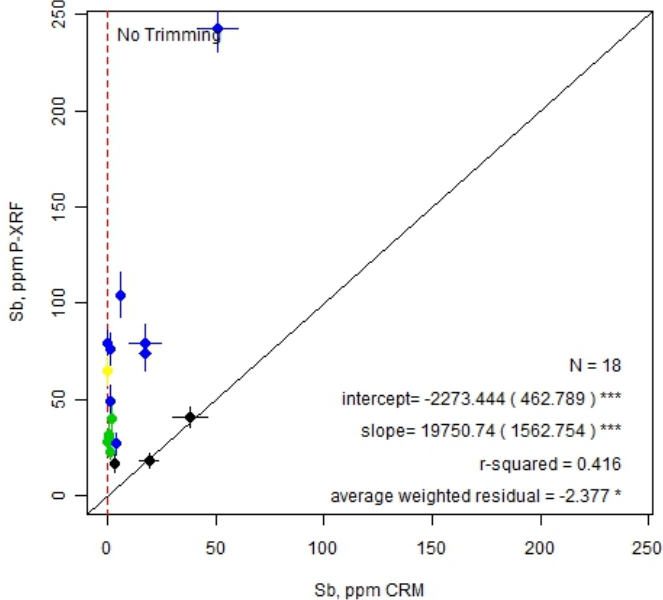
Bench Top-BTBS-Soil Mode



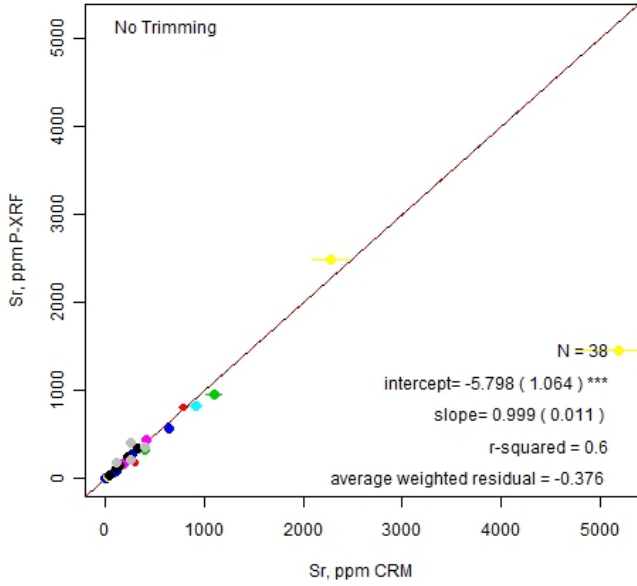
Handheld-HHAS-Soil Mode



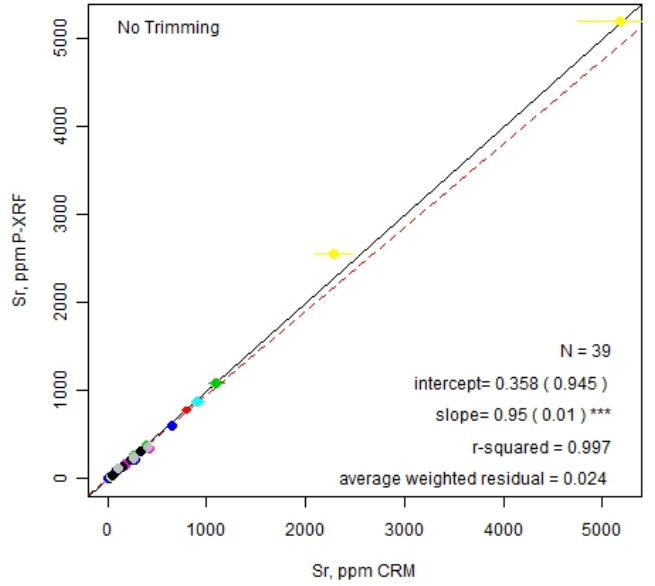
Handheld-HHCS-Soil Mode



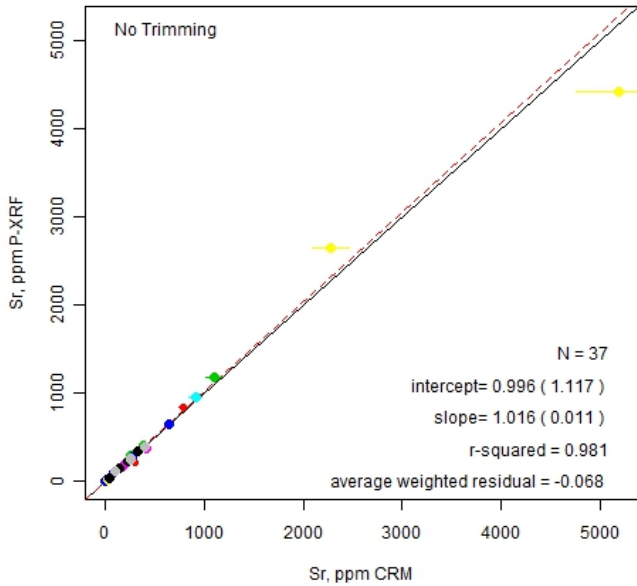
Bench Top-BTAS-Soil Mode



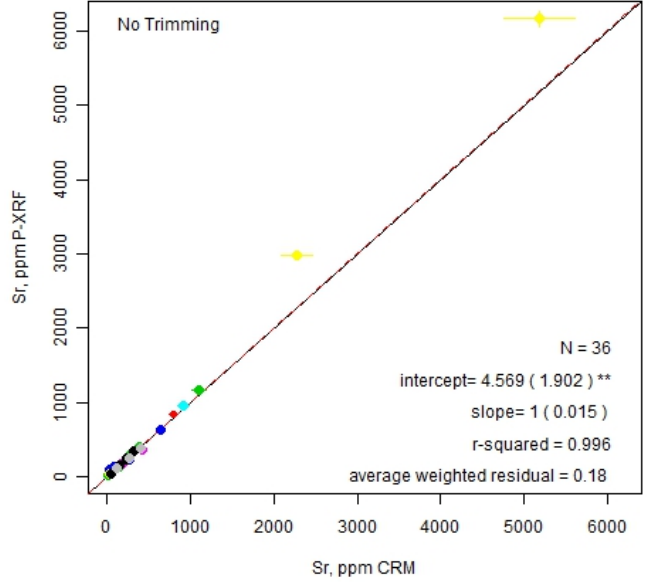
Bench Top-BTBS-Soil Mode



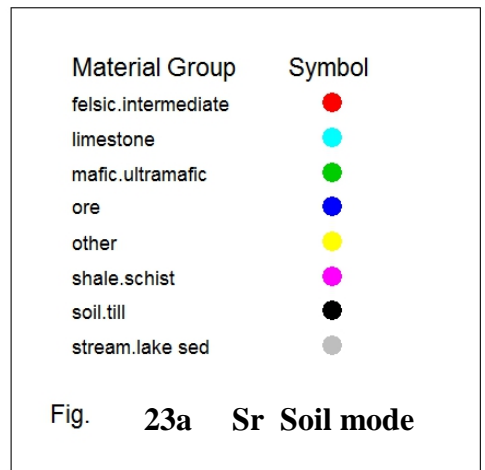
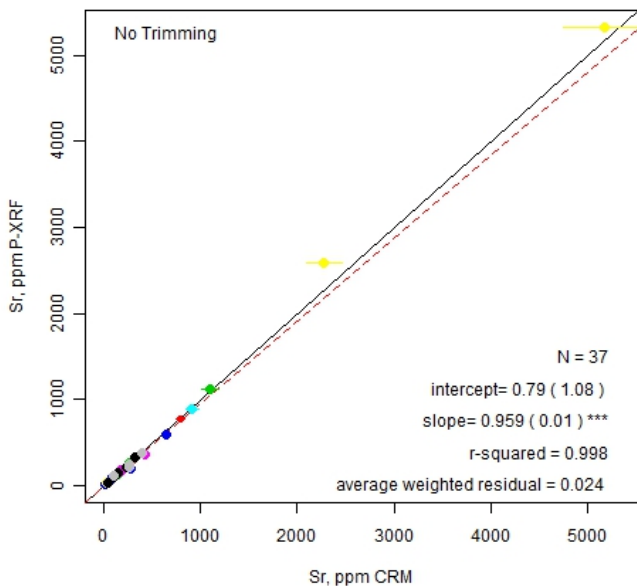
Handheld-HHAS-Soil Mode



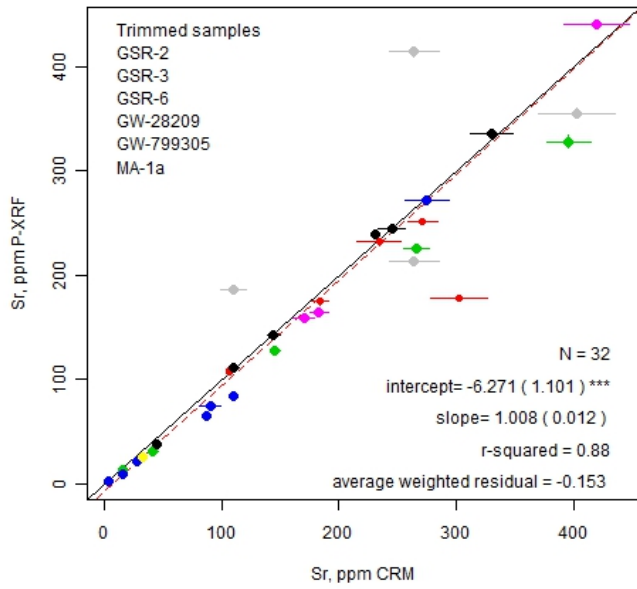
Handheld-HHBS-Soil Mode



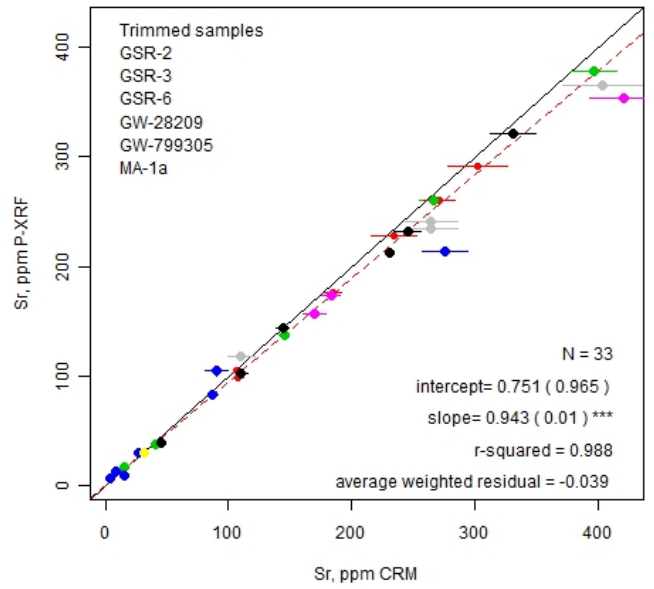
Handheld-HHCS-Soil Mode



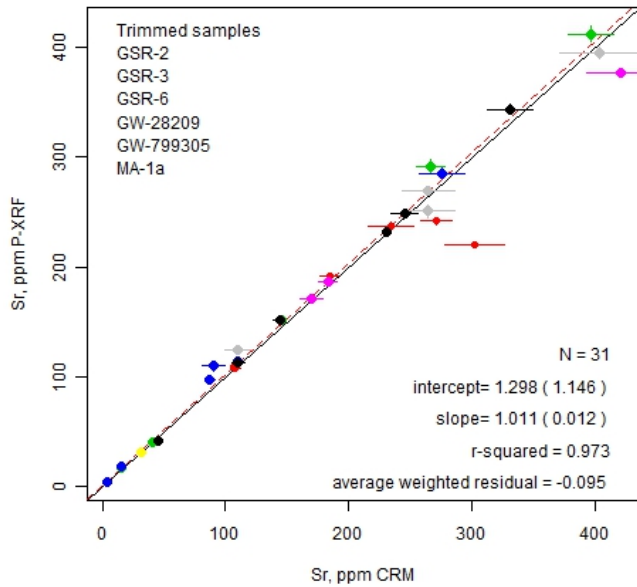
Bench Top-Machine A-Soil Mode



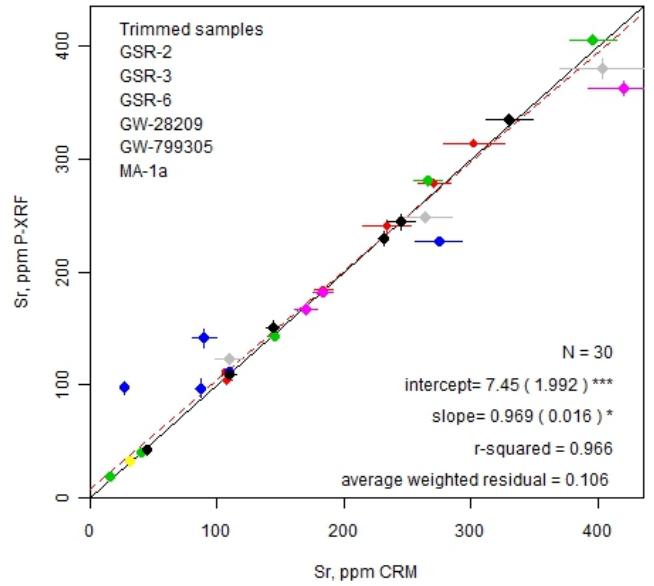
Bench Top-BTBS-Soil Mode



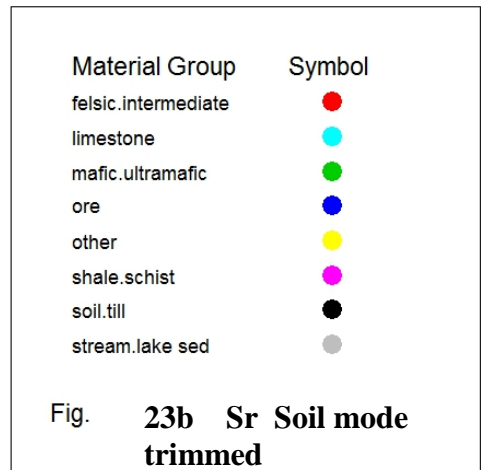
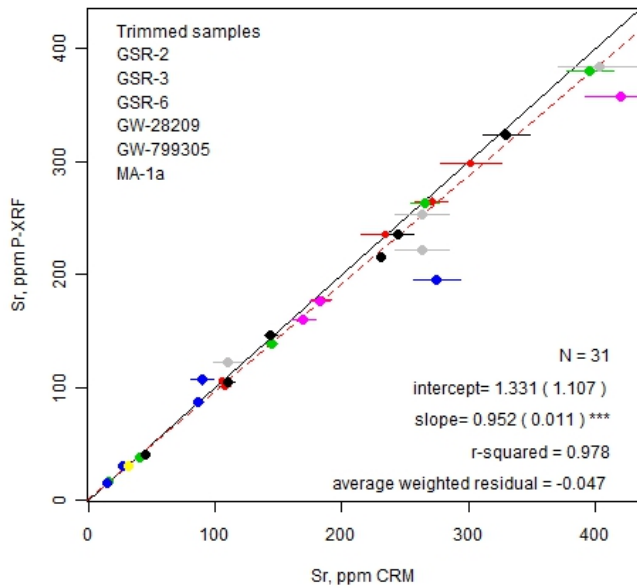
Handheld-HHAS-Soil Mode



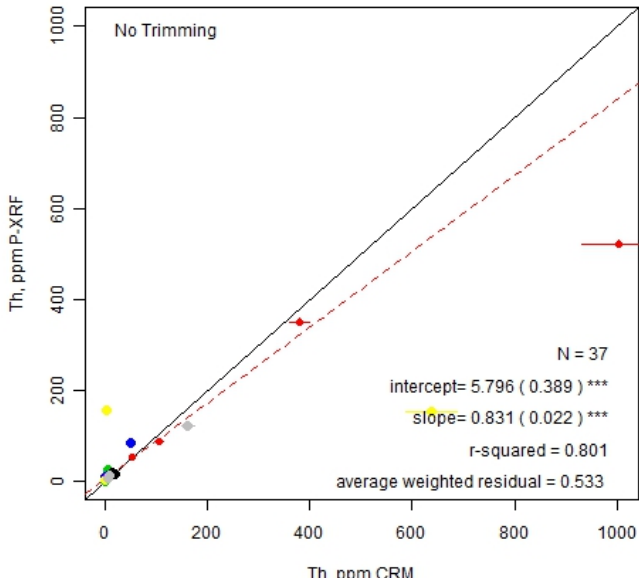
Handheld-HHBS-Soil Mode



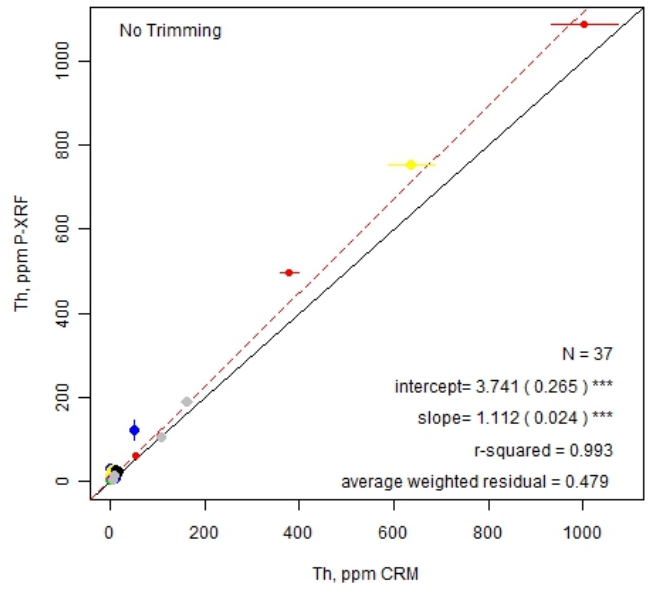
Handheld-HHCS-Soil Mode



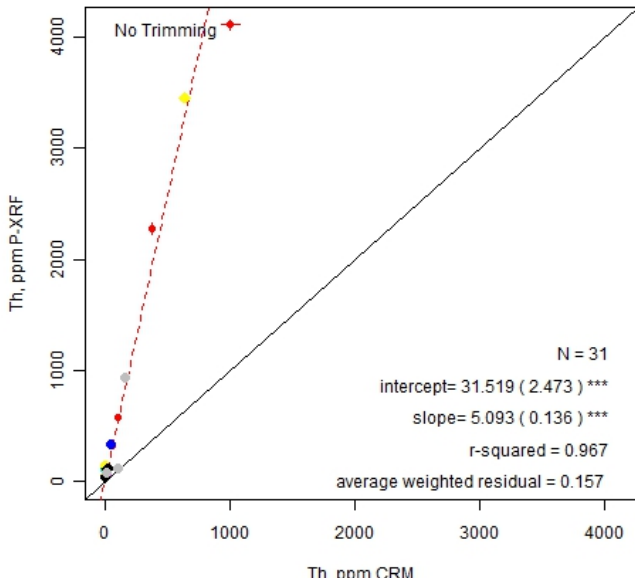
Bench Top-BTAS-Soil Mode



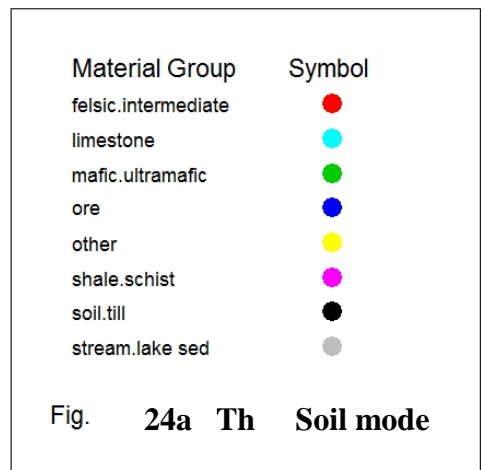
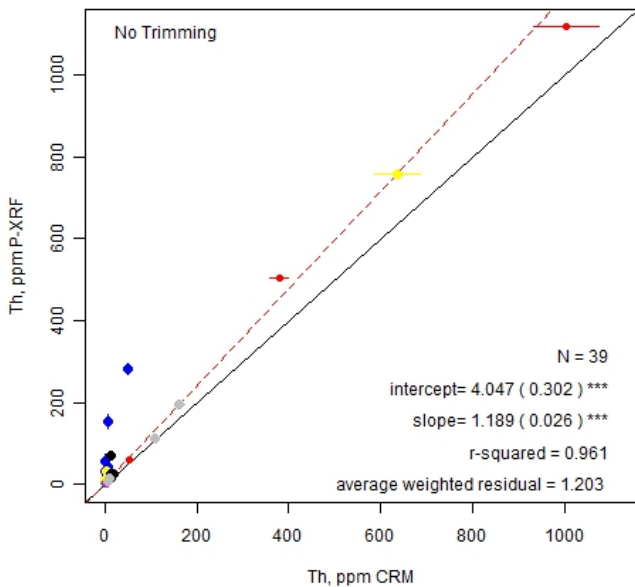
Bench Top-BTBS-Soil Mode



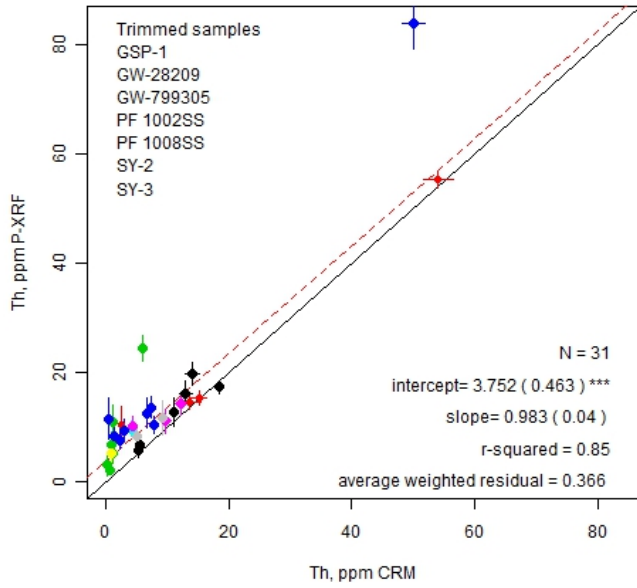
Handheld-HHAS-Soil Mode



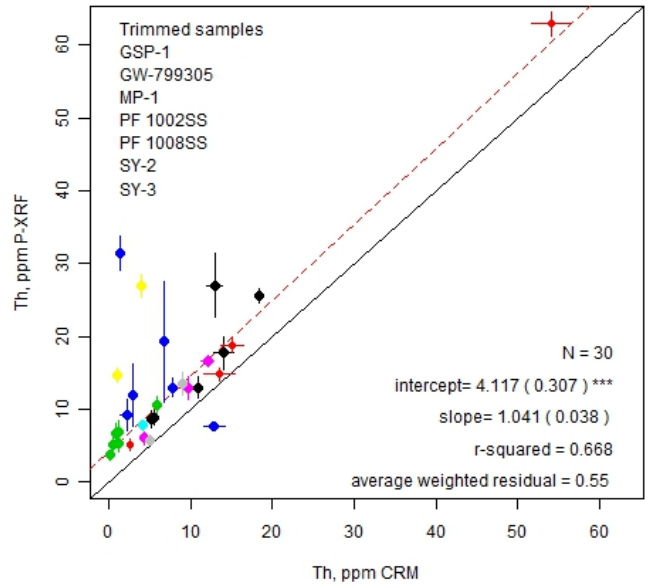
Handheld-HHCS-Soil Mode



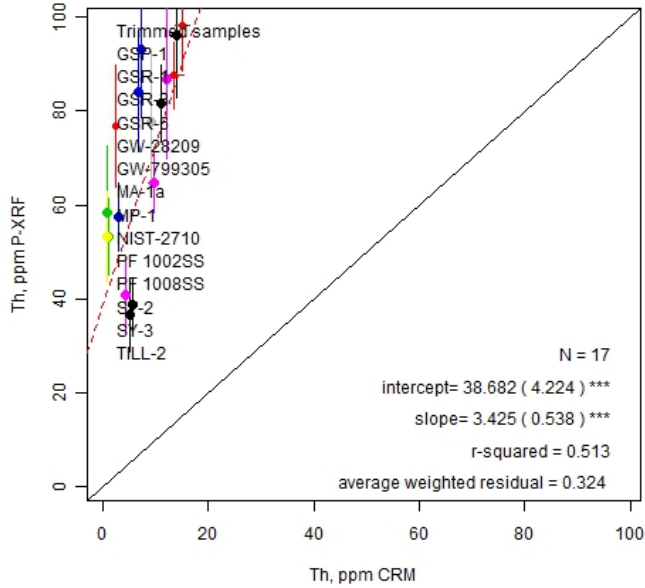
Bench Top-Machine A-Soil Mode



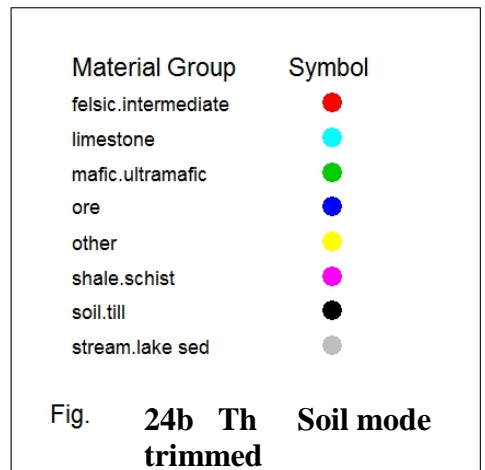
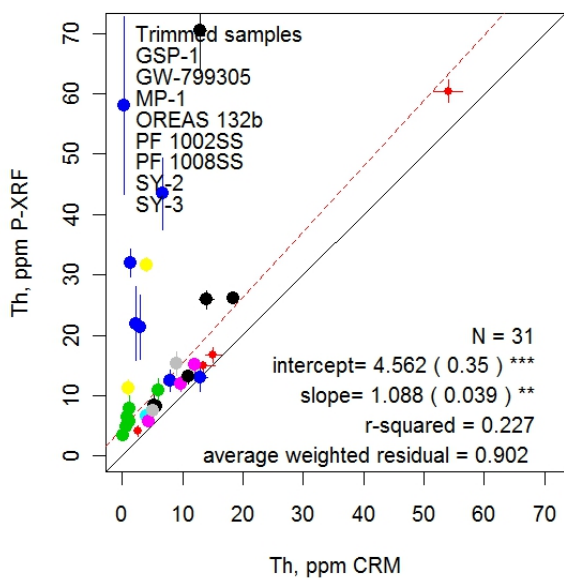
Bench Top-BTBS-Soil Mode



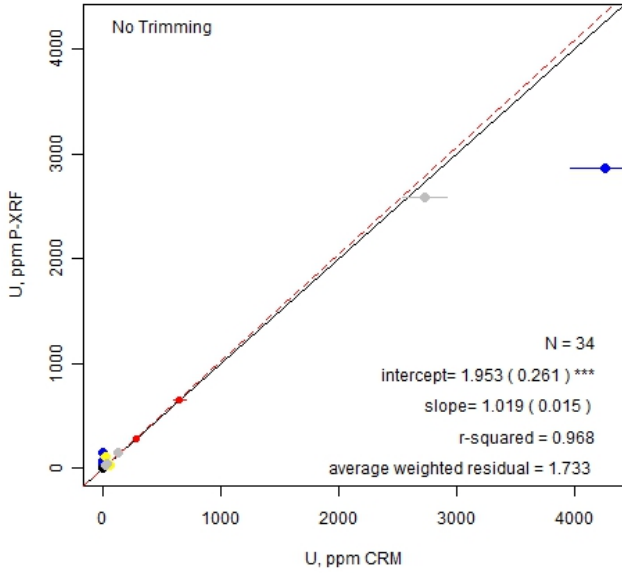
Handheld-HHAS-Soil Mode



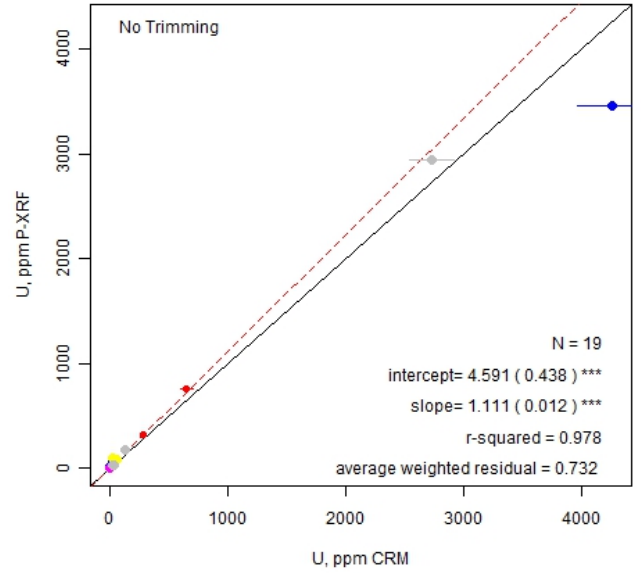
Handheld-HHCS-Soil Mode



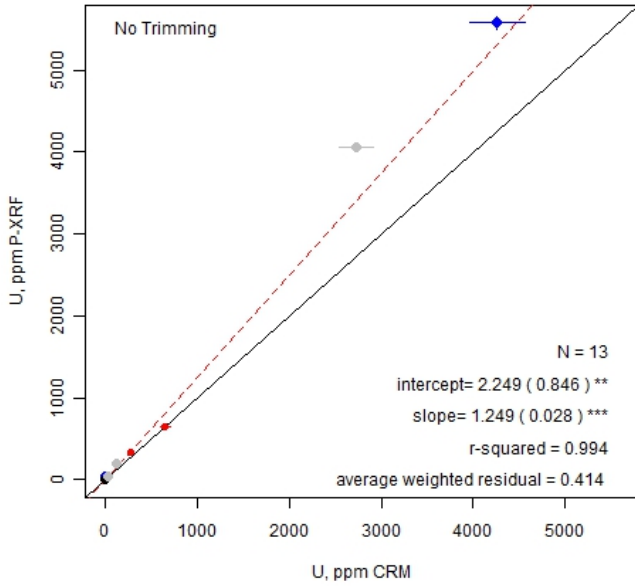
Bench Top-BTAS-Soil Mode



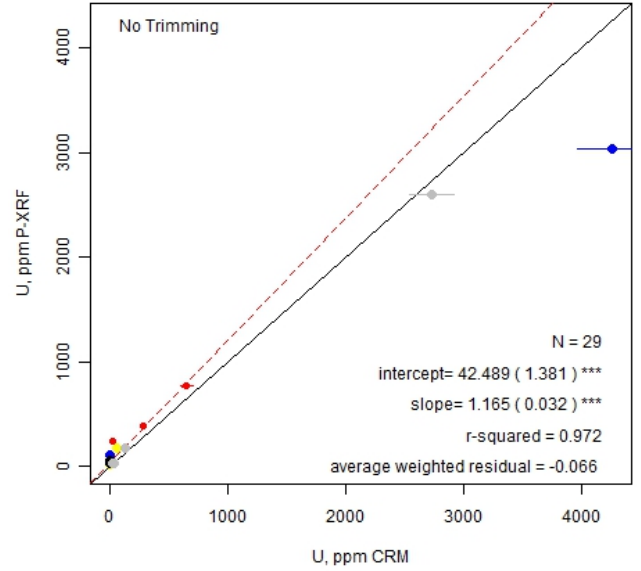
Bench Top-BTBS-Soil Mode



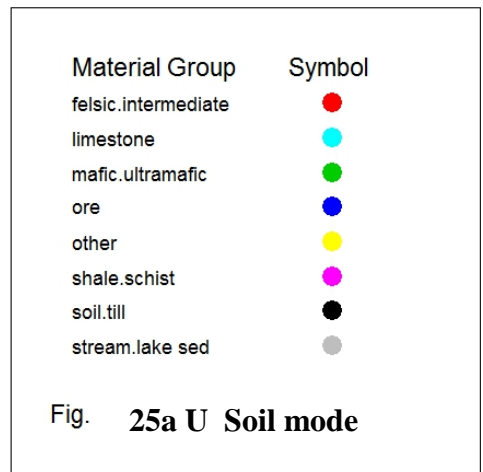
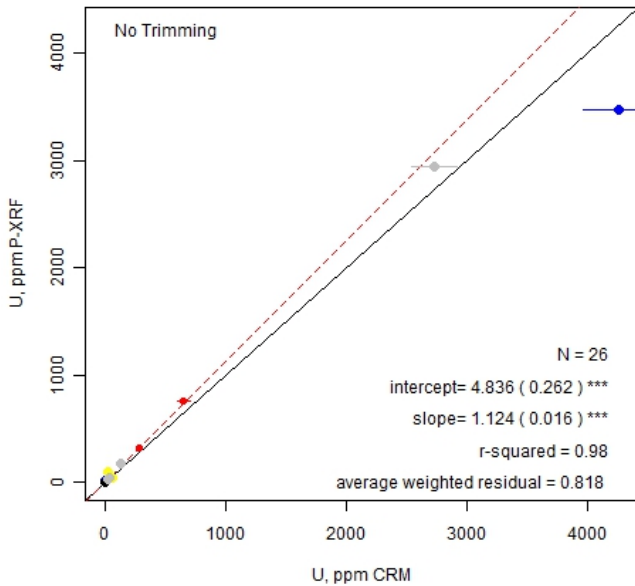
Handheld-HHAS-Soil Mode



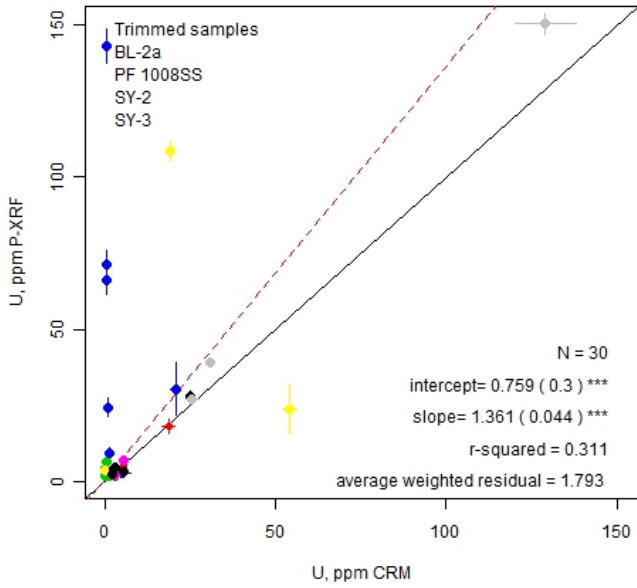
Handheld-HHBS-Soil Mode



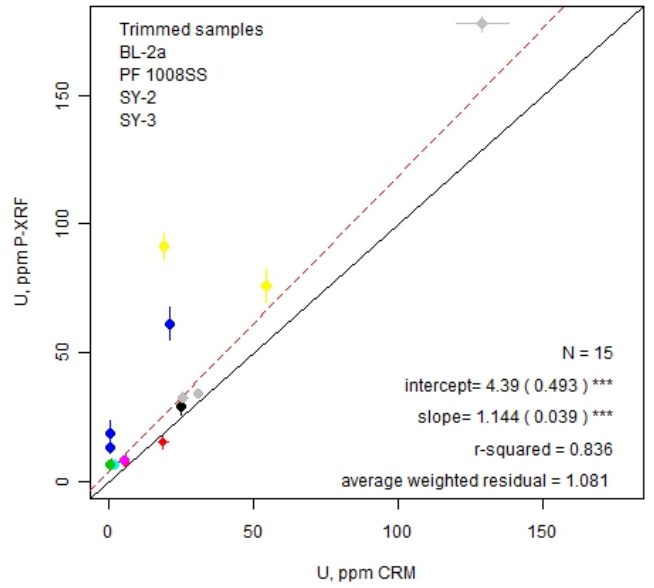
Handheld-HHCS-Soil Mode



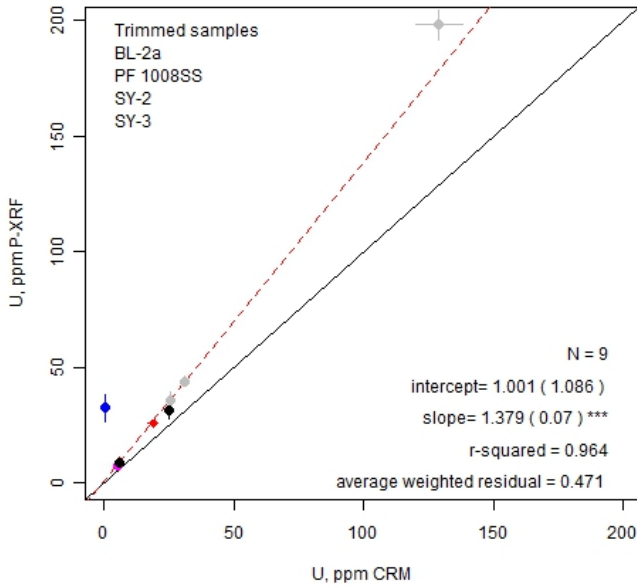
Bench Top-Machine A-Soil Mode



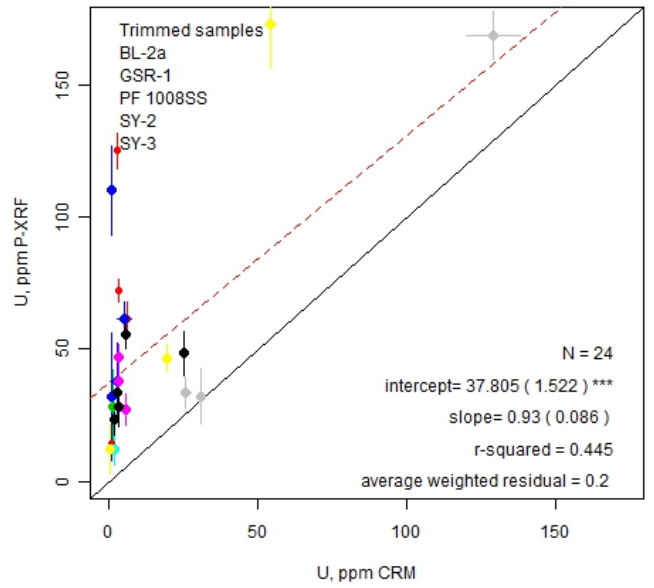
Bench Top-BTBS-Soil Mode



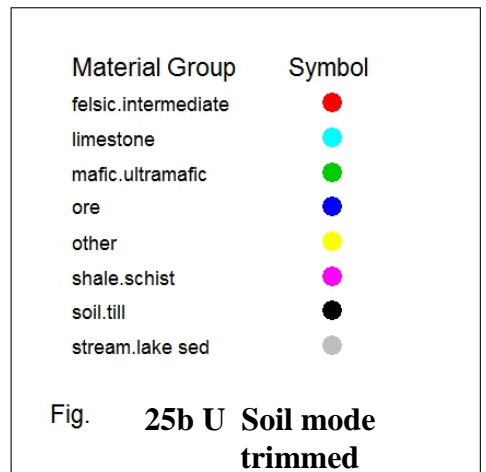
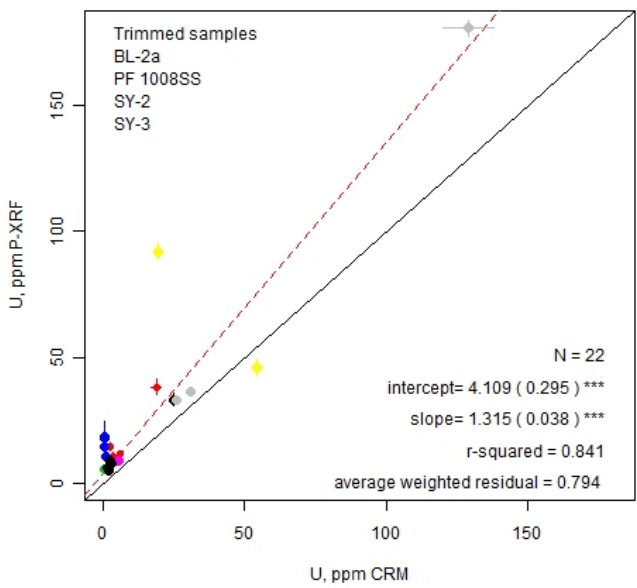
Handheld-HHAS-Soil Mode

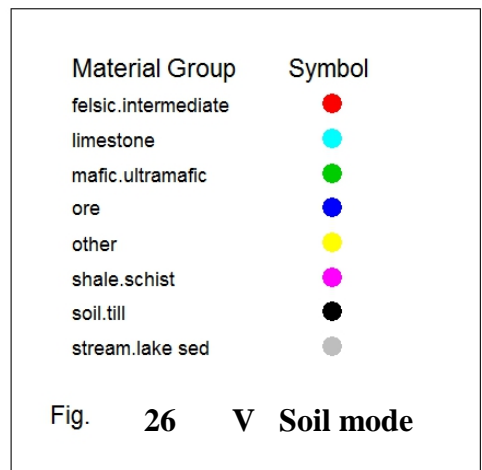
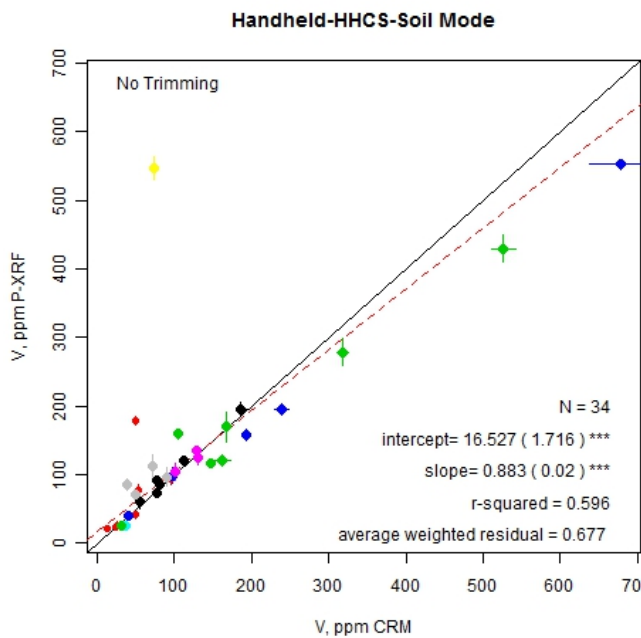
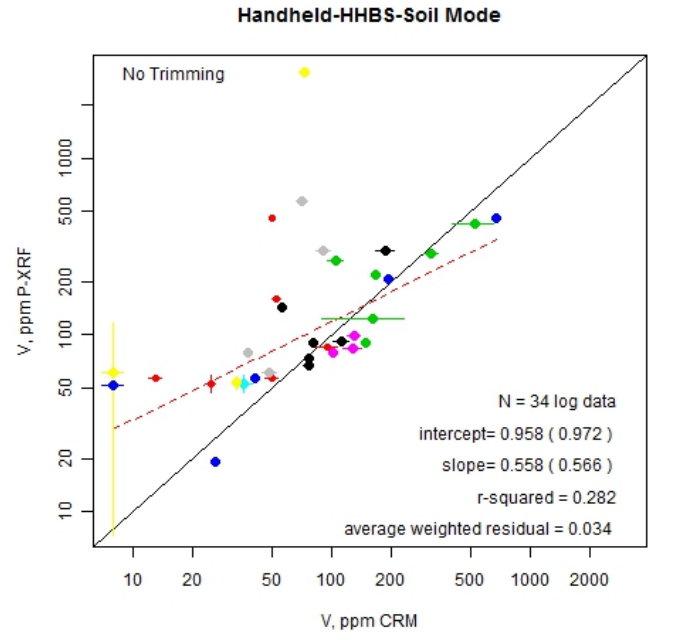
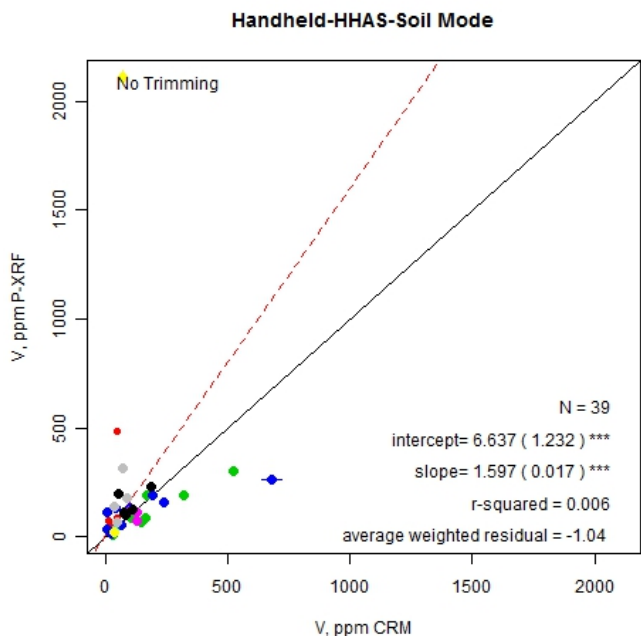
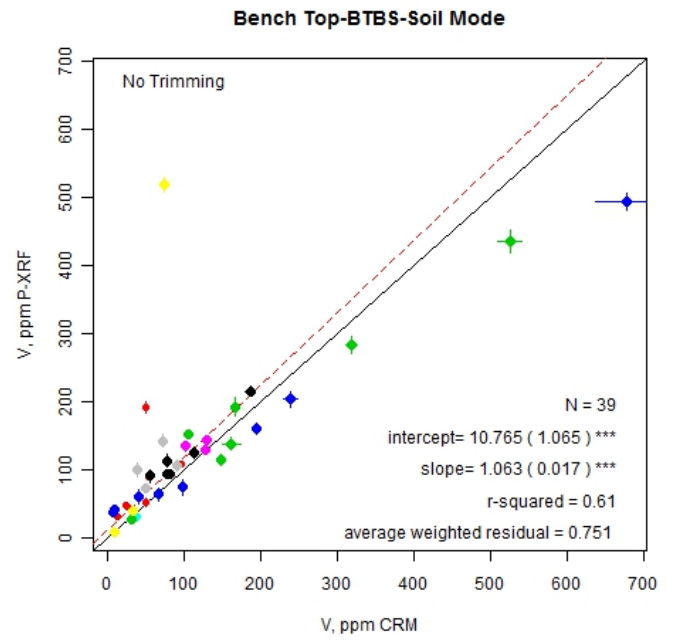
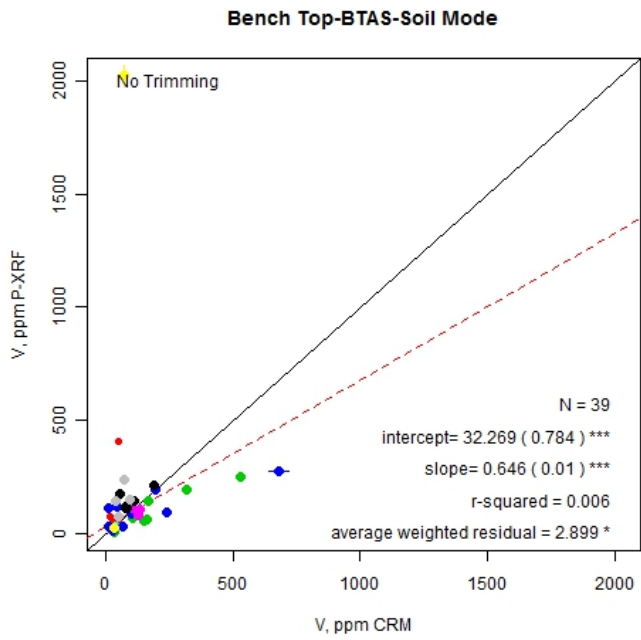


Handheld-HHBS-Soil Mode

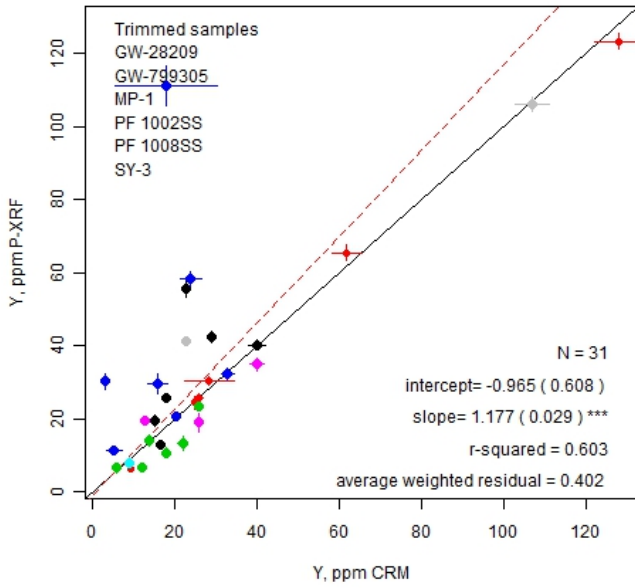


Handheld-HHCS-Soil Mode

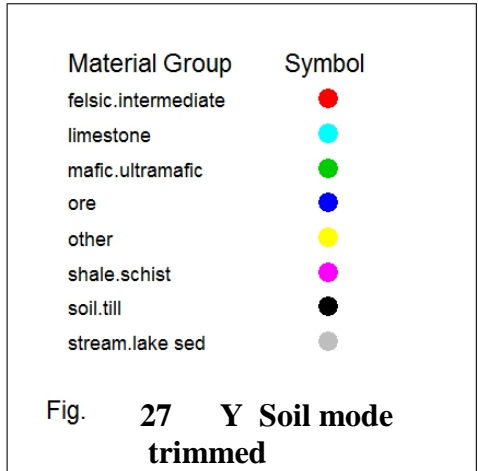
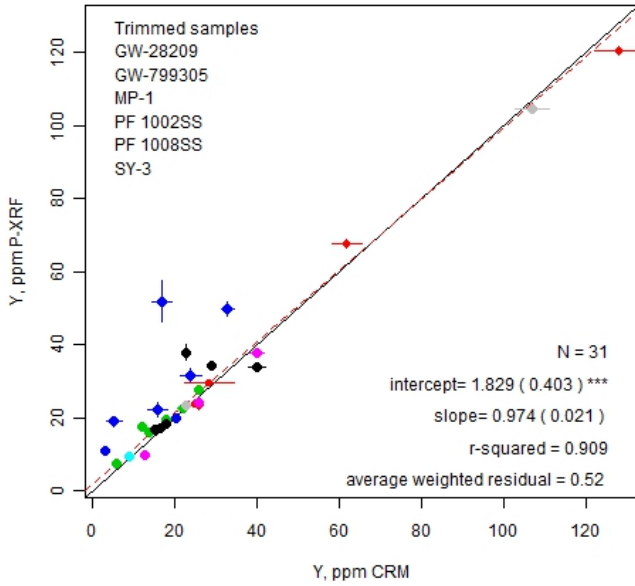




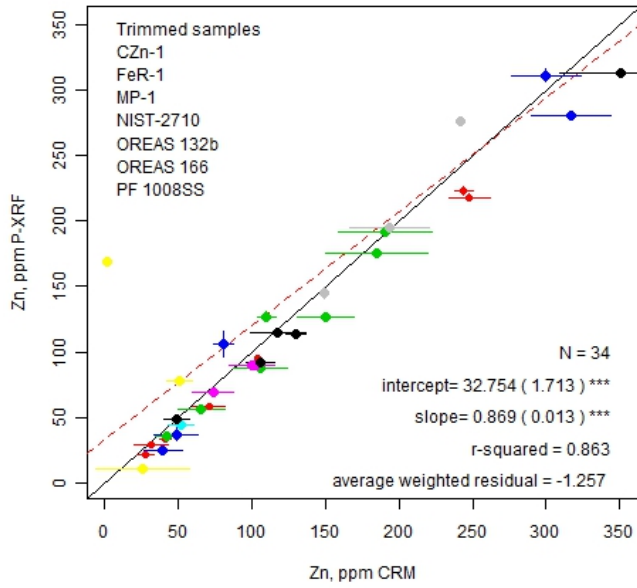
Bench Top-BTAS-Soil Mode



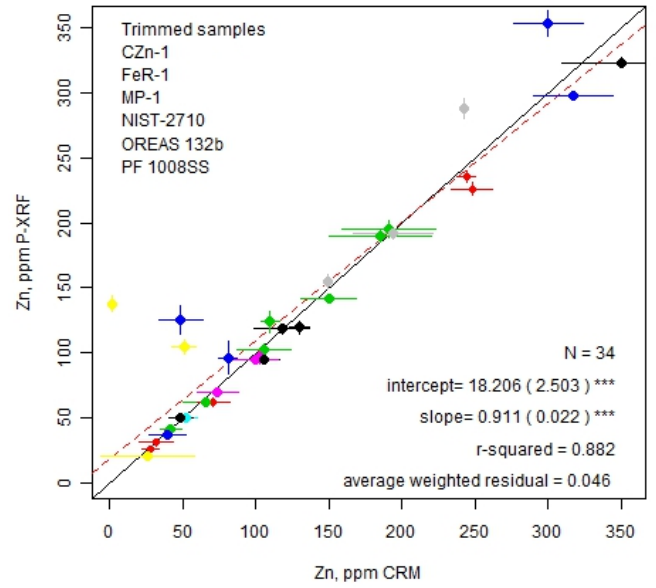
Handheld-HHAS-Soil Mode



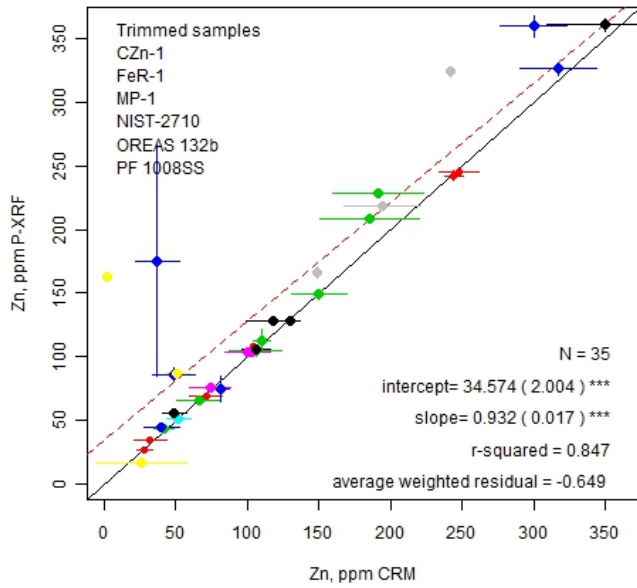
Bench Top-Machine A-Soil Mode



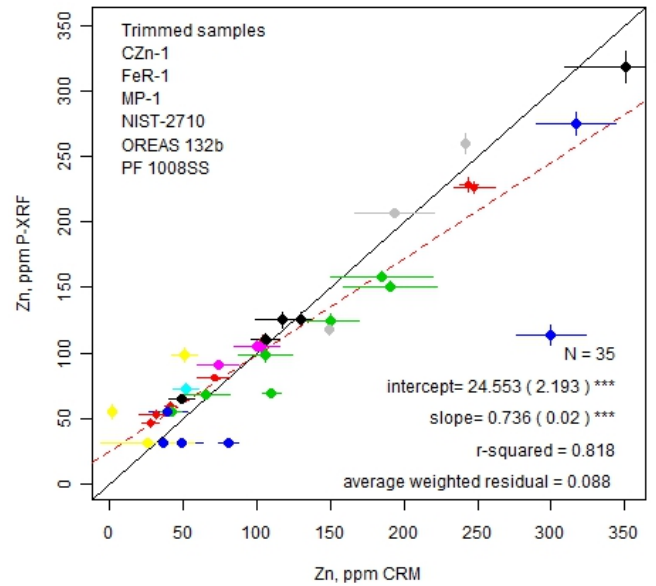
Bench Top-BTBS-Soil Mode



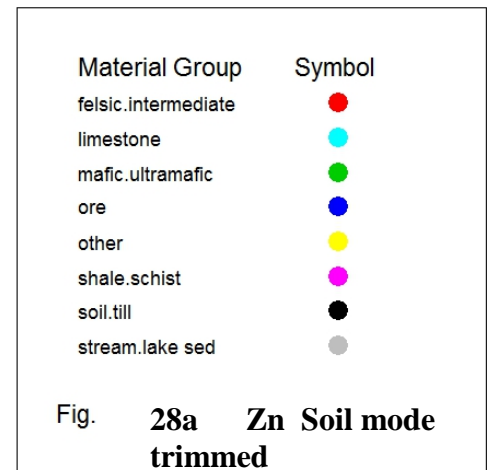
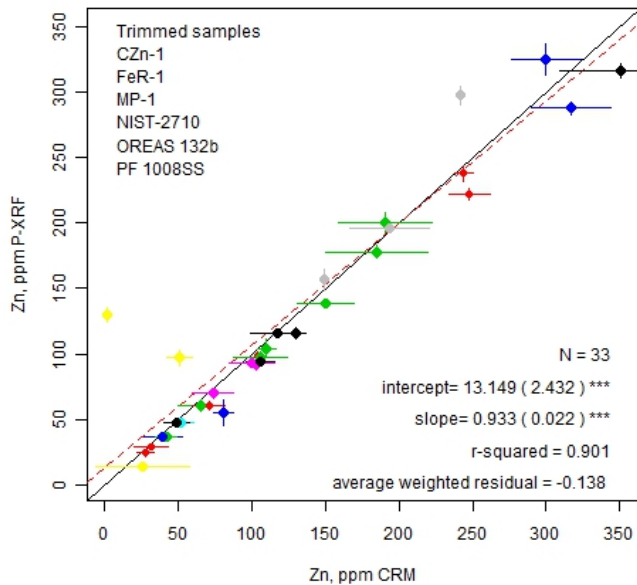
Handheld-HHAS-Soil Mode



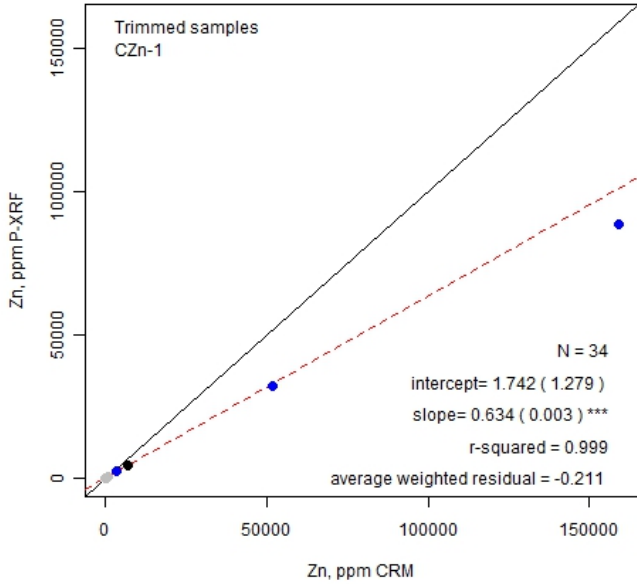
Handheld-HHBS-Soil Mode



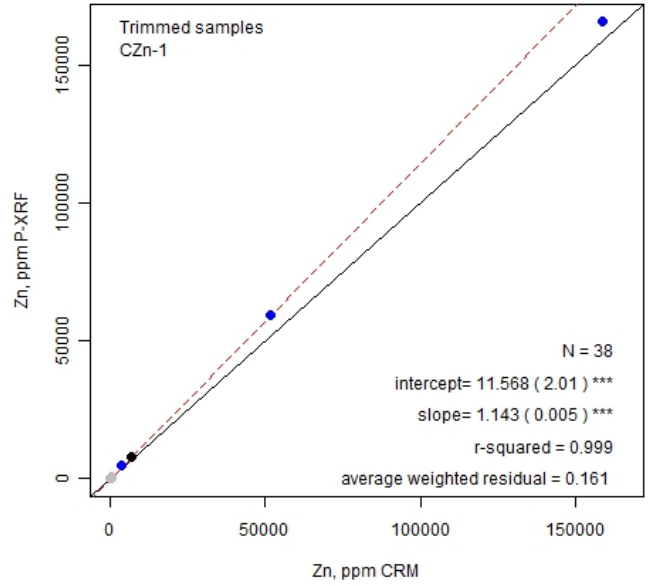
Handheld-HHCS-Soil Mode



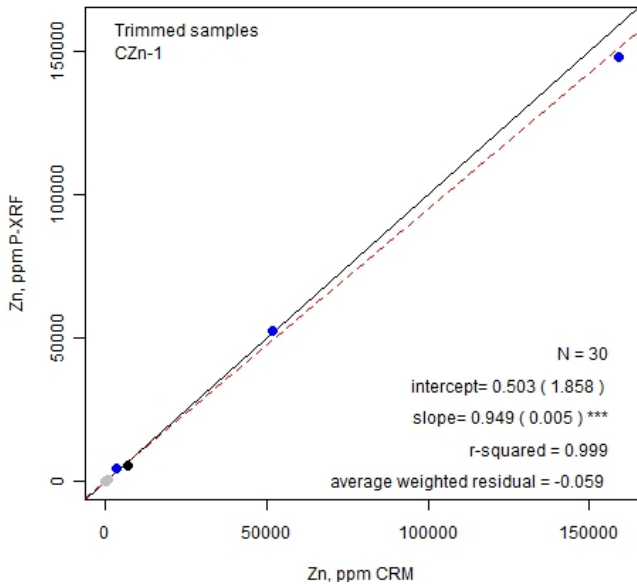
Benchtop-BTAM-Mining Mode



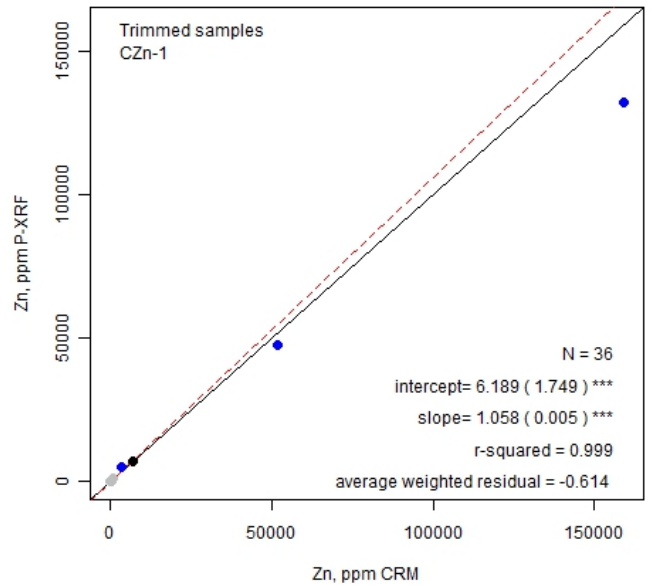
Handheld-BTBM-Mining Mode



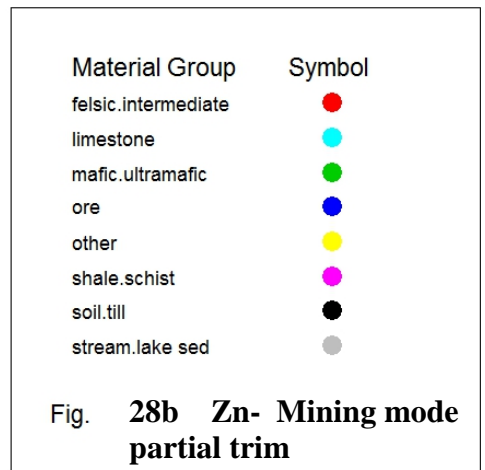
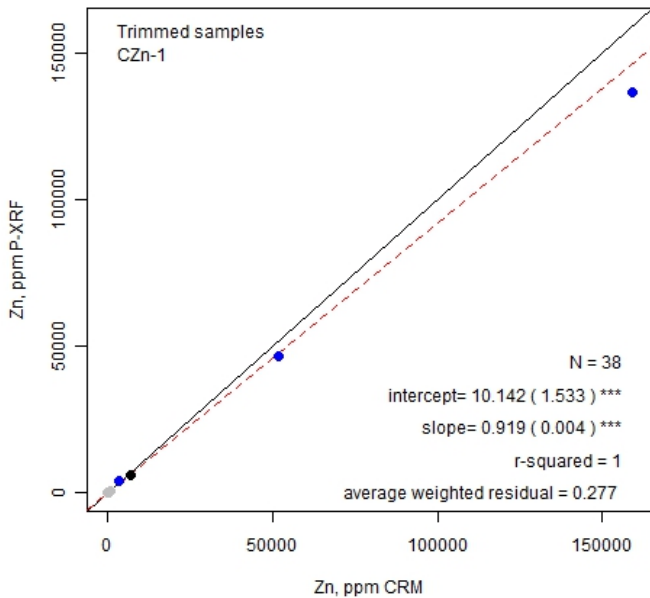
Handheld-HHAM-Mining Mode



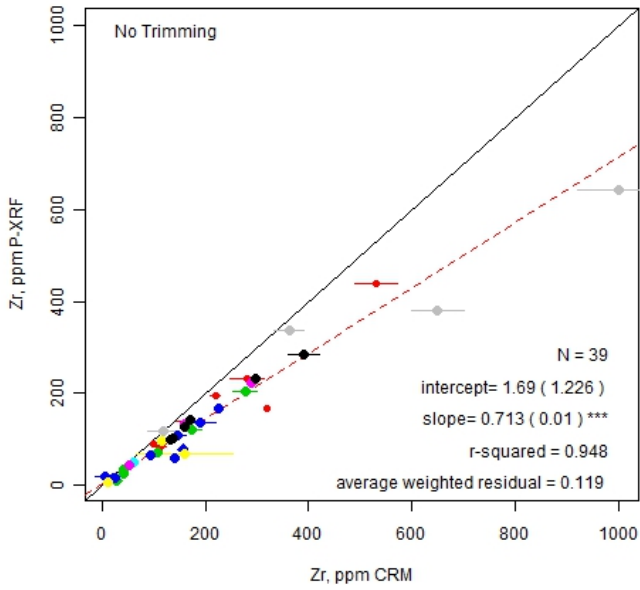
Handheld-HHBM-Mining Mode



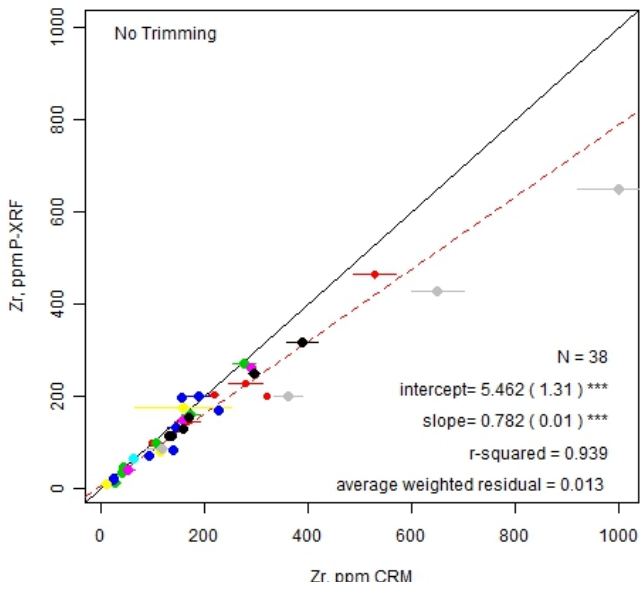
Handheld-HHCM-Mining Mode



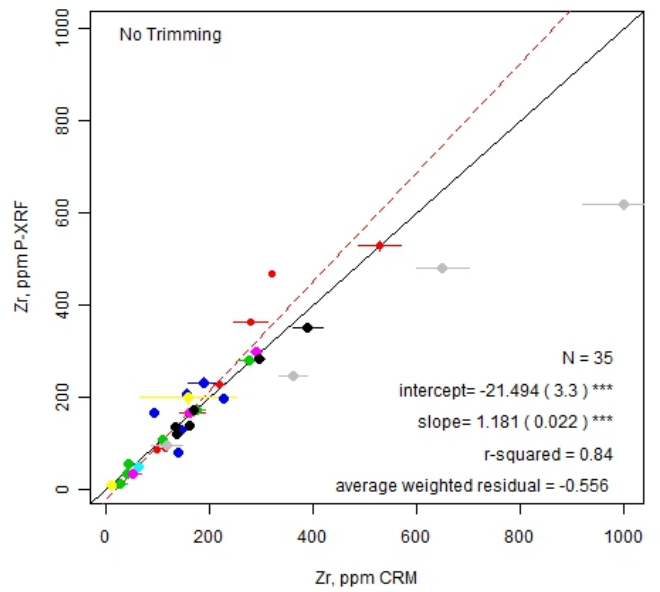
Bench Top-BTAS-Soil Mode



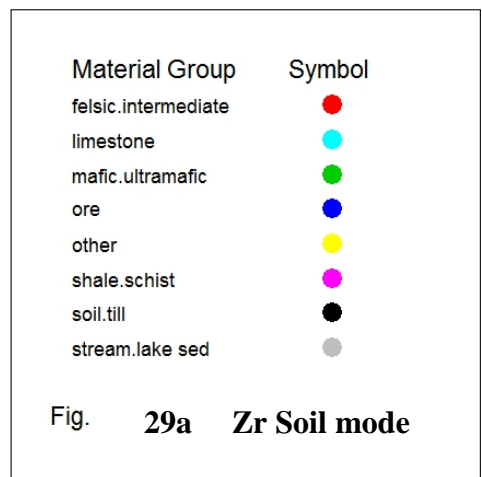
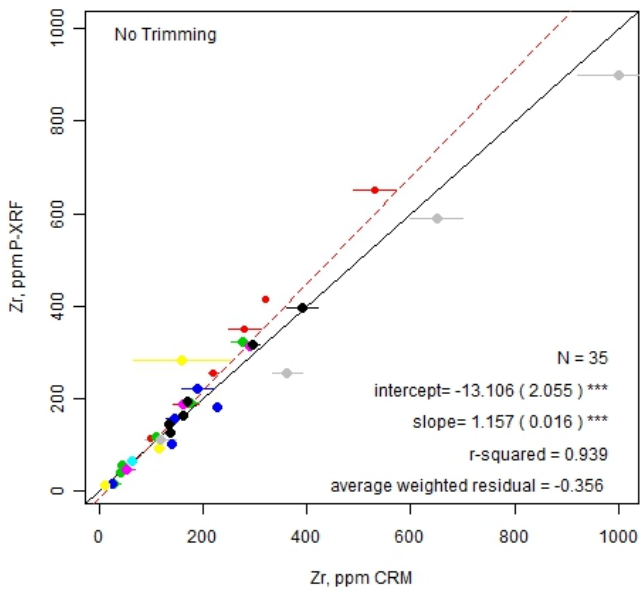
Handheld-HHAS-Soil Mode



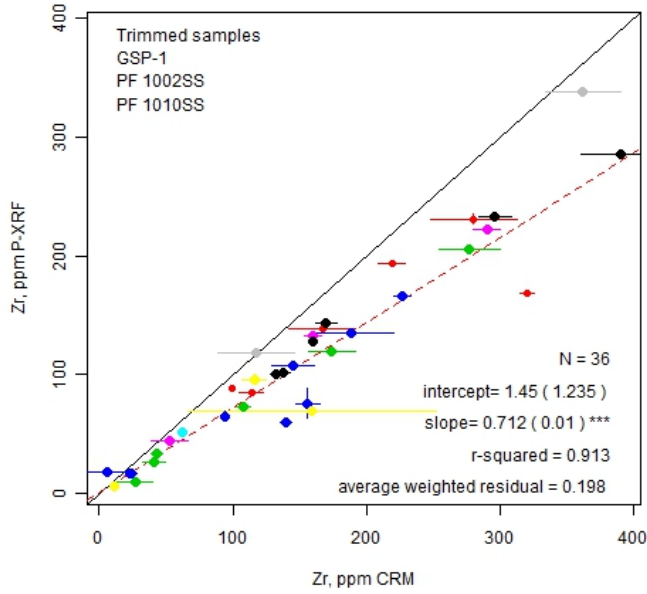
Handheld-HHBS-Soil Mode



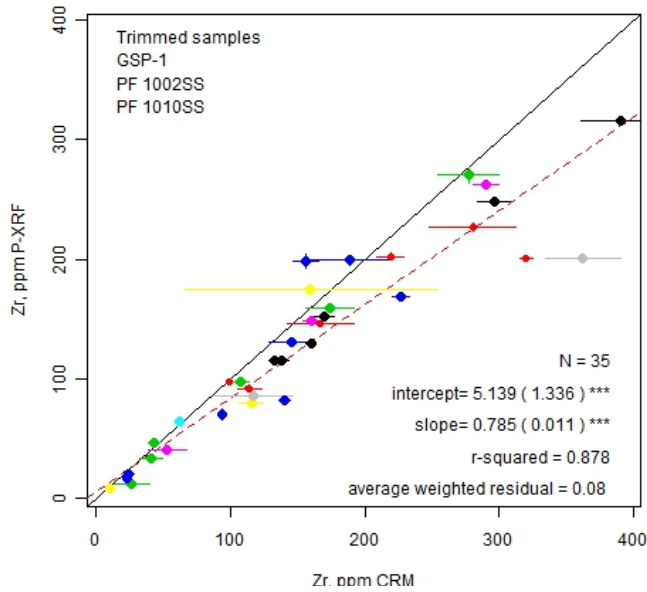
Handheld-HHCS-Soil Mode



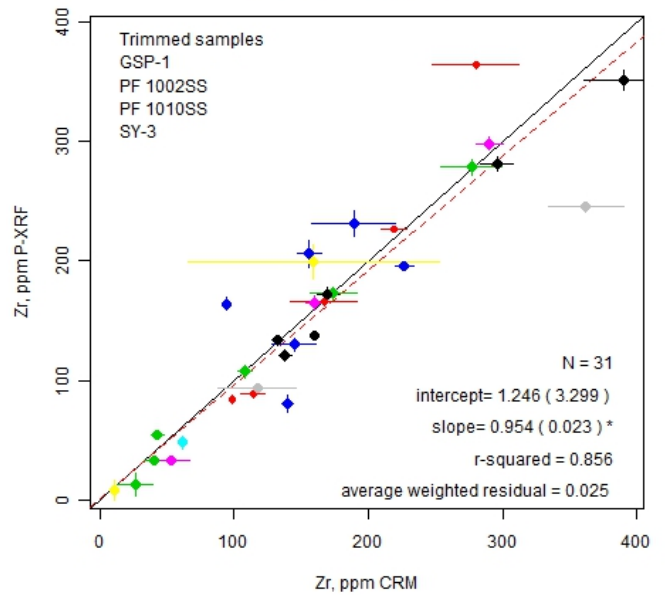
Bench Top-Machine A-Soil Mode



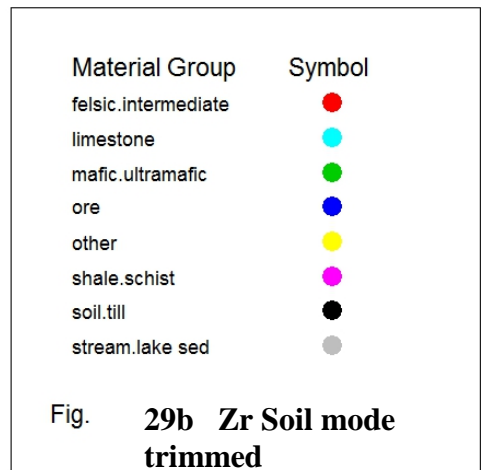
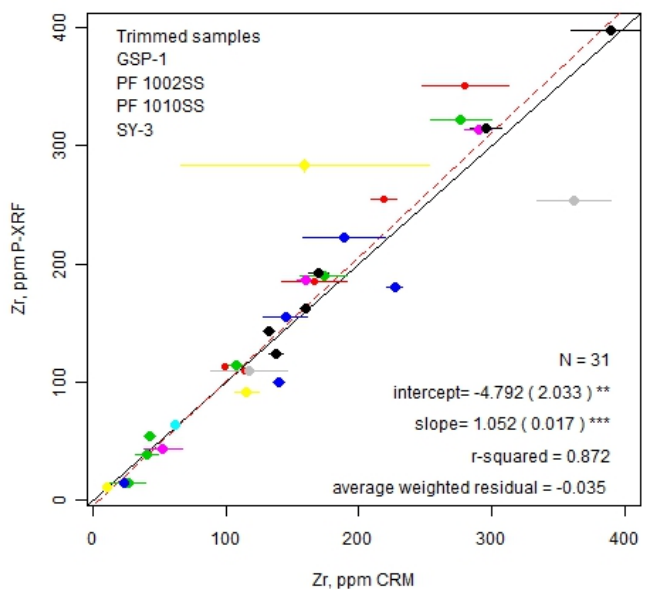
Handheld-HHAS-Soil Mode



Handheld-HHBS-Soil Mode



Handheld-HHCS-Soil Mode



4.3.3 Summary and discussion of accuracy and precision graphs

Because there are a very large number of graphs and tables, we decided to attempt some summary tables, to facilitate generalization and to provide users with an easy guide. It should be emphasized, however, that these summary tables are somewhat subjective, and users are encouraged to look at the detailed graphs and tables for particular elements of interest.

Separate summary tables have been generated for soil mode and mining mode. In the mining mode, the main interest is on the major elements and on ore materials, so the statistics refer to untrimmed data. For the soil mode, the focus is more on trace elements and without the potentially interfering ore-type samples, so the statistics are calculated from values shown on the trimmed plots.

One purpose of the summary plots is to allow a generalized ranking of elements, based on both precision and goodness of fit. A simplified classification of the slope and r^2 values was made using the following subjective criteria. Thus a slope within 5 % of 45° (rotational bias ± 5 %) is considered 'good, and one greater than 20 % is 'bad'. A goodness of fit (GOF) better than 90 % is considered 'good', whereas one less than 50 % is 'bad'. Given the challenging suite of diverse sample types analysed, our ratings are probably too critical.

	Accuracy	Precision	
	Slope	Goodness-of-fit	
	abs(b - 1)	r²	Weight
Good (G)	<0.05	>0.9	3
Fair (F)	0.05 - 0.10	0.8 - 0.9	2
Poor (P)	0.10 - 0.20	0.5 - 0.8	1
Bad (B)	>0.20	<0.5	-1

The following tables show the classification of each machine for each element, by mode, so that a comparison of machines is possible, and a summary across all 5 machines. In this way, elements can be ranked by an average rating (across rows of the tables), expressed as a weighted sum. For elements not measured on all 5 machines, the weighted sum is normalised by multiplying by 5/k, where k=number of machines reporting. This allows elements not measured on all machines to be compared with the others. A separate 'secondary' table following each 'primary' table shows values for elements measured on fewer than 3 machines.

SOIL MODE ON 'TRIMMED' GRAPHS

Rating based on combination of accuracy and precision across all machines

Primary list. Elements measured on at least 3 machines.

Elem.	BT-A-S			BT-B-S			HH-A-S			HH-B-S			HH-C-S			Wt.Sum
	n	Acc.	GOF													
Sr	32	G	F	33	F	G	31	G	G	30	G	G	31	G	G	28
Rb	34	F	F	36	P	G	33	G	P	32	G	G	36	P	G	22
Cu	33	P	F	32	P	F	30	G	G	31	F	G	32	P	P	19
Ca	30	B	F	34	F	F	30	B	G	30	G	G	32	G	G	19
K	34	B	G	38	F	G	32	B	G				37	F	G	17.5
Zn	34	P	F	34	F	F	35	F	F	35	B	F	33	F	G	17
Fe	34	F	F	34	P	F	28	B	G	34	F	G	34	P	F	17
Ti	33	G	P	34	B	G	36	P	F	32	P	P	31	P	G	15
Zr	36	B	G				35	B	F	31	G	F	31	F	F	15
As	34	P	G	29	G	F	34	B	G	18	P	F	26	P	B	14
Mn	36	F	P	35	G	B	37	G	F	32	P	P	31	P	P	13
Th	31	G	F	30	G	P	17	B	B				31	F	B	8
Pb	27	B	B	31	G	G	20	B	P	13	B	B	26	G	G	8
Nb	32	G	P				30	P	P	4	B	B				6.6
Ba	34	F	G	29	B	P				23	P	P	28	B	B	6.25
Cd	10	G	G	6	B	F				21	B	P	9	B	B	6.25
Cr	34	P	P	31	P	P	35	P	P	21	B	P	17	B	P	6
U	30	B	B	15	P	F	9	B	G	24	B	B				4.25
Sb	36	G	G	15	B	B							11	B	B	3.3
Mo	23	P	F	22	P	B	11	B	P				17	B	B	1.25
V	31	B	B	33	F	P	31	B	B	23	B	B	29	F	P	0
Ni	19	B	B	26	B	B	10	B	B	12	G	G	26	P	B	0
Co	32	B	B	23	B	P	33	B	P	28	B	B	13	B	B	-6
S	27	B	F	22	B	B	4	B	B				22	B	B	-6.25
Sn	37	B	P	24	B	B							11	B	B	-6.6

Secondary list of elements on fewer than 3 machines

Elem.	BT-A-S			BT-B-S			HH-A-S			HH-B-S			HH-C-S			Wt.Sum
	n	Acc.	GOF													
La	23	F	G													25
Y	31	P	P				31	G	G							20
Ce	23	P	P													10
Ag	6	P	G				4	B	B							5
Sm	7	B	P													0
Se	22	B	P	6	B	B										-5
W	24	B	B	5	B	B										-10
P	26	B	B				5	B	B							-10
Hg	11	B	B													-10
Nd	14	B	B													-10
Ta										7	B	B				-10

GOF: Goodness of fit

The following observations (and some conclusions) may be made from the soil summary table. Note that the soil table uses trimmed data, so that any samples with values of an element greater than the cutoff are excluded. It therefore focuses on the non-extreme values.

1. Of the 25 elements listed in the primary trimmed soil table, Sr is ranked ‘best’ and Sn ranked ‘worst’. The top group of 11 elements (weighted sum > 10) in order from best to worst are: Sr, Rb, Cu, Ca, K, Zn, Fe, Ti, Zr, As and Mn. The bottom group of 14 elements (weighted sum < 10), again in decreasing order of ranking, are Th, Pb, Nb, Ba, Cd, Cr, U, Sb, Mo, V, Ni, Co, S and Sn.
2. There is no unanimity of ranking between machines. Seldom do all the machines tell the same story. This has important implications for users with more than a single machine, (unless perhaps it is an identical model, with the same version of the software—an untested situation here) because they may well be giving significantly different results. What is more, there is no clear advantage of using one machine over another. Each machine is good on some elements, less good on others.
3. There is no obvious difference in performance between handheld and benchtop machines in either the top or bottom group of elements.
4. The top list of elements has reported values for over n=30 of the 41 samples. The unreported samples are presumably below detection, or troubled by interferences. A small number of samples have been trimmed—but usually fewer than 5. The bottom list has reported numbers of samples (n) that can differ greatly between machines. For example, Nb gives results for n=32 samples by BT-A-S, 30 by HH-A-S but only 4 by HH-B-S. Ni gives n=19 by BT-A-S, 26 by BT-B-S, 10 by HH-A-S, 12 by HH-B-S and 26 by HH-C-S. It is uncertain whether this is due to differences between algorithms (some more restrictive than others, for certain elements, others less so)—or other reasons. This appears to be more problematic with the less well-ranked elements, so may not be too significant, because results from these elements likely will not be trusted anyway.
5. Some elements ranked low in the list still have good results from one machine, but bad on the other machines. For example, Ni (ranked very low across 4 machines) has good results by HH-B-S (slope within 5 % of 45° line, r^2 better than 90 %). Similarly Sb has ‘good’ results by BT-A-S, ‘bad’ by BT-B-S and HH-C-S. This reinforces the observation of differences between machines, but is perhaps an encouraging sign that as improvements are made to hardware and software especially that acceptable results will eventually be possible for more elements.
6. The secondary list of elements (measurements on only 1 or 2 machines), includes elements that are mostly problematic. Best of the group are La and Y, followed in decreasing order of rank by Ce, Ag, Sm, Se, W, P, Hg, Nd and Ta.

ACCURACY AND PRECISION RATING ON UNTRIMMED MINING MODE

Primary list of elements measured by at least 3 machines

Elem.	BT-A-M			BT-B-M			HH-A-M			HH-B-M			HH-C-M			Wt.Sum
	n	Acc.	GOF													
Fe	41	G	G	40	G	G	41	P	G	40	F	G	40	F	G	25
Ca	38	B	G	40	G	G	40	B	G	40	F	G	40	F	G	22
Zn	34	B	G	38	P	G	30	F	G	36	F	G	38	F	G	21
Pb	32	B	G	22	F	G	29	P	F	19	F	G	22	F	G	20
Cu	37	B	G	31	F	G	41	P	G	35	P	G	30	F	G	20
Si	41	G	F	40	P	F	41	F	F	40	F	F	40	P	F	19
K	36	P	G	37	G	G	30	B	G	36	B	G	37	P	G	18
Al	33	G	G	38	B	F	38	B	G	40	G	F	36	F	F	18
S	29	B	G	29	G	G	28	B	G	26	G	G	30	B	G	18
Cr	35	B	F	36	F	G	34	B	G	8	F	G	36	P	G	17
As	10	B	G	11	G	P	17	B	G	16	G	G	10	B	G	16
Ni	29	B	G	23	P	G	36	P	G	21	P	G	17	B	G	16
Mn	41	B	G	40	F	G	41	P	G	38	B	G	38	B	G	15
Ti	39	B	F	38	B	G	39	B	G	33	F	G	40	P	G	14
Sr				13	B	G				35	B	G	33	P	G	13.3
Rb				12	B	G				28	F	G	20	P	F	13.3
P	19	B	G	34	B	G	17	B	F	19	F	G	12	B	G	12
Mg				23	B	F	8	B	G	36	G	P	6	G	F	12
Cd	2	B	G	3	G	G	36	B	P	6	B	G	3	B	G	12
Zr	34	G	P	14	B	F	39	B	P	34	B	B	34	F	G	8
Co	13	B	F	8	B	F	33	B	F	9	P	G	5	B	B	5
Mo	4	B	G	2	B	G	12	B	G	3	B	B	9	B	B	2
V	35	B	B	38	B	P	37	B	B	23	B	B	39	B	B	-8
Sn				34	B	B	39	B	B							-10

Secondary list of elements measured on fewer than 3 machines

Elem.	BT-A-M			BT-B-M			HH-A-M			HH-B-M			HH-C-M			Wt.Sum
	n	Acc.	GOF													
U										6	F	G				25
Ba				39	P	G							38	B	G	15
Ag				39	G	B							3	P	F	12.5
Ce										5	B	G				10
Hf										3	B	G				10
Nb				2	B	G				10	B	B	8	B	B	-2
W	9	P	B				14	B	B							-5
Bi				9	B	B							8	B	B	-10
Cl				4	B	B							17	B	B	-10
Ta										13	B	B				-10
Sb							40	B	B							-10

GOF: Goodness of fit

MINING MODE. RATING BASED ON PRECISION ONLY. UNTRIMMED.

List of elements measured on at least 3 machines

Elem.	BT-A-M		BT-B-M		HH-A-M		HH-B-M		HH-C-M		Wtd.
	n	GOF									
Ca	38	G	40	G	40	G	40	G	40	G	15
Zn	34	G	38	G	30	G	36	G	38	G	15
K	36	G	37	G	30	G	36	G	37	G	15
Rb			12	G			28	G	20	G	15
Sr			13	G			35	G	31	G	15
Fe	41	G	40	G	41	G	40	G	40	G	15
Mn	41	G	40	G	41	G	38	G	38	G	15
Cu	37	G	31	G	41	G	35	G	30	F	15
S	29	G	29	G	28	G	26	G	30	G	15
Ni	29	G	23	G	36	G	21	G	17	G	15
Pb	32	G	22	G	29	F	19	G	22	G	14
P	19	G	34	G	17	F	19	G	12	G	14
Ti	39	F	38	G	39	G	33	G	40	G	14
Cr	35	F	36	G	34	G	8	G	36	G	14
Al	33	G	38	F	38	G	40	F	12	G	13
Cd	2	G	3	G	36	P	6	G	3	G	13
As	10	G	11	P	17	G	16	G	10	G	13
Si	41	F	40	F	41	F	40	F	40	F	10
Mg			23	F	8	G	36	P	6	F	10
Co	13	F	8	F	33	F	9	G	5	P	10
Mo	4	G	2	G	12	G	3	B	9	B	7
Zr	34	P	14	F	39	P	34	B	34	G	6
V	35	B	38	P	37	B	23	B	39	B	-3
Sn			34	B	39	B					-5

Secondary list of elements measured by fewer than 3 machines.

Elem.	BT-A-M		BT-B-M		HH-A-M		HH-B-M		HH-C-M		Wtd. Sum
	n	GOF									
U							6	G			15
Ce							5	G			15
Hf							3	G			15
Ba			39	G					38	G	1.6
Nb			2	G			1				
Ag			0	B					8	B	1.6
Bi			39	B					3	F	-5
Cl			9	B					8	B	-5
Ta			4	B					17	B	-5
W							1				
Sb	9	B			14	B	3	B			-5
					40	B					-5

GOF: Goodness of fit

The summary table for mining mode is based on untrimmed data, as this mode is better suited to samples such as ores with higher element concentrations. The mining mode is particularly good for major elements. Here, two summaries are provided, one with a ranking based on both accuracy and goodness of fit (similar to the soil table) and a separate ranking in another table based on goodness of fit only. This is because the mining mode is designed for user-prepared calibration for particular materials, and poor accuracy can probably be diminished by fitting lines to calibration samples with 'true' concentration values measured by some other method.

The main observations are as follows.

1. There are 19 elements with weighted sum values greater than 10. In order, best-worst these are: Fe, Ca, Zn, Pb, Cu, Si, K, Al, S, Cr, As, Ni, Mn, Ti, Sr, Rb, P, Mg and Cd. Despite the variety of materials amongst the CRM samples, with no custom calibration, the performance of the mining mode on these elements generally is superior to the soil mode, particularly for goodness of fit (i.e. less scatter about the best fit line). Nevertheless, bias (upward or downward) is for most elements a significant problem, and often differs in both magnitude and sign between machines. Again this is an indication of inter-machine differences, and should be a caveat unless user-calibration is carried out.
2. The less satisfactory elements in the primary list, in decreasing order of rank, are: Zr, Co, Mo, V and Sn.
3. In the secondary list, reported on by only 1 or 2 machines, the best is U, followed by Ba, Ag, Ce and Hf (above a weighted sum of 10), with Nb, W, Bi, Cl, Ta, and Sb bringing up the rear.
4. In the summary table that ranks elements in mining mode on goodness of fit only, there are 10 elements that have r^2 better than 90 %. These are Ca, Zn, K, Rb, Sr, Fe, Mn, Cu, S, and Ni. For these elements, on any of the 5 machines, recalibration would likely produce excellent goodness of fit results. For Pb, P, Ti, Cr and Cd, 4 out of 5 machines give r^2 better than 90 %, and Al and As are 'good' on 3 out of 5 machines. Mg, Co, Mo, Zr, V and Sn give inferior results, generally unusable.
5. In the secondary mining mode list based on goodness of fit, U, Ce, Hf, Ba and possibly Nb give better than 90 % r^2 on at least 1 machine. Ag, Bi, Cl, Ta, W and Sb give poor results.

4.4 Precision and detection limits

In this section precision was estimated as *repeatability* on a sub-suite of the CRMs and this allowed, in some cases, a definition of optimum detection limit.

Overall precision in geochemistry takes into consideration all steps from sampling to analysis and thus variance is a function of the associated standard deviations:

$$\text{Variance} = \sigma_{\text{sampling}}^2 + \sigma_{\text{prep}}^2 + \sigma_{\text{analysis}}^2$$

where ‘sampling’ refers to the representivity of that sample aliquot, ‘prep’ to the various preparation steps that might be involved (crushing, grinding, sieving) and ‘analysis’ to the analytical technique methodology (e.g. ICP-AES, ICP-MS, XRF). Usually the variability associated with the latter is insignificant compared to that of preparation and certainly to that of sampling. In methods based on ICP-MS or fire assay, for example, where a sample is put through a decomposition procedure, the variability associated with the ‘analysis’ includes all steps taken in the lab (digestion, separation from the matrix AND the analysis itself). In direct analysis by pXRF, where there is little to no sample preparation and no sample digestion or separation step, the variance associated with the analysis should be very small. The inherent precision of pXRF, then, is based on the counting statistics; this error is the number provided with each datum and indeed it is usually very low. For example, the ‘RSD’ (standard error/concentration in %) associated with one analysis of the granite, GSR-1, is typically as follows: ± 0.4 % for Fe (at 1.59 % Fe); ± 2 % for Sr (at 108 ppm); ± 0.4 % for Rb (at 460 ppm); and ± 1.3 % for Rb (at 146 ppm) (data from HH-A-S). Clearly this noise increases at low count rates, at levels close to detection level, as seen for example for As, at ± 25 % at concentrations below 10 ppm and for Cr at ± 10 % at a concentration below 40 ppm.

Noise also increases dramatically in certain regions of the spectrum where there are numerous interferences and a large (variable) background and the error shown by the instrument will indicate that it is unwise to use the concentration reported. For example, Sn is reported by one instrument at $\sim 150 \pm 180$ ppm in the rhyolite, RGM-1; in fact, the certified concentration of Sn in RGM-1 is 4.1 ppm. So it is critical to pay attention to that error, though it certainly does not always indicate inaccuracy. In the case of Sn, it would have been preferable for the manufacturer to eliminate reporting Sn under those circumstances, as was done by other vendors. The more corrections the software is designed to make, the more noise one would assume to be associated with the number reported.

Ten non-ore samples were selected from the CRM suite to test precision and detection limits. They were analysed 10 times each in completely random fashion, so as to include any variability encountered by repositioning the sample. Their results – as mean, SD and RSD (CV) - are attached in Appendices 8a (Precision_soil), 8b (Precision_mining Ag_Mn) and 8c (Precision mining Mo_Zr). When not all 10 analyses per sample produced readings, but $n \geq 5$, these data are included for viewing (see later discussion in this section). Unfortunately there are numerous non-detects amongst some trace elements (e.g. Cd, Mo) and that is the reason for the blank areas in the tables. Also provided in the tables are (1) the ‘mean’ RSD across the 10 samples per instrument and (2) the mean of the mean RSDs per element across the instruments. In situations where $n < 10$ for a sample, that mean was not used in the calculation of RSDs. As is well known, RSD varies with concentration, and therefore taking the mean RSD across these samples as

representative can be misleading. However, many of the ranges in concentration are not that large and the calculation affords some attempt at summarizing the data, as shown in the table below.

Analytical precision by pXRF across the five (or fewer, depending on the element) instruments for the suite of 10 CRMs. DLs in ppm unless otherwise indicated.

Element	Mean RSD, %	Optimum DL, ppm	Comments on precision
Soil mode			
Ag	8.1 ± 4.6	4	BT-B-S data are erroneous, so RSD is invalid
As	11.0 ± 5.7	10	Good precision ≠ good accuracy, especially at low levels
Au		NA	Data are <i>highly</i> erroneous
Ba	10.7 ± 10.7	6	HH-B-S exceptionally noisy
Bi			Too low in [Bi] to determine
Ca	1.7 ± 1.1	400	Tight data
Cd	17.8 ± 14.6	10	HH-B-S, BT-A-S very noisy
Ce	(57)		Only BT-A-S data, 3 results
Cl		(300)	Only BT-A-S data, 1 result
Co	12.9 ± 7.4	3	Very high DLs by HH-C-S, BT-B-S
Cr	6.0 ± 0.6	20	Hard not to encounter interference at low levels
Cs	(8.3 ± 0.5)		Only HH-C-S, BT-B-S reported, data are highly erroneous
Cu	5.6 ± 2.2	5	Fairly consistent across models
Fe	0.9 ± 0.8	300	Consistent across models
Hg		NA	Data are <i>highly</i> erroneous
K	2.4 ± 1.1	300	Consistent, BT-B-S exceptionally good SDs
La			Only reported by BT-A-S, n≠10 in any sample
Mn	3.6 ± 1.6	50	Consistent across models
Mo	15.5 ± 10.5	4	n is highly variable across models
Nb	9.6 ± 2.3	3	Precise data by HH-A-S, BT-A-S
Nd			Only by BT-A-S but highly erroneous
Ni	13.6 ± 6.5	20	Highly variable results across models; n=4 for two cases
P			Only 1 result, by BT-A-S
Pb	6.2 ± 1.1	5	n=4 for HH-B-S, [Pb] too low
Pd			Data are <i>highly</i> erroneous
Pr			Only reported by BT-A-S, highly erroneous
Rb	4.1 ± 0.6	3	Very consistent
S	10.4 ± 4.6	300	Highly variable, numerous non-detects
Sb	22.7 ± 11.7	5	n=2-5 for most
Sc			Highly erroneous data

Se	31	(3)	Only enough data by BT-A-S, could be good DL if no interferences
Sm			Only by BT-A-S, no samples with 10 readings >0
Sn	21.9 ± 13.1	5	Variable, only 9 results
Sr	1.9 ± 1.3	5	Extremely consistent across all models
Ta			Only by BT-A-S, highly erroneous data
Te			6 results, all so inaccurate
Th	15.5 ± 2.9	5	Good across 3 models, very inaccurate by HH-A-S
Ti	2.5 ± 1.5	100	Very consistent across all 5
U	14.4 ± 8.4	5	BT-A-S shows U can be determined to 5 ppm in 'clean' samples. HH-B-S much too high.
V	9.9 ± 9.0	10	Precision by HH-B-S inferior to that of the other 4.
W	(13.2 ± 13.2)		Only 6 results reported, most inaccurate
Y	4.6	3	Just using data by HH-A-S
Zn	2.6 ± 0.9	5	Consistent across all 5 models
Zr	3.1 ± 1.2	5	Consistent across all 5 models
Mining mode			
Al	6.7 ± 4.8	0.2 %	Highly variable RSDs, from 2.6 % by BT-B-M to 11.9 % by BT-A-M
Ca	1.1 ± 0.6	0.03 %	Very consistent across all models
Fe	0.6 ± 0.1	0.03 %	Very consistent across all models
K	1.9 ± 0.9	0.03 %	Consistent RSDs
Mg	14.9 ± 9.1	1 %	Highly variable across models, many results <DL
Mn	5.0 ± 1.7	50	Consistent across the five
P	28 ± 39	0.02 %	Highly variable, many non-detects, one instrument (BT-B-M) clearly superior (3 % RSD)
S	5.9 ± 4.1	0.03 %	Consistent across 4 (HH-B-M inferior), RSDs typically 3-5 %
Si	1.5 ± 1.0	0.3 %	Consistent
Ti	2.8 ± 1.5	0.03 %	Consistent

Data-sets for many elements are based on four or five instruments but for elements such as Ag, Cs, La, Sc and Y this number is reduced. The precision for some elements such as Mo may appear to be much worse for one instrument because the element is being reported to low levels by that instrument and not by others (i.e. the cut-off for reporting by the others is set higher or not all 10 readings are reported and therefore not used in the RSD calculation). BT-A-S has a mean RSD of 24 % for Mo (n=9) compared to only 7 % by HH-C-S where only 4 samples are reported. At other times an instrument displays inferior precision to that of the others for no obvious reason: an example is for V by HH-B-S where its mean RSD is 26 % compared to 4-8 % for the other four instruments and all samples are reported. In this case it appears that a fairly

high detection limit of 52 ppm has been set for HH-B-S as samples of low V content report at this level. This is not a bad practice by the vendors where interferences are rampant and users can be misled by data reported below *real* detection limits where many matrices will suffer from interferences. Of the elements that are reported high because of interferences, Au, Pd and Hg are particularly treacherous because the precision appears to be good. For example, Au in GSR-6 and Hg in BHVO-1 by HH-A-S are reported at 5.3 ± 0.5 ppm (9.2 % RSD, n=10) and 13.1 ± 1.5 ppm (11.6 % RSD), respectively, good precision which belies the accuracy as these two CRMs contain less 1 *ppb* Au and 5.6 *ppb* Hg, respectively.

From the table and the appendices, typical RSDs for the CRMs fall into the following groups: <2.5 % for Fe, Ca, K, Si; 2.5-4.9 % for Mn, Rb, Sr, Ti, Y, Zn, Zr; 5-10 % for Ag, Cr, Cu, Pb, V, Al, S; 11-20 % for As, Ba, Cd, Co, Ni, S, Th, U, Mg; and > 20 % for Sb, Se, Sn and P. Also shown in the table is an ‘optimum detection limit’. This is based on three times the standard deviation of one of these samples containing the element at ~ 3-10 times the expected detection limit. This is *optimum*: the silicate samples used are not of complex matrix, do not contain unusually high concentrations of otherwise ‘trace’ elements, and are homogeneous and fine-grained. The large data-set in this report attests to the huge variability of detection limit (assuming accuracy) in different geological matrices. It should be borne in mind that the detection limit proffered by the manufacturers is usually defined as three times the standard deviation of a *pure element standard* which produces a ‘clean’ spectrum.

The data shown in italics in the precision tables indicate that fewer than 10 readings for that element in that sample have been reported ($5 \leq n < 10$). This provides the user with a good idea of the detection limit in that particular matrix. However, if the matrix changes, as it can well do in a survey or down a core, the level at which such randomness of reporting may rise and the user may be unaware that the number that is being reported is indeed at the new detection level (and therefore could be wrong). The table below provides examples of samples where not all 10 readings are reported by the instrument and yet the concentration levels that *are* reported appear to be above the instrument’s ‘usual’ or ‘best’ detection limit. The limestone (GSR-6) and the gabbro (MRG-1) are obviously problematic matrixes for these elements using this soil calibration. Thus, one reading of Co in MRG-1, for example, might read <DL or 0, depending on the nomenclature used by the manufacturer, and another might read ~ 300 ppm.

Examples of data where $5 \leq n < 10$; concentrations are near DL for that matrix

Element	Sample	Instrument	Mean \pm SD ppm	Accepted value, ppm
Co	MRG-1	HH-C-S	320 ± 76	87.0
Ni	NIST 2710	HH-C-S	41 ± 7	14.3
Ni	GSR-6	HH-A-S	33 ± 8	27
Sb	NIST 2711	HH-A-S	39 ± 4	19.4
Sc	GSR-6	BT-B-S	175 ± 33	6
Sr	GSR-6	HH-A-S	979 ± 13	913
Th	MRG-1	HH-A-S	54 ± 9	0.9
W	MRG-1	BT-B-S	36 ± 7	0.3

The geochemist is not in the habit of taking multiple readings so he/she would either follow up on a false anomaly or miss one by not realizing that the region of the *real* detection limit has changed. It would be safer for the user if the software was designed to work with variable detection limits and eliminate reporting concentrations below these limits according to the degree of interference encountered, as indeed some manufacturers do. This is further reinforcement that the user must become familiar with the constraints in the performance of pXRF and *their particular* instrument.

4.5 Thin-film Study

Graphs for GSR-1, GSR-3, LKSD-4, OREAS 166 and SY-3, showing the data for this study, are at the end of this section. Overall, Mg (detected in GSR-3 only), Al and Si transmittance display the greatest sensitivity to thin-film material and thickness. Transmittance for these elements in samples analysed falls within the following ranges:

Thin-film	Mg transmittance % (in GSR-3 only)		Al transmittance % range		Si transmittance % range	
	HH-A-M	BT-A-M	HH-A-M	BT-A-M	HH-A-M	BT-A-M
	Mylar 2.5	65	62-72	65-76	77-80	81-87
Mylar 3.6	59	62-71	61-68	69-78	75-81	
Mylar 6.0	ND	44-46	42-55	54-61	62-69	
PP 3.0	92	85-88	80-89	89-91	87-93	
PP 4.0	67-71	80-86	74-89	85-89	87-92	

- Material

In general and as expected, greater transmittance is observed for PP (polypropylene) than for Mylar of similar thickness (i.e. 3-4 μm vs 3.6 μm , respectively). This difference can be explained primarily by differences in density between materials, Mylar being denser than PP. Differences in density absorption effects predominate in the low keV region. In all samples, pronounced differences in transmittance for Mg, Si, Al, Si, S (most cases), K and Ca are observed for pellets lined with Mylar vs. PP. For example, Al transmittance in GSR-1 lined with Chemplex PP (3 and 4 μm) by HH-A is 82 % in contrast to Chemplex Mylar (6 μm) where Al transmittance is only 65 %, resulting in a difference of 17 %. This highlights the impact in choice of thin-film material on light element accuracy and detectability. The use and choice of bags in sampling programs should be considered carefully, especially where light elements are concerned. GSR-3 measured by HH-A-M provides a good example in illustrating how differences in transmittance between materials are attenuated as energy (keV) increases, where transmittance between materials (and thickness) becomes increasingly similar (smaller gap or overlap between blue square and red symbols) with keV.

- Thickness

Our results highlight that thickness does indeed play a great role in transmittance, particularly for light elements, or more precisely for lower keV elements. For a given thin-film material (e.g. Mylar in blue in the graphs), thickness influences transmittance, and this too is highly evident with respect to the lighter elements. For example, the LKSD-4 pellet combined with 6.0 μm Mylar yields Si transmittance of 45 % while 2.6 μm Mylar yields 72 % (a difference of 27 %). Furthermore, Al from the OREAS 166 pellet with 2.6 μm Mylar results in 76 % transmittance while Al is not detected whatsoever with 6.0 μm Mylar.

Moreover, differences in thickness are more pronounced for Mylar than for PP, likely a function of material density. For example, transmittance with 3.0 μm PP for Al in LKSD-4 vs. 4.0 μm PP is 4 % higher, while 2.5 μm Mylar transmittance relative to 3.6 μm Mylar (difference of 1.1 μm) transmittance is 9 % higher. In general, the effect of thickness on transmittance decreases with increasing energy (keV) for a particular thin-film (i.e. symbols of same colour are closer or overlap).

- Impurities

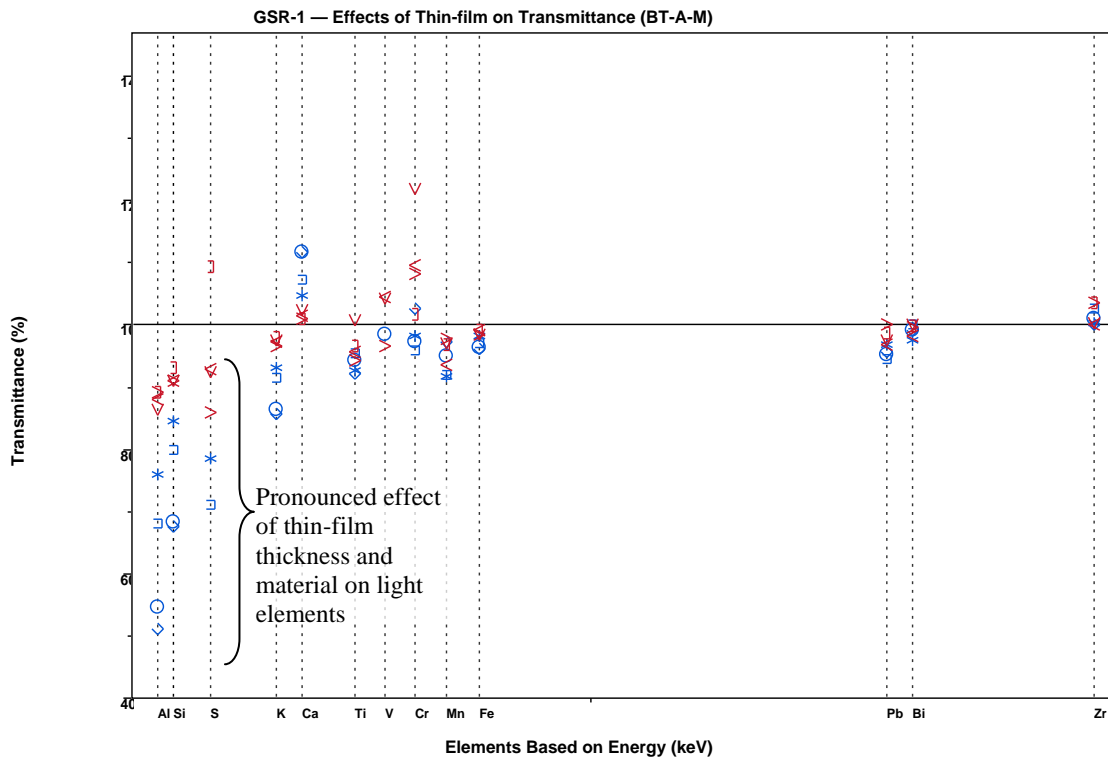
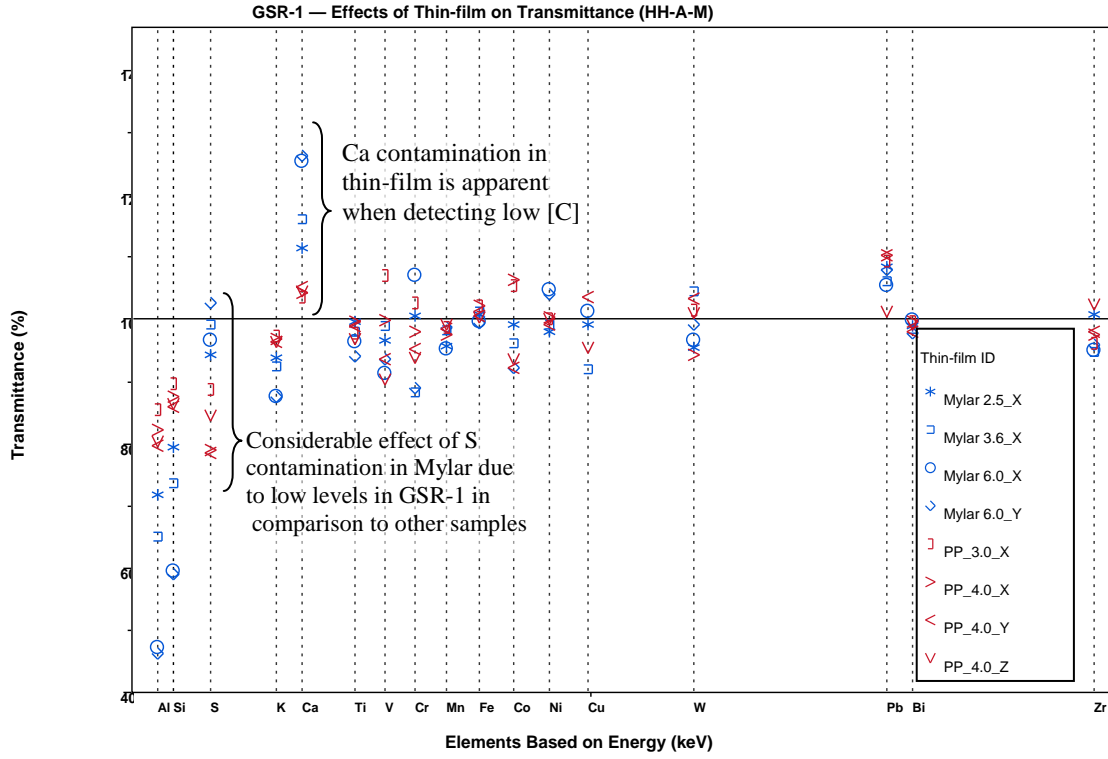
Contamination was interpreted as transmittance greater than 100%, i.e., when the concentration of an element detected with the use of thin-film is higher than without the use of thin-film. Because both analysers (i.e. HH-A and BT-A) were calibrated using PP, impurities in Mylar were not accounted for by a lower offset in the calibration. As such, Mylar impurities were apparent. In general, there are no significant differences in impurities between manufacturers (e.g. different triangles in graphs) for a given material. Also, in some cases impurities are observed with one analyser but not the other. This too highlights the complexities of dealing with low detection elements. Nonetheless, some differences in thin-film material impurities come to the fore-front when found and detected in low quantities in the samples. For example, low but detectable levels of P in the GSR-3 (HH-A), LKSD-4 (HH-A and BT-A) and SY-3 (HH-A and BT-A) pellets are falsely amplified by the P impurity in Mylar. Interestingly, while transmittance of P in GSR-3 (BT-A) is not greater than 100% for either material, Mylar transmittance is higher than PP – a well-known contradiction in transmittance potential between these materials – underlining the role of the P contamination in Mylar falsely boosting P transmittance.

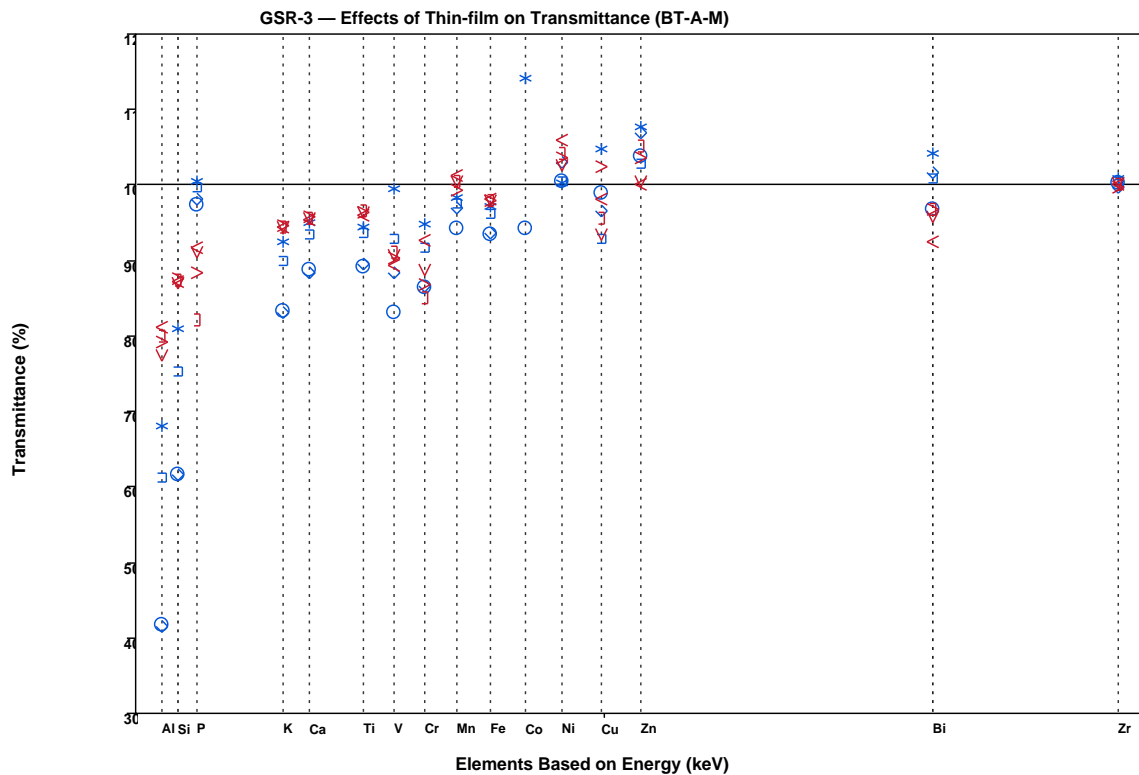
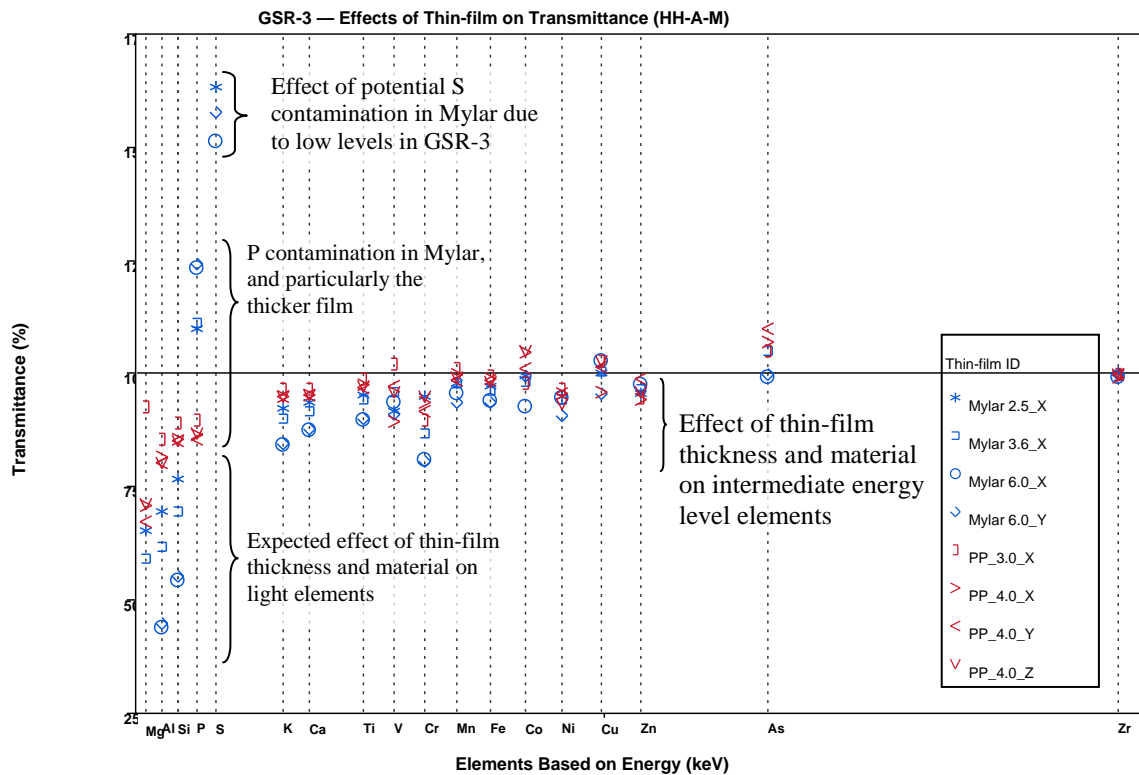
Sulphur also serves as another example of thin-film material impurity in Mylar for samples bearing low but detectable levels of S samples. For instance, S transmittance in GSR-3 (HH-A) is 1.6 times greater than the pellet without thin-film. Transmittance of S in this sample is also greater than PP, a tell-tale sign of S contamination in Mylar. In contrast, due to high concentrations of S in OREAS 166 (11.29 %) in comparison to all other samples, the effect of S contamination in Mylar is not perceptible for this sample. This underscores the importance of analyte concentrations in determining the extent of impact on accuracy by an impurity. It is worthwhile to carry out a similar exercise if thin-films are to be used and if target levels are in the ppm range, i.e. the same range as impurities.

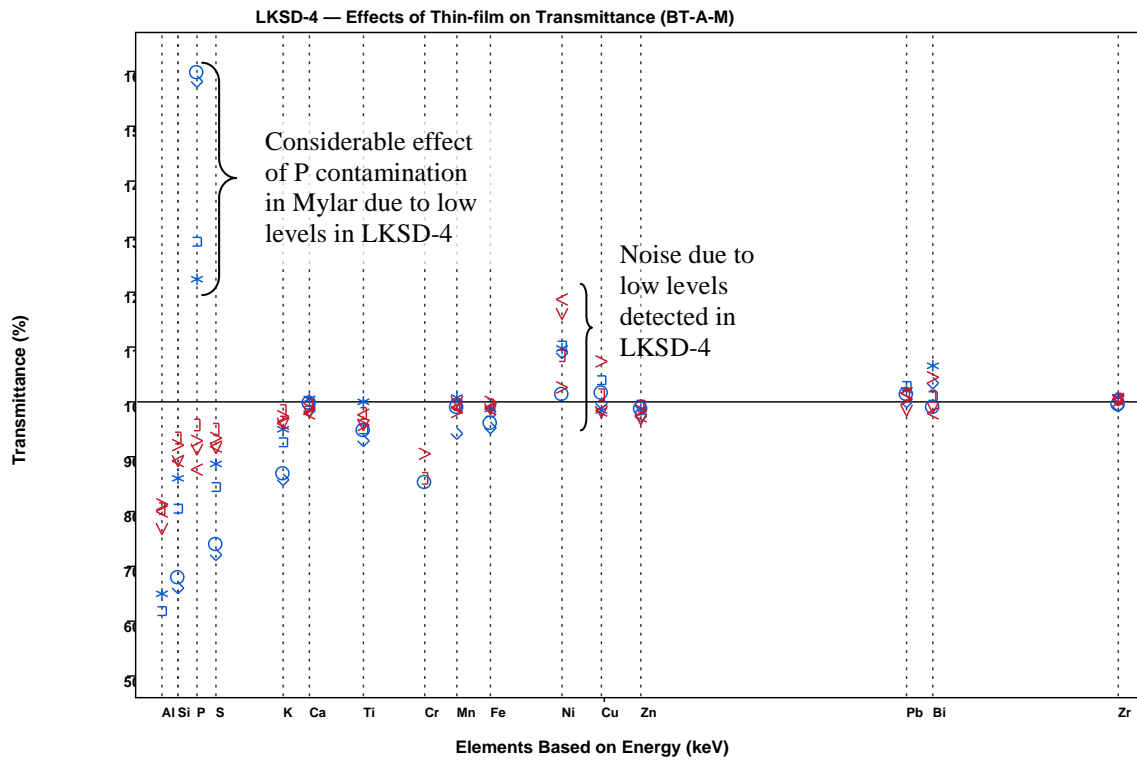
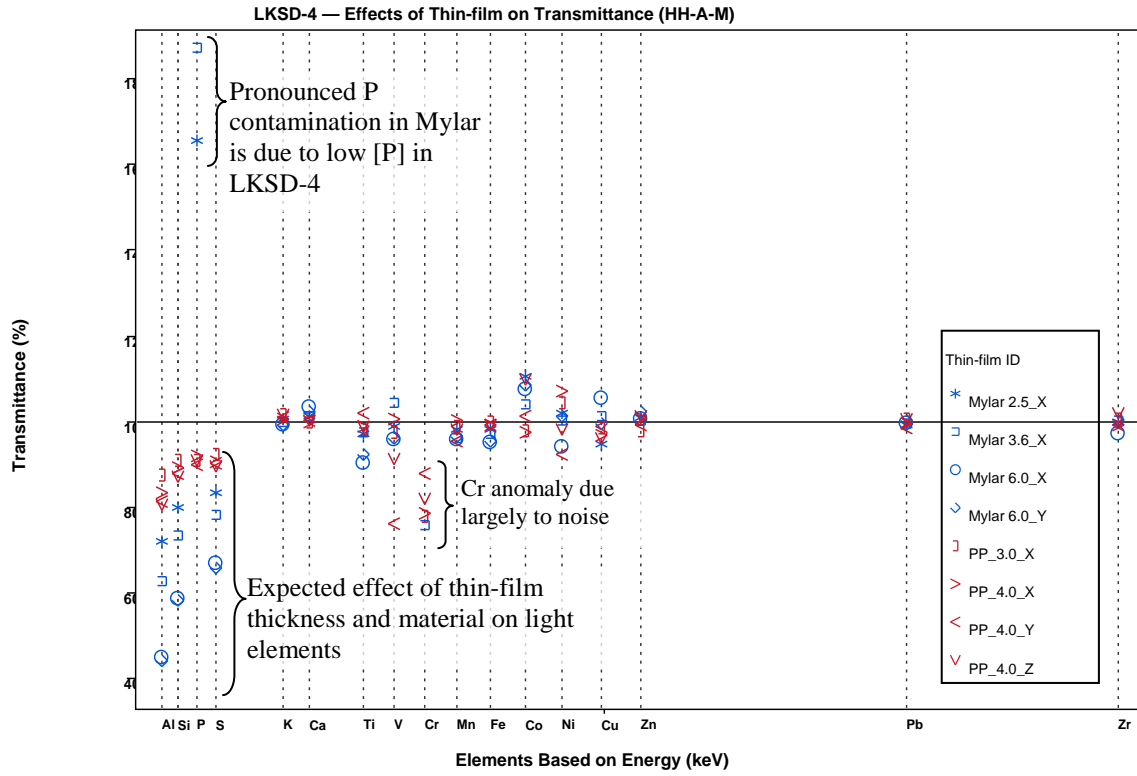
Interestingly, the trends between HH-A and BT-A for GSR-1 are inverted: S transmittance with Mylar for HH-A is higher than with PP, whereas the opposite is observed for BT-A. We suspect that differences for detection between both analysers may relate to factors such as detectability and noise but this trend could not be fully explained.

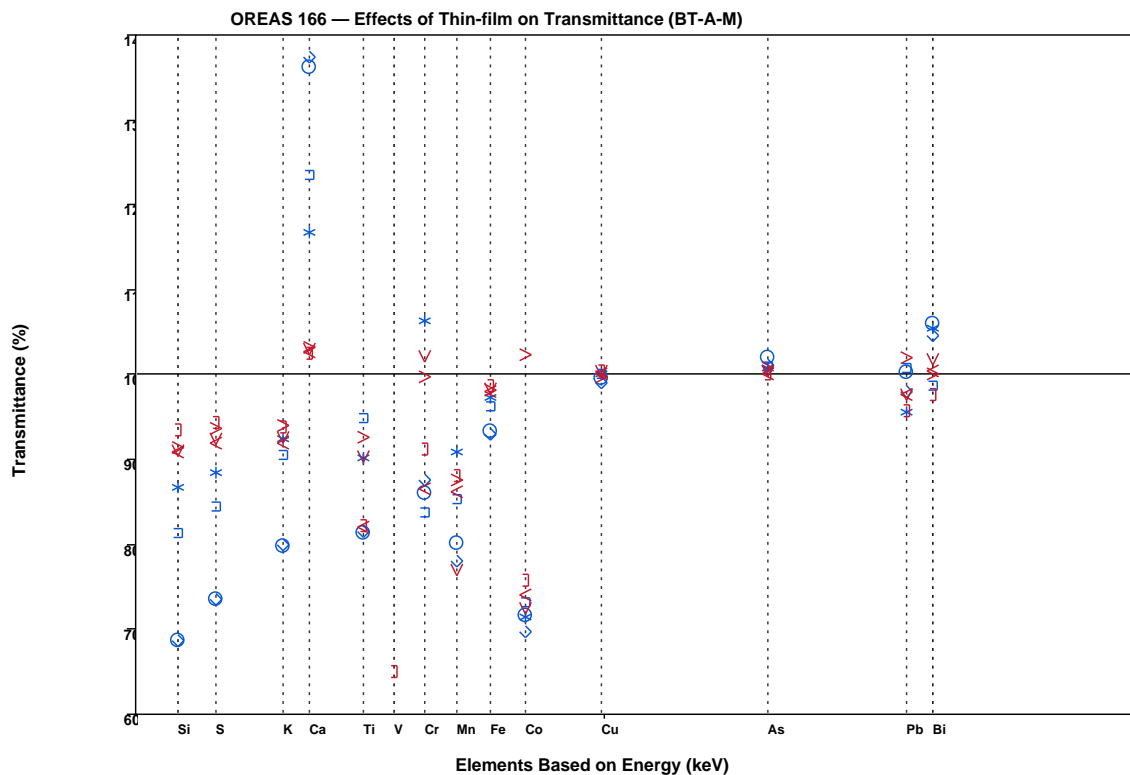
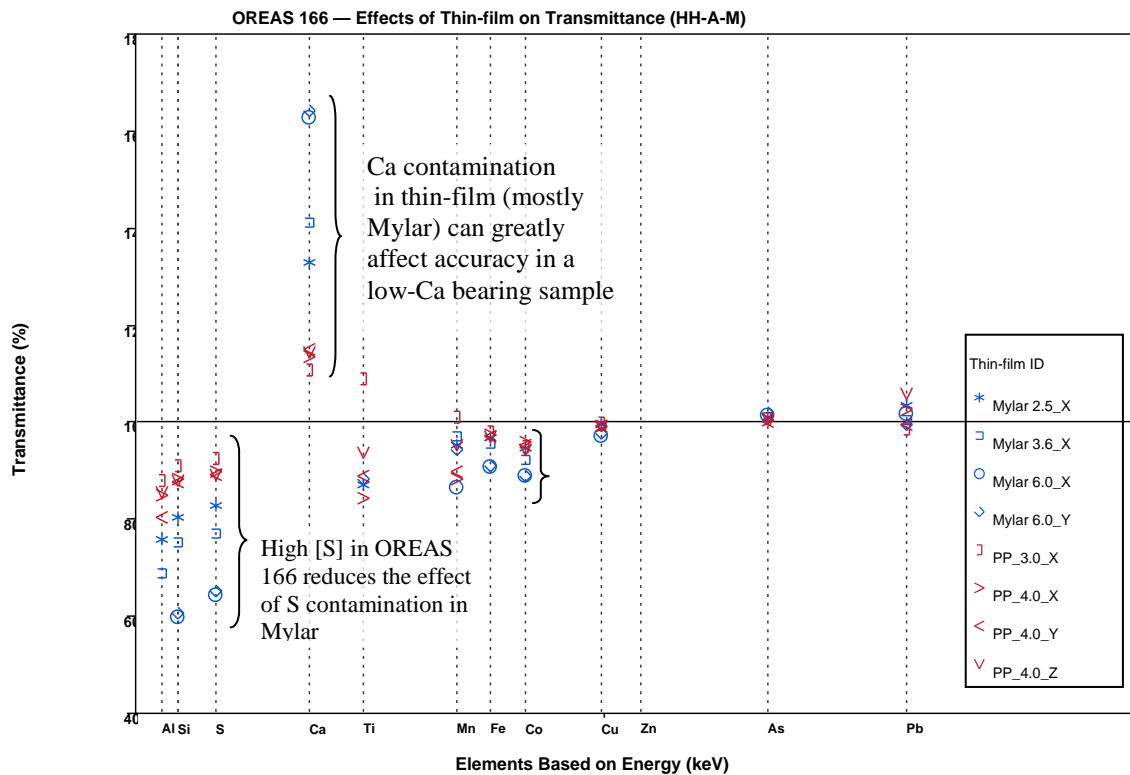
Another common impurity is Ca, observed for the OREAS (HH-A and BT-A) and to a lesser extent in GSR-1 (HH-A and BT-A) pellets. The Ca in Mylar for OREAS is magnified due to the low levels in the sample.

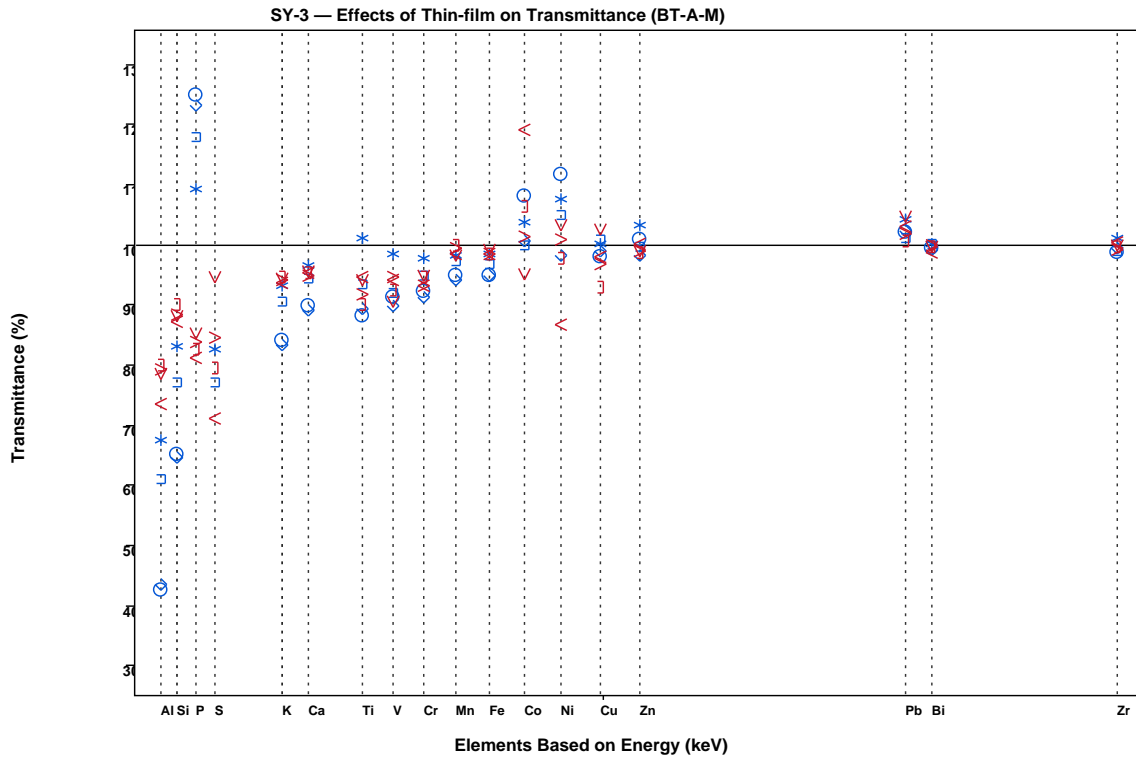
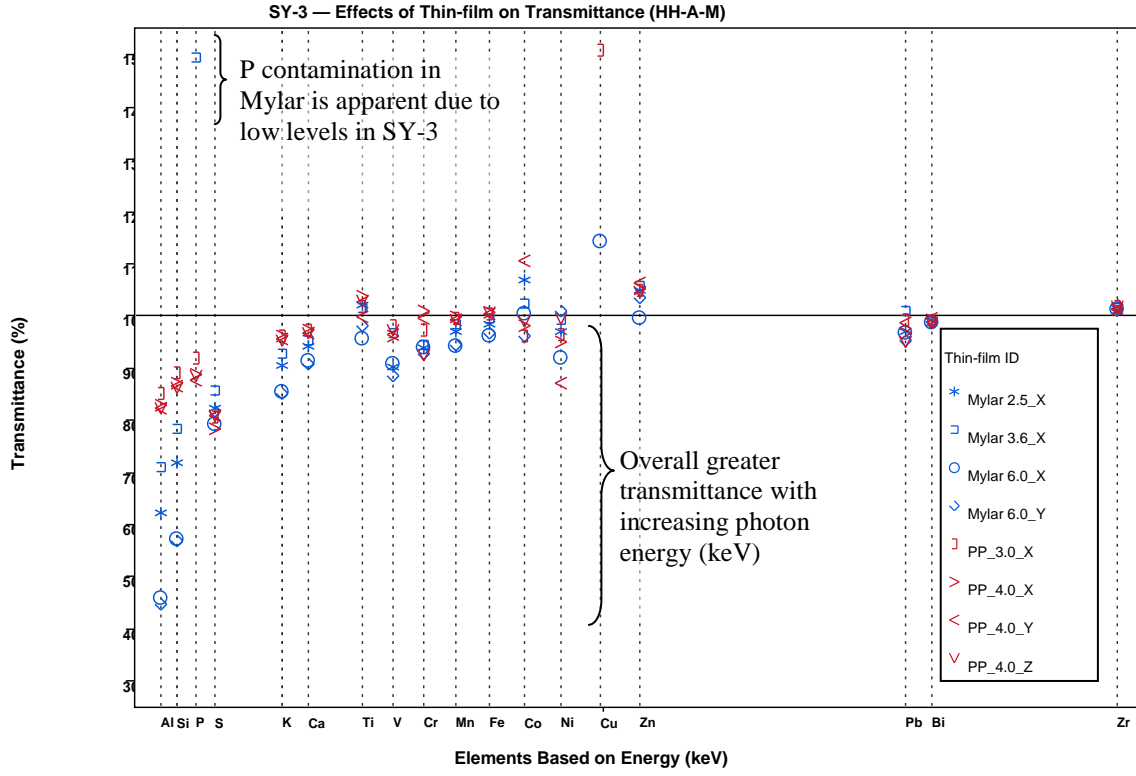
Other anomalies in data trends include Cr in GSR-1 (HH-A), Co in GSR-3 (BT-A), Cr (HH-A) and Ni (BT) in LKSD-4, Cr in OREAS (BT) and Cu in SY-3 (HH-A), which all hovered near detection. Additional factors such as sample homogeneity (even for these reference materials) could play a role at low levels. For example, the Cu anomaly in SY-3 is in part due to noise given the low concentration of Cu reported (17 ppm) in comparison to, for instance, OREAS 166 (87 500 ppm). However, Cu concentrations in other samples (e.g. LKSD-4) are detected within the same range as SY-3 but do not display this trend. While Cu is a typical impurity in PP, its absence as an impurity for LKSD-4 data refutes thin-film as an explanation for these results. The Cu concentration measured for the SY-3 pellet with no film may have been slightly underestimated, highlighting all the high sensitivity of circum-detection data and sample homogeneity in results. That being said, only multiple measurements when dealing with near-detection levels can assist in determining accurate and representative values for samples.





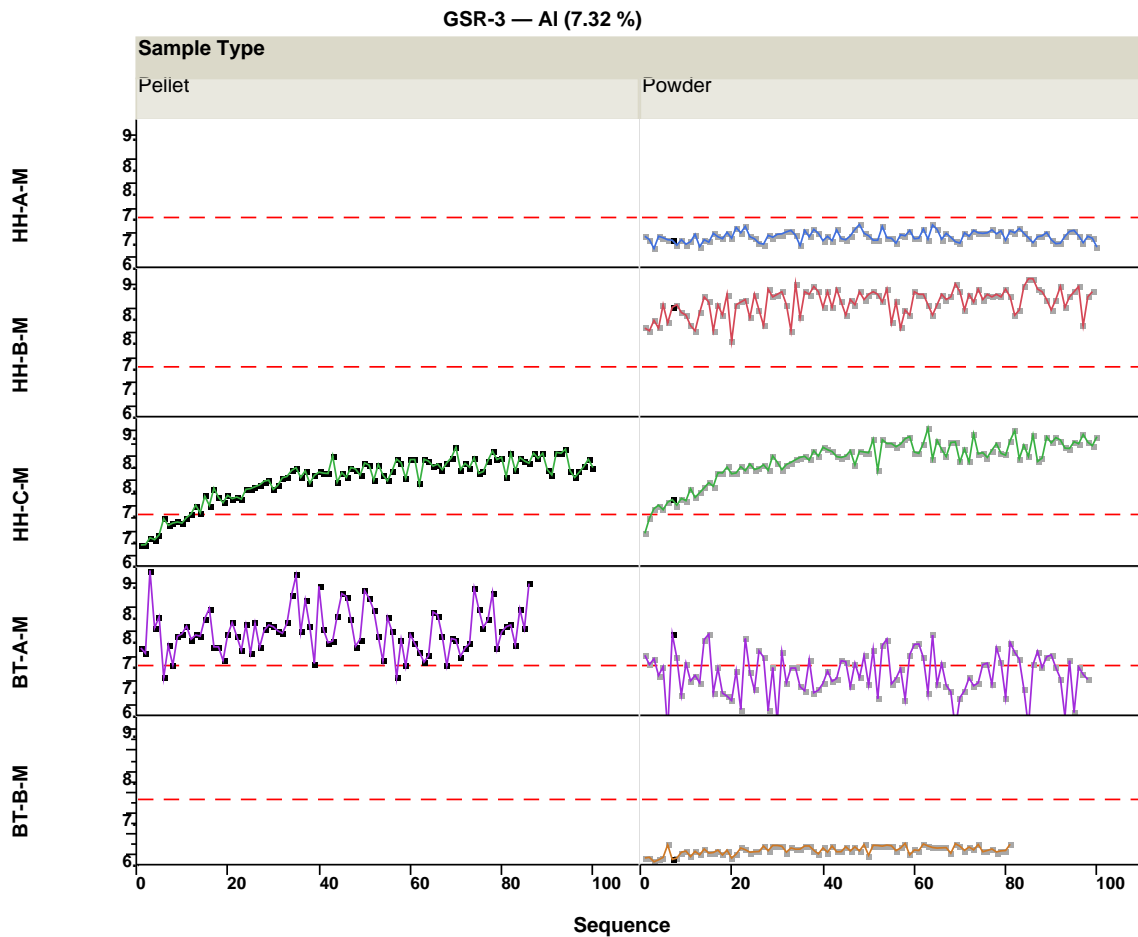






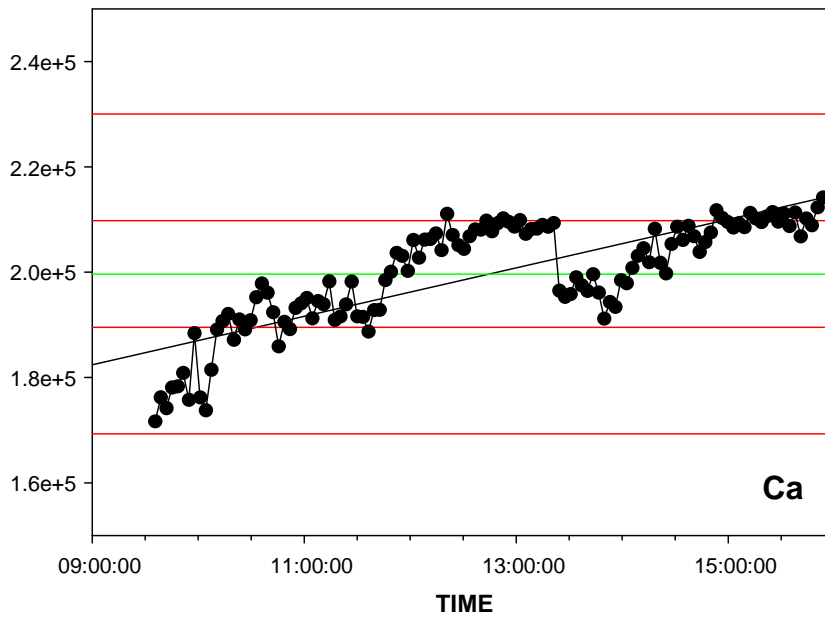
4.6 Drift

Drift has been demonstrated in Section 4.2 on the optimization of beam time. Other instances of drift have been observed throughout the project. The figure below illustrates changes in concentration reported for Al in GSR-3 as it was analysed in the mining mode ~ 100 times in sequence. While simply the noise of analysis is evident for four instruments, HH-C-M displays a significant increase in signal with time for GSR-3 in both the pellet and powder form. Note the magnitude of this shift, from ~ 6.7 % to ~ 8.3 % in Al. The actual amount of noise in these readings is not high and certainly superior, for example, to that shown by BT-A-M. There would probably be an increase in temperature of the sample over this period but it would be surprising if this accounted for such a shift in absolute signal. This is a problem that the manufacturer has to address.

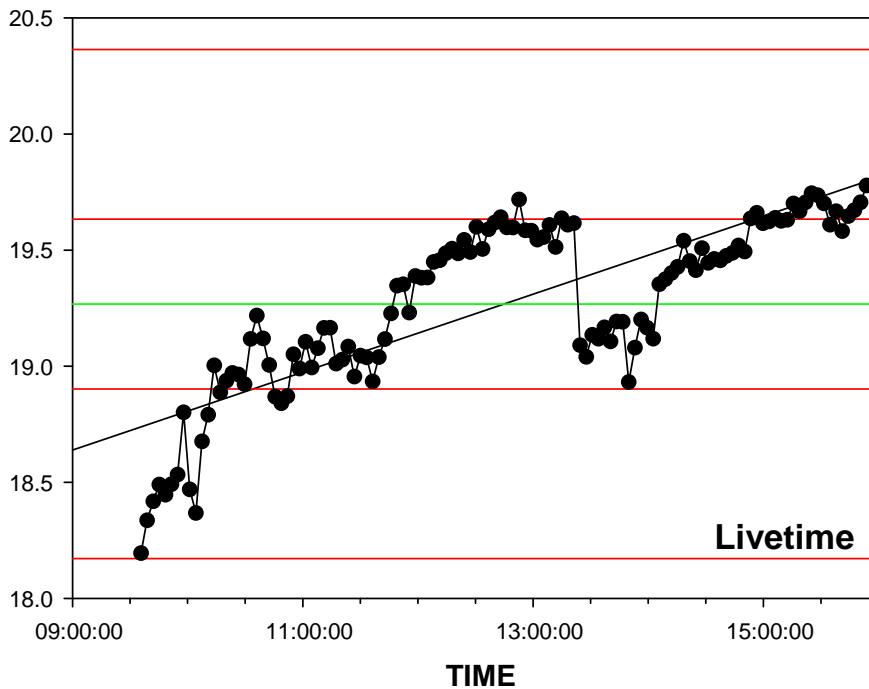


A large drift was also seen for all the elements (e.g. Ca, Ti, K, S) reported by the low energy beam using BT-A-S. This is illustrated for GXR-3 run consecutively throughout the day. It was determined that this drift was caused by a drift in live-time, as shown by the second graph. Again, this is a problem that has to be solved by the manufacturer.

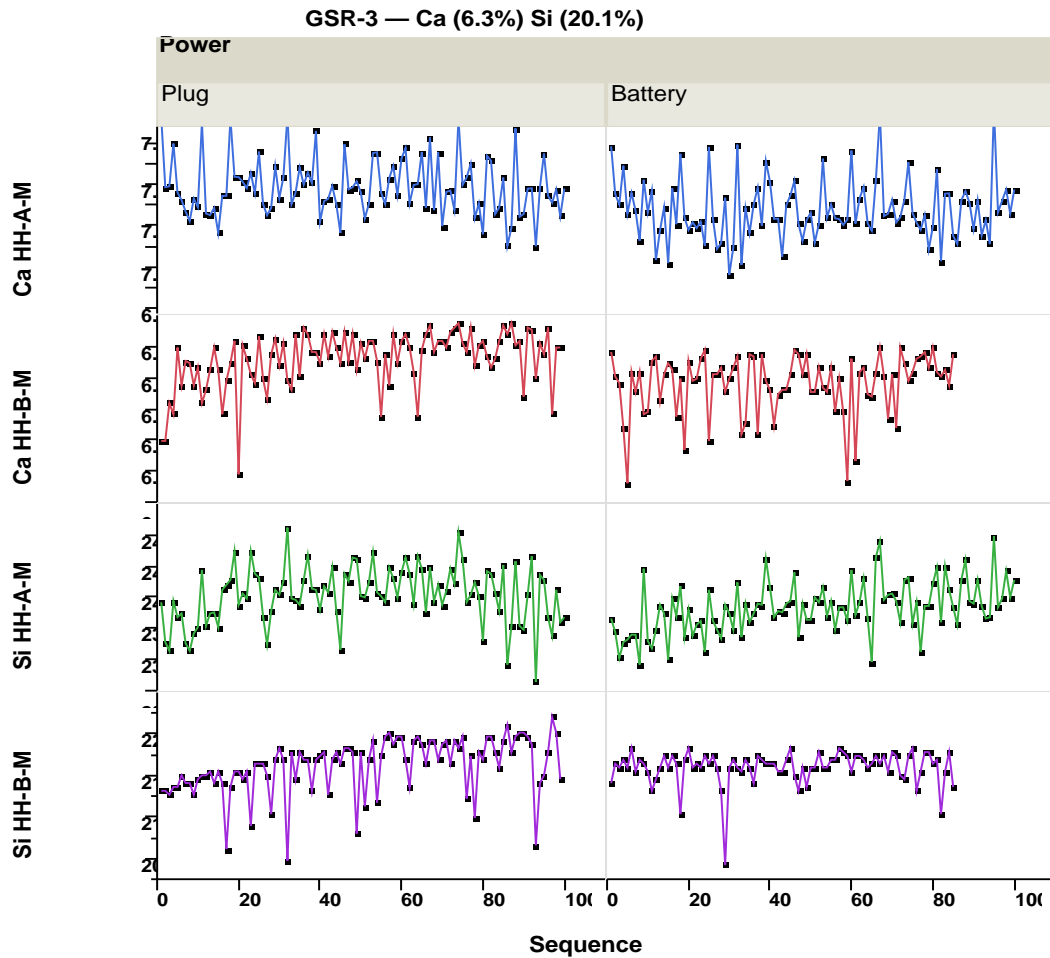
GXR-3 (soil mode, 60 s)



GXR-3 (soil mode, 60 s)



The possibility of drift using the battery for extended periods was also investigated. The figure below shows the results for Ca and Si in GSR-3 run consecutively ~ 100 times (60 s beam time) using HH-A-M and HH-B-M on both battery and mains supply. There is a warm-up period of drift in the first few analyses using both power sources but there is a drift upwards for Si using HH-B-M on mains, not evident for the battery. There is a similar drift, though of less magnitude, for Si using HH-A-M off the battery.



5. RECOMMENDATIONS FOR MANUFACTURERS OF PXRF ANALYSERS

This section provides recommendations for manufacturers of pXRF analysers. Recommendations provided address the areas of pXRF documentation, factory calibration, analyser performance, general analyser use, user calibration, results, accessories and upgrades.

Documentation

It is recommended that manufacturers provide pXRF users with an operator/user manual that has accurate and complete instrument user instructions. The manual should contain these items:

- Installation instructions of hardware and software (even if performed by the instrument manufacturer);
- a functional description of the analyser, its intended use and general operating instructions;
- instructions on all integrated functional components, configuration and linkage of integrated components (e.g. test stand), user interface specifications of both the analyser and the computer software;
- a description of the hardware (e.g. tube voltage, anode/collimator material) which will help facilitate data interpretation of interferences or of spurious results when elements of interest correspond to elements present in analyser material (e.g. Ag, Pd);
- analyte lines (photon energy lines) used to quantify an element so potential overlaps can be investigated;
- a list of elements known to interfere with the analytes of interest;
- cautions in terms of mining applications limitations and established limits of detection;
- an assurance of data accuracy, (i.e. published certified values of certified material *and* ranges in values expected to be obtained by the analyser);
- preparation requirements for a sample, matrix specifications and information on available sample supports (i.e. cups and thin-film, backing), and on how a sample can be tested and stored;
- the amount of sample needed for testing (e.g. minimum depth or infinite thickness) based on a list of penetration depths for each element based on key common geological matrices;
- instructions on preventative maintenance to ensure that the instrument will perform correctly, will have less downtime, and will reduce other maintenance/repair costs;
- a description of environmental and maintenance requirements;
- a list of warning/error messages and their appropriate corrective action;
- a description of the software that includes a file/output structure, field descriptions, user definable database options;
- a description of software-performed calculations and a description on how to recalibrate spectra;
- a mechanism on how users can update the manual and firmware when new features are available.

With the continuing advances in technology, it is recommended that the user guide be in a format that facilitates additions, deletions, and corrections so that documentation provided be up-to-date and reflect the features of the analyser.

Factory calibrations

In general, information on calibration procedures should be communicated so that conditions can be matched if the user intends to use the Default Factory modes in order to optimize accuracy. It is recommended that all relevant information on factory calibration of analysers be communicated to the user in the documentation provided.

Measurement time for analyser calibration

It is recommended that measurement time (count time) on each beam/filter used to calibrate instruments be communicated to the user. If the user chooses to proceed by measuring a sample for a shorter duration, this information may assist in adjusting expectations in terms of accuracy and/or precision.

Standards used for calibration

It is recommended that an indicator of calibration quality (i.e. r^2) of the regression (slope and intercept) for each element in each mode be provided to the user. This indicator will assist the user in evaluating the quality of their results.

- Accuracy of data generated from the default Factory modes can be largely dependent on the quality of calibration. The number of samples and matrices used to calibrate each element within each mode will in most cases affect analyser performance.
- The user may be able to recalibrate the instrument with more samples; however, if the default Factory mode is based on a poor calibration, there may be inherent limitations to the extent of improvement that a user's calibration can achieve.
- Information on Factory calibration quality can greatly assist a user in determining how best to proceed and invest in recalibrating an instrument.

Consistency in use of thin-film

It is highly recommended that every manufacturer adopt a policy for consistency in thin-film used to calibrate the instruments and in thin-film provided to the user (blanks and reference material). This should be clearly communicated to the user in the accompanied documentation. Transmittance success is dependent on thin-film thickness (gauge). If a thicker thin-film, for instance, is employed by the end-user when running the Factory Default modes, lower counts rates may result leading to falsely lower concentrations especially with regard to light elements.

It would only be beneficial to both the manufacturer and user that the user be aware and recommended to use the same thin-film as that used to calibrate the instrument. Matching calibration conditions will only provide the user with improved accuracy and greater satisfaction.

Analyser performance

Analyser stability

It is recommended that

- Drift be investigated prior to releasing an analyser. In turn, users can be informed of the necessary start-up time required for analyser stability.
 - A 5-min warm-up period when starting up does not always suffice.
 - Drift can occur throughout the day. This can be analyser-, mode- or element-specific.
 - Communicating general and common trends in analyser behaviour can really benefit in informing the user of necessary set-up time to ensure maximum precision and accuracy.
- Manufacturers investigate every analyser for live-time stability in each mode available on the analyser prior to releasing the analyser.
- Manufacturers inform users on how long analyser stability should be expected. Perhaps a mechanism built into the analyser to monitor usage should be set-up to prompt a warning message after a pre-defined duration to inform the user that diagnostic testing and check-up is recommended/required.

Certified reference material

It is recommended that

- Certified reference material be provided in the same condition (i.e. cup and thin-film material *and* thickness) as that used to calibrate the instrument. The added accuracy will provide a higher level of certainty for the user, especially for a newer user who may not be familiar with the ‘expected’ percent error that would be consistently observed for these materials.
- Replacements of thin-film for standards be provided to the user so that analyser monitoring using these supports can be as consistent as possible.

Blanks

It is recommended that

- Blanks (i.e. SiO₂ blank) powder be also provided in the same condition (i.e. thin-film and cup) used to calibrate the instrument. Thin-film should be consistent to eliminate the false reading of persistent contamination in the analyser in fact due to contamination in the thin-film.
- Manufacturers provide the user with more guidance on handling ‘legacy’ or new contaminants observed in the blanks.

General analyser use

Mode or beam selection

It is recommended that the manufacturer provide more information on the applicability of each mode and beam/filter available on the analyser. For instance, what is the cut-off in determining the use of the soil vs. mining mode? More guidance on interpreting results in two modes or beams should also be provided.

Element suites in modes

It is recommended that caveats be integrated in both the documentation and analyser interface when dealing with ‘accessory’ elements, i.e. elements not optimized for a given mode and/or

filter/beam. For instance, if a mode is designed for light elements or REEs only, it should be explicitly specified that all other elements be interpreted with a lesser degree of confidence.

User calibration (i.e. User Factors, ‘CalFactors’, or ‘Type Standardization’)

It is recommended that the manufacturer provide guidance on user-performed calibrations for matrix matching. Procedures for calibrating the analyser at the factory could serve as a guidance tool (and be included in the documentation) for user-performed calibration. This guidance would also include information on thin-film, cups, standards best suited for the analytes of each client, etc.

Mining mode recalibration

It is recommended that guidance be provided (and included in the documentation) on the necessity of calibrating the analyser in the mining mode. This may be addressed by incorporating a built-in message in the user interface of the analyser indicating that re-calibrations are highly recommended when operating under the mining mode. For mining customers, ensure that one of their matrix-matched calibrations is available on the analyser when purchased.

Soil mode recalibration

It is recommended that manufacturers provide information on when the soil mode recalibration is necessary. Should the user run a sample on the mining mode first to determine whether a sample’s elemental concentrations are fit and applicable for soil mode (Compton normalization)? At what point does Compton Normalisation start to waiver?

Results

Data display and consistency

It is recommended that

- Manufacturers incorporate an option for users to display (both on the interface and in the export file) elements in oxides or elemental form based on user preference, with specifications on the form in which the element has been modeled/calculated.
- Output results obtained by running the analyser directly or via the computer (i.e., test-stand) be synchronized and consistent.

Spectral viewer

It is recommended that

- More features be available for spectral analysis for users interested in investigating spectra. Additional features may include:
 - Displaying where baselines have been drawn under each peak (auto calibration);
 - Flexibility in redrawing baseline as a user sees fit, and cautions in doing so;
 - Highlighting the peak used to interpret/quantify the element;
 - Options for displaying the energy window (keV min and max) in which an element peak is interpreted;
 - Scrolling throughout an entire spectrum at a certain magnification;
 - Annotating spectra;

- Graded transparency for spectrum filling with the overlay function so that smaller peaks of the overlain spectrum can still be observed;
- Manufacturers consider in general the ease in viewing, saving, copying spectra for other applications (word document).

Accessories for the mining industry

It is recommended that manufacturers consider development of a test-stand designed for core. Holding the analyser over cores (or samples too large to fit in the test-stand chamber) can be very demanding energetically. A test-stand designed to have the analyser facing down would be useful for cores that could be shuffled underneath.

Firmware upgrades

It is recommended that manufacturers

- communicate with all users via email feed and website on firmware updates, commonly reported issues, and a status of issues that have been resolved.
- provide any information on firmware updates that may include changes to algorithms. Such changes will result in differences on how spectra are interpreted, and in turn affect data consistency and comparability.

6. REFERENCES

- Argyraki, A., Ramsey, M.H. and Potts, P.J., 1997. Evaluation of portable X-ray fluorescence instrumentation for in situ measurements of lead on contaminated land. *Analyst*, 122, 743–749.
- Berger, M., Zou, L. and Schleicher, R., 2010. Analysis of sulfur in the CopperBasin and Muddy River sites using portable XRF instrumentation. *Proceedings of the Annual International Conference on Soils, Sediments, Water and Energy*, 13, Article 2.
- Binstock, D.A., Gutknecht, W.F., McWilliams, A.C., 2008. Lead in soil by field portable X-ray fluorescence spectrometry – an examination of paired in-situ and laboratory ICP-AES results. *Proceedings of the Annual International Conference on Soils, Sediments, Water and Energy*, 13, Article 3.
- Chemplex, 2011. Chemplex Industries Inc. Catalog, 2011
<http://www.chemplex.com/>
- Gonzalez-Fernandez, O. and Queralt, I., 2010. Fast elemental screening of soil and sediment profiles using small-spot energy-dispersive X-ray fluorescence: application to mining sediments geochemistry. *Applied Spectroscopy*, 64, 1045-1053.
- Haffert, L. and Craw, D., 2009. Field quantification and characterisation of extreme arsenic concentrations at a historic mine processing site, Waiuta, New Zealand. *New Zealand Journal of Geology and Geophysics*, 52, 261-272.
- Hall, G.E.M. and Bonham-Carter, G.F., 1988. Review of methods to determine gold, platinum and palladium in production-oriented geochemical laboratories, with an application of a statistical procedure to test for bias. *Journal of Geochemical Exploration* 30, 255-286.
- Hall, G.E.M. and Pelchat, P., 1997. Determination of As, Bi, Se, Sb and Te in fifty-five reference materials by hydride generation ICP-MS. *Geostandards Newsletter*, 21, 85-91.
- Houlihan, T, Ramsay, S. and Povey, D., 2003. Use of field portable X-ray fluorescence spectrum analysers for grade control – a presentation of case studies. *Proceedings of the 5th International Mining Geology Conference* (see <http://www.ausimm.com.au>), Bendigo, 9p.
- Hou, X., He, Y. and Jones, B.T., 2004. Recent advances in portable X-Ray fluorescence spectrometry. *Applied Spectroscopy Reviews*, 39, 1-25.
- Hughes, N. and Rowe, H.D., 2009. Application of energy-dispersive X-ray fluorescence (ED-XRF) in chemostratigraphy of organic-rich mudstones of Texas. *Geological Society of America, Abstracts with Programs*, 41, p. 438.

- Hughes, N. and Rowe, H.D., 2010. Advancing the hand-held ED-XRF instrument as a quantitative tool for deciphering paleoceanographic conditions in Phanerozoic mudrock sequences. *American Geophysical Union*, Fall Meeting 2010, abstract #PP13B-1519.
- Jones M.C., Williams-Thorpe O., Potts, P.J. and Webb, P.C., 2005. Using field-portable XRF to assess geochemical variations within and between dolerite outcrops of Preseli, south Wales. *Geostandards and Geoanalytical Research*, p. 251-269.
- Kalnicky, D.J. and Singhvi, R., 2001. Field portable XRF analysis of environmental samples. *Journal of Hazardous Materials*, 83, 93-122.
- Kenna, T.C., Nitsche, F.O., Herron, M.M., Mailloux, B.J., Peteet, D., Sritrairat, S., Sands, E. and Baumgarten, J., 2011. Evaluation and calibration of a field portable X-Ray fluorescence spectrometer for quantitative analysis of siliciclastic soils and sediments. *Journal of Analytical Atomic Spectrometry*, 26, 395-405.
- Lachance, G.R. and Traill, R.J., 1966. A practical solution to the matrix problem in X-ray analysis. *Canadian Spectroscopy*, 11, 43-48.
- Makinen, E., Korhonen, M., Viskari E.-L., Haapamaki, S., Jarvinen. M. And Lu, L., 2006. Comparison of XRF and FAAS methods in analysing CCA contaminated soils. *Water, Air and Soil Pollution*, 171, 95-110.
- Margui, E., Jurado, A., Hidalgo, M., Pardini, G., Gispert, M. and Queralt, I., 2009. Application of small-spot energy dispersive X-ray fluorescence instrumentation in phytoremediation activities around metal mines. *Applied Spectroscopy*, 63, 1396-1402.
- Markey, A.M., Clark, S., Succop, P.A. and Roda, S., 2008. Determination of the feasibility of using a portable X-Ray fluorescence (XRF) analyser in the field for measurement of lead content of sieved soil. *Journal of Environmental Health*, 70, 24-29.
- Mielke, H.W., Gonzales, C.R., Cahn, E., Brumfield, J., Powell, E.T. and Mielke Jr., P.W., 2010. Soil arsenic surveys of New Orleans: localized hazards in children's play areas. *Environmental Geochemistry and Health*, 32, 431-440.
- Morris, P.A., 2009. Field-portable X-ray fluorescence analysis and its application in GSWA. *Geological Survey of Western Australia*, Record 2009/7, 23p.
- Peinado, F. M. Ruano, S. M. Gonzalez, M. G. Molina, C. E., 2010. [A rapid field procedure for screening trace elements in polluted soil using portable X-ray fluorescence \(PXRF\)](#). *Geoderma*, 159, 76-82.
- Potts, P.J., 1987. *A Handbook of Silicate Rock Analysis*, Blackie & Son Ltd, Glasgow, 622 pp.
- Potts, P.J. and Webb, P.C., 1992. X-ray fluorescence spectrometry. *Journal of Geochemical Exploration*, 44, 251-296.

- Potts P.J., Webb P.C., Williams-Thorpe O. and Kilworth R., 1995. Analysis of silicate rocks using field-portable X-ray fluorescence instrumentation incorporating a mercury (II) iodide detector: A preliminary assessment of analytical performance. *The Analyst*, 120, 1273-1278.
- Potts P.J., Webb P.C. and Williams-Thorpe O., 1997a. Investigation of a correction procedure for surface irregularity effects based on scatter peak intensities in the field analysis of geological and archaeological rock samples by portable X-ray fluorescence spectrometry. *Journal of Analytical Atomic Spectroscopy*, 12, 769-776.
- Potts, P.J. and West, M., 2008. Portable X-Ray Fluorescence Spectrometry. Capabilities in *In-Situ* Analysis. RSC Publishing, ISBN 978-0-85404-552-5.
- Potts P.J., Williams-Thorpe O. and Webb P.C., 1997b. The bulk analysis of silicate rocks by portable X-ray fluorescence: Effects of sample mineralogy in relation to the size of the excited volume. *Geostandards Newsletter*, 21, 29-41.
- Potts, P.J., Bernardini, F., Jones, M.C., Williams-Thorpe, O. and Webb, P.C., 2006. Effects of weathering on *in situ* portable X-ray fluorescence analyses of geological outcrops: dolerite and rhyolite outcrops from the Preseli Mountains, South Wales. *X-Ray Spectrometry*, 35, 8-18.
- Ripley, B.D. and Thompson, M., 1987. Regression techniques for the detection of analytical bias. *The Analyst* 112, 377-383.
- Rousseau, R.M., 1989. Concepts of influence coefficients in XRF analysis and calibration. In: S.T. Ahmedali (Editor), X-Ray Fluorescence Analysis in the Geological Sciences: Advances in Methodology. *Geological Association of Canada Short Course Vol. 7*, 141-220.
- Royal Society of Chemistry, 2002. Fitting a linear functional relationship to variables with errors on both variables. *Analytical Methods Committee AMC Technical Brief 10*, 2.
- Sheppard, P., Trichereau, B. and Milicich, C., 2010. Pacific obsidian sourcing by portable XRF. *Archaeology in Oceania*, 45, 21-30.
- Sherman, J., 1955. The theoretical derivation of fluorescent X-ray emission intensities from mixtures. *Spectrochimica Acta*, 7, 283-306.
- Simandl, G.J., Paradis, S., Fajber, R., Rogers, N., 2011. Hand-held portable XRF in exploration for carbonate-hosted sulphide and nonsulphide Pb-Zn deposits, British Columbia; *British Columbia Ministry of Forests, Mines and Lands*, Geofile 2011-6, poster.
- Solazzi, M.J., 1985. X-ray fluorescence thin-film sample support materials. *American Laboratory*, 17 (11). Also available in Chemplex, 2011.

Vanhoof, C., Corthouts, V. and Tirez, K., 2004. Energy-dispersive X-ray fluorescence systems as analytical tool for assessment of contaminated soils. *Journal of Environmental Monitoring*, 6, 344-350.

Wegrzynek, D., Markowicz, A. and Chinea-Cano, E., 2003. Application of the backscatter fundamental parameter method for *in situ* element determination using a portable energy-dispersive X-ray fluorescence spectrometer. *X-Ray Spectrometry*, 32, 119-128.

Acknowledgements

We are very grateful to the Geological Survey of Canada for housing this study and for use of the various facilities. We particularly thank Pierre Pelchat, Carrie Bolton and Simon Jackson for their extensive assistance in the project. We also thank ALS and SGS laboratories for their excellent analyses and InnovX, Niton and Bruker for generously providing the instruments and training.